

https://dspace.org/

Environmental analysis of modern speleothems from Sterkfontein Caves and its implications for reconstructing palaeoenvironments

Venter, Claudia Nicole

2017

https://hdl.handle.net/10539/24030

Venter, Claudia Nicole (2017) Environmental analysis of modern speleothems from Sterkfontein Caves and its implications for reconstructing palaeoenvironments, University of the Witwatersrand, Johannesburg, <http://hdl.handle.net/10539/24030>

Downloaded from a DSpace repository. https://dspace.org/



Environmental Analysis of Modern Speleothems from Sterkfontein Caves and its Implications for Reconstructing Palaeoenvironments

MSc Dissertation

Claudia Venter

A dissertation submitted to the Faculty of Science, University of the Witwatersrand, Johannesburg, in fulfilment of the requirements for the degree of Master of Science.

Johannesburg, 2017

Declaration

I declare that this dissertation is my own unaided work. It is being submitted for the degree of Master of Science at the University of the Witwatersrand, Johannesburg. It has not been submitted before for any degree or examination in any other university.



(Signature of candidate)

Date: 17/08/2017

Acknowledgements

I would like to thank my supervisors Dr Christine Steininger and Dr Dominic Stratford for all their guidance, support and encouragement throughout this research project. My thanks also go out to Lucas and Sipho, the technicians at Sterkfontein Caves, who diligently collected my drip water samples for the course of a year, and recorded the cave climatic data during the collection of these samples, and to Dr Dominic Stratford for overseeing this process and assisting with the field work component of this dissertation. My sincere gratitude is also expressed to Dr Christine Steininger, who funded the analysis of the drip water samples.

I would also like to express gratitude to Mike Butler and Osborne from iThemba Labs, Gauteng, who ran the carbon and oxygen stable light isotope analyses on my speleothem samples, and assisted me in preparing these samples for analysis. My thanks also go out to Professor Tamiru Abiye from the School of Geosciences for running the oxygen stable light isotope analyses on my drip water samples. Many thanks go out to Professor Chris Curtis from the School of Geography, Archaeology and Environmental Studies, for the use of his water laboratory and YSI probe equipment in the hydrochemical analysis of my drip water samples. I would also like to thank Professor Marion Bamford, for her assistance with the vegetation aspects of this study. Many thanks also go to the South African Weather Service, Gauteng, for providing the 10 year temperature and precipitation records from various weather stations in Gauteng.

Lastly, I would like to thank my parents for all their continued support, love and interest, and especially for helping me out with the grammatical aspects of this dissertation. I would also like to express my gratitude to my fiancé, Wyzen Bogaard for his continued support, love, and reassurance when things felt impossible. This dissertation would not have been possible without all of your steadying hands helping me.

This dissertation was funded by the National Research Foundation Scarce Skills Scholarship, the National Research Foundation Grantholder’s bursary to Dr Dominic Stratford, and the African Origins Platform Grant to Dr Christine Steininger.

Abstract

During the Plio-Pleistocene, the Earth experienced a period of gradual cooling, leading to a decrease in atmospheric temperature and increased seasonality. This resulted in the aridification of large parts of Africa, and this is believed to have encouraged human evolution and innovation. Palaeoenvironmental analyses using sediment deposits as palaeoclimate proxies in the Cradle of Humankind have been used to understand the timing and intensity of this aridification by determining how changes in environmental conditions and seasonal cycles affected the South African landscape. These changes are recorded within the carbon and oxygen isotopic signatures of speleothems, which have precipitated within the Sterkfontein Caves system. The aim of this study is to understand the degree to which modern speleothems represent the modern climate and environment, and thereby deduce the reliability of speleothem deposits in the Sterkfontein Caves system as palaeoclimate proxies. Samples of modern speleothems were collected from different chambers of the Sterkfontein Caves, along with the collection of modern drip water samples bi-weekly over a period of 14 months. Oxygen and carbon stable light isotope analyses of these modern speleothem and drip water samples were used to obtain modern temperature, precipitation and vegetation data. These data were then compared to modern climatic and environmental records for atmospheric temperatures and precipitation from weather stations around the Sterkfontein Caves area. The $\delta^{13}C$ trends produced from the modern speleothem samples reflected the current vegetation distribution in terms of C_4 and C_3 vegetation very well, while the temperatures calculated from the $\delta^{18}O$ values of the modern speleothem and drip water samples displayed variations related to kinetic fractionation effects, rendering these data less useful in reflecting the current atmospheric temperatures. The $\delta^{18}O$ values of the drip water samples, along with the measured drip rate reflected current precipitation seasonality, taking into account groundwater residence time and recharge rate. The conditions within the cave conducive to formation of the speleothems was well reflected by the pH and electro-conductivity values produced from the drip water samples. These values also provided further insight into the exterior climatic conditions.

Overall, the carbon and oxygen stable light isotope data revealed patterns present in the modern speleothem and drip water samples, which could be further related to changes in local climate during the precipitation of these modern speleothems from drip water sources. This, to a certain degree, provides evidence of the reliability of speleothems in the Sterkfontein Caves system as suitable palaeoclimate proxies with regards to vegetation and precipitation

interpretations, over a longer term scale and at higher sampling resolution.

Contents

Acknowledgements **I**

Abstract **II**

List of Figures VII

List of Tables XII

Chapter 1: Introduction **1**

1.1 Introduction 1

1.2 Rationale and Research Question 2

1.3 Significance of Research and Aims 3

1.4 Dissertation Structure 4

Chapter 2: Background **5**

2.1 Introduction 6

2.2 Geology and Stratigraphy 7

2.2.1 General Geology and Stratigraphy 7

2.2.2 Dating of Cave Stratigraphy 13

2.2.3 Speleothems 14

2.2.4 Cave Formation 15

2.3 Palaeoclimate and Human Evolution 16

2.3.1 Cenozoic Palaeoclimate and Human Evolution in Africa 16

2.3.2 Faunal and Floral Evolution in Africa during the Cenozoic 19

2.3.3 Cenozoic Palaeoclimate Record of the Cradle of Humankind 20

2.3.4 Hominin Evolution with regard to Palaeoenvironments 27

2.3.5 Speleothem Analysis 28

2.4 Palaeoenvironmental Analysis 31

2.4.1 Carbon Isotope Analysis 31

2.4.2 Drip Water Analysis 33

2.4.3 Oxygen Isotope Analysis 36

2.4.4 Dust Flux Analysis 41

2.4.5 Miscellaneous Palaeoclimate Analyses 42

Chapter 3: Methods & Materials **44**

3.1 Introduction 44

3.2 Sample Location and Sampling 45

3.2.1 Sample Location 45
3.2.2 Speleothem Sampling 46
3.2.3 Drip Water Sampling 49
3.2.4 Vegetation Survey 51
3.3 Preparation and Analysis 51
3.3.1 Speleothem Analysis 51
3.3.2 Drip Water Analysis 52
3.3.3 Hydrochemical Analysis 54
3.4 Calibration and Correction 55
3.5 Statistical Analyses and Correlations 58
3.6 Data Analysis 59
3.6.1 Temperature 59
3.6.2 Precipitation 63
3.6.3 Vegetation 64
3.6.4 Hydrochemistry 65
Chapter 4: Results **66**
4.1 Exterior Climate for the Cradle of Humankind 66
4.1.1 Atmospheric Temperatures 66
4.1.2 Precipitation 67
4.2 Cave Climatic Conditions 69
4.2.1 Measured Cave Air Temperature 69
4.2.2 Humidity 71
4.2.3 Cave Atmospheric Pressure 72
4.2.4 Vegetation 73
4.3 Speleothem Isotopes 74
4.3.1 Carbon Isotopes 75
4.3.2 Oxygen Isotopes 78
4.4 Drip Water 80
4.4.1 Oxygen Isotopes 80
4.4.2 Temperature 86
4.4.3 Fractionation 98
4.4.4 Drip Rate and Precipitation 102
4.5 Hydrochemistry 107

4.5.1 Electro-conductivity 107
4.5.2 pH 108
4.6 Summary 109
Chapter 5: Discussion **111**
5.1 Vegetation 111
5.1.1 Modern Speleothem Carbon Isotopes 111
5.1.2 Observed Vegetation 115
5.1.3 Overall Vegetation Distribution 116
5.2 Temperature 117
5.2.1 Modern Speleothem Oxygen Isotopes 117
5.2.2 Drip Water Oxygen Isotopes 120
5.3 Precipitation 131
5.3.1 Modern Speleothems 131
5.3.2 Drip Water 132
5.4 Hydrochemistry 137
5.4.1 Electro-conductivity 137
5.4.2 pH 140
Chapter 6: Conclusions **142**
6.1 Modern Environment 142
6.2 Implications for Palaeoenvironmental Analysis 146
References **150**
Appendices **177**
Appendix A 177
Appendix B 178
Appendix C 186
Appendix D 195
Appendix E 201
Appendix F 215
Appendix G 217

List of Figures

Figure 1.1	Locality map showing Sterkfontein Caves in the Cradle of Humankind.	1
Figure 2.1	Map showing the regional geology surrounding the Cradle of Humankind World Heritage Site, including the location of the Sterkfontein Caves site. Adapted from Obbes, 2000.	8
Figure 2.2	North-south section of Sterkfontein showing the stratigraphy and relative locations of the 6 members (Clarke, 2006).	9
Figure 2.3	Profile through a section of the Sterkfontein Caves site showing stratigraphic relationships (Reynolds & Kibii, 2011).	12
Figure 2.4	An example of speleothems in the form of flowstones and drip water from the Jacovec Cavern.	14
Figure 2.5	Oxygen and carbon isotope date in blue and red respectively from the T8 speleothem from the Makapansgat site (Holmgren et al., 2003).	23
Figure 2.6	Stable oxygen isotope variations, associated palaeotemperature variations, and stable carbon isotope variations associated with $\%C_4$ vegetation. (Talma & Vogel, 1992).	24
Figure 2.7	Rainfall records from the Tswaing Impact Crater site (Partridge et al., 1997).	26
Figure 2.8	The use of oxygen and carbon stable light isotope analysis of speleothems to reconstruct palaeoclimates using temperatures (de Cisneros & Caballero, 2013).	30
Figure 2.9	Examples of drip water from flowstone deposits in the Jacovec Cavern of Sterkfontein Caves.	34
Figure 2.10	Oxygen isotope curve for the last 900 Ka (Bassinot et al., 1994).	37

Figure 2.11	Oxygen isotope curve produced from the analysis of benthic foraminifera, dating from the Cretaceous to the Plio-Pleistocene.	38
Figure 2.12	Climate change data from the Vostok ice core temperature change records (Petit et al., 1999) and from the global SPECMAP record (Imbrie et al., 1984).	40
Figure 3.1	Map of Sterkfontein Caves, with chamber locations and samples collected from these chambers indicated by the red arrow. Adapted from Reynolds et al., 2003.	46
Figure 3.2	Simplified diagram showing the sample vial set up in the autosampler trays, as well as the double needle set up. (Thermo-Fischer Scientific, 2014).	52
Figure 3.3	Map of South Africa, showing the locations of the three weather stations used.	64
Figure 4.1	Temperature record from 2011 to 2016 from the Lanseria Weather Station.	67
Figure 4.2	Temperature record from 2006 to 2016 from the Johannesburg Botanical Gardens weather station.	67
Figure 4.3	Rainfall record from 2006 to 2016 from Krugersdorp and Johannesburg Botanical Gardens weather stations.	68
Figure 4.4	Line graph displaying the cave air temperature trends measured from the Jacovec Cavern, Antechamber 1 and Antechamber 2.	70
Figure 4.5	Comparison of the measured cave air temperatures to the measured average atmospheric temperatures.	71
Figure 4.6	Line graph displaying the humidity trends measured from the Jacovec Cavern, Antechamber 1 and Antechamber 2.	72
Figure 4.7	Line Graph showing the atmospheric pressure measured for the Jacovec Cavern, Antechamber 1 and Antechamber 2.	73

Figure 4.8	(A) Photograph of some of the grasses and herbaceous plants present at the Sterkfontein site. (B) Overall view of some of the typical shrubs, grasses and trees present at Sterkfontein.	74
Figure 4.9	$\delta^{13}C$ versus $\delta^{18}O$ for modern speleothem samples from the Sterkfontein Caves system.	75
Figure 4.10	$\delta^{13}C$ values for modern speleothem samples from Sterkfontein Caves.	76
Figure 4.11	Bar graph showing the percentage distribution of C_3 and C_4 vegetation for each speleothem sample, calculated using the carbon isotope data from the speleothem samples.	77
Figure 4.12	Pie chart showing the overall average percentage distribution of C_3 and C_4 vegetation for the environment above the Sterkfontein Caves system, deduced from the d13C values.	78
Figure 4.13	$\delta^{18}O$ values from modern speleothem samples from the Sterkfontein Caves system.	79
Figure 4.14	Comparison of ideal temperatures produced using the empirical and experimental equations for deriving temperatures from speleothems, and the measured air temperatures in the cave system.	80
Figure 4.15	Comparison of $\delta^{18}O$ data from 328 drip water samples with the global meteoric water line.	81
Figure 4.16A, B	$\delta^{18}O$ results from the Jacovec Cavern, without the 4 outlier samples for 26 weeks.	83
Figure 4.17A, B	$\delta^{18}O$ trends for Antechamber 1 for 26 weeks. The 14 outlier samples have been disregarded.	84

Figure 4.18	$\delta^{18}O$ results for Antechamber 2 for 26 weeks. The 8 outlier samples have been disregarded.	85
Figure 4.19	Monthly average $\delta^{18}O$ values for the Jacovec Cavern, Antechamber 1 and Antechamber 2.	86
Figure 4.20	Temperatures calculated from the Jacovec Cavern average $\delta^{18}O$ values using equation 1, and compared to the average measured atmospheric temperatures.	88
Figure 4.21	Temperatures calculated from the Antechamber 1 average $\delta^{18}O$ values using equation 1, and compared to the average measured atmospheric temperatures.	89
Figure 4.22	Temperatures calculated from the Antechamber 2 average $\delta^{18}O$ values using equation 1, and compared to the average measured atmospheric temperatures.	90
Figure 4.23	Measured cave air temperatures versus the temperatures calculated from the Jacovec Cavern, Antechamber 1 and Antechamber 2 using equation 1.	92
Figure 4.24	Temperatures calculated from the Jacovec Cavern average $\delta^{18}O$ values using equation 2, and compared to the average measured atmospheric temperatures.	93
Figure 4.25	Temperatures calculated from the Antechamber 1 average $\delta^{18}O$ values using equation 2, and compared to the average measured atmospheric temperatures.	94
Figure 4.26	Temperatures calculated from the Antechamber 2 average $\delta^{18}O$ values using equation 2, and compared to the average measured atmospheric temperatures.	96
Figure 4.27	Measured cave air temperatures versus the temperatures calculated from the Jacovec Cavern, Antechamber 1 and Antechamber 2 using equation 2.	98
Figure 4.28	Comparison between the idealised temperatures calculated using equation 1, and the temperatures calculated from the three chambers using equation 1.	100

Figure 4.29	Comparison between the idealised temperatures calculated using equation 2, and the temperatures calculated from the three chambers using equation 2.	102
Figure 4.30	Drip Rate for Jacovec Cavern, Antechamber 1 and Antechamber 2, from July 2015 to August 2016.	103
Figure 4.31	Drip rate for the Jacovec Cavern, Antechamber 1 and Antechamber 2 in comparison to the average measured rainfall for July 2015 to August 2016.	104
Figure 4.32	Drip rate trends from the Jacovec Cavern, Antechamber 1 and Antechamber 2 compared to the $\delta^{18}O$ values measured from the drip water of the three chambers.	106
Figure 4.33	Average monthly measured rainfall compared to the $\delta^{18}O$ values from drip water.	107
Figure 4.34	Electro-conductivity results for the modern drip water samples.	108
Figure 4.35	pH results for the modern drip water samples from Sterkfontein Caves.	109
Figure 5.1	Diagram showing the vegetation cover in relation to the cave chambers. Adapted from Reynolds et al. (2003).	116
Figure 5.2	Comparison of the idealised temperatures produced from the modern speleothem samples using the experimental equation for calculating temperature from speleothems, the measure cave air temperature and the average atmospheric air temperature during the period in which the samples were taken and cave air temperature measured.	120

List of Tables

Table 3.1	Description of speleothem samples and the chambers from which they were collected.	48
Table 3.2	Description of speleothem samples and the chambers from which they were collected.	50
Table 3.3	In-house standards used during the oxygen and carbon stable light isotope analysis of the speleothems.	56
Table 3.4	In-house standards used during the oxygen stable light isotope analysis of the drip water samples.	57
Table 3.5	Classification of r values according to strength of correlation between data.	59
Table 3.6	Statistical data for the modern drip water oxygen isotope values.	61

Chapter 1

A general overview of the Cradle of Humankind and the associated palaeontological discoveries is provided in Section 1.1 of this chapter, followed by the project rationale and a description of the research question pertinent to this study, as well as the significance and overall aims of the research (Sections 1.2 to 1.3). Section 1.4 provides a description of the overall structure of the presented study.

1.1 Introduction

The Cradle of Humankind comprises fossil-bearing cave sites, and is situated 40km northwest of Johannesburg, South Africa, encompassing an area of around 47 000 hectares (Figure 1.1). It was declared a World Heritage Site in 2000, due to the famous Plio-Pleistocene hominin fossil discoveries in the caves of Sterkfontein, Swartkrans and Kromdraai, and the associated fauna (Hilton-Barber & Berger, 2002). Several genera and species of hominins have been discovered in the cave sites, including *Australopithecus africanus*, *A. sediba*, *Paranthropus robustus*, *A. prometheus*, early *Homo*, and *H. ergaster* (Brain, 1993; Tobias, 2000; Dirks & Berger, 2012; Clarke, 2013). The discovery of these hominin fossils has contributed greatly to our understanding of hominin evolution (Dart, 1925; Broom, 1936; Robinson, 1953; Clarke, 1985; Berger et al., 2010), and has contributed to the development of a diverse range of palaeontological studies.



Fig. 1.1: Locality map showing Sterkfontein Caves in the Cradle of Humankind. Modified after: Stratford (2011).

1.2 Rationale and Research Question

The Earth experienced numerous climatic fluctuations and shifts in variability during the Plio-Pleistocene (approximately 5.3 – 0.7 Ma (million years ago)), which resulted in an overall decrease in global atmospheric temperatures and increased seasonality, due to a global period of gradual cooling (de Menocal, 2004; Shackleton et al., 1984; Kennett, 1995; Reynolds, 2007). It has been suggested that these climate fluctuations precipitated important evolutionary changes with regard to African fauna and flora, including key stages of human evolution and innovation (de Menocal, 2004; Reynolds, 2007). Palaeoenvironmental analyses using speleothems as palaeoclimate proxies have been used to understand these climatic variations by determining how changes in environmental conditions and seasonal cycles affected the South African landscape (Gascoyne, 1992; Talma & Vogel, 1992; Ayliffe et al., 1998; Dorale et al., 1998; Moriarty et al., 2000; Holmgren et al., 2003; Richards & Dorale, 2003; Tan et al., 2003; Vaks et al., 2003; Fleitmann et al., 2004; McDermott, 2004; Mickler et al., 2004; White, 2004; Cruz et al., 2005; Nordhoff, 2005; Hopley et al., 2007; Sundqvist et al., 2007; Pickering et al., 2011; Tremaine et al., 2011). These changes may be recorded within the carbon and oxygen isotopic signatures of speleothems which have precipitated within the cave systems of the Cradle of Humankind (Talma & Vogel, 1992; Ayliffe et al., 1998; Dorale et al., 1998; Moriarty et al., 2000; Holmgren et al., 2003; Richards & Dorale, 2003; Vaks et al., 2003; Mickler et al., 2004; White, 2004; Pickering et al., 2011). Oxygen and carbon stable light isotope data produced from the analysis of speleothems provides information regarding atmospheric temperatures, precipitation events, and the distribution of vegetation during the precipitation of the speleothems, allowing for complex palaeoclimate and palaeoenvironmental reconstructions to be completed (Gascoyne, 1992; Dorale et al., 2002; Vaks et al., 2003; Fleitmann et al., 2004; McDermott, 2004; Mickler et al., 2004; Lachniet, 2009). Determining the level of accuracy and reliability in the use of speleothems as palaeoclimate proxies is therefore important in order to assess the reliability of the palaeoenvironmental and palaeoclimatic reconstructions produced from this analysis. This study questions the extent to which modern climatic reconstructions produced from the oxygen and carbon stable light isotope analysis of modern speleothem and drip water samples reflects current climatic and environmental conditions, in order to determine the reliability of speleothems as palaeoclimate proxies.

1.3 Significance of Research and Aims

Oxygen and carbon stable light isotope analysis of speleothems has been used in the past in order to obtain precipitation, temperature and vegetation data (Vaks et al., 2003; Fleitmann et al., 2004; McDermott, 2004). These data have then been used for palaeonvironmental and palaeoclimate reconstructions of the Quaternary and compared to global, regional, and local records of climate change during that period. de Menocal (2004) had suggested that more arid and open environments existed in Africa from 2.8 Ma, and many palaeoclimate and palaeoecological work has been done in East Africa showing a similar pattern (Cerling, 1992; de Menocal, 1995; Dupont & Leroy, 1995; Clemens et al., 1996; Bobe, 2006; Fernandez & Vrba, 2006), but conditions particular to South Africa may vary in this regard (Talma & Vogel, 1992; Avery, 2001; Holmgren et al., 2003; Hopley et al., 2007).

This research will include the analysis of oxygen and carbon stable light isotopes from modern speleothem examples as well as from drip water sources, and comparing the precipitation and temperature data produced from this analysis with modern records for local temperatures and mean annual rainfall. Vegetation data produced from carbon isotope analysis of speleothems will be compared to current vegetation cover and overall floral environment of the environment above the cave system. This will produce an indication of whether modern examples of speleothems are reliable sources of precipitation, temperature and vegetation data, and therefore whether speleothems produce reliable environmental and climatic reconstructions. These results will be used to ascertain whether ancient speleothems are reliable palaeoclimate proxies. The overall aim of this study is to understand the degree to which modern speleothems represent the modern climate and environmental conditions by using stable light isotope analysis of oxygen and carbon from modern speleothem samples from Sterkfontein Caves to provide temperature, precipitation and vegetation data.

The main aims of this study are:

1. To ascertain whether modern speleothems are reliable sources of precipitation, temperature and vegetation data in terms of the current environment and climate.

2. To ascertain from the comparison of climatic data produced from the modern speleothems and the current environment whether ancient speleothems would be reliable palaeoclimate proxies.

1.4 Dissertation Structure

Chapter 1 includes an overall introduction to the study, including the research question, research rationale, and significance and aims of the research. Chapter 2 provides a detailed background to the study, which includes a literature review. Chapter 3 details the methodology and materials used in conducting this study. Chapter 4 provides a detailed description of the results produced from the study. Chapter 5 discusses these results in detail and provides interpretations for the results produced, and Chapter 6 provides overall interpretations and conclusions. This is followed by an extensive reference list, and a series of appendices.

Chapter 2
Background

The introduction to this chapter provides a brief overview of the history of the excavations undertaken in the Cradle of Humankind, particularly at Sterkfontein Caves, as well as an overview of the important palaeontological and archaeological discoveries from Sterkfontein Caves. These discoveries are described in order to reveal the palaeontological and archaeological context of this study. This introduction (Section 2.1) is followed by a description of the overall geological and stratigraphic context of the Sterkfontein Caves in Section 2.2, providing detailed descriptions of the six stratigraphic members comprising the Sterkfontein Formation, as well as the caverns and chambers located in the Sterkfontein site in Section 2.2.1. A description of the dating of cave deposits follows this in Section 2.2.2., followed by a detailed description of speleothem deposits in Section 2.2.3 and the overall formation of cave deposits in Section 2.2.4. Section 2.3 provides a detailed description of Cenozoic palaeoclimates and human evolution with regards to palaeoclimatic variations, particularly within the Cradle of Humankind. Section 2.3.1 provides detailed descriptions of Cenozoic palaeoclimates and the evolution of humans in Africa, particularly in southern and eastern Africa. This is followed by an overview of the faunal and floral evolution in Africa during the Cenozoic in Section 2.3.2. Section 2.3.3 details the Cenozoic palaeoclimate record with particular reference to the Cradle of Humankind, and is followed by a description of human evolution with regard to palaeoenvironments in Section 2.3.4, with particular reference to hypotheses proposed for human evolution in the context of palaeoenvironmental change. Section 2.3.5 provides a detailed description of speleothem deposits and the analysis thereof, including examples of studies conducted by Ayliffe et al. (1998), Moriarty et al. (2000), Pickering et al. (2011) and Hopley et al. (2007), using speleothems as palaeoclimate proxies. Section 2.4 describes numerous methods used in the analysis and reconstruction of palaeoenvironments and palaeoclimates, and details various analyses including climate analyses, carbon stable light isotope analyses, speleothem drip water analyses, oxygen stable light isotope analyses, dust flux analyses, as well as numerous other methods of palaeoenvironmental analysis (Sections 2.4.1 to 2.4.5).

2.1 Introduction

Excavation of the cave sites in the Cradle of Humankind began in the late 1890s, when limestone miners discovered fossils in the caves and brought them to the attention of scientists (Berger & Tobias, 1994; Curnoe, 2010; Herries et al., 2010; Pickering & Kramers, 2010). Since then, the Cradle of Humankind has been the subject of numerous studies, including studies undertaken on the stratigraphy, sedimentology and lithostratigraphy of the caves (Butzer, 1976; Partridge, 1978, 1982, 2000; Clarke, 1994). These studies have resulted in the division of the cave deposits of Sterkfontein, Swartkrans and Kromdraai into numerous members based on the colour, grain size and calcium carbonate content of the sediments in the caves (Partridge, 1978, 1979, 1982).

The first adult *Australopithecus* specimen (TM1511) was discovered on 17 August 1936 at the Sterkfontein cave site by Robert Broom (Broom, 1936; Stratford, 2011; Clarke, 2013), who initially named it *A. transvaalensis* (Broom, 1936). This was changed to *A. plesianthropus* after the 1938 discovery of a juvenile sympheseal fragment (Broom, 1938). An extensive number of other *Australopithecus* fossil discoveries at Sterkfontein include large toothed males and smaller toothed females (Clarke, 2013; Tobias, 1973). Robinson (1954) grouped all these discoveries into the *A. africanus* species in 1954, and in 1972 he attempted to move them to the genus *Homo*, which was rejected. In 1947, Robert Broom discovered an almost complete *A. africanus* adult female, or possibly male skull, which was initially named *Plesianthropus transvaalensis* ('Mrs Ples'), which was later absorbed into *A. africanus* (Tobias & Hughes, 1977; Curnoe, 2010; Herries et al., 2010; Pickering & Kramers, 2010; Pickering et al., 2011). In 1948, Raymond Dart discovered hominin fossils at Makapansgat, which he named *Australopithecus prometheus*. Since then, numerous fossil discoveries have been attributed to this species, as well as to the *A. africanus* species (Tobias, 1973; Berger & Tobias, 1996; Clarke, 2013). Tobias and Hughes (1969) renewed excavations at Sterkfontein in 1966, and excavations have been continually maintained to date (Tobias, 1973). During this time, numerous other hominin fossils have been discovered at Sterkfontein, including a hominin cranium, a maxilla with teeth as well as loose teeth, all discovered in situ (Tobias, 1973). Ronald Clarke discovered a third almost complete *Australopithecus* skeleton in 1997 in the Sterkfontein caves (Clarke, 1998). This *Australopithecus* skeleton is the most complete hominin skeleton ever discovered. These hominin discoveries contributed to the overall study and characterization of the stratigraphic layers and palaeoenvironments with regard to hominins within the Cradle of Humankind, and particularly within the Sterkfontein Caves.

Excavations at Sterkfontein Caves have yielded enormous faunal assemblages and the only floral fossil remains yet found in the Cradle of Humankind (Bamford, 1999). The faunal remains have allowed for detailed stratigraphic analysis of the host deposits, as well as providing one of the earliest means of dating associated hominin fossil remains (Partridge, 1982; Vrba, 1982, 1995; Stratford, 2011). Fossil wood has been recovered from the Member 4 deposits in the Sterkfontein Caves (Bamford, 1999). Numerous stone tools have also been recovered from the Sterkfontein cave site, including stone tools from the Oldowan and Acheulean industries (Brain, 1958; Tobias, 1973; Stiles & Partridge, 1978; Clarke, 1985; Kuman, 1994a, b, 1996, 1998). Assemblages from the Earlier Stone Age, as well as from the Middle Stone Age have been recovered from Sterkfontein, and this has been interpreted to show that hominins regularly visited the Sterkfontein site for tool making purposes (Reynolds & Kibii, 2011).

2.2 Geology and Stratigraphy

2.2.1 General Geology and Stratigraphy

The caves of the Cradle of Humankind have formed within Late Archean age (2.5-2.6 Ga) Malmani Subgroup dolomite, deposited under epeiric conditions in the intracratonic Transvaal Basin (Button, 1973; Martini et al., 2003; Stratford, 2011) (Figure 2.1). The Malmani Subgroup, in which the caves have formed, has been divided into five formations (Oaktree, Monte Christo, Lyttelton, Eccles and Frisco Formations) (Eriksson & Truswell, 1974; Eriksson et al., 2006), based on the abundance of chert present in each sedimentary unit (Martini et al., 2003). The Sterkfontein Formation extends across the lithological boundary between the Oaktree Formation and Monte Christo formation (Martini et al., 2003; Stratford, 2011). The sedimentary infills of the cave have recorded landscape, environment, and hominin evolution over approximately 3 Ma (Partridge et al., 2003). Initial work on the sediments of the Cradle of Humankind lead to the interpretation that the sediments were deposited in a ‘layer- cake’ manner (Partridge, 1978), and comprised 6 sedimentary members (Members 1-6; M1-M6). All faunal and hominin assemblages are currently referred to by which member they were excavated from.

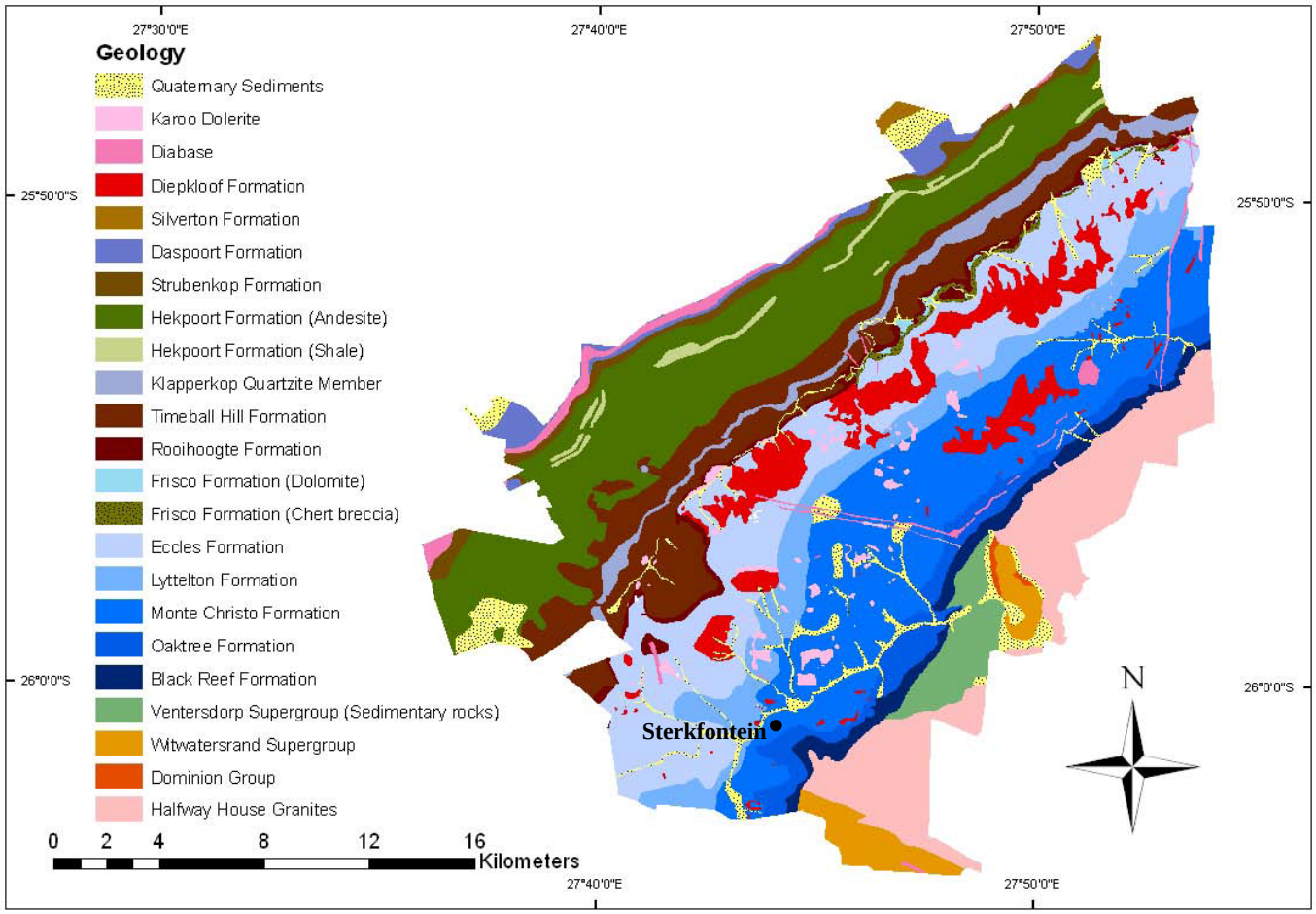

Fig. 2.1: Map showing the regional geology surrounding the Cradle of Humankind World Heritage Site, including the location of the Sterkfontein Caves site. Adapted from Obbes, 2000.

The basal unit of the Malmani Subgroup is the Oaktree Formation, which is 180m thick and is characterised by very chert-poor sediments. The Monte Christo Formation overlies the Oaktree Formation, and is a 700m thick chert-rich unit, with oolitic beds at the base of the formation. This formation also hosts the Lincoln and Fault caves. The Sterkfontein Formation straddles the boundary between these two formations (Martini et al., 2003; Stratford, 2011). The strata here have a dip of about 30° north-west. A long, subvertical, silicified fault exists in the cave system, trending North-South (Martini et al., 2003). Numerous dolerite dykes and sills have been identified in the area around the Sterkfontein Cave system, but none occur within the cave system itself. A dolerite sill occurs just below the cave system (Martini et al., 2003).

The Sterkfontein Cave System comprises an interconnected network of passages and channels which formed as a result of the dissolution of host rock material along joints and fractures, accompanied by ceiling collapse (Stratford, 2011) (Figure 2.2). These channels and passages amount to approximately 5.23km (Martini et al., 2003). Cooke (1938) conducted the first geological studies on the deposits at the Sterkfontein Cave System. Deposits at Sterkfontein

were initially characterised as a single, conformable breccia (Brain, 1958), and later interpreted as numerous distinct breccia bodies. Three disparate breccia bodies were initially recognized by Robinson (1962), namely a pink Lower Breccia, which hosts numerous *Australopithecus* fossils, a reddish-brown Middle Breccia, hosting stone tools, and a dark brown Upper Breccia, which is the youngest deposit of the three described. Robinson (1962) also proposed that the initial infill of material collapsed into deeper areas within the cave systems (Robinson, 1962; Martini et al., 2003). More recent studies have proposed a model of successive sequences of talus cone deposits, or the sedimentary infilling of separate caverns, in place of the model of layer cake deposition comprising six sedimentary units (Partridge, 2000; Reynolds & Kibii, 2011) (Figure 2.2).

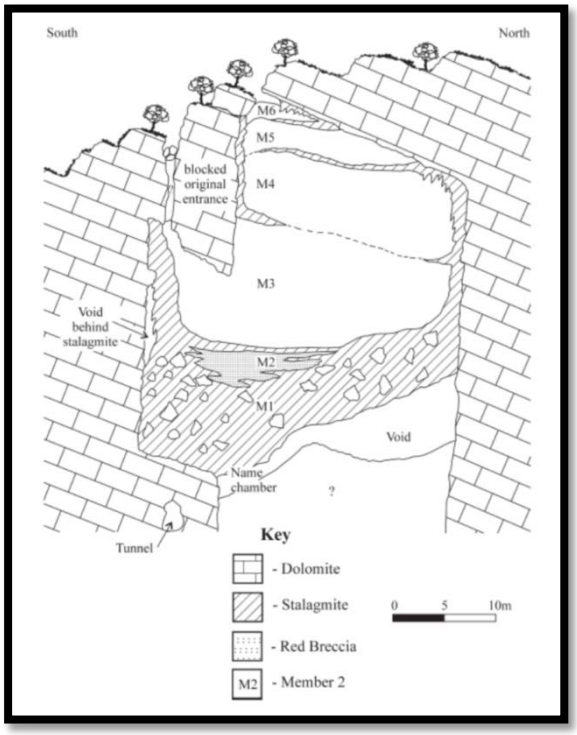

Fig. 2.2: North-south section of Sterkfontein showing the stratigraphy and relative locations of the 6 members From Clarke (2006).

Member 1 is a sterile deposit which formed while the cave entrances were closed or very small (Partridge, 2000; Martini et al., 2003; Reynolds & Kibii, 2011). It is exposed on the floor of the Silberberg Grotto, overlying a dolomitic floor and underlying Member 2 (Ogola, 2009; Reynolds & Kibii, 2011), and is also exposed as a hanging remnant in some of the younger chambers, such as the Name Chamber (Partridge, 2000; Martini et al., 2003; Reynolds & Kibii, 2011).

Member 2 is exposed within the Silberberg Grotto in the Sterkfontein Cave system. It unconformably overlies Member 1, and comprises two distinct sedimentary facies. Member 2 comprises silty sand, as well as fossiliferous breccias containing highly calcified sediments with variably sized chert and dolomite blocks (Martini et al., 2003; Reynolds & Kibii, 2011; Stratford, 2011). A flowstone layer separates Member 1 and Member 2 in some locations. Member 2 has also produced the most complete and oldest *Australopithecus* hominin skull (StW 573) in association with its skeleton (Ogola, 2009).

The Jacovec Cavern has been inferred to be contemporaneous with Member 2 deposits (Partridge et al., 2003), and hosts some of the deepest fossil-bearing deposits in the system, having yielded 11 *Australopithecus* specimens in addition to other non-hominid fauna (Wilkinson, 1983, 1985; Kibii, 2000; Reynolds & Kibii, 2011). The cavern comprises two different fossil-bearing breccia deposits (Reynolds & Kibii, 2011). The older Orange Breccia was deposited first, and following its deposition, collapsed onto the cavern floor. In situ remnants of the Orange Breccia can be found as hanging remnants in the cavern. (Partridge et al., 2003; Reynolds & Kibii, 2011). Following the collapse and erosion of the Orange Breccia, the Brown Breccia was deposited as a talus cone. Partial slumping and collapse of the Brown Breccia resulted in some mixing of the two deposits (Reynolds & Kibii, 2011).

Member 3 comprises the largest deposit within the Sterkfontein Cave System, and exhibits localized areas of fossiliferous material (Ogola, 2009). It comprises reddish-brown clayey, silty sand overlying a flowstone layer (Martini et al., 2003). Member 3 is exposed primarily in the Silberberg Grotto (Martini et al., 2003) (Figure 2.3).

Member 4 is a very large deposit located towards the eastern end of the exposed breccias at the surface of the Sterkfontein Cave system (Ogola, 2009; Pickering & Kramers, 2010) (Figure 2.3). Member 4 is subdivided into four stratigraphic beds, namely Bed A, B, C and D, which comprise a large amount of calcified sediments (Partridge, 1978). These beds are all exposed in the Type Site (the north-eastern part of Member 4) and in the Lower Cave within Sterkfontein Caves (Beds A, C and D) (Reynolds & Kibii, 2011). Bed B is also exposed in the lower levels of the ‘Extension Site’ (Ogola, 2009; Reynolds & Kibii, 2011). Both Beds B and C have yielded *Australopithecus* specimens and the Sts 5 specimen ‘Mrs Ples’ was recovered from Bed C (Partridge, 1978; Reynolds & Kibii, 2011). Member 4 has proven to be an important deposit with regard to the recovery of *Australopithecus* specimens (Kibii & Clarke, 2003; Kibii, 2004; Ogola, 2009; Kibii et al., 2011; Stratford, 2011), and has also yielded the only fossil wood from the cave site (Bamford, 1999). Recent studies have also suggested that

Member 3 deposits may in actual fact be distal deposits of Member 4 (Pickering & Kramers, 2010; Stratford, 2011). If confirmed, the volume of Member 4 deposits would be much larger than previously thought. It would also account for the great palaeoenvironmental variation currently observed in Member 4, as the deposit would have accumulated over a longer period of time (Reynolds & Kibii, 2011).

The Name Chamber comprises the Silberberg Grotto and the Milner Hall cavern, as well as numerous interconnecting passages, and lies directly beneath Member 5 (Clarke, 1994; Stratford et al., 2012).The Name Chamber comprises a large collapsed talus cone consisting of two allogenic deposits, namely the Eastern and Western Talus cones (Clarke, 1994; Reynolds, 2003; Reynolds & Kibii, 2011), as well as a central deposit which includes a mixture of Member 2 deposits hosting the StW 573 'Little Foot' fossils, Member 3 deposits, the *Australopithecus* bearing Member 4 deposits, Oldowan bearing Member 5 deposits and sediments from the western extremity of the Lincoln-Fault Cave System (Stratford, 2011; 2012). Member 1 deposits are also found here, as well as throughout the entire cave system (Clarke, 2006). Infilling encompasses three distinct phases, namely the Ancient Brecciated Deposit, followed by the Old Brecciated Deposit, and lastly the Younger Soft Deposit (Straford, 2011; Stratford et al., 2012).

The Member 5 deposit rests unconformably on Member 4 (Figure 2.3), and comprises three almost geologically uniform units of loam and rock debris (Martini et al., 2003; Stratford, 2011). The Member 5 deposits are exposed from the 'Extension Site' to the western end of the Type Site (Robinson, 1962; Partridge, 1978; Reynolds & Kibii, 2011; Stratford, 2011) (Figure 2.3). These three units include the StW 53, the Member 5 East deposit and the Member 5 West deposit (Kuman & Clarke, 2000; Ogola, 2009). These infill deposits are fossiliferous, and the Member 5 East infill deposit hosts one of the earliest records of Oldowan industry stone tool use in southern Africa (Reynolds & Kibii, 2011). Numerous *Paranthropus robustus* fossils have also been recovered from the Member 5 East infill deposit (Reynolds & Kibii, 2011; Stratford, 2011). The Member 5 West deposits contain stone tool artefacts from the Acheulean industry (Kuman, 1994a, b, 1998; Reynolds & Kibii, 2011; Stratford, 2011). The StW 53 infill deposit is also the host deposit in which the StW 53 cranium was discovered (Hughes & Tobias, 1977).

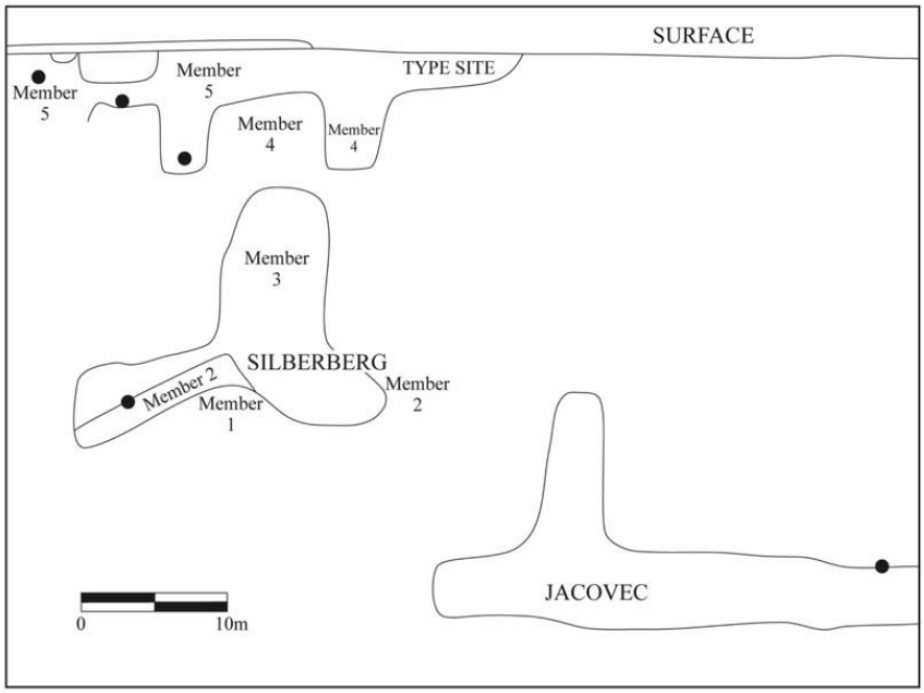

Fig. 2.3: Profile through a section of the Sterkfontein Caves site showing the relationships between members 4 and 5 exposed at the surface, and members 1, 2 and 3 exposed in the Silberberg Grotto and Jacovec Cavern. From Reynolds & Kibii, 2011, redrawn after Clarke, 2006.

Member 6 represents a relatively small, unexcavated hanging remnant of the original deposit overlying a flowstone layer capping the Member 5 West deposit (Robinson, 1962; Brain, 1981; Kuman & Clarke, 2000; Ogola, 2009; Reynolds & Kibii, 2011). Member 6 is interpreted to have filled in a small space between the dolomitic roof and the Member 5 breccias, prior to the erosion of a channel situated between Member 5 East and West, in the northern area (Ogola, 2009). Following this, the channel was infilled with the Post-Member 6 infill (Kuman & Clarke, 2000; Ogola, 2009).

The Post-Member 6 infill, or L/63 infill comprises the youngest breccia deposit exposed at the surface of the Sterkfontein Cave System excavations (Kuman & Clarke, 2000; Reynolds & Kibii, 2011). The Post-Member 6 infill also contains a rich assemblage of fossils, dating from the mid to late Pleistocene (Ogola, 2009).

The Lincoln-Fault Cave system is one of the longest cave systems in the Cradle of Humankind, measuring approximately 1 665 m (Reynolds, 2003). It is situated approximately 7 m from the northern-most excavations of the Sterkfontein Cave System, and comprises two fossiliferous deposits (Reynolds et al., 2007). These include a hard breccia deposit in the north (Lincoln Cave North Deposit), and a soft, poorly calcified breccia in the south (Lincoln Cave South Deposit), dating from the mid to late Pleistocene (Reynolds & Kibii, 2011; Reynolds, 2003).

These two deposits roughly correlate to the Post-Member 6 infill, and extend the limit of hominin and human occupation to less than 115 Ka (Reynolds et al., 2003, 2007; Reynolds & Kibii, 2011).

2.2.2 Dating of Cave Stratigraphy

The dating of the various features within cave systems of the Cradle of Humankind has proven to be difficult and contentious, due to the diverse range of dates which have been produced by numerous different methods. Dates produced from faunal and archaeological analysis also do not agree with dates produced from absolute dating methods. The complexity of karst deposits seems to be partly responsible for the contention surrounding dates produced from the Cradle of Humankind. Karst deposits result from varying processes at different temporal and spatial scales. This includes large-scale climatic scales down to individual catchment site conditions (Reynolds & Kibii, 2011). U-Pb and U-Th methods have recently been used to date flowstone layers interbedded between fossilifierous deposits, in order to obtain more reliable dates for the deposits in the Sterkfontein Cave system (Pickering & Kramers, 2010). Using these methods, absolute date ranges have been obtained for the fossiliferous deposits. Member 2 dates range between 2.8±0.28 Ma and 2.6±0.30 Ma. Member 4 produced dates between 2.65±0.30 Ma and 2.01±0.05 Ma (Pickering & Kramers, 2010). The date produced from the deposits located at the top of Member 4 (2.01±0.05 Ma) has constrained the last appearance of *Australopithecus africanus* to 2 Ma (Pickering & Kramers, 2010).

Flowstones located in the Silberberg Grotto and associated with the StW573 ‘Little Foot’ fossil have produced a U-Pb date of approximately 2.2 Ma (Pickering & Kramers, 2010; Granger et al., 2015; Kramers & Dirks, 2017; Stratford et al., 2017). U-Th dating of some deposits within the Sterkfontein Cave System has shown that there are substantial deposits younger than 400 Ka underlying older deposits. This shows that the stratigraphy within the cave system is more complex than a layer cake stratigraphy (Pickering & Kramers, 2010). Recent studies into techniques such as palaeomagnetic dating, cosmogenic nuclide dating and isotope decay may also yield more accurate results in the future, if a combination of these techniques is used (Partridge, 2005; Stratford, 2011). However, current individual use of these methods is fraught with complications (Berger et al., 2002). Recent research into TIMS U-Pb dating has also begun to yield some reliable dates (Walker et al., 2004).

2.2.3 Speleothems

Speleothems are calcium carbonate structures which include stalagmites, stalactites and flowstones, as shown in figure 2.4. These structures developed in the Sterkfontein Cave system when the cave environment changed from a phreatic to a vadose system (Stratford, 2011). Calcium carbonate precipitates from a $CaCO_3$ rich solution which filters through joints and fractures in the host dolomitic rock, forming speleothem structures (Stratford, 2011). Speleothems exposed to air movement may also form evaporite deposits in the form of 'popcorn' (Stratford, 2011) and aragonite crystals on cave walls. The amount of aragonite present in the speleothems also relates to the concentration of magnesium in the groundwater, which has played a part in the precipitation of the speleothems (Martini et al., 2003, Stratford, 2011).



Fig. 2.4: An example of speleothems in the form of flowstones and drip water from the Jacovec Cavern.

The presence of elements such as uranium within speleothem deposits has also allowed these structures (particularly flowstones) to be dated by U-series techniques (Edwards et al., 1987; Li et al., 1989; Dorale et al., 2004; Walker et al., 2006; Pickering et al., 2006; Pickering et al., 2010; Pickering & Kramers, 2010) Uranium series dating has proven to be useful in the dating of speleothem deposits, as the most accurate uranium series dating is produced from calcium carbonate bearing deposits such as speleothems, calcretes and biogenic carbonates (Schwarcz, 1992). Uranium bearing minerals generally follow numerous decay chains, involving a variety

of radioactive isotopes which ultimately ends up in the production of stable ^{206}Pb (Faure, 1986). Uranium series dating using the U-Th decay chain is possible for speleothem deposits due to the varying degrees of solubility of U and Th within groundwater. Uranium is more soluble in groundwater than thorium, and this results in a separation of the two elements when speleothem calcite deposits are precipitated from drip water (Schwarcz, 1989; Blackwell & Schwarcz, 1995). This results in speleothem deposits which contain radioactive uranium, but no thorium. If any thorium is detected within the speleothem deposit, it can be deduced that this thorium is a decay product from the uranium present in the speleothem deposit (Schwarcz & Latham, 1989). The ratio between $^{230}Th/^{234}U$ can then be used to produce ages for the sedimentary deposits surrounding the speleothems, as the thorium produced within the speleothem is a direct result of the radioactive decay of the *in situ* ^{234}U (Schwarcz, 1992; Blackwell & Schwarcz, 1995).

Dating of speleothems using this technique however has proven to be problematic, as many speleothems may precipitate, recrystallise, be removed and then precipitate into newly formed fractures or fissures (Bruxelles et al., 2014). Speleothems have also been extensively used to reconstruct palaeoenvironments for the cave deposits and water table levels (Wilkinson, 1973; Vaks et al., 2003; Fleitmann et al., 2004; McDermott, 2004; Tan et al., 2006; Kluge et al., 2008), as well as for recording the relative timing of deposition of sediments in the cave system.

2.2.4 Cave Formation

The formation of fossil-bearing cave deposits in the Cradle of Humankind is described as a 6-stage process by Brain (1958, 1981). During stage one, ground water in the phreatic zone forms a cavity in the dolomitic host rocks by dissolution of the rock along structurally weak zones such as fractures. During stage two, the water table begins to drop due to river incision, surface erosion or climatic changes, allowing the cavity created in stage one to enlarge, and gradually become filled with air. During stage three, speleothems and avens start to form in the dolomitic roof above the cavern. This cavern eventually opens up to the surface to form a cave. During stage four, the newly formed cave is progressively filled with sediments, bones and rock debris, which accumulate to form a talus cone. During stage five, this talus cone becomes increasingly calcified due to calcium carbonate rich solutions dripping from the roof onto the talus cone, and eventually forms a breccia. During stage six, the roof of the cave is eroded away and the breccias are exposed to surface weathering (Brain, 1981).

There are numerous complications regarding the deposition of sediments in caves. Stratigraphic analyses as well as interpretations regarding the associations and contexts of fossils and artefacts may become difficult and even misleading. This is due to the variability in the structure, history and properties of the sedimentary deposits (Stratford, 2011). A lack of understanding regarding the processes which produce the deposition of sediments, as well as post-depositional processes affecting the deposit has led to misinterpretations of fossil deposits (Stratford, 2011). The factors which contribute to stratigraphic complexities may be divided into two sections. These sections include deposit formation factors, and deposit interpretation factors (Stratford, 2011). Factors in the formation of the deposit contributing to stratigraphic complexities include primary sedimentation of the deposit, secondary sedimentation or re-working, and transport of sediments (Stratford, 2011). Deposit interpretation factors contributing to stratigraphic complexities include inadequate sampling, unrecognized stratigraphic boundaries and unrecognized depositional indicators (Stratford, 2011).

2.3 Palaeoclimate and Human Evolution

Over the past 100 million years, the Earth's climate has undergone dramatic variations, swinging from 'greenhouse' conditions during the mid-Cretaceous, to 'ice house' conditions in the Late Cenozoic (Lear et al., 2000; Shackleton & Kennett, 1975; Miller et al., 1987). The long-term cooling trend exhibited, owing to the transition from greenhouse to icehouse conditions resulted from numerous factors. These include variations in atmospheric greenhouse gases, particularly CO_2, variations in the Earth's albedo, and variations in ocean-atmospheric circulation (Lear et al., 2000). Current Cenozoic paleoclimate records used to reconstruct these climatic conditions have been obtained primarily from deep sea marine core records, and marine sedimentation, as well as foraminifera (Elderfield & Ganssen, 2000; Lear et al., 2000; Kos, 2001). These have been used to reconstruct global temperatures during the Cenozoic (Chappell & Shackleton, 1986; Richards & Dorale, 2004; Bobe, 2006). Continental sedimentation is discontinuous with regard to vertical and lateral extents, as opposed to marine sedimentation which is relatively continuous, suggesting that marine sedimentation records would be better for palaeoclimate analysis (Bobe, 2006).

2.3.1 Cenozoic Palaeoclimate and Human Evolution in Africa

The climate of the early Eocene (at around 50 Ma) was characterised by warm temperatures and warm ocean waters, which provided large amounts of moisture to the atmosphere, resulting in high precipitation (Zachos et al., 2001). This was succeeded by an increasingly arid climate

in Africa, with decreasing marine temperatures and precipitation (Lear et al., 2000; Zachos et al., 2001). The Eocene-Oligocene boundary (approximately 33.7 Ma) is characterised by a dramatic decrease in marine temperatures, which is attributed to the build-up of Antarctic ice (Lear et al., 2000; Zachos et al., 2001; Coxall et al., 2005; Bobe, 2006). The early Miocene experienced a warming trend from 18 Ma to 14 Ma, followed by another period of global cooling (Vrba, 1985; Lear et al., 2000; Zachos et al., 2001; Bobe, 2006). The Late Miocene is characterised by greater rainfall seasonality, and more open environments (Street, 1981; Traverse, 1982, 1988; Laporte & Zihlman, 1983; Vrba, 1985; Wolfe, 1985; Lear et al., 2000; Zachos et al., 2001; Wynn, 2004; Bobe, 2006; Magill et al., 2013; Tipple, 2013). C_4 vegetation also spread during this period, evident from the analysis of carbonate palaeosols and dental enamel (Morley & Richards, 1993; Morgan et al., 1994; Cerling et al., 1997; Wynn, 2004; Bobe & Behrensmeyer, 2004; Bobe, 2006). This cooling trend in the late Miocene has been tentatively attributed to the expansion of the Antarctic ice sheet (Woodruff et al., 1981; van Zinderen Bakker & Mercer, 1986; Zachos et al., 2001; Bobe, 2006). It has also been linked to the closing of the Indonesian Seaway, affecting the Indian Ocean sea surface temperatures and, as a result, precipitation within Africa at the time (Cane & Molnar, 2001; Bobe, 2006). A tentative link has also been made between this cooling and aridification trend in Africa, and the closing of the Panama isthmus and the effects thereof on Atlantic Ocean circulation (Haug & Tiedemann, 1998; Haug et al., 2001; Bobe, 2006). Alternatively, Trauth et al. (2009) attributed these climate variations to variations in low-latitude solar heating, rather than that of high latitude ice volume variations.

A reversal in this cooling trend occurred during the early Pliocene (Lear et al., 2000), with temperatures, documented by marine oxygen isotopes, being the warmest during the last 5 million years (Wara et al., 2005). Temperatures began to cool again after 3.5 Ma (Bobe, 2006). The marine climate record has shown that the period preceding 2.8 Ma exhibited variations in the African climate at periodicities of 19 000 and 23 000 years, reflecting African monsoonal variability resulting from low latitude precessional forcing of the monsoonal climate (de Menocal, 1995; de Menocal, 2004; Tipple, 2013). Increases in climate variability, and particularly in aridity, during the Plio-Pleistocene occurred in a step-like fashion near 2.8 Ma, 1.7 Ma and 1.0 Ma (Tiedemann et al., 1994; de Menocal, 1995; Clemens et al., 1996; de Menocal, 2004; Bobe, 2006; Reynolds & Kibii, 2011). This step-like increase in climate variability and aridity has been attributed to orbital eccentricity variations of the earth, and coincides with the onset and intensification of glacial cycles at the polar regions (Ruddiman &

Janecek, 1989; Clemens & Prell, 1991; Tiedemann et al., 1994; de Menocal, 1995; Shackleton, 1995; Clemens et al., 1996; Clarke et al., 1999; Zachos et al., 2001; de Menocal, 2004; Fernandez & Vrba, 2006; Tipple, 2013). The period postdating 2.8 Ma has shown climate variations at periodicities of 41 000 years. Climate variations changed again during the 1.2 Ma middle Pleistocene transition, and continued after 1.0 Ma to 100 000 year periodicities (Clarke et al., 1999; de Menocal, 2004; Bobe, 2006). These intervals coincide with the development of more arid and open environments and an increase in rainfall seasonality, as well as with key stages of early hominin evolution (de Menocal, 2004). Palaeoclimate analysis has also shown that more arid conditions persisted in east, central and west Africa, when Atlantic sea surface temperatures were cooler during the Pleistocene transition (de Menocal, 1995). During this period, savannah and desert environments also spread throughout northern (Dupont & Leroy, 1995) and southern Africa (Vrba, 1974, 1975; de Menocal, 1995; de Menocal & Bloemendal, 1995; Potts, 1998; Avery, 2001). In general, variations in African climate during this period can be described as cycles of wet and dry conditions, with a longer shift towards aridity with step-like shifts in the earth's periodicity and amplitude (Burckle, 1995; Dupont & Leroy, 1995; de Menocal, 2004; Fernandez & Vrba, 2006; Reynolds & Kibii, 2011).

These climate variations after 2.8 Ma coincide with variations in the onset and intensification of high-latitude ice sheets and the cooling of the sub polar oceans (Shackleton et al., 1990; Raymo et al., 1990; Shackleton, 1995; Fernandez & Vrba, 2006), and support Milankovitch theory of glaciations driven by orbital variations (Clarke et al., 1999). These large scale shifts in global climate are responsible for changing the ecology of landscapes, which in turn leads to faunal adaptation and speciation pressures. This precipitates genetic selection and innovation of fauna, including hominins (de Menocal, 2004). In general, it has been proposed that climatic changes during the last 7 Ma have resulted in hominin speciation pressures, increases in hominin cranial capacities, the shift to bipedality in hominins, adaptations regarding behaviour, cultural innovations as well as wide spread geographic dispersal of hominins (Cohen et al., 2009). The Savannah Hypothesis, which explains the evolution of hominins as a result of the step-like intervals of cooler, more open and arid environments, proposes that this presence of bipedality and larger brain sizes were a result of hominins residing in an open savannah environment (Dart, 1925; Vrba, 1988; de Menocal, 1995; Bobe et al., 2002; de Menocal, 2004; Behrensmeyer, 2006). These intervals of increased aridity also coincide with bursts of biotic change, as described by Vrba's (1985) turnover pulse hypothesis.

In addition, understanding the palaeoenvironments in which hominins existed can provide evidence for early hominin ecology, which includes predator-prey relationships, diet and locomotive adaptations as well as speciation and extinction events (Hopley & Maslin, 2010).

2.3.2 Faunal and Floral Evolution in Africa during the Cenozoic

During the late Mesozoic to early Cenozoic, the global climate was warm, providing excellent conditions for the propagation of woody vegetation and closed environments in eastern and southern Africa (Bobe, 2006; Magill et al., 2013). A period of extinction of large herbivorous mammals towards the end of the Mesozoic allowed woody vegetation to flourish without the threat of large herbivores consuming the young vegetation and opening forests by uprooting trees (Bobe, 2006; Magill et al., 2013). African environments were dominated by lush moist forests boasting C_3 vegetation (Bobe, 2006; Magill et al., 2013; Tipple, 2013) that characterised the more coastal adjacent moisture-rich areas of the continent. Some of the more central, water stressed areas were characterised by savannahs, boasting acacia vegetation (Bobe, 2006; Magill et al., 2013). This demonstrates the heterogeneity of environments produced in Africa due to climatic variations on different areas in the continent.

In conjunction with the changing climatic and environmental conditions in the African continent during the Miocene, Pliocene and Pleistocene, there was an increase in the diversity of megafauna, particularly in large herbivorous mammals, which peaked during the Pliocene, as well as an increase in C_4 vegetation approximately 5 Ma-8 Ma (de Menocal & Bloemendal, 1995; Hill, 1995; Cerling, 1997; Kingston et al., 2007). This increase in C_4 vegetation is thought to have resulted from atmospheric CO_2 falling below the critical threshold for C_3 photosynthesis (Cerling, 1997), and has also been attributed to climatic variations and glacial-interglacial cycles (Cerling, 1997). Fauna during the Pliocene in general underwent an increase in seasonality, developing a more savannah-mosaic character (Cerling, 1997). This diversification went hand in hand with the aridification trend, as the megafauna created and maintained more open environments characteristic of arid climates. In particular, bovids are seen to increase in abundance during specific stages, namely in the Late Miocene after 6 Ma, in the Late Pliocene after 3 Ma and in the Plio-Pleistocene after 2 Ma.

The increase in bovids and other fauna at 6.5 Ma has been attributed to the spread of C_4 vegetation during this period, as well as tentatively being related to the Messinian Salinity crisis occurring during this time period in the Mediterranean (Cerling et al., 1997; de Menocal,

2004). The second increase in bovid populations after 3 Ma may be related to changing climate variations occurring at around 2.8 Ma (Bobe & Eck, 2001; Bobe et al., 2002; Bobe & Behrensmeyer, 2004; de Menocal, 2004; Bobe, 2006). The third shift in bovid populations after 2 Ma may be related to the more modern development of grassland environments in Africa at the time (Bobe & Behrensmeyer, 2004; de Menocal, 2004). In general, fauna occupied more open and arid environments from 2.9 Ma to 2.4 Ma, and again after 1.8 Ma (Bonnefille, 1995; Reed, 1996; de Menocal, 2004; Behrensmeyer, 2006; Fernandez & Vrba, 2006). Flora was C_3 dominated, with C_4 components on the increase from 4 Ma to 1.8 Ma, with C_4 vegetation dominating after 1.8 Ma (Bobe & Behrensmeyer, 2004; Cerling, 1992; Reed, 1996). In general, faunal evidence from this time period has also suggested that not all environments evolved due to climatic changes in a homogenous way, accounting for the diversity of fauna and flora across the continent (de Menocal, 2004).

Stable carbon isotope measurements from the Plio-Pleistocene palaeosols of the Turkana Basin in Kenya, as well as palaeoprecipitation estimates, have yielded a high resolution record of the aridification trend in Africa during the last 4.3 Ma (Wynn, 2004). These isotope measurements have also provided a record of increasing C_4 biomass during this period (Wynn, 2004). Carbon isotope data derived from deep sea cores has also provided valuable information on the nature of the global carbon cycle, as well as on changes in deep-sea circulation patterns. These changes might have either triggered, or resulted from climatic changes (Zachos et al., 2011).

2.3.3 Cenozoic Palaeoclimate Record of the Cradle of Humankind

Palaeoenvironmental analysis of the Cradle of Humankind has shown that during the Plio-Pleistocene from 4 Ma to about 2 Ma more open, arid environments spread, while closed, forested environments decreased (Vrba, 1985, 1988; Reynolds & Kibii, 2011). The border between moist and arid savannah environmental conditions lay close to the Cradle of Humankind, alongside the arid grassland savannah ecotone (Vrba, 1982; Cadman & Rayner, 1989; Avery, 2001). Faunal, floral and isotopic studies conducted within the Cradle of Humankind have revealed that a mosaic environment existed in the area during the early to middle Pleistocene. This mosaic environment included patches of open grasslands and woodlands hosting C_3 and C_4 vegetation, as well as forested areas (Reed, 1996; Sponheimer & Lee-Thorp, 2003; Reynolds, 2007; Reynolds & Kibii, 2011). Analysis of the Member 4 deposits in the Sterkfontein cave site has also revealed that a mosaic environment existed during the deposition of these sediments (Kibii, 2004; Reynolds & Kibii, 2011). Habitat reconstructions of the Cradle of Humankind indicate that the area was characterised by a

medium density forest interspersed with an open savannah environment (Vrba, 1985, 1988; Benefit & McCrossin, 1990; Mckee, 1991; Clarke & Tobias, 1995; Berger & Tobias, 1996; Reed, 1996; Potts, 1998; Reynolds & Kibii, 2011). The mean annual precipitation varied between 310 mm and 550 mm, with a summer aridity index of 3.8-4.1. Palaeoclimate analysis has shown that atmospheric temperatures would have been higher than today, but with a smaller temperature range (Avery, 2001).

Flowstone and breccia successions in the Cradle of Humankind, as well as U-series dates and stable light isotope data provide a 600 Ka record of climate variations in the area. These factors suggest that climate variations in the area can be attributed to a strong allocyclic control, which is a result of changes in atmospheric circulation (Ayliffe et al., 1998; Potts, 1998; Holmgren et al., 2003). Palaeoenvironmental analysis of the Cradle of Humankind shows that in general glacial periods were drier, with wetter interglacial periods. However, cooler temperatures during glacial periods also implies increased evaporation and increased precipitation (Pickering, 2007). The Cradle of Humankind experienced cycles of warm, wet recovery periods following glacials, which are characterised by the growth of C_3 vegetation. Less seasonal precipitation, as well as higher atmospheric temperatures, and more arid conditions attributed to interglacial periods which are dominated by C_4 vegetation (Vogel, 1993; Lourens et al., 1996). These climate variations can be attributed to orbital forcing, with precessional changes in solar output controlling climate variations in the area, as well as glacial-interglacial cycles. Thus, these above-mentioned cycles cannot alone account for the complex climate variations in the Cradle of Humankind (Partridge, 2002; Pickering, 2007). After around 60 Ka, these precessional forces decreased and atmospheric variations over Antarctica dominated variations in African climate (Partridge et al., 1997, 2004; de Menocal, 2004).

The Cradle of Humankind has varied considerably in its appearance over the last 4 million years, due to numerous physical factors modifying the landscape. These factors include river incision and erosion, which degraded older African planation surfaces, and valley widening associated with incision, which accommodated denuded sediments (Dirks & Berger, 2010). The denudation of cover rocks resulted in the exposure of dolomitic rocks hosting the caves (Partridge, 1973; Dirks & Berger, 2010). Tectonic factors which influenced the evolution of the Cradle of Humankind landscape include complex interactions between numerous small fractures and joints controlled by uplift (Dirks & Berger, 2010). A link has been tentatively established between the uplift of the African plateau, and the climate and landscape variations. These climate and landscape variations include the aridification trend since the Miocene and

the development of extensive grasslands (Bobe & Behrensmeyer, 2004; Feakins et al., 2005; Dirks & Berger, 2010). The uplift of the southern African plateau resulted in the creation of the southern African 'highveld', with a characteristic climate of cool winters, summer storms and grassland environments. This shows that the development of the palaeoenvironment and palaeoclimate of the Cradle of Humankind are controlled by global climate change patterns, as well as the tectonic uplift of the southern African plateau. The caves of the Cradle of Humankind opened after the African erosion surface had degraded and lowered by incision. Tectonically active landscapes have also been responsible for rejuvenating the landscape at regular intervals and countering some of the negative effects of climate change (Dirks & Berger, 2010).

A modern analogue of the palaeoenvironment present at the Sterkfontein Cave Site during the Plio-Pleistocene can be found 200 km west and southwest of the Cradle of Humankind, with an altitude 250 m lower than today (Dirks & Berger, 2010). All three of the above mentioned vegetation types, namely forested areas, grasslands and woodlands, interweave in the area South of Mafikeng (Avery, 2001; Dirks & Berger, 2010). However rainfall in this area is higher than the precipitation expected from the palaeoenvironmental analysis of the Cradle of Humankind (Dirks & Berger, 2010). The areas near Kuruman and Kimberley exhibit a similar climate to the palaeoclimate deduced for the Sterkfontein Valley, where arid savannah vegetation merges with grassland vegetation (Avery, 2001).

Palaeoclimate analyses conducted in southern Africa have also contributed to the reconstruction of regional and local palaeoclimate. Carbon and oxygen stable light isotope data obtained from stalagmites in the Makapansgat Valley at a high resolution have resulted in the documentation of local climate variations in southern Africa (Holmgren et al., 2003). Uranium dating of this stalagmite indicated that growth of the stalagmite occurred between the Late Pleistocene and Holocene, from 24.4-12.7 Ka and 10.2-0 Ka, with a halt in growth occurring for 2.5 Ka (Holmgren et al., 2003). Carbon and oxygen stable light isotope data from this stalagmite indicated that a period of post-glacial warming occurred at around 17 Ka, which was interrupted by a period of cooling, flowed by a period of warming after 13.5 Ka (Holmgren et al., 2003). Warm conditions were documented during the Early Holocene, followed again by warm conditions from 2.5 Ka to 1.5 Ka (Holmgren et al., 2003) (Figure 2.5).

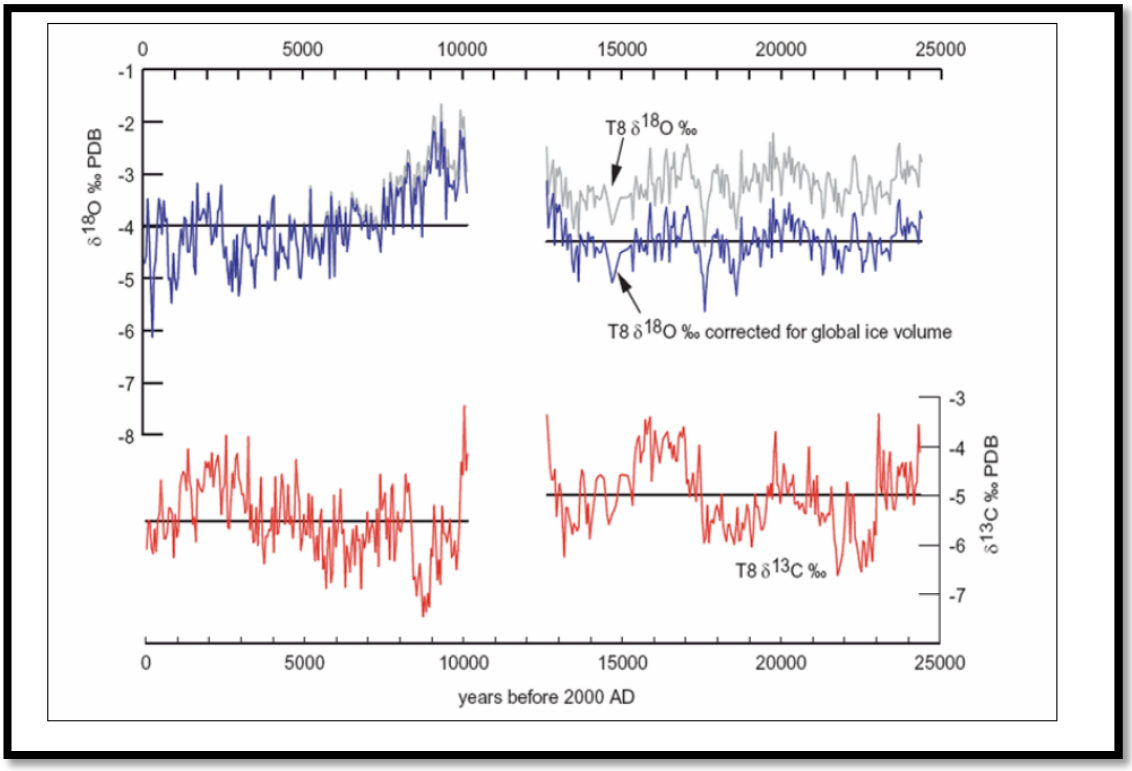

Fig. 2.5: Oxygen and carbon isotope date in blue and red respectively from the T8 speleothem from the Makapansgat site (Holmgren et al., 2003).

A speleothem deposit from the Cango Caves in the Western Cape has provided a record of climate change for a greater part of the last 30 Ka, as depicted by figure 2.6. $\delta^{18}O$ records from the speleothem has provided data on local temperature changes by using the isotopes present in the confined groundwater of the Uitenhage aquifer, which is of a similar age (Talma & Vogel, 1992). These temperature data indicate that temperatures were approximately 6°C lower during the last glacial maximum compared to today (Figure 2.6) (Talma & Vogel, 1992). Changing vegetation patterns were also documented using the $\delta^{13}C$ values from the speleothem as shown in the third graph in figure 1.3, showing that the period from 47 Ka to 13 Ka was dominated more by woodlands, with increasing grassland encroachment (Talma & Vogel, 1992).

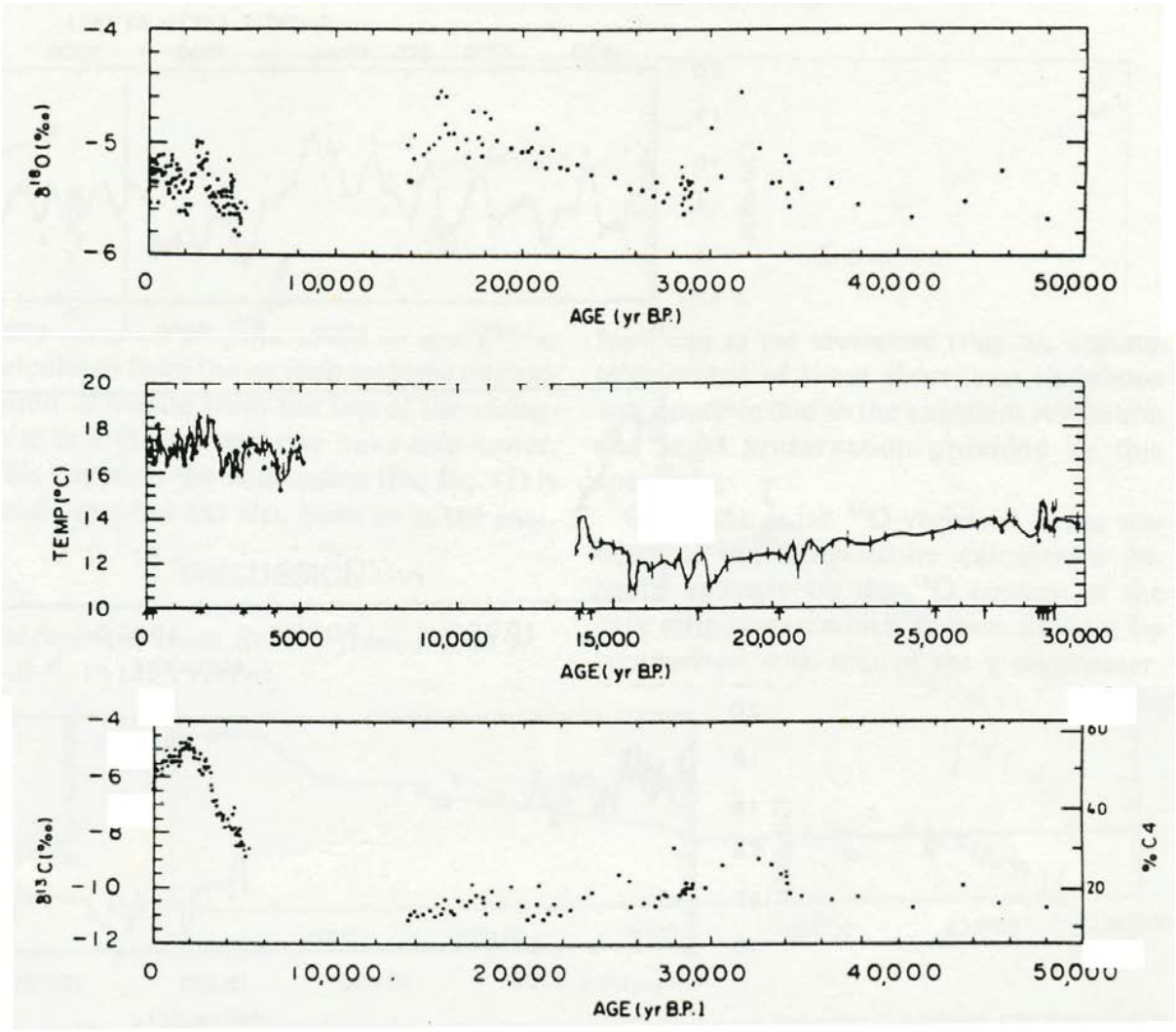

Fig. 2.6: stable oxygen isotope variations and associated palaeotemperature variations, and stable carbon isotope variations associated with $\%C_4$ vegetation. (Talma & Vogel, 1992).

Palaeoclimate reconstructions have also been created using sediments and stratigraphic sequences, along with facies analysis of those sequences. Facies analysis allows for palaeoenvironmental reconstructions by providing information about depositional environments (Boggs, 2001). These depositional environments are controlled by tectonics, sea level change and climate variations (Boggs, 2001). Kos (2001) used this approach, and related cycles of erosion and deposition of sediments within cave systems during the last interglacial period to groundwater variations, which relates to surface environmental conditions. Brain (1995) used the sedimentation sequence of the Member 5 deposit from Swartkrans to model variations in climate which controlled the sedimentation of this deposit (Brain, 1995). It has also been suggested that the degree of calcification in clastic sedimentary layers may distinguish climate changes. Layers exhibiting no calcification have been proposed to correlate to arid periods, or moist periods characterised by very fast sedimentation (Moriarty

et al., 2000). Clastic layers interbedded with flowstone layers and well-calcified sediments would provide evidence for a wetter climate (Moriarty et al., 2000).

Pollen analysis has been conducted on the Wonderkrater spring sediments in the Limpopo Province of South Africa, and has provided valuable information on environmental changes within the savannah biome during the late Quaternary (Scott et al., 2003). The data obtained from the pollen samples has produced temperature and moisture patterns for the last 20 Ka, and has documented colder conditions at around 17 Ka, with warmer conditions occurring at around 13 Ka (Scott et al., 2003). These temperature and moisture data can be compared to the temperature and precipitation data produced for the same period from stable oxygen isotope analysis of speleothems.

Carbon and oxygen isotope analysis of the Tswaing Crater Lake sediments indicates that carbonate precipitation took place under arid to semi-arid conditions, where evaporative conditions dominated (Horstmann & Bühman, 1999). A study combining the change in the soil sediment texture of vertical facies and an age-depth model for the lake sediments resulted in a record of rainfall for the last 200 Ka (Partridge et al., 1997). This rainfall record reflects the presence of nine cycles of orbital precession, and the presence of the main periodicity at 23 Ka (Partridge et al., 1997) (Figure 2.7).

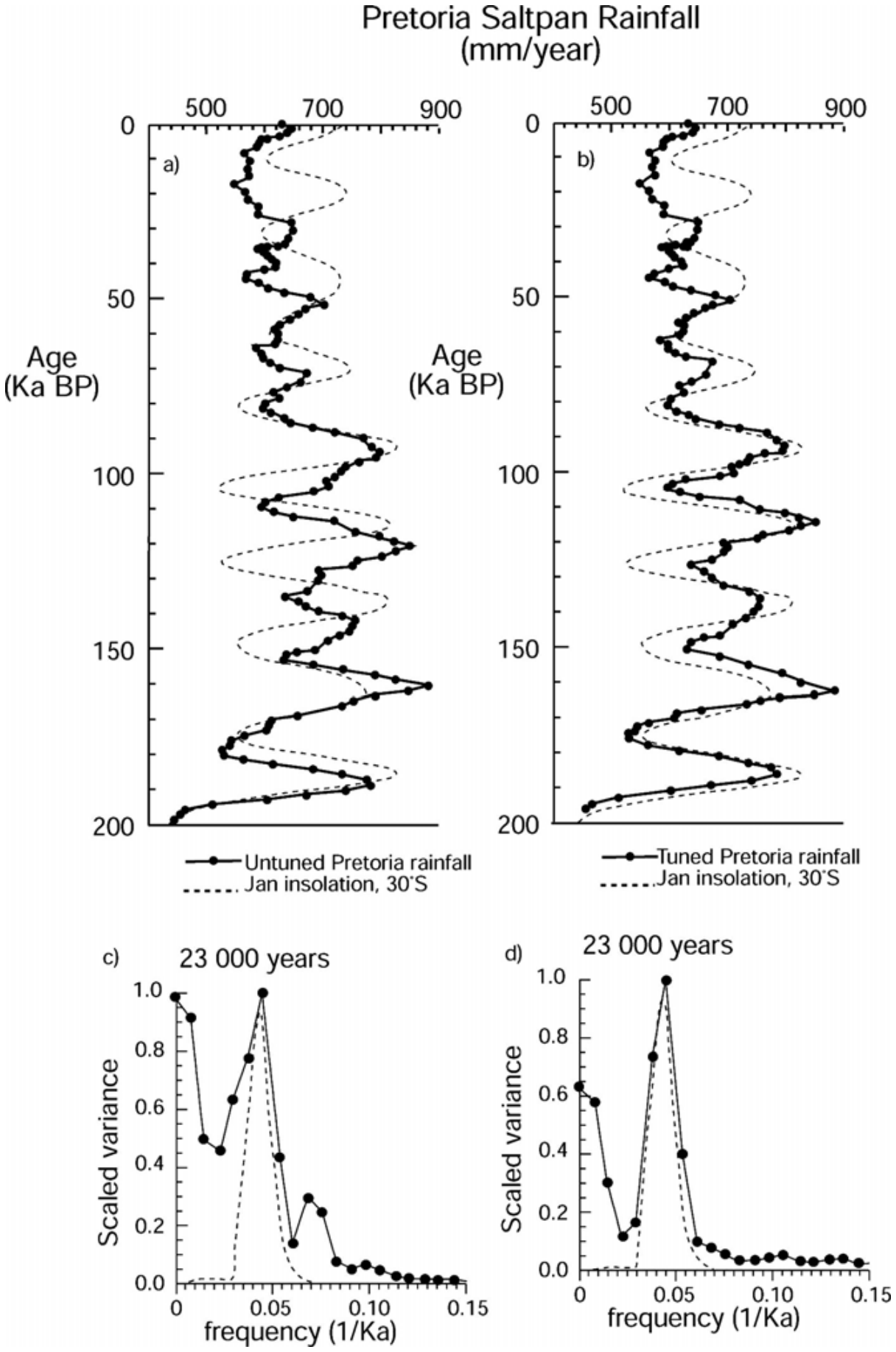

Fig. 2.7: Rainfall records from the Tswaing Impact Crater site (top), with related 23 Ka cyclicity frequency histograms (bottom) (Partridge et al., 1997).

2.3.4 Hominin Evolution with regard to Palaeoenvironments

Environmental hypotheses of African faunal evolution are generally 'habitat specific' hypotheses, as faunal adaptations are analysed in a specific environment (Potts, 1998, 2007). This environment is most commonly the grassland-savannah environment, which first occurred in Africa after the late Miocene (Cerling, 1992, 1997; de Menocal, 2004). Another hypothesis has also been used in faunal analysis of African environments, namely the 'variability selection' hypothesis (Potts, 1996, 1998). This hypothesis includes African palaeoclimatic variability patterns recorded from deep sea sediments and the importance thereof as a mechanism for natural selection (de Menocal, 2004). These hypotheses have also been applied to hominin evolution.

A habitat specific account of hominin evolution resulted in the development of the savannah hypothesis. Current interpretations of this hypothesis state that evolution of African fauna, including hominins, was attributed to the development of cooler, more arid and open environments in a step-like manner since the late Miocene (de Menocal, 2004; Bobe & Behrensmeyer, 2004). The shift to more arid conditions during the mid-Pliocene (3.2-2.6 Ma) is said to have particularly favoured the evolution of fauna adapted to more arid environments. This period has also been said to have influenced early hominin evolution and behaviour significantly (Vrba, 1988; de Menocal, 1995, 2004; Bobe et al., 2002). A variant of the savannah hypothesis was developed by Elisabeth Vrba (1980, 1985, 1988, 1995) based on the first and last appearance data for bovids, namely the turnover pulse hypothesis (McKee, 2001; de Menocal, 2004; Bobe & Behrensmeyer, 2004). This hypothesis suggested that 'bursts of biotic change', or turnover, were initiated by significant variations in the African climate occurring near 2.8 Ma, 1.8 Ma and 1.0 Ma (Vrba, 1988; de Menocal, 1995, 2004; Clemens et al., 1996). An alternate hypothesis based on fossil pollen records from 3.3 Ma to 3.0 Ma, the forest hypothesis, was developed by Rayner and others (1993). This hypothesis suggests that closed vegetation, such as forests and woodlands, constituted the environment in which early bipeds adapted and evolved (Rayner et al., 1993). A third hypothesis was proposed by Blumenschine (1987), which suggests that tool-making hominins evolved in grassland-woodland mosaic environments (Reed, 1996; de Menocal, 2004; Bobe & Behrensmeyer, 2004).

Three hypotheses have also been proposed to account for trends observed in the hominin fossil-bearing members of the Sterkfontein Formation. The first hypothesis is the Climate Change Hypothesis, which suggests that the observed evolutionary trends are a result of global and

local cooling and aridification (McKee, 1991). This hypothesis also proposes that a savannah-grasslands environment replaced an earlier environment comprising denser, more wooded vegetation (McKee, 1991). The second hypothesis is the Taphonomy Hypothesis, which explains changes in the representation of relative species with regard to bone accumulating agents (McKee, 2001). The third hypothesis is the Species Interaction Hypothesis, which is a variation of the Red Queen Hypothesis (see van Valen, 1973). This hypothesis suggests that the dynamics of species interactions, which includes competition and commensalism, was responsible for evolutionary changes and extinctions (McKee, 1991).

These hypotheses in general have proposed that climatic changes during the last 7 Ma have resulted in hominin speciation pressures, rapid increases in hominin cranial capacities, the shift to bipedality in hominins, hominin adaptations regarding behaviour, cultural innovations as well as wide spread geographic dispersal of hominins (Cohen et al., 2009).

Understanding the palaeoenvironments in which hominins existed can provide evidence for early hominin ecology, which includes predator-prey relationships, diet and locomotive adaptations as well as speciation and extinction events (Hopley & Maslin, 2010).

2.3.5 Speleothem Analysis

Speleothems, which include stalagmites, stalactites and flowstones, are regarded as informational archives of terrestrial palaeoclimates (Cruz et al., 2006; Pickering & Kramers, 2010). They provide information about past climates, vegetation, hydrology, sea-levels, water-rock interactions, landscape evolution and tectonics, as they form in very specific conditions (Richards & Dorale, 2003; Pickering, 2007). In recent years, speleothem research and analysis has contributed to numerous palaeoclimate and palaeoenvironmental records during the Plio-Pleistocene (Cruz et al., 2006). They may be useful archives of palaeoclimate information, as they occur in numerous locations worldwide, they may be sampled at high resolutions, and may be reliably dated using U-Pb dating techniques (Richards & Dorale, 2003). They also allow for the construction of long duration (103-104 Ka) records (Fleitmann et al., 2004). Accurate dating of speleothems allows these deposits to be compared to independent records from the terrestrial environment, oceans and cryosphere, so that the pattern of speleothem growth in response to different climatic forcing events may be investigated (Richards & Dorale, 2003).

There are numerous palaeoclimate proxies which are used when analysing speleothems for palaeoclimate reconstructions. The presence or absence of speleothems may act as a proxy for

palaeoclimate analysis, as the deposition of speleothems depends on a range of sufficient water supply and soil carbon dioxide to enable the dissolution and transport of the reactants responsible for the formation of the deposits (Richards & Dorale, 2003). The growth of speleothem deposits may also provide insight into changes in the vadose water chemistry, flooding events, aridity, permafrost conditions and shifts in flow routing (Richards & Dorale, 2003).

Other proxies include growth intervals within speleothem deposits, which are identified by U-Pb dating, and are used to identify wetter versus drier or warmer versus colder climatic intervals (Ayliffe et al., 1998; Spotl et al., 2005; Cruz et al., 2006). Alternating layers of calcite and aragonite present within the speleothem deposits may also be used as a proxy for climate change, as the alternating layers represent different depositional environments controlled by climate oscillations (Melis et al., 2013).

Oxygen isotope ratios obtained from speleothems constitute another palaeoclimate proxy, and are used to interpret variations in temperatures and precipitation properties within cave environments (McDermott, 2004; Cruz et al., 2006) (Figure 2.8). Carbon isotope ratios are also used as palaeoclimate proxies, and are used to interpret changes in the overlying vegetation (C_3 versus C_4 vegetation) and vegetation density (Dorale et al., 1998; Baldini et al., 2008) (Figure 2.8). Carbon isotope ratios are controlled by biogenic carbon dioxide supply from surrounding soils, which is in turn controlled by secondary rainfall and temperature (Cruz et al., 2006). The contribution of carbon isotopes to the speleothem deposit depends on mechanisms controlling bedrock dissolution and carbonate precipitation within the cave system (Cruz et al., 2006).

Annual laminae thickness may be used as another palaeoclimate proxy with regard to speleothem analysis, and this is used as a proxy for the amount of precipitation accompanying the formation of the speleothem deposits, as well as the mean annual temperature (Polyak & Asmerom, 2001; Tan et al., 2003; Fleitmann et al., 2004; Cruz et al., 2006). Trace elements are also used as a proxy, and provide information on the precipitation, vegetation and growth rate, and may also provide seasonal information (Fleitmann et al., 2004; Cruz et al., 2006).

Additional palaeoclimate proxies used when analysing speleothems include deuterium concentrations in speleothem fluid inclusions (Fleitmann et al., 2003), pollen and lipid biomarkers (Cruz et al., 2006; Blythe et al., 2007). Sulphur concentrations, as well as the concentrations of its isotopes have also been used to provide information on atmospheric

sources and palaeo-pH (Wynn et al., 2008), and noble gases have been used as indicators of palaeotemperatures (Kluge et al., 2008). Multiproxy studies of speleothem deposits allow for the precise determination of climate variations (Cruz et al., 2006). In general, speleothem deposits have been noted to grow during warm, wet interglacial periods, especially at around 128 Ka during the penultimate interglacial (Richards & Dorale, 2003). However, in desert environments, speleothem deposits have been revealed to grow during glacial periods, which are accompanied by an increase in effective precipitation (Ayliffe et al., 1998; Richards & Dorale, 2003).

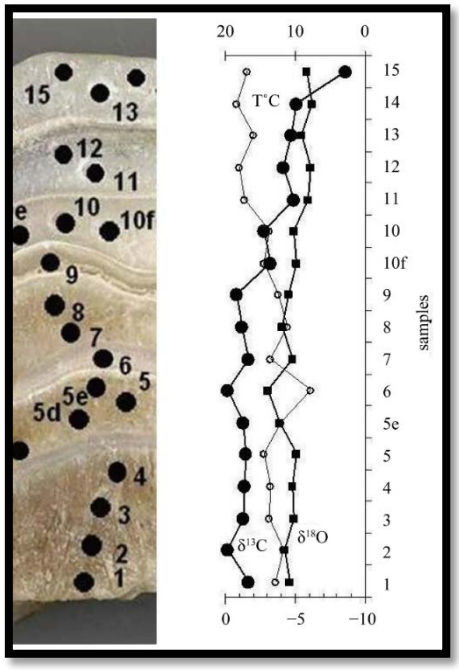

Fig. 2.8: An example of how oxygen and carbon stable light isotope analysis of speleothem may be used to reconstruct palaeoclimates using temperatures. Two trends appear on the graph for oxygen and carbon isotopes, with a temperature scale on the top horizontal axis. (de Cisneros & Caballero, 2013).

Analysis of speleothems was done by Ayliffe et al. (1998), who dated speleothems at the Naracoorte Caves using the TIMS-U series method. Ayliffe et al. (1998) argues that these speleothems document changes in precipitation over the last 500 Ka. They were able to show that the speleothem deposits document four different phases of growth, occurring at 20-115 Ka, 155-220 Ka, 270-300 Ka and 340-420 Ka. These phases correspond to stadials and cool interstadials. The indicated lack of speleothem growth during the interglacials shows that these periods were relatively arid in South Australia (Ayliffe et al., 1998).

Moriarty et al. (2000) also conducted research on the speleothems and flowstone at the Naracoorte Caves, and interpreted the development of these deposits to have occurred in a moist environment, with considerable vegetation outside the cave. Moriarty et al. (2000) developed

more specific palaeoenvironmental interpretations from the flowstone forms and growth rates (Moriarty et al., 2000).

U-Pb radiometric dates obtained from flowstone sheets interbedded between cave sediments at the Swartkrans Cave Site have provided bracketing ages for the fossiliferous deposits (Pickering et al., 2011). These new U-Pb dates have also allowed the developmental pattern of the flowstones to be established. Flowstone formation events have also been recognized and correlated across different cave sites. Overlapping flowstone formation events have been recognized at Sterkfontein and Swartkrans at around 2.29 Ma and 1.77 Ma, and at Sterkfontein and the Malapa cave site at around 2.02 Ma (Pickering et al., 2011). These events have suggested that a regional control existed with regard to the nature and timing of speleothem formational events in cave deposits, and that these flowstones could assist in the correlation of internal and specific deposits between cave sites (Pickering et al., 2011).

Hopley et al. (2007) used high resolution oxygen and carbon stable light isotopes from two flowstone deposits located in the hominin-bearing Makapansgat Caves to reconstruct Plio-Pleistocene palaeoenvironments for the region. The oxygen isotope measurements reveal variations in monsoonal precipitation intensity. The carbon isotopes reflect that during the late Miocene/early Pliocene, the environment was dominated by C_3 vegetation, while the Plio-Pleistocene was dominated by a mixture of C_3 and C_4 vegetation (Hopley et al., 2007). The carbon isotope measurements reveal that C_4 vegetation expanded at around 1.7 Ma, which Hopley et al. (2007) suggested was a response to an increase in aridity in southern Africa due to the initiation of Walker Circulation in the Pacific Ocean (Hopley et al., 2007).

2.4 Palaeoenvironmental Analysis

2.4.1 Carbon Isotope Analysis

Carbon has two stable, naturally occurring isotopes ^{12}C and ^{13}C, and one unstable isotope, ^{14}C. These isotopes fractionate in a variety of processes. Two of these processes include photosynthesis, and isotope exchange reactions between carbon compounds (Faure, 1986). During photosynthesis, the ^{12}C isotope is enriched, while isotope reactions between carbon dioxide and aqueous carbonates results in the enrichment of ^{13}C (Faure, 1986). As a result, the abundance of ^{13}C in terrestrial carbonates varies by approximately 10% (Faure, 1986). Photosynthesis involves the uptake of CO_2 gas by green vegetation and the incorporation of the carbon into simple sugars by way of numerous complex biochemical steps (Faure, 1986).

The $\delta^{13}C$ value for atmospheric carbon is greatly enriched during this process (Faure, 1986). Vegetation which makes use of photosynthesis may be divided into three main groups based on the chemical pathways used by each group during one stage of photosynthesis. These three groups include C_3 plants, C_4 plants and CAM (Crassulacean Acid Metabolism) plants (Vogel, 1993). C_3 plants make use of a photosynthetic pathway which involves only three carbons, as well as the enzyme rubisco (Vogel, 1993; Potts, 1998). C_4 plants make use of a photosynthetic pathway which involves four carbons, and does not include rubisco (O'Leary, 1981, 1993; Potts, 1998). In addition to this, C_4 plants exhibit a different cellular arrangement compared to C_3 plants, and are able to fix carbon in low CO_2 conditions (O'Leary, 1981, 1993, Vogel, 1993). This photosynthetic pathway is a modification of the C_3 pathway, and is relatively modern. C_4 plants generally include monocotyledonous plants like grasses and sedges (O'Leary, 1981, 1993; Potts, 1998). The C_3 and C_4 pathways result in differing degrees of fractionation of carbon within plants, ultimately resulting in a significantly different $\delta^{13}C$ values for C_3 and C_4 plants (Vogel, 1993).

C_3 and C_4 plants may also be grouped into different climatic zones, based on their geographic distribution (Vogel, 1993). C_3 plants dominate areas which experience winter rainfall, while C_4 plants dominate areas which experience warm, arid summer rainfall (Vogel, 1993). As a result, these climate characteristics of C_3 and C_4 plants, as well as the different carbon isotope signatures of the two groups, may be used as proxy for climate change (Vogel, 1993).

Carbon isotopes may be used in the study of speleothems. Dissolved carbon from water seeping into caves and ultimately precipitating speleothems may be derived from atmospheric carbon, decaying organic matter or root respiration in the soil above the cave, and dissolved limestone or dolomite lying along the flow route to the cave (Richards & Dorale, 2003). Numerous chemical factors result in a complex system (see Richards & Dorale, 2003), where the most useful information derived from $\delta^{13}C$ values from speleothems relates to vegetation changes in the area (Richards & Dorale, 2003). Variations in $\delta^{13}C$ may also relate to seasonal changes, where the $\delta^{13}C$ value increases during summer and decreases during winter.

Carbon isotope analyses, along with the analysis of non-vascular (bryophyte) plant fossils has recorded atmospheric CO_2 concentrations from the Mesozoic and early Cenozoic (Fletcher et al., 2008). Carbon isotopes fractionate within terrestrial bryophytes. This fractionation depends strongly on atmospheric CO_2 during the photosynthetic uptake of carbon (Fletcher et al., 2008). The changes recorded within these CO_2 concentrations coincide with climate shifts in the Mesozoic, and explain the presence of cold intervals which coincide with lower concentrations,

within a greenhouse atmosphere (Fletcher et al., 2008). This method represents the terrestrial analogue of the marine phytoplankton carbon proxy, which is used to reconstruct glacial-interglacial CO_2 changes from Pleistocene peat cores (Fletcher et al., 2008).

Stable carbon isotope measurements from the Plio-Pleistocene palaeosols of the Turkana Basin in Kenya, as well as palaeoprecipitation estimates, have yielded a high resolution record of the aridification trend in Africa during the last 4.3 Ma (Wynn, 2004). These isotope measurements have also provided a record of increasing C_4 biomass during this period (Wynn, 2004). Carbon isotope data derived from deep sea cores has also provided valuable information on the nature of the global carbon cycle, as well as on changes in deep-sea circulation patterns. These changes might have either triggered, or resulted from climatic changes (Zachos et al., 2011).

Carbon isotope data derived from deep sea cores has also provided valuable information on the nature of the global carbon cycle, as well as on changes in deep-sea circulation patterns. These changes might have either triggered, or resulted from climatic changes (Zachos et al., 2011).

2.4.2 Drip Water Analysis

Drip water within cave systems is regarded as the solution from which speleothems ultimately form, and can be seen forming on the tips of modern speleothems (Figure 2.9). The temperature measured from the $\delta^{18}O$ values of drip water feeding speleothem deposits usually resembles the ambient cave temperature. These temperatures measured from the $\delta^{18}O$ values of the drip water also include a range of temperatures which resemble the variations of the mean annual temperature on the ground surface (Nordhoff, 2005; Mandice et al., 2013). The $\delta^{18}O$ values of cave drip water also remain constant during the course of a year, and average the mean annual precipitation at the ground surface (Nordhoff, 2005). Due to these factors, drip water temperature values may be used to document long term changes in local and global climatic variations (Mandice et al., 2013). $\delta^{18}O$ values from drip water may also provide interpretations with regard to seasonality, as the $\delta^{18}O$ values of meteoric precipitation which drip water values average, change depending on seasonal temperature and precipitation changes (Nordhoff, 2005). The air and drip water temperature within a cave system is inversely proportional to the fractionation and ultimate $\delta^{18}O$ composition within precipitated speleothem deposits (Nordhoff, 2005). Therefore, an increase in the overall air and drip water temperature would result in a decrease in the fractionation of oxygen isotopes between drip water and the precipitated speleothem deposits, and result in a decrease in $\delta^{18}O$ in precipitated speleothem deposits (Nordhoff, 2005). In general, variations in $\delta^{18}O$ between precipitated calcite and drip

water are caused by numerous factors. These include changes in the $\delta^{18}O$ values within ocean water at the time, which varies according to changes in ice sheet volumes, variations in the flow of water between the area affected by precipitation and the source of the water, and variations in the isotopic composition as well as the quantity of rain and vadose waters (Dorale et al., 1992; Richards & Dorale, 2003). Negative variations in $\delta^{18}O$ values may be due to variations in ocean water $\delta^{18}O$ during glacial-interglacial transition periods, as well as due to the amplification of rainfall patterns and the seasonality of rainfall (Dorale et al., 1992; Richards & Dorale, 2003). The isotopic study of the T8 stalagmite from Makapansgat by Holmgren et al. (2003) concluded that variations in $\delta^{18}O$ values within the stalagmite represent variations in the types of precipitation occurring in the area during the precipitation of the stalagmite. The $\delta^{18}O$ variations from this stalagmite have shown that lower, more depleted $\delta^{18}O$ values may represent drier, more arid climatic conditions, and less depleted $\delta^{18}O$ values represent wetter, warmer environments (Holmgren et al., 2003).

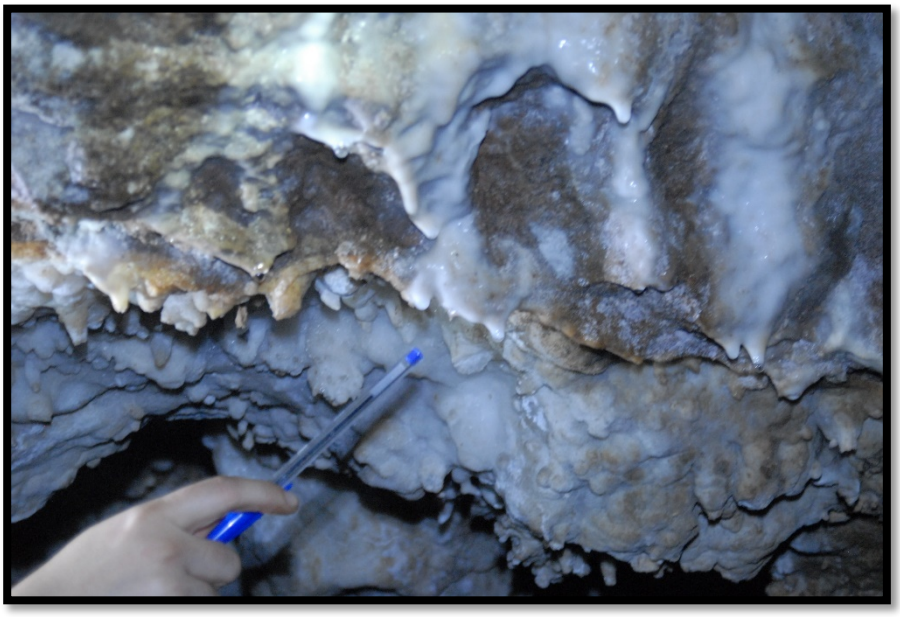

Fig. 2.9: Examples of drip water from flowstone deposits in the Jacovec Cavern of Sterkfontein Caves.

The degree to which drip water temperature represents the mean annual temperature on the ground surface is dependent on numerous fractionation factors. Overall fractionation of oxygen isotopes in drip water may be related to mass differences of the respective isotopes, where heavier isotopes such as ^{18}O move and react much slower compared to ^{16}O, which has a lighter mass (Noah, 2010). This is referred to as isotopic equilibrium fractionation and generally occurs between two different phases of a particular compound, $CaCO_3$ (Harmon et al., 2004). In this regard, ^{18}O would be more enriched in speleothem carbonate than in drip water CO_2

(White, 2004). Oxygen isotopes are affected by two types of fractionation, namely equilibrium fractionation and kinetic fractionation.

There are numerous different types of kinetic fractionation. These include evaporative cooling, fracture flow and heat transport process, and cave air ventilation processes. Evaporative cooling effects may significantly alter the recorded temperature of drip water with regard to the mean temperature on the ground surface, as cooling results in more negative, depleted oxygen isotope values and therefore lower temperatures, making temperature data from drip water samples unreliable when comparing them to mean temperature data from the ground surface (Cuthbert et al., 2014). Unless evaporative effects are taken into account, drip water samples which have undergone evaporative cooling will not accurately represent the mean annual temperature at the ground surface (Cuthbert et al., 2014). Fracture flow and heat transport processes can result in a dramatic increase in drip water temperatures (Cuthbert et al., 2014). Cave air ventilation processes affect drip water temperatures by changing the relative humidity within the cave environment, which in turn controls the rate of evaporation, and therefore the rate of cooling of the drip water. This can result in drip water temperatures which do not represent the mean temperatures on the ground surface (Cuthbert et al., 2014). The temperature differences between the cave interior and exterior environment may result in corresponding pressure changes in the cave system, resulting in the movement of air from cave entrances to the cave roof (Noah, 2010). This movement of air may result in changes in the temperatures produced from $\delta^{18}O$ values of speleothems and drip water, and changes in humidity, which also affects the $\delta^{18}O$ values produced (Wigley & Brown, 1976).

The amount of precipitation (Gascoyne 1992; Sundqvist et al., 2007) and the atmospheric air temperatures (van Beynen & Febbroriello, 2006; Sundqvist et al., 2007) also contribute to fractionation effects with regards to $\delta^{18}O$ signatures, and are related to Rayleigh distillation, which takes place during the course of the hydrological cycle, and within the cave system (Noah, 2010). With regards to the cave system, Rayleigh distillation may be responsible for kinetic fractionation of oxygen isotopes, which takes place during the removal of CO_2 and calcite of varying isotopic signatures from the drip water solution (Wynn et al., 2005). The removal of gaseous CO_2 from the drip water solution usually takes place at a constant rate in order to preserve calcite supersaturation; however this results in the enrichment of ^{18}O in the drip water solution (Hendy, 1971; Noah, 2010). This may therefore result in abnormally enriched $\delta^{18}O$ values within drip water solutions. With regards to the hydrological cycle, fractionation caused by Rayleigh distillation usually occurs during the evaporation or

condensation of water (Fairchild et al., 2006), and the effects thereof are usually determined by the amount of precipitation, leading to a gradual depletion of ^{18}O isotopes during heavy rainfall events (White, 2004; Noah, 2010).

These factors also contribute to variations in the fractionation of $\delta^{18}O$ during speleothem precipitation, as the speleothem precipitates from the affected drip water (Spotl et al., 2005; Cuthbert et al., 2014). If all of these factors are taken into account and are corrected for, the drip water temperatures can be successfully correlated to the mean temperatures on the ground surface.

In order for palaeoenvironmental analyses to be accurate with regards to speleothem stable light isotope proxies, the conditions under which the speleothem originally formed must be determined (Hendy, 1971; Ouelette, 2013). During the precipitation of speleothem deposits from drip water, the fractionation ratio between oxygen isotopes in the drip water and deposited speleothem is only a function of temperature if thermodynamic equilibrium within the cave system is achieved (Hendy, 1971; Richards & Dorale, 2003; Cuthbert et al., 2014). Thermodynamic equilibrium is usually achieved as a result of slow degassing rates, and no presence of evaporation (Nordhoff, 2005). These conditions are usually met in environments like the back of very deep caves, where humidity values are high and air flow is reduced (Richards & Dorale, 2003; Nordhoff, 2005).

2.4.3 Oxygen Isotope Analysis

Oxygen has three stable, naturally occurring isotopes, ^{16}O, ^{17}O and ^{18}O. These isotopes fractionate between sea water, fresh water and air, as well as occurring in calcium carbonate precipitates. This fractionation is temperature dependent, and therefore values of $\delta^{18}O$ can be used to determine climate changes and variability, with colder climates indicated by positive values, and warmer climates indicated by negative values (Faure, 1986; Pickering, 2007; Zachos et al., 2011) (Figure 2.10). This use of oxygen isotopes has been applied to speleothems, deep sea core and ice cores, which has provided palaeoclimate data when coupled with dating techniques (Faure, 1986; Pickering, 2007; Zachos et al., 2011). Oxygen isotope analysis from deep-sea cores has allowed precise patterns of cold and warm climatic phases during the Quaternary to be deduced (Shackleton & Opdyke, 1973; Pickering, 2007) (Figure 2.10). Cold phases are characterised by large amounts of atmospheric water precipitating in Polar Regions, causing a build-up of polar ice sheets. This ice is depleted in ^{18}O and enriched in ^{16}O compared to sea water, and is therefore isotopically ‘lighter’ than sea water (Potts, 1998; Pickering, 2007).

During these cold phases, sea levels were about 130 m lower than today, as large amounts of sea water was trapped in ice masses. As the climate warmed, this ice melted into the sea water, therefore making the sea water isotopically 'lighter' than the ice sheets (Potts, 1998). These changes were recorded in the shells formed by marine organisms, particularly those of foraminifera. These shells were continuously deposited onto the ocean floors, ultimately preserving a record of climate changes through the Quaternary (Chappell & Shackleton, 1986; Potts, 1998) (Figure 2.11). Oxygen isotope analysis of these foraminifera from deep sea cores has allowed a pattern of cold and warm phases from the Quaternary to be created and confirmed. There is also a strong correlation between $\delta^{18}O$ and latitude, with the $\delta^{18}O$ value decreasing towards higher latitudes, as well as further inland.

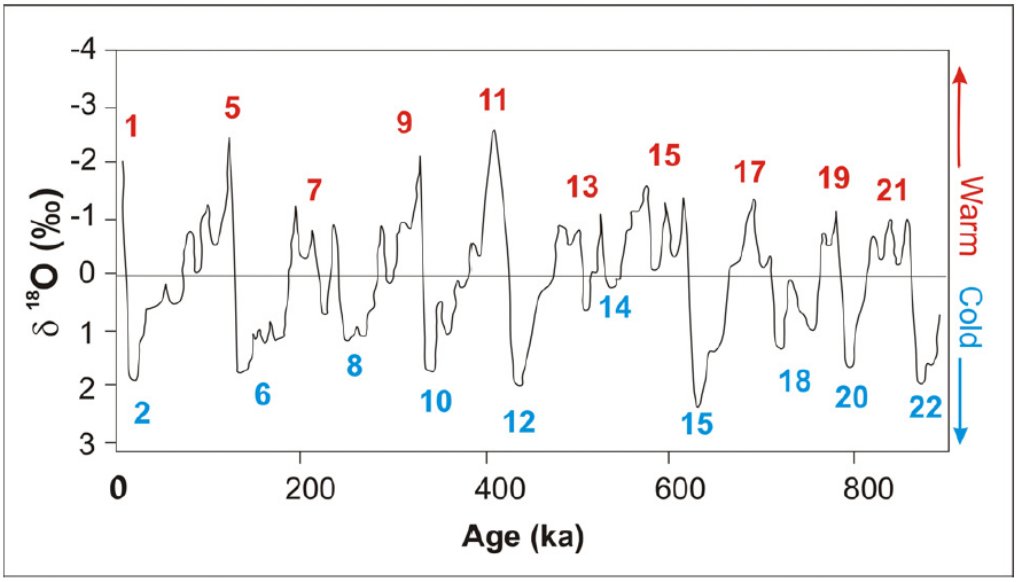

Fig. 2.10: Oxygen isotope curve for the last 900 Ka. The odd numbers represent interglacial periods, and the even numbers represent glacial periods. From Bassinot et al., (1994).

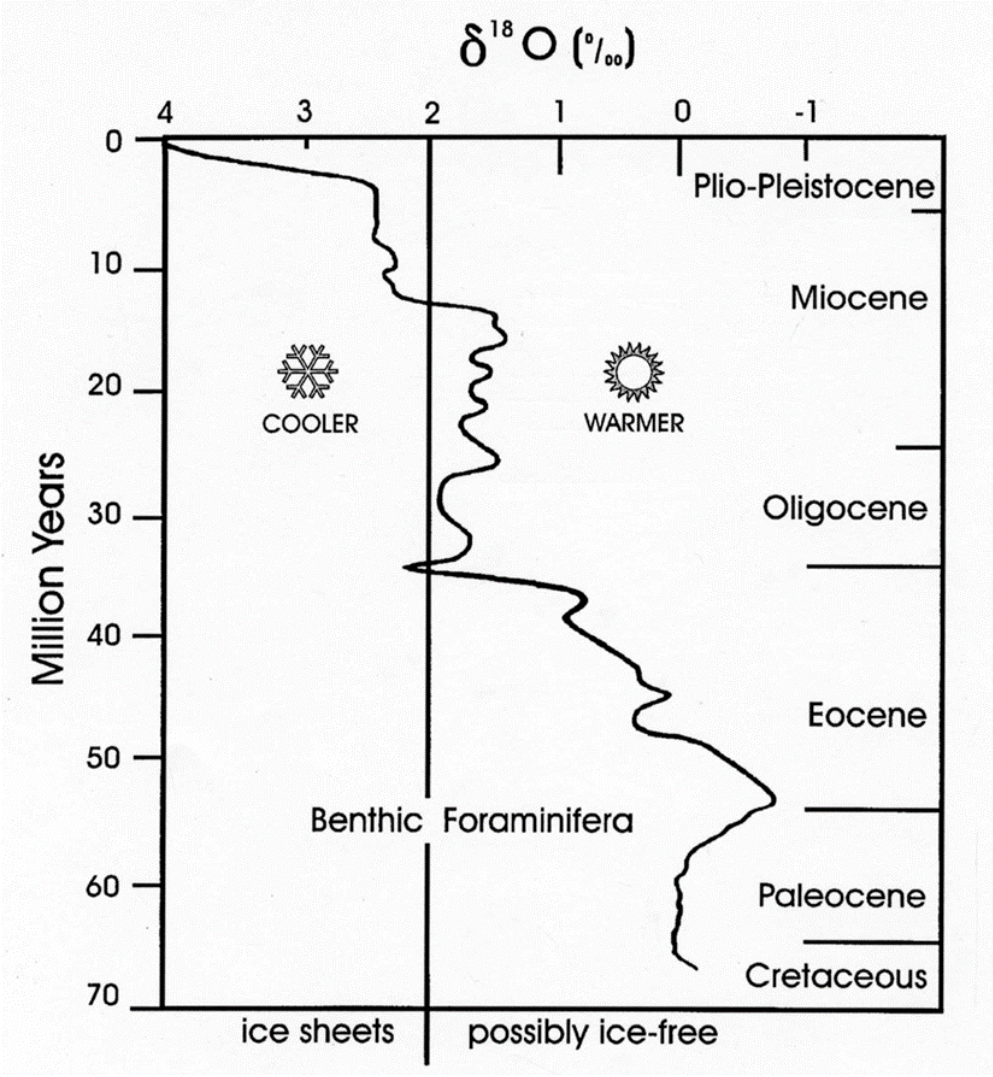

Fig. 2.11: Oxygen isotope curve produced from the analysis of benthic foraminifera, dating from the Cretaceous to the Plio-Pleistocene, with interpretations (Source Unknown).

Numerous high resolution records of Quaternary climate change exist which may be used in comparison to other records (Imbrie et al., 1984). The most common of these records which pertain to studies conducted in the southern hemisphere include the SPECMAP record of sea level change, and the Vostok ice core record of temperature changes (Imbrie et al., 1984; Pickering, 2007). The SPECMAP Archive No.1 contains climate data of the past 700 Ka for 17 sediment cores which originate from the Atlantic Ocean (Imbrie et al., 1984) (Figure 2.12). Included in these records are quantitative data documenting the species and assemblages of planktonic fauna and flora, which reflect variations in the surface conditions of the Atlantic Ocean, as well as data used to interpret continental ice volumes (Imbrie et al., 1984; Zachos et al., 2011). Oxygen and carbon isotope data from the benthic and planktonic assemblages provide additional palaeoclimate data (Imbrie et al., 1984; Lear et al., 2000). Using these

measurements, a model of global sea level changes was created for the last 780 Ka, using changing ice volumes during this period (Imbrie et al., 1984). The Vostok ice core record originates from an ice sheet in east Antarctica, and provides a record of global climate change for the last 420 Ka (Potts, 1998; Petit et al, 1999) (Figure 2.12). Four glacial-interglacial cycles are recorded in this ice core record. These ice cores provide palaeoclimate data which ranges from local temperatures deduced from deuterium content within the cores, precipitation rates, moisture source conditions, wind strength, as well as the flux of aerosols of marine, terrigenous, cosmogenic, volcanic and anthropogenic origin (Petit et al., 1999) (Figure 2.11). Oxygen isotope analysis of these ice cores has allowed global ice volume changes, as well as ice volume changes within the hydrological cycle, to be determined (Potts, 1998) (Figure 2.12).

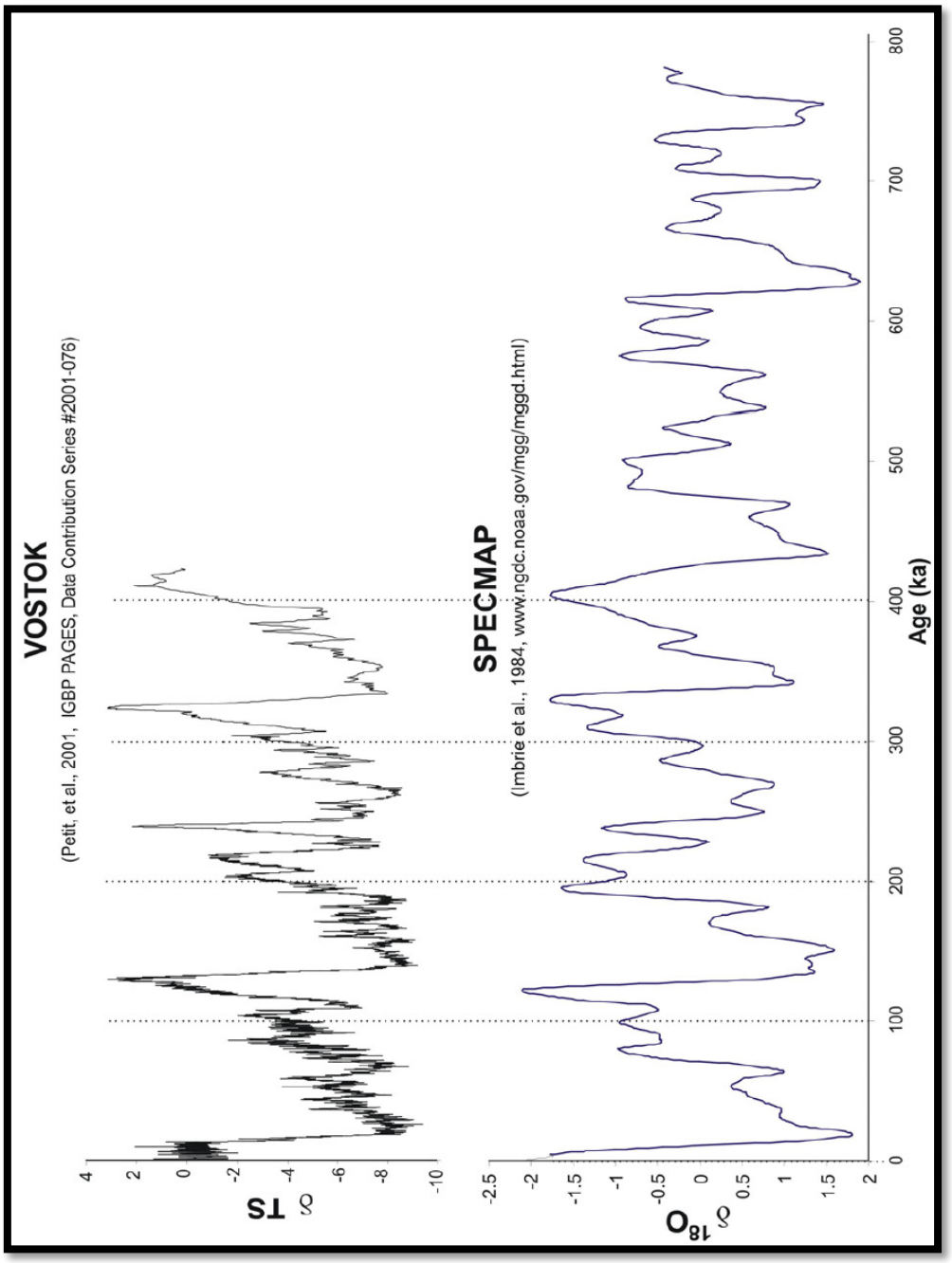

Fig. 2.12: Graphs showing climate change data from the Vostok ice core temperature change records (Petit et al., 1999) and from the global SPECMAP record (Imbrie et al., 1984).

Oxygen isotope analysis of speleothem deposits have provided palaeoclimate data pertaining to variations in temperatures and precipitation variations within cave environments. In a system which has achieved isotopic equilibrium, the distribution of ^{18}O between calcite and water during the precipitation of the speleothem deposits is dependent on temperature (Friedmann & O'Neil, 1977; Richards & Dorale, 2003). Variations of oxygen isotope concentrations within ancient calcite is attributed to temperature shifts, as well as changes in the ^{18}O of sea water, variations in the path of water from its source to the site of precipitation, and the isotopic

composition and volume of rain and vadose water (Richards & Dorale, 2003). Negative shifts in ^{18}O values are attributed to glacial-interglacial changes in ocean ^{18}O values, as well as the intensification of rainfall and seasonal rainfall patterns (Richards & Dorale, 2003). Long, high resolution records of climate changes from oxygen isotope variations of speleothem deposits may be compared to marine sediment core records, and ice core records (Figure 2.12), in order to provide a complete, more accurate record of global climate changes (Richards & Dorale, 2003).

2.4.4 Dust Flux Analysis

Ocean dust records come about as a result of dust plumes forming over the oceans from terrigenous material. These plumes form due to strong seasonality in rainfall, as well as a result of the winds which carry the dust from the continents to the oceans (Potts, 1998). Dust accumulations in ocean sediment cores therefore provide a record of changes in seasonality and prevailing wind conditions over a considerable amount of time (Potts, 1998). These dust cores may also provide a history of vegetation cover on the continents, as large areas of open vegetation and desert increase the chance of erosion and transport of terrigenous material (Potts, 1998).

The analysis of terrigenous dust flux from marine and lacustrine sediments has provided records of trends, rhythms and events with respect to African climate during the Plio-Pleistocene (Trauth et al., 2009). Samples used for dust flux analysis have been obtained from marine sediments in the eastern Mediterranean Sea, the Arabian Sea, and off the coast of subtropical West Africa, as well as from lacustrine sediments from eastern Africa (Trauth et al., 2009). Dust flux analysis has attempted to remove inconsistencies between marine climate variability records and terrestrial climate variability records (Behrensmeyer et al., 2006; Trauth et al., 2009). Analysis of marine records containing Saharan dust has revealed that major steps in faunal and hominin evolution occurred during climatic shifts towards more arid, variable climatic conditions. This has been shown to have occurred during the onset and intensification of high-latitude glacial cycles which occurred at around 2.8 Ma, 1.7 Ma and 1.0 Ma (de Menocal, 1995, 2004; Trauth et al., 2009). However, dust flux analysis conducted on Plio-Pleistocene lake sediments from eastern Africa with regard to lake level variations have suggested that in fact these periods were dominated by wetter and more seasonal conditions (Trauth et al., 2009). Dust records have also revealed that precessional (19 to 23 Ka) and obliquity (41 Ka) forcing is continuous throughout the records (de Menocal, 2004; Trauth et

al., 2009). Dust flux records also provide evidence for the modulation of precession by eccentricity up until 5 Ma (Trauth et al., 2009). This suggests that the modulation of precession by eccentricity has a major effect on the hydrological cycle within tropical Africa (Trauth et al., 2009). It also suggests that that large amplitude variations in African climate are not related to the onset and intensification of high latitude glacial cycles, as suggested by numerous other studies (de Menocal, 1995, 2004; Trauth et al., 2009). Dust layers from glacial periods have shown to be thicker and contain more aeolian material, than those of interglacial periods (de Menocal, 2004).

2.4.5 Miscellaneous Palaeoclimate Analyses

The ratio between magnesium and calcium in benthic foraminiferal calcite has been used to produce a deep sea temperature record for the past 50 Ma (Lear et al., 2000). The temperature record produced from these data is very similar to the record produced from benthic oxygen isotope data. In general, these data define an overall cooling trend of about 12°C of deep ocean water, with four main cooling phases, over the past 50 Ma. They also provide estimates of global ice volumes (Lear et al., 2000).

Micromammalian fossils from the Sterkfontein Member 5 East and Swartkrans Members 1-3 have contributed palaeoenvironmental information to the period between 2 Ma and 1 Ma, and have allowed for palaeoenvironmental reconstructions of the Cradle of Humankind (Avery, 2001).

Large ice sheets, such as those of the Arctic or Antarctic, are also used for large scale palaeoclimate analysis as they play an important part in amplifying, pacing, and driving global climate change over large time periods (Potts, 1998; Clarke et al., 1999). The influence of ice sheets on climate include changing ocean surface temperatures, ocean circulation, continental water balance, vegetation, and albedo, all of which affect the global climate system (Clarke et al., 1999). It has been suggested that the underlying geological substrate beneath the ice sheets has helped modulate the response of ice sheets to insolation forcing. These responses manifest as effects the ice sheets have on global climate, and may explain climate variability over the past 2.5 Ma (Clarke et al., 1999).

Palaeoclimate reconstructions have also been created using sedimentation and stratigraphic sequences, along with facies analysis of those sequences. Facies analysis allows for palaeoenvironmental reconstructions by providing information about depositional environments (Boggs, 2001). These depositional environments are controlled by tectonics, sea

level change and climate variations (Boggs, 2001). Kos (2001) used this approach, and related cycles of erosion and deposition of sediments within cave systems during the last interglacial period to groundwater variations, which relates to surface environmental conditions. Studies have shown that in Australia, the last glacial period is represented by a hiatus in sedimentation and speleothem development within cave systems, and may be accompanied by erosion. This has been related to more arid surface conditions by Kos (2001). Brain (1995) used the sedimentation sequence of the Member 5 deposit from Swartkrans to model variations in climate which controlled the sedimentation of this deposit (Brain, 1995). It has also been suggested that the degree of calcification in clastic sedimentary layers may distinguish climate changes. Layers exhibiting no calcification have been proposed to correlate to arid periods, or moist periods characterised by very fast sedimentation (Moriarty et al., 2000). Clastic layers interbedded with flowstone layers and well-calcified sediments would provide evidence for a wetter climate (Moriarty et al., 2000).

Diatoms present in lake sediments are environmentally sensitive organisms, and may provide a history of lake depth, salinity and alkalinity (Potts, 1998). These lake properties are strongly influenced by climatic and tectonic variations, therefore a study of diatoms within the lake sediments would allow for the reconstruction of rates of environmental changes (Potts, 1998).

Chapter 3
Methods and Materials

3.1 Introduction

The methodology used in collecting samples from the Sterkfontein Caves, as well as in conducting the isotopic and climatic analyses on the samples produced is described in this chapter. Overall, 16 modern speleothem samples were personally collected, and 328 drip water samples were collected bi-weekly in vials over a period of 14 months by technical staff at the Sterkfontein Caves site. The speleothem samples were personally prepared for oxygen and carbon stable light isotope analyses which were conducted at iThemba Labs at the University of the Witwatersrand using a Finnigan Gasbench II. The drip water samples were sent for oxygen isotope analyses at the Hydrogeology Research Laboratory in the School of Geoscience at the University of Witwatersrand, where the samples were prepared for analysis and analysed for oxygen isotopes. Hydrochemical analyses were conducted personally on the drip water samples at a private water analysis laboratory at the Department of Archaeology, Geography and Environmental Science at the University of the Witwatersrand, which included an analysis of the pH and electro-conductivity of each drip water sample. Overall climatic data was collected from within Sterkfontein Caves during the collection of the drip water samples, and overall atmospheric climatic data was obtained from nearby weather stations. Pearson's product-moment correlation statistical analyses were performed on the resulting data in order to interpret correlations and trends. The localities of each sample collected are described in this chapter, as well as the sampling procedure, which is detailed for both the modern speleothems and drip water. The preparation and analysis of these collected samples is then described, in terms of laboratory stable light isotope analyses, and hydrochemical analyses performed on the drip water samples. A detailed description of the calibration and correction used in processing the stable light isotope results is provided, followed by a description of the statistical analyses used to interpret the data sets with regards to correlations and trends. This is followed by a detailed section on the analysis and interpretation of the speleothem and drip water stable light isotope data in terms of temperature, precipitation and vegetation, as well as hydrochemical interpretations and interpretations with respect to the modern climatic data.

3.2 Sample Location and Sampling

3.2.1 Sample Location

The interior of the Sterkfontein Cave system was examined in terms of geology, geomorphology and physical attributes in order to collect samples which would reflect a variety of differing climatic and geological conditions within the cave system. Modern speleothem and drip water samples were collected from the Silberberg Grotto, Milner Hall, Jacovec Cavern, and two narrow antechambers (Figure 3.1). The Silberberg Grotto was selected for modern speleothem sampling, due to the Grotto's proximity to a main cave entrance, and due to the direct vertical ground water flow from the ground surface into the Grotto. Milner Hall was selected because it is exposed and subject to continual climatic variations due to its' proximity to tourist path, as well as being the site of the Milner Lake, a source of static ground water in the cave system. Climatic variations would be expected along the tourist path due to disturbed air flow currents, which could affect the humidity, atmospheric pressure and temperature variations within the cave system along these routes (Dominguez-Villaer et al., 2010). The Jacovec Cavern was selected due to its' high initial humidity, which promotes fewer kinetic fractionation effects, and the large number of active flowstones in the cavern. The two antechambers were chosen for sampling due to the isolation of these areas and the high humidity measured in these areas. A map showing the sample locations is provided (Figure 3.1)

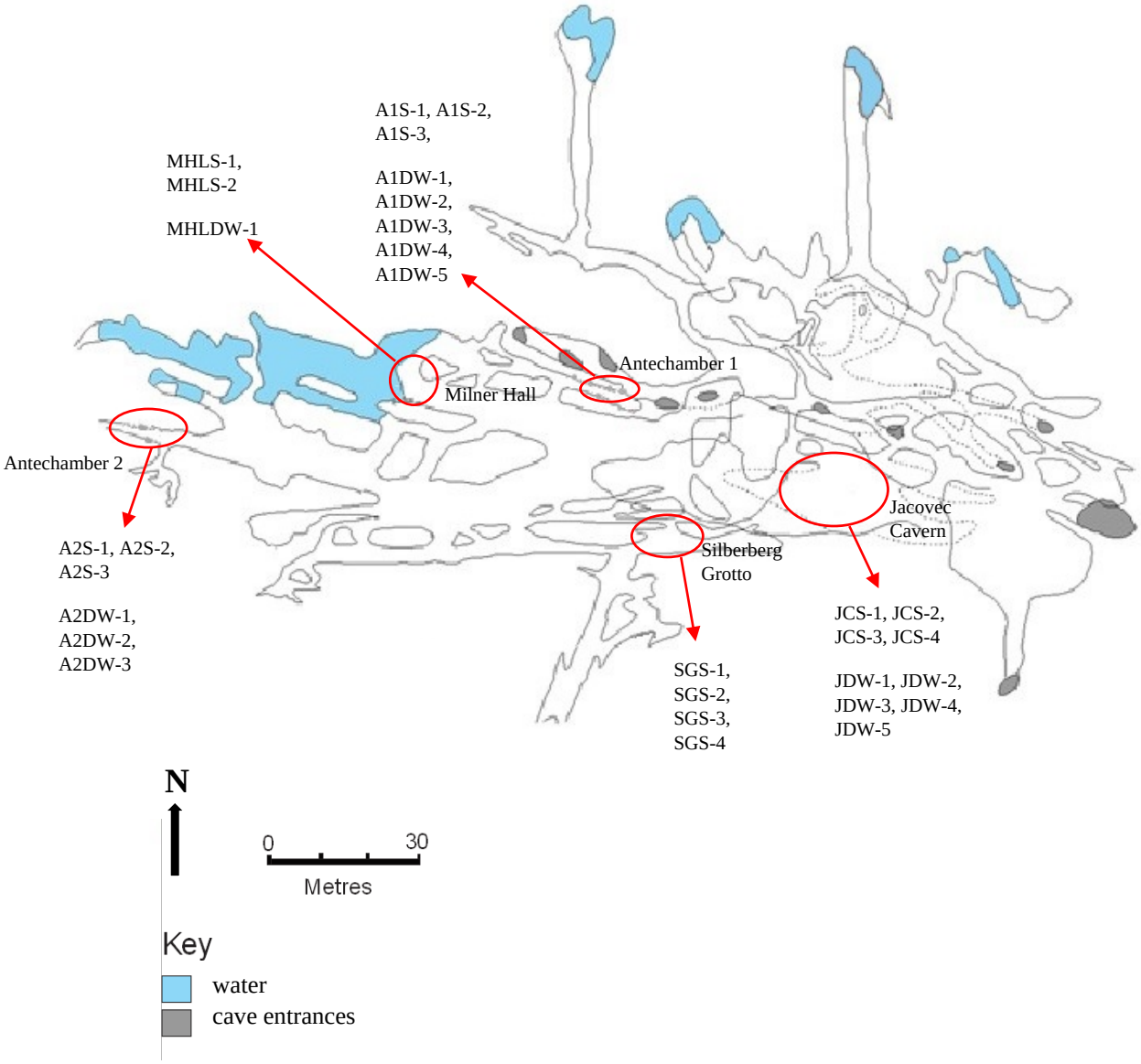

Fig. 3.1: Map of Sterkfontein Caves, showing chamber locations circled in red, and samples collected from these chambers indicated by the red arrow. The dotted line displays the outline of overlying cave chambers. Adapted from Reynolds et al. (2003).

3.2.2 Speleothem Sampling

Sixteen modern speleothem samples were personally taken in the field from currently precipitating flowstone layers using a chisel. Each sample measured approximately 3 mm to 10 mm in length. These speleothem samples were put into small sample bags and labelled with a sample name, depending on the sample location. These samples were taken from various locations within the Sterkfontein caves system, including the Silberberg Grotto, Milner Hall lake site, Jacovec Cavern and two smaller antechambers (Figure 3.1). Each sample locality was recorded with the Total Station using x, y and z co-ordinates measured for each sample by a combination of an electronic theodolite and electronic distance meter. Speleothem samples are listed in Table 3.1.

Samples of speleothems which had recently precipitated onto the dolomite roof host rock of the cave system were taken, as well as samples which had precipitated over older speleothems along the cave walls (Table 3.1). Data from these three types of samples were compared in order to ascertain how the environment onto which the speleothems precipitated and the manner in which the speleothems precipitated affected the oxygen and carbon isotope values. Samples were also taken from locations at different levels within the cave system as well as at different distances from cave entrances, in order to account for the impact of variability on the stable light isotopes of the samples with regards to humidity and sources of wind. Samples at higher levels and closer to cave entrances would experience less humidity and greater wind interference, which is represented by the samples collected from the Silberberg Grotto and Milner Hall, whereas samples at deeper levels and further away from cave entrances would experience the opposite, represented by samples collected from Antechamber 1, Antechamber 2 and the Jacovec Cavern (Table 3.1).

Table 3.1: Description of speleothem samples and the chambers from which they were collected. Total station co-ordinates for each sample can be found in Appendix A. Fresh calcite refers to newly precipitated speleothems/calcite. Clean calcite refers to calcite without any dirt/impurities. Abbreviations: D-dolomite, C-calcite, B-breccia, V-ventilated, H-humidity.

Sample Name	Chamber Location	Sample Description	Chamber Description	Elevation (masl)
SGS-1	Silberberg Grotto	Fresh speleothem	Well V., close to main entrance, moderate H., small.	1462.304
SGS-2	Silberberg Grotto	Fresh speleothem	Well V., close to main entrance, moderate H., small.	1461.171
SGS-3	Silberberg Grotto	Older speleothem	Well V., close to main entrance, moderate H., small.	1462.059
SGS-4	Silberberg Grotto	Top of speleothem on D.	Well V., close to main entrance, moderate H., small.	1462.502
MHLS-1	Milner Hall Lake	Flowstone below older speleothem precipitated on D.	Well V., access to numerous minor entrances, low H., very large and exposed.	1 440.092
MHLS-2	Milner Hall Lake	Recrystallized speleothem	Well V., access to numerous minor entrances, low H., very large and exposed.	1 440.827
JCS-1	Jacovec Cavern	Fresh C. from flowstone precipitated onto older speleothem	Moderately V., small minor entrances, high H., medium size, low roof.	1 446.280
JCS-2	Jacovec Cavern	Fresh C. with modern speleothem	Moderately V., small minor entrances, high H., medium size, low roof.	1 444.358
JCS-3	Jacovec Cavern	Fresh C. from modern speleothem precipitated on D.	Moderately V., small minor entrances, high H., medium size, low roof.	1 444.255
JCS-4	Jacovec Cavern	Fresh C. from modern speleothem precipitated on older B.	Moderately V., small minor entrances, high H., medium size, low roof.	1 445.990
A1S-1	Antechamber 1	Clean C. from modern speleothem precipitated onto older B.	Poorly V., one small minor entrance, high H., narrow and small.	1 448.098
A1S-2	Antechamber 1	Clean C. from modern speleothem precipitated onto older B.	Poorly V., one small minor entrance, high H., narrow and small.	1 448.199
A1S-3	Antechamber 1	Clean C. from modern speleothem precipitated onto older speleothem and B.	Poorly V., one small minor entrance, high H., narrow and small.	1 447.332
A2S-1	Antechamber 2	Fresh C. from modern speleothem precipitated over older speleothem	Poorly V., one small minor entrance, high H., very narrow and small, high roof.	1448.727
A2S-2	Antechamber 2	C. from modern speleothem precipitated onto D.	Poorly V., one small minor entrance, high H., very narrow and small, high roof.	1443.623
A2S-3	Antechamber 2	Fresh C. from modern speleothem precipitated over older speleothem	Poorly V., one small minor entrance, high H., very narrow and small, high roof.	1443.199

During the collection of these samples, the cave humidity, atmospheric temperature, dew point temperature, altitude and atmospheric pressure at the sample location were also recorded using a Kestrel 4500 Pocket Weather Tracker, in order to establish the ambient cave environment under which the modern speleothems formed (see Appendix D). These measurements were

collected over a period of 14 months, from June 2015 to August 2016, every two weeks. These physical measurements were also essential in order for temperature and precipitation climatic data to be deduced and understood correctly. Measurements scheduled to be taken as per the bi-weekly system were not taken on 17th December 2015, 31st December 2015, and 28th April 2016.

In order for palaeoenvironmental analyses to be accurate with regards to both drip water and speleothem stable light isotope proxies, the conditions under which the speleothem originally formed must be determined (Hendy, 1971; Ouelette, 2013). During the precipitation of speleothem deposits from drip water, the fractionation ratio between oxygen isotopes in the drip water and deposited speleothem is only a function of temperature if thermodynamic equilibrium within the cave system is achieved (Hendy, 1971; Richards & Dorale, 2003; Cuthbert et al., 2014). Thermodynamic equilibrium is usually achieved as a result of slow degassing rates, and no presence of evaporation (Nordhoff, 2005). These conditions are usually met in environments like the back of very deep caves, where humidity values are high and air flow is reduced (Richards & Dorale, 2003). Measuring the humidity, air temperature, air pressure and dew point temperature for both the drip water and speleothem samples would allow for the conditions under which the speleothems and drip water formed to be established.

3.2.3 Drip Water Sampling

Approximately 20 to 30 ml drip water samples were collected bi-weekly for 14 months from July 2015 to August 2016, in pre-cleaned and pre-treated 30 ml polyethylene bottles using a funnel, from 13 different drip water locations within the Sterkfontein cave system. These locations include sample points in the Silberberg Grotto, Milner Hall lake site, Jacovec Cavern, and two smaller antechambers (Table 3.2). A sample of the lake water from the Milner Hall Lake site was also taken. Samples were collected in the same manner as was done for the speleothem samples with respect to location, bi-weekly collection dates, and cave climatic data, and were collected by technical staff at Sterkfontein Caves. Drip water samples collected from Antechamber 1 and Milner Hall were the closest to the tourist path, therefore closer to the influence of tourist activity, with samples collected from Antechamber 2 and the Jacovec Cavern being further away from the tourist paths, and therefore further from the influence of tourist activity. As the Sterkfontein Caves are open to tourists every day, the samples were thus collected from all the chambers during varying, unpredictable tourist visits over the course of the 14 month sampling period. Drip water samples are listed in Table 3.2. Samples were not collected on 17th December 2015, 31st December 2015, and 28th April 2016.

Table 3.2: Description of speleothem samples and the chambers from which they were collected. Fresh calcite refers to newly precipitated speleothems/calcite. Clean calcite refers to calcite without any dirt/impurities. Total station co-ordinates for each sample can be found in Appendix A. Abbreviations: D.W.-drip water, D-dolomite, C-calcite, B-breccia, V-ventilated, H-humidity.

Sample Name	Chamber Location	Sample Description	Chamber Description	Elevation (masl)
JDW-1	Jacovec Cavern	D.W. from fresh C. precipitated onto older speleothem	Moderately V., small minor entrances, high H., medium size, low roof.	1 444.876
JDW-2	Jacovec Cavern	D.W. from fresh C. with modern speleothem	Moderately V., small minor entrances, high H., medium size, low roof.	1 444.243
JDW-3	Jacovec Cavern	D.W. from fresh C. precipitated on D.	Moderately V., small minor entrances, high H., medium size, low roof.	1 443.868
JDW-4	Jacovec Cavern	D.W. from fresh C. precipitated on older B.	Moderately V., small minor entrances, high H., medium size, low roof.	1 443.815
JDW-5	Jacovec Cavern	D.W. from fresh C. precipitated on modern speleothem	Moderately V., small minor entrances, high H., medium size, low roof.	1 444.489
A1DW-1	Antechamber 1	D.W. from clean C. precipitated onto older B.	Poorly V., one small minor entrance, high H., narrow and small.	1 446.660
A1DW-2	Antechamber 1	D.W. from clean C. precipitated onto older B.	Poorly V., one small minor entrance, high H., narrow and small.	1 447.136
A1DW-3	Antechamber 1	D.W. from clean C. precipitated onto older speleothem and B.	Poorly V., one small minor entrance, high H., narrow and small.	1 444.724
A1DW-4	Antechamber 1	D.W. from clean C. precipitated over older B.	Poorly V., one small minor entrance, high H., narrow and small.	1 444.355
A1DW-5	Antechamber 1	D.W. from clean C. precipitated over older speleothem	Poorly V., one small minor entrance, high H., narrow and small.	1 447.088
A2DW-1	Antechamber 2	D.W. from fresh C. precipitated over older speleothem	Poorly V., one small minor entrance, high H., very narrow and small, high roof.	1443.623
A2DW-2	Antechamber 2	D.W. from C. from modern speleothem precipitated onto D.	Poorly V., one small minor entrance, high H., very narrow and small, high roof.	1445.312
A2DW-3	Antechamber 2	D.W. from fresh C. from modern speleothem precipitated over older speleothem	Poorly V., one small minor entrance, high H., very narrow and small, high roof.	1441.749

During the collection of these samples, the drip rate, cave air humidity, cave atmospheric pressure and temperature were also recorded using a Kestrel 4500 Pocket Weather Tracker, using the same technique carried out when collecting the speleothem samples (see Appendix D). These variables were measured over a period of 13 months, from July 2015 to July 2016. Measurements were not taken on 17th December 2015, 31st December 2015, and 28th April 2016, and drip rates were not measured on 19th May 2016.

3.2.4 Vegetation Survey

A general field survey was conducted at Sterkfontein Caves to assess the extent of the biodiversity of the local flora around the Sterkfontein Cave site, which included a vegetation percentage overview analysis of the different species, and to what degree C_3 and C_4 vegetation were present in the area (Mogg, 1975). This was completed by noting the occurrence of C_3 or C_4 or CAM plants, as well as the percentage coverage of this vegetation over the environment above the cave system. Photographs of the overall vegetation distribution around the Sterkfontein Caves site were taken, in order for a general visual overview of the C_3 and C_4 vegetation distribution to be obtained. A reference book, 'Important Plants of Sterkfontein' was used in order to identify plant species and overall vegetation distribution (Mogg, 1975).

3.3 Preparation and Analysis

3.3.1 Speleothem Analysis

The 16 speleothem samples were personally prepared and analysed for oxygen and carbon stable light isotopes at iThemba Labs at the University of the Witwatersrand (see Appendix C). With regards to preparation, the speleothem samples were crushed into a powder, and 0.5 mg to 0.6 mg of each sample was accurately weighed out and transferred into a vial for further stable light isotope analysis. Each sample was divided into two, resulting in a total of 32 vials. Two in-house carbonate standards were used for this analysis, namely the CSS and MHS1 standards. The CSS in-house standard produces intermediate negative ^{13}C and ^{18}O values, with a smaller range than MHS1, which produces very negative ^{13}C values and more positive ^{18}O values, with a large range. 0.3 mg of each standard was measured out four times, resulting in a total of four CSS standard vials, and four MHS1 standard vials. These two standards were chosen as they display a large range of negative values for ^{13}C and ^{18}O, which allow for the accurate calibration of speleothem sample results relative to PeeDee Belemnite (PDB) (Vaks et al., 2003; Mattey et al., 2008).

The speleothem samples were analysed using the Finnigan GasBench II. Sample vials were loaded into a sample tray. Slots one to nine on the sample tray were occupied by blank samples which only contained helium. Slots 10 to 13 hosted the vials containing the standards, which included two CSS standard vials and two MHS1 standard vials. The rest of the samples were then loaded into the remaining slots, with the last four slots occupied by standards again (Figure 3.2). The tray was then heated to 72°C in order to speed up the reaction that would take place

between the carbonates and the acid with which the samples were dosed. This also reduced the time required to reach isotopic equilibrium in each sample. In order to measure oxygen and carbon stable light isotopes simultaneously in carbonate samples, each sample was dosed with phosphoric acid in order to yield CO_2, which reflects the isotopic value of the CO_3^{2-} carbonate ion. In order to measure carbonates for oxygen and carbon stable light isotope data, the double needle set up was used in the GasBench, which allowed one sample to be dosed with phosphoric acid while simultaneously measuring the oxygen and carbon stable light isotopes of another sample (Figure 3.2). Prior to this, each sample was flushed with 100 ml of helium for five minutes, in order to remove all air in the sample vials, and to allow for equilibration. Following this, one needle automatically transported phosphoric acid into a sample vial, while another needle sampled gas from the headspace of one of the sample vials (Figure 3.2). In order for the CO_2 in the sampling vials dosed with acid to equilibrate, it was necessary to wait one hour. Samples were run twice, as the first run did not reproduce well. Raw data reproduced as a chromatograph, and values were automatically entered into Microsoft Excel. The oxygen and carbon stable light isotope data were analysed together and against each other in order to establish any correlations.

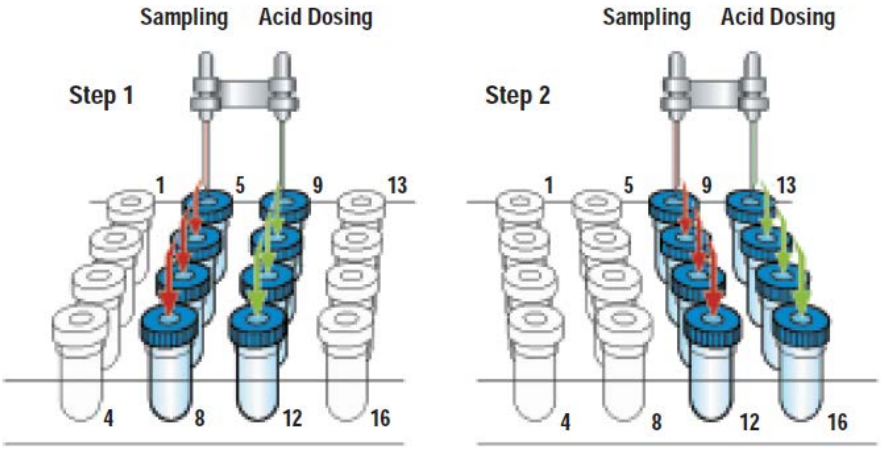

Fig. 3.2: Simplified diagram showing the sample vial set up in the autosampler trays, as well as the double needle set up. (Thermo-Fischer Scientific, 2014).

3.3.2 Drip Water Analysis

328 drip water samples were sent to the Hydrogeology Research Laboratory at the School of Geoscience at the University of Witwatersrand for oxygen stable light isotope analysis (Appendix C), and to a water laboratory at the Department of Archaeology, Geography and

Environmental Science at the University of the Witwatersrand for hydrochemical analyses (Appendix F).

Oxygen stable light isotope analysis of the drip water samples was conducted using an LGR Liquid Water Isotope Analyser model 45-EP. This equipment makes use of cavity enhanced absorption spectrometry, where laser absorption is measured within a cavity with mirrors boasting high reflectivity in order to generate paths of several kilometres (Aggarwal et al., 2009). This results in the lines of laser absorption from various water molecules being clearly separated and distinguishable, and results in an increase in measured absorption compared to other technical systems. The results produced from this equipment display high signal to noise ratios, and therefore precise isotopic measurements (Aggarwal et al., 2009). Overall, the equipment consists of a laser analysis system with an internal computer, a liquid autosampler and autosampler tray, a small membrane vacuum pump, and an intake line that passes air through a Drierite column for the removal of moisture (Aggarwal et al., 2009). During sample preparation, 0.75 µL of sample was injected through a PTFE septum in the autosampler using a Hamilton microliter syringe. The autosampler injection port is heated to 46°C, in order to vaporize the sample during injection under vacuum conditions. This vapour is then transported down the transfer line into the mirrored laser analysis chamber. One millilitre of each standard and sample is pipetted into a 2 ml marked glass vial placed in the autosampler tray in the correct position, and sealed with a PTFE cap. Typically, three in-house reference materials for the analysis of oxygen stable light isotopes in water samples are used for this analysis. In the first position on the autosampler tray, a blank sample is placed. Position two is held by the heavy isotope calibration reference material, position three by the light isotope calibration reference material, and position four by the control reference material. The next five to nine positions are then for the water samples to be placed in the autosampler tray. Positions 10 to 12 are then again filled by the three reference materials used, followed by five of the water samples, and then the three reference materials again, until all the water samples have been placed on the autosampler tray. The maximum number of positions which may be occupied per run is 52, with an extra 53rd sample included, which will be de-ionised water to clean the syringe after the sample analysis (Aggarwal et al., 2009). Before the run begins, the autosampler septum is checked to see whether a replacement is needed, which occurs every 325 injections. Typically, a run of 53 samples requires 318 injections. The active Drierite level in the column of the equipment is also checked, in order to insure that there is sufficient Drierite for the run (Aggarwal et al., 2009). The spectrum of the laser is also checked, in order to ensure that the correct absorption spectrum and absorption peak is within the shaded area on the plot displayed

(Aggarwal et al., 2009). After these checks, analysis of the samples in the autosampler tray is initiated.

The standard deviation for the oxygen isotope values produced from the drip water samples was calculated in order to determine the reliability of the results, and these oxygen isotope results were compared to the δ^2H values measured from the drip water samples, and both data sets were analysed against one another, in comparison to the Global Meteoric Water Line, in order to assess the suitability of the isotope results for interpretation. The δ^2H and $\delta^{18}O$ data produced from each sample was used to plot the samples relative to the Global Meteoric Water Line, calculated using the equation $\delta^2H = 8\ \delta^{18}O + 10‰$ (Craig, 1961), in order to deduce whether the sample data followed a similar trend compared to the Global Meteoric Water Line. A positive correlation between the sample data and Global Meteoric Water Line would indicate the suitability of the sample data for further interpretation.

3.3.3 Hydrochemical Analysis

Hydrochemical analyses were personally conducted on the drip water samples at a laboratory at the Department of Archaeology, Geography and Environmental Sciences, University of the Witwatersrand. The samples underwent pH and electro-conductivity analyses using a YSI Professional Plus hydrochemical probe (Appendix F). For pH analyses (Thermo-Fischer Scientific, 2014), the probe was calibrated by using two Fluka pH buffer reference materials, one with a pH of 7 at 20°C and another with a pH of 4 at 20°C. Each pH buffer was poured into separate beakers, and the probe was dipped into each pH buffer solution for approximately three minutes. The probe was rinsed with tap water and de-ionised water between calibrating with each pH buffer. The probe recorded a pH of 7.13 for the first pH standard, and a pH of 4.29 for the second pH standard. After this calibration, the probe was rinsed with tap water and finally de-ionised water again. For electro-conductivity analyses, the probe was calibrated using a standard conductivity solution measuring 1413 µS/cm at 25°C. The conductivity solution was poured into a 20 ml tube, and the probe was dipped into this tube for approximately one minute. The probe produced a reading of 1446 µS/cm, due to factoring in the ambient room temperature of 26.5°C as the conductivity is temperature dependent.

One set of drip water samples from each month for a period of 14 months (July 2015 to August 2016) was then selected, and the probe was used to measure the electro-conductivity and pH of each sample. Some of the drip water from each sample was poured into a 20 ml tube, and the probe was dipped into this tube for two minutes to allow for the pH reading to settle, and

one minute for electro-conductivity. The probe and tube was rinsed with tap water and de-ionised water after each sample analysis was complete.

3.4 Calibration and Correction

All speleothem samples were calibrated according to similar analyses performed on standards of known isotopic composition. Two in-house standards, namely CSS and MHS1 were used by iThemba Labs, Gauteng, in order to calibrate the data and determine correction factors. Both of these standards are measured relative to PeeDee Belemnite (PDB) (Table 3.3). PDB is a reference standard used particularly in palaeotemperature studies with regard to variations in oxygen and carbon isotopes in calcite materials (Epstein et al., 1953; Craig, 1965; Gonfiantini et al., 1995), and thus is a particularly useful reference material for the standards used in the oxygen and carbon stable light isotope analyses conducted on the modern speleothem samples. PDB comprises $CaCO_3$ from the rostrum of a belemnite from the Cretaceous period, discovered in the Peedee Formation in South Carolina (Gonfiantini et.al., 1995). The CO_2 produced from PDB by treatment with 100% phosphoric acid at 25°C is used as the reference standard for oxygen and carbon isotope variations in calcite and aragonite, as PDB exhibited similar $^{18}O/^{16}O$ ratios as that of calcium carbonate precipitated in thermodynamic equilibrium in modern ocean water at 16.5°C (Epstein et al., 1953; Craig, 1965; Gonfiantini et al., 1995). The CSS and MHS1 standards were chosen for this analysis as they display a large range of negative values for ^{13}C and ^{18}O, which allow for the accurate calibration of speleothem sample results relative to PeeDee Belemnite (PDB) (Vaks et al., 2003; Mattey et al., 2008).

The mean and standard deviation of the ^{13}C and ^{18}O values for each standard used was calculated in order to calibrate samples, and to measure an error range on the sample data respectively. The raw data produced from the stable light isotope analysis of the standards was analysed against the expected values for carbon and oxygen stable light isotopes for the two standards (provided by iThemba Labs, Gauteng) in Microsoft Excel, and two trend lines were produced using these data for the oxygen and carbon isotope standards respectively, using the equation $y = 0{,}9963x - 0{,}1318$ for carbon isotopes, and $y = 1{,}0297x - 16{,}993$ for oxygen isotopes. These trend lines were used to calibrate the data, and the equation for these trend lines were used to correct the data produced. This was done in order to ensure that the results produced from the oxygen and carbon stable light isotope analysis of the speleothem samples are accurate, and so that any outlier results may be correctly identified, and that skewing of results due to equipment drift may be explained. In order for these trend

lines to be meaningful for the calibration of the rest of the sample results, it is necessary for the values of the standards to cover a wide range of values (Mattey et al., 2008).

The difference between the values obtained for the measured and expected results were used as a measure of the drift of the GasBench equipment (Thermo Electron Corporation, 2004). Oxygen and carbon isotope values were reported in per mil (‰) relative to the PeeDee Belemnite scale for the speleothem samples, and the oxygen isotope values will be reported relative to Vienna Standard Mean Ocean Water (VSMOW) for the drip water samples.

Table 3.3: In-house standards used during the oxygen and carbon stable light isotope analysis of the speleothems.

Standards Relative to PDB		
	CSS	MHS1
^{13}C	-6.80	-2.82
^{18}O	-8.20	-14.60

All drip water samples were also calibrated according to similar analyses performed on in-house reference materials of known isotopic composition, provided by the Hydrogeology Research Laboratory in the School of Geoscience, at the University of Witwatersrand (Table 3.4). Five in-house standards provided by the Hydrogeology Research Laboratory were used in order to calibrate the data and determine correction factors. The Liquid Water Isotope Analyser equipment automatically calibrates itself using these reference materials, and then proceeds with the oxygen isotope analysis. The equipment produces results with a precision of approximately 1 ‰ for δ^2H and 0.2 ‰ for $\delta^{18}O$ in liquid water samples of up to at least 1000 mg/L dissolved salt concentrations. The standards used during the analysis of the drip water samples are tabulated in Table 3. These standards were chosen by the Hydrogeology Research Laboratory due to the very large range of both positive and negative values for hydrogen and oxygen. This large range allows for the accurate calibration of drip water sample results relative to Vienna Standard Mean Ocean Water (VSMOW) (Mattey et al., 2008). The mean and standard deviation of the hydrogen and oxygen isotope values for each standard used was calculated in order to calibrate samples, and to measure an error range on the sample data respectively (Mattey et al., 2008). The raw data produced from the stable light isotope analysis of the standards was analysed against the expected values for hydrogen and oxygen stable light isotopes for the five standards (provided by the Hydrogeology Research

Laboratory, University of the Witwatersrand) in Microsoft Excel, and trend lines were produced using these data for the oxygen and hydrogen isotope standards. These trend lines were used to calibrate the data, and the equations for these trend lines were used to correct the data produced. This was done in order to ensure that the results produced from the oxygen and hydrogen stable light isotope analysis of the speleothem samples are accurate, and so that any outlier results may be correctly identified, and that skewing of results due to equipment drift may be explained. In order for these trend lines to be meaningful for the calibration of the rest of the sample results, it is necessary for the values of the standards to cover a wide range of values (Mattey et al, 2008). All oxygen stable light isotope data produced from the analysis of the drip water samples was reported in per mil (‰) relative to VSMOW. VSMOW is an oxygen and hydrogen isotope ratio primary reference water sample distributed in order to enable the calibration of $^{2}H/^{1}H$ and $^{18}O/^{16}O$ ratio variations, and has an isotopic composition very similar to the Standard Mean Ocean Water (SMOW) described by Craig (1961). The VSMOW reference samples were produced by mixing distilled water from the Pacific Ocean collected at a latitude of 0° and longitude of 180° with smaller amounts of additional water samples until the desired $^{18}O/^{16}O$ isotopic composition was obtained (Gonfiantini et al., 1995). VSMOW is currently the main calibration reference material for hydrogen and oxygen isotopic ratio variations in natural compounds (Gonfiantini et al., 1995).

Table 3.4: In-house standards used during the oxygen stable light isotope analysis of the drip water samples. Columns are represented by the letter ‘C’.

Reference Materials Relative to VSMOW					
Autosampler Positions	5C	4C	3C	2C	1C
^{2}H (‰)	-9.2 ±0.5	-51.6 ±0.5	97.3 ±0.5	-123.7 ±0.5	-154±0.5
^{18}O (‰)	-2.69±0.15	-7.94±0.15	-13.39±0.15	-16.24±0.15	19.49±0.15

In order for the oxygen stable light isotope data from the drip water samples to be referenced to VSMOW correctly, VSMOW/VSLAP (Vienna Standard Light Antarctic Precipitation) scaling needed to be performed. VSLAP is a water reference material for $^{17}O/^{16}O$, and is considerably depleted with regards to heavy isotopes in comparison to VSMOW. The isotopic composition of VSLAP in comparison to VSMOW is defined by the values

$\delta^2H = -428.0‰$, $\delta^{18}O = -55.50‰$, which are used to fix the δ^2H and δ^{18}O scales (Gonfiantini et al., 1995). VSMOW/VSLAP scaling is needed in order to normalize the experimental fractionation factors of hydrogen and oxygen isotopes, and is performed using the equation $\delta = ((R_{SAMPLE} / R_{VSMOW}) - 1) \cdot \delta_{VSMOW} / ((R_{VSLAP} - R_{VSMOW}) / R_{VSMOW})$ (Gonfiantini et al., 1995), where *R* is the measured isotopic ratio of D/H (O^{18}/O^{16}).

In order to do this, two reference water samples of differing compositions were also included in the analysis of the drip water samples. The scaling factor produced was 0.9946 for this system (Hilkert & Avak, 2008).

3.5 Statistical Analyses and Correlation

All correlations, similarities and trends were statistically analysed using PAST v3.14 software. Pearson product-moment correlation tests were performed on all data sets requiring the analysis of correlations and trends. Tests were performed on δ^{18}O values from the modern speleothem and drip water samples, as well as on the temperatures calculated from the modern speleothem and drip water samples using equation 1 and equation 2 in comparison to the measured average monthly atmospheric temperatures. Pearson product-moment correlation tests were also conducted on the calculated temperatures in comparison to the measured cave air temperatures and the calculated idealised temperatures. The calculated idealised cave air temperatures and the measured cave air temperatures were analysed together using a Chi-squared statistical test. The drip rates were analysed using the Pearson product-moment correlation test, as well as the monthly measured average rainfall and drip water δ^{18}O values versus the drip rates. The drip water δ^{18}O values were also analysed in this manner in comparison to the monthly measured average rainfall. Pearson product-moment correlation tests were also conducted for humidity and atmospheric pressure.

The Pearson product-moment correlation test assumes a normal distribution for all data, and is a parametric test for correlation (Hammer et al., 2001). A Shapiro-Wilk normality test was conducted on the data sets using PAST v3.14, producing p values of <0.9 which indicates a normal distribution of data (Hammer et al., 2001). The Pearson product-moment correlation test produces Pearson correlation coefficient values (*r*), which range in value from +1 to -1. A value of 0 indicates no correlation between the data sets. A value greater than 0 indicates a progressively positive correlation relationship towards +1 between data sets, and a value less

than 0 indicates a progressively negative correlation relationship or inverse relationship towards -1 between data sets. The value of *r* indicates the amount of variation of the data around a calculated line of best fit for the data sets, and indicates the strength of correlation between data sets (Table 3.5) (Hammer et al., 2001). A confidence level of 90% was used for these statistical analyses.

Table 3.5: Classification of r values according to strength of correlation between data sets (Adapted from Hammer et al., 2001).

	Correlation Coefficient, *r*	
Strength of Correlation	Positive	Negative
Weak	0.1 to 0.3	-0.1 to -0.3
Intermediate	0.3 to 0.5	-0.3 to -0.5
Strong	0.5 to 1.0	-0.5 to -1.0

The Chi-squared statistical test is a non-parametric test used to determine the independence of two variables, and to determine significant differences between observed and expected data sets (Hammer et al., 2001). This statistical test uses a confidence level (p) of 95%. The p value indicates the probability of producing the observed results, when the null hypothesis is true. If the p value is greater than the confidence level of 0.05, the null hypothesis for the test is considered to be true, and no significant differences between data sets are noted. (Hammer et al., 2001)

3.6 Data Analysis

3.6.1 Temperature

Oxygen stable light isotope data from the speleothem samples were analysed using Microsoft Excel and PAST v3.14 software in order to determine general temperature trends and correlations. The measured data were used to calculate an idealised temperature at which these speleothems precipitated, and therefore idealised temperatures for the cave environment over a period of 14 months (July 2015 to August 2016). This can be done by assuming that no fractionation has occurred during the precipitation of the speleothem from the drip water solution. Two different equations were used in the calculation of temperatures using the oxygen stable light isotope data –the empirically determined speleothem temperature equation

$T℃ = 16.9 - 4.2(\delta_c - \delta_w) + 0.13\ (\delta_c - \delta_w)^2$ (eq1), (Epstein et al., 1953; Kim & O'Neil, 1997; Schwarcz, 2007; Lachniet, 2009; Feng et al., 2014), where T is temperature (K), δ_c is oxygen isotope value from the solid calcite, and δ_w is the oxygen isotope value from drip water,

and the widely used experimentally determined speleothem temperature equation

$10^3 \ln\alpha = 2.78(10^6 T^{-2}) - 2.89$ (eq2) (Epstein et al., 1953; Kim & O'Neil, 1997; Schwarcz, 2007; Lachniet, 2009; Feng et al., 2014), where α is the fractionation factor and T is temperature (K). The fractionation factor α was calculated using the equation $\alpha_{c-w} = \frac{\delta_{calcite}}{\delta_{water}}$ (eq3) (Epstein et al., 1953; Coplen, 1996; Kim & O'Neil, 1997; Lachniet, 2009; Feng et al., 2014).

In order to produce an idealised result assuming no fractionation, the δ_{water} value was calculated by simply using the speleothem stable oxygen isotope data and converting this data to values relative to VSMOW, using the equation

$\delta^{18}O_{VSMOW} = 1.03086(\delta^{18}O_{PDB}) + 30.86$ (eq4) (Friedmann & O'Neil, 1977; Schwarcz, 2007; Lachniet, 2009; Feng et al., 2014). The results from the two temperature equations (Appendix E) were compared to one another, and to the measured cave air temperature measured during the collection of the speleothem samples using Pearson's product-moment correlation test, in order to determine which equation produces the most accurate and reliable results. The results were then graphed for analysis of the data, in order to determine trends and correlations within the data.

Oxygen isotopes measured from drip water samples were used in conjunction with the oxygen isotope data measured from the speleothem samples to determine the real temperature at which the speleothems formed, and to determine to what extent fractionation had occurred. Outliers in the oxygen isotope data were identified and removed using two methods. All oxygen isotope values lying outside the standard deviation of the mean were considered outliers and removed, as these results plotted far from the local meteoric water line, and indicate the presence of significant kinetic fractionation effects (Talma & Vogel, 1992; Fleitmann et al., 2004). Oxygen isotope values lying outside of the interquartile range (IQR) were also considered outliers and removed from the data set. These two methods were used simultaneously, as the standard deviation for the data and the IQR were very similar (Table 3.6).

Table 3.6: Statistical data for the modern drip water oxygen isotope values.

Mean	-2.34719
Standard deviation	1.901663
Median	-2.657103
25th Percentile (Q1)	-3.543593
75th Percentile (Q3)	-1.575095
Interquartile Range (IQR) (Q3-Q1)	1.968498

Equation 1 (eq1) and equation 2 (eq2) were used to determine the temperature from these oxygen isotope values (Appendix E). The oxygen isotopes from the speleothems were measured relative to PDB, and represent δ_c, while the oxygen isotopes measured from the drip water samples were measured relative to VSMOW and represent δ_w. Fractionation factors were determined beforehand using equation 3 (eq3). The temperature data produced using these equations over a period of 14 months (July 2015 to August 2016) were analysed along with the idealised temperature data produced from the speleothem oxygen isotopes, the measured cave atmospheric temperatures, and with the measured atmospheric temperatures obtained from the weather stations. The temperature data produced was compared to the measured atmospheric temperatures in order to determine the correlation of variations between the two data sets. This allowed for the variations between the two data sets to be accounted for, as temperatures calculated from the $\delta^{18}O$ values of the drip water include a range of temperatures which should resemble the variations of the mean annual temperature on the surface (Nordhoff, 2005; Mandice et al., 2013). This comparison also allowed for an analysis of the level of seasonality within the two data sets, as well as the level of openness of the cave system.

The extent of the effects of the exterior temperatures to the measured cave air temperatures, speleothem precipitation, and hydrochemistry within the cave system was also analysed using the comparison between the calculated temperatures, measured cave air temperatures, and the measured atmospheric temperatures. Correlations, trends and similarities were then drawn between the three data sets using Pearson's product-moment test for correlation.

Fractionation factors (α) between the oxygen stable light isotope data from the speleothem samples and the drip water samples were determined prior to temperature calculations using

equation 3. These fractionation factors were used to assess to what extent fractionation has played a part in the precipitation of the speleothems, and to what degree it has overprinted and obscured the oxygen isotope signatures used in the calculation of the temperatures.

All of the temperature data sets produced were then analysed against regional modern day records of climatic data from the Johannesburg Botanical Gardens Weather Station, and Lanseria Weather Station, in order to assess how well these data compare to the regional records, and whether there were any significant trends or correlations. The data sets underwent the same statistical analyses as for the temperature data sets.

The calculated temperature data from the idealised calculations and from the calculations incorporating the measured stable oxygen isotope values for speleothems and drip water were then compared to annual atmospheric temperatures measured at the Johannesburg Botanical Gardens Weather Station weather station and the Lanseria Weather Station (Figure 3.3) from 2006 to 2016. The Lanseria Weather Station is significantly closer to the Sterkfontein Caves site, compared to the Johannesburg Botanical Gardens Weather Station (Figure 3.3), and therefore should represent the atmospheric temperatures for Sterkfontein more accurately. However, as the Lanseria Weather Station is not exactly at the Sterkfontein Caves site, it may be limited by some variation between the atmospheric temperatures at Sterkfontein deduced from the oxygen isotope values, and the measured atmospheric temperatures from these weather stations, due to varying climatic conditions, as the variation between the two temperature data sets may result in unreliable correlations. The Johannesburg Botanical Gardens Weather Station should show some variation with regard to atmospheric temperatures compared to the Lanseria Weather Station. These data sets were analysed together using Pearson's product-moment test for correlation in order to determine any trends and correlations between the data sets, as was done for the initial temperature data, and therefore to determine the accuracy of the temperatures obtained from the oxygen stable light isotope data of the speleothems and drip water in mirroring atmospheric temperatures. This comparison allows for the resemblance of variations between the produced temperatures and the measured atmospheric temperatures to be analysed and accounted for, as temperatures measured from the $\delta^{18}O$ values of the drip water include a range of temperatures which resemble the variations of the mean annual temperature on the surface (Nordhoff, 2005; Mandice et al., 2013). It also allows for a comparison between the seasonality shown by the measured atmospheric temperatures and the seasonality deduced from the calculated temperatures. This provides insight into whether modern speleothems can be used to indicate

modern climatic conditions, and therefore whether fossil speleothems would be reliable indicators of palaeoclimates.

3.6.2 Precipitation

The oxygen stable light isotope data from drip water samples was used to deduce the amount and general type of precipitation which had occurred during a period of 14 months (July 2015 to August 2016) over which the samples were collected, based on whether the oxygen isotopes were depleted or not. The oxygen stable light isotopes from the speleothem samples were analysed in the same manner, but on a broader time scale. These data sets were then compared to the measured precipitation for the Cradle of Humankind for this time period obtained from the weather stations from Krugersdorp, the Johannesburg Botanical Gardens, and Lanseria (Figure 3.3). The Krugersdorp and Lanseria Weather Stations are significantly closer to the Sterkfontein Caves site, with the Krugersdorp Weather Station being in closest proximity to Sterkfontein (Figure 3.3). These weather stations should therefore represent the precipitation for Sterkfontein more accurately, however, as they are not exactly at the Sterkfontein Caves site, there may be limited by some variation between the precipitation at Sterkfontein represented by the oxygen isotope values, and the measured precipitation from these weather stations. The Johannesburg Botanical Gardens Weather Station should show some variation with regard to precipitation amount and intensity compared to the other two stations, as this station is limited due to its' distance with regards to the other two, and therefore is used comparatively only. The Krugersdorp and Johannesburg Botanical Gardens Weather Stations provide precipitation data from 2006 to 2016, while the Lanseria Weather Station provides precipitation data from 2011 to 2016. The precipitation data represented by the oxygen stable light isotopes were analysed with the actual measured precipitation using Pearson's product-moment test for correlation, in order to determine trends and correlations, and to determine how accurate the oxygen isotopes were in reflecting precipitation. The rate of dripping of the drip water samples was also used as an indication of the amount of precipitation occurring during the collection of the drip water samples. This data was compared to the oxygen stable light isotope data using Pearson's product-moment test for correlation, in order to determine whether the data sets correlate with one another, and to what extent.

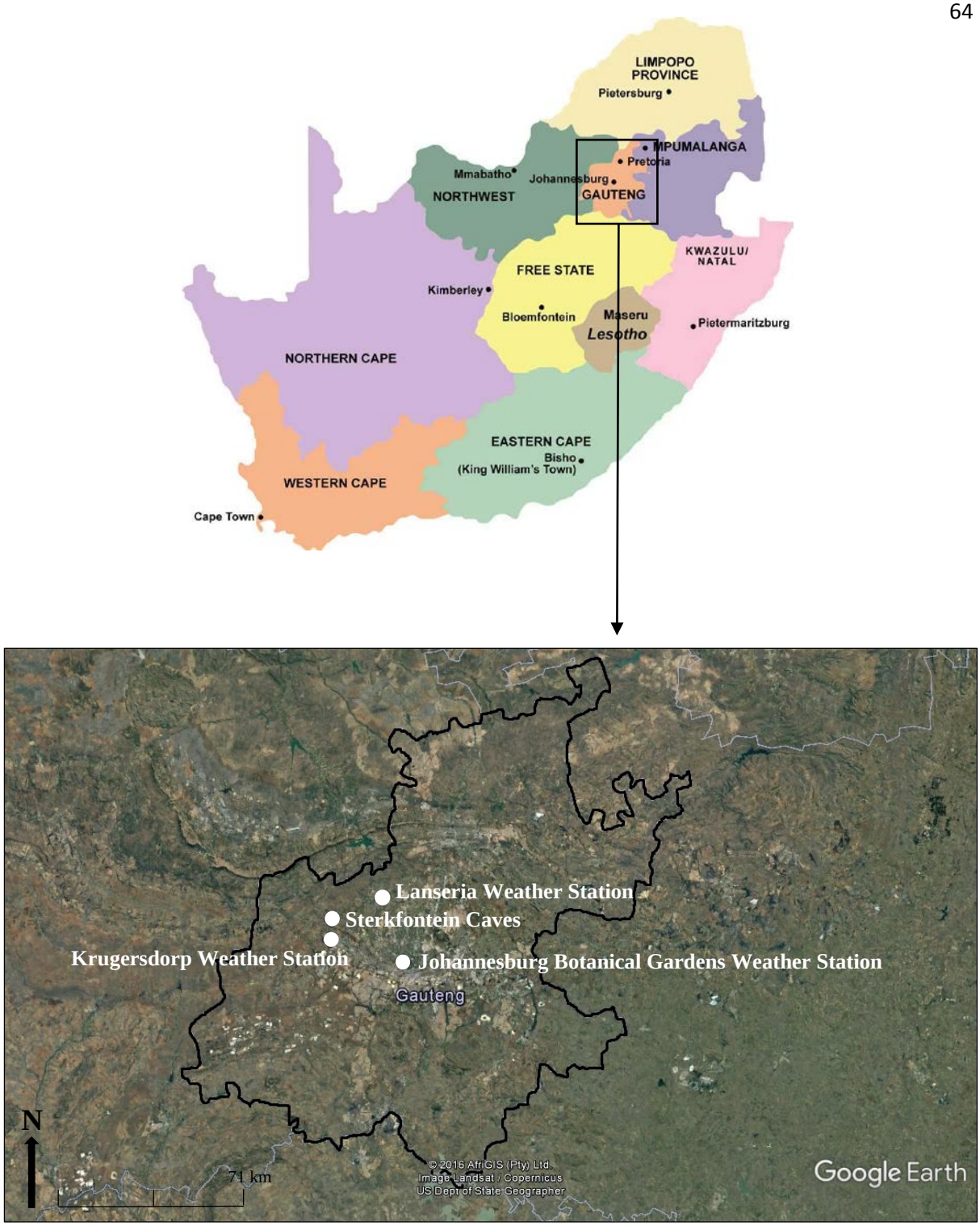

Fig. 3.3: Map of South Africa, showing the location of the province of Gauteng, and a map of Gauteng showing the locations of the three weather stations used. Map of South Africa from http://www.towns.bookingsouthafrica.com/.

3.6.3 Vegetation

Carbon stable light isotope data produced from the analysis of the modern speleothem samples at iThemba Labs were analysed and interpreted with regard to C_3 and C_4 vegetation,

with more depleted carbon isotope values on the graph indicative of the presence of C_3 vegetation, and the more enriched values indicative of the presence of C_4 vegetation. This data was used to calculate the dominance of the vegetation types on the overlying environment, using Talma and Vogel's (1992) estimate of 100% C_4 vegetation dominance being represented by a value of +1.2‰, and 100% dominance of C_3 vegetation being represented by a value of -12‰. These estimates were used to calculate percentages of C_4 and C_3 vegetation on the modern surface environment, from the carbon stable light isotope data obtained from the modern speleothem samples. The results of the modern vegetation distribution survey were compared to the percentages of C_4 and C_3 vegetation obtained from the carbon stable light isotope data in Microsoft Excel, in order to establish to what degree the vegetation information provided by the carbon stable light isotopes represented the actual vegetation on the modern surface environment.

3.6.4 Hydrochemistry

The samples were sent to the Hydrogeology Research Laboratory in the School of Geoscience at the University of the Witwatersrand for oxygen stable light isotope analyses. The samples were also sent to a hydrochemical analysis laboratory at the School of Geography, Archaeology and Environmental Studies at the University of the Witwatersrand in order to measure the pH and electro-conductivity of the samples.

Obtaining the pH and electro-conductivity of the drip water samples is important, as it provides information with regard to the chemistry of the drip water. pH is a measure of the concentration of hydrogen ions within the drip water, and may be either basic (pH > 7), neutral (pH=7) or acidic (pH<7) (Bates, 1973). A measure of the pH of the solution would provide a measure of how acidic or basic the solution is, and allow for the calculation of basic or acidic ions within the water solution (Bates, 1973). The electro-conductivity of the drip water is a measure of the water's ability to conduct electricity and is used to determine the ionic content of a solution. This is important, as it will enable the chemistry and exact nature of the drip water to be determined, as well as any dissolved solids within the water sample (Gray, 2004). All of these properties will allow the conditions under which the drip water formed to be established, which is crucial for accurate palaeoenvironmental analyses (Hendy, 1971; Ouelette, 2013).

Chapter 4

Results

The exterior climate of the Cradle of Humankind is described in Section 4.1, displaying precipitation and temperature data from the Lanseria, Johannesburg Botanical Gardens and Krugersdorp weather stations, as well as the observed vegetation specifically above the Sterkfontein Caves site. Section 4.2 provides details concerning the ambient cave climatic conditions for the Sterkfontein Caves, which includes the measured cave air temperature, relative humidity and atmospheric pressure. Section 4.3 describes the carbon and oxygen isotope results with regards to the modern speleothem samples, in context of vegetation distribution and temperatures. This is followed by Section 4.4, which describes the oxygen stable light isotope results of the modern drip water samples in terms of raw $\delta^{18}O$ values, temperature, fractionation and precipitation. Section 4.5 provides the results of the hydrochemical analysis of the modern drip water samples in terms of electro-conductivity and pH, and this is followed by a synopsis of the main results produced in Section 4.6.

4.1 Exterior Climate for the Cradle of Humankind

4.1.1 Atmospheric Temperatures

The monthly atmospheric temperatures from the Lanseria and Johannesburg Botanical Gardens weather stations from 2011 to 2016 and from 2006 to 2016 respectively show typical seasonal temperature cycles, which lie within a distinct range (Figures 4.1 and 4.2). This seasonal range of temperatures increases gradually towards 2016, with average lowest and highest temperatures increasing. This trend is the same for the temperatures from both the Lanseria and the Botanical Gardens weather stations.

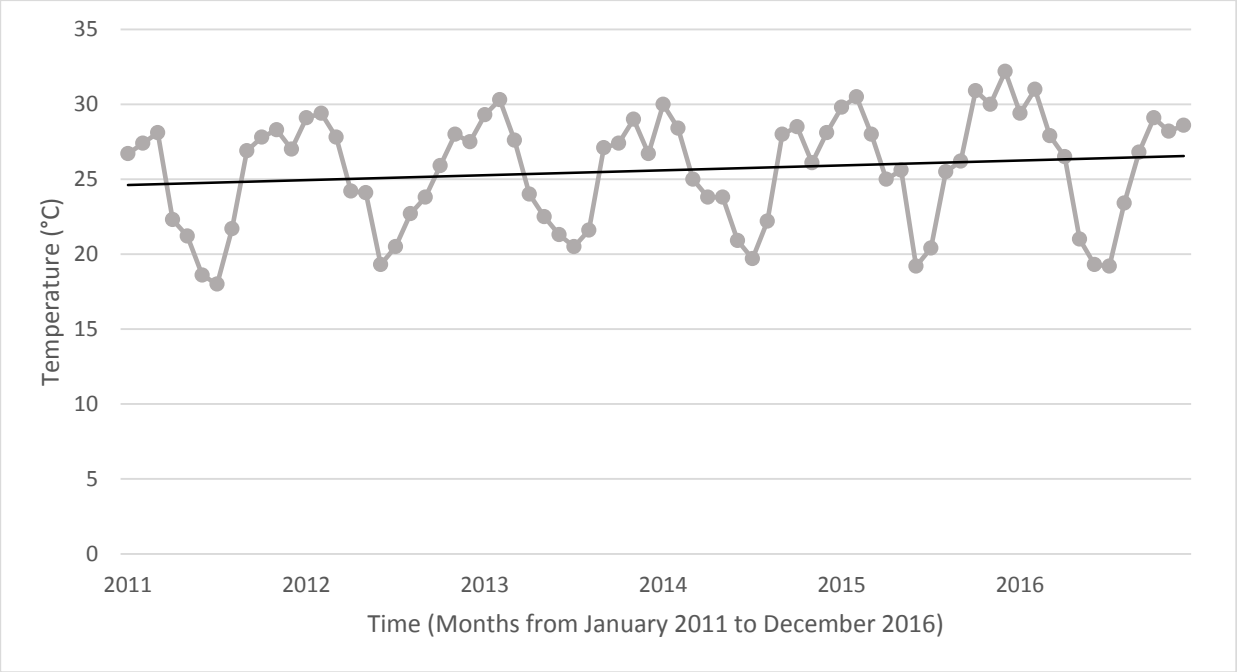

Fig. 4.1: Temperature record from 2011 to 2016 from the Lanseria Weather Station.

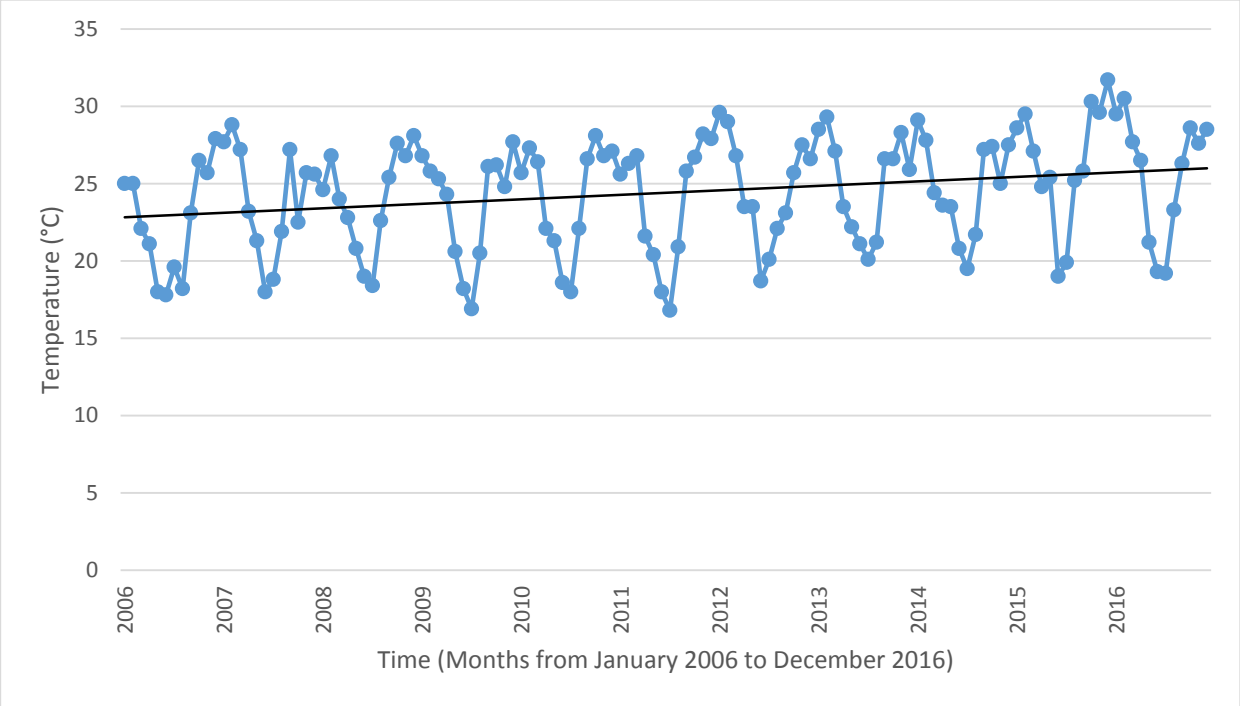

Fig. 4.2: Temperature record from 2006 to 2016 from the Johannesburg Botanical Gardens weather station.

4.1.2 Precipitation

Rainfall patterns for individual years generally follow expected yearly seasonal variations, with early to late summer rainfall. The amount and intensity of rainfall from 2006 to 2016 from Krugersdorp weather station and the Botanical Gardens weather station does not display any prominent trends and remains variable on a yearly scale (Figure 4.3). The year 2010 seemed to

receive a significantly increased amount of rainfall compared to the other years for the Botanical Gardens, as well as the year 2011 for Krugersdorp. The Botanical Gardens saw an increase in average rainfall from 2007 to 2010, followed by a decrease from 2011 to 2014. A slight increase occurs again from 2015 to 2016. Krugersdorp displays a decrease in rainfall from 2008 to 2010. There is an increase in rainfall again.in 2011, followed by a decrease from 2012 to 2013. The year 2014 saw an increase in rainfall, with a subsequent decrease in 2015 and 2016. Overall, Krugersdorp displays higher overall rainfall compared to the Johannesburg Botanical Gardens, especially during 2007, 2011 and 2013 to 2014, and has a smaller range of rainfall values compared to the Johannesburg Botanical Gardens weather station. This difference between the rainfall recorded by the two stations could be due to the distance between them (see Chapter 3, section 3.6.2). As the Krugersdorp weather station is situated closer to the Sterkfontein Caves site, the rainfall patterns from this weather station, especially for 2015 and 2016, should reflect the rainfall conditions at the Sterkfontein Caves site more accurately, and may be reflected in the $\delta^{18}O$ values produced from the modern drip water and speleothems, as well as the drip rates measured.

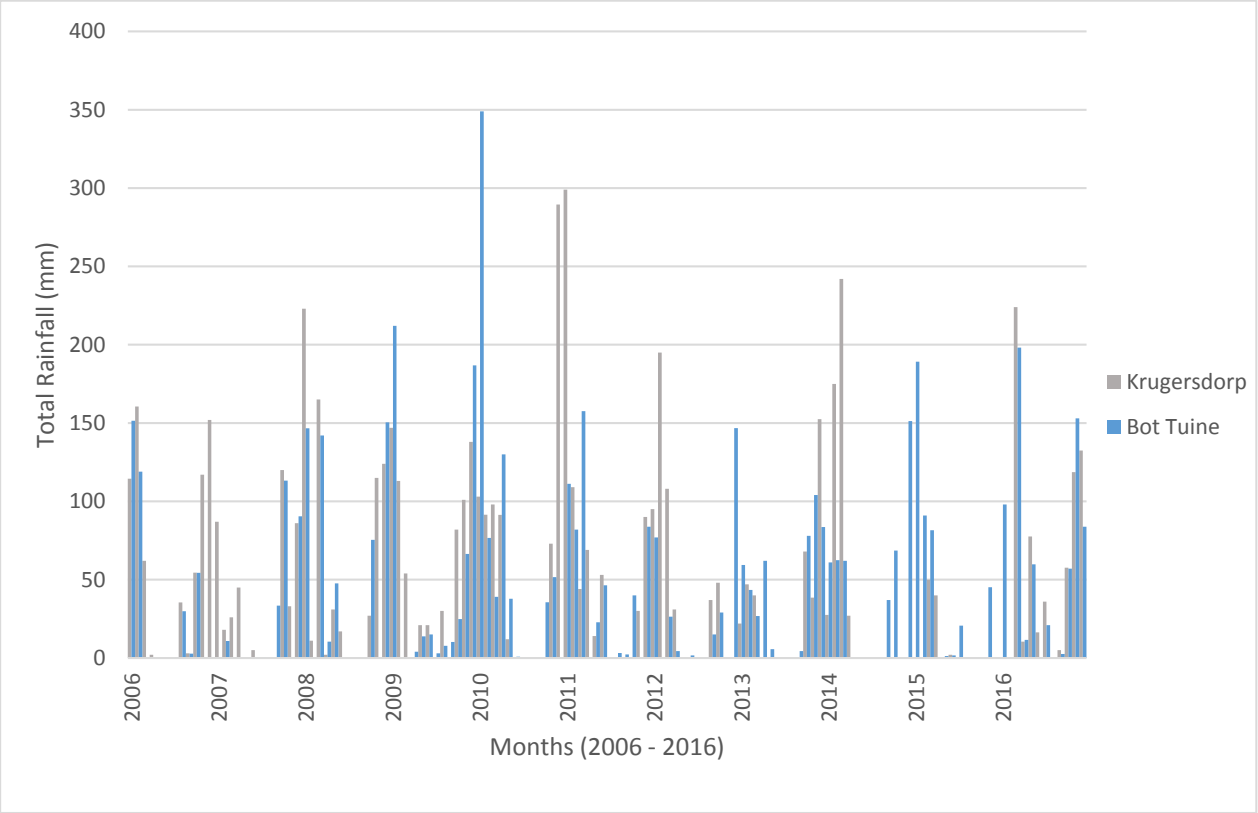

Fig. 4.3: Rainfall record from 2006 to 2016 from Krugersdorp and Johannesburg Botanical Gardens weather stations.

4.2 Cave Climatic Conditions

4.2.1 Measured Cave Air Temperature

The overall air temperature for the cave environment ranged from between 15.5°C to 24°C over the course of a year. Cave air temperatures were measured during the collection of drip water samples from the Jacovec Cavern, Antechamber 1 and Antechamber 2. Each chamber displayed its' own cave air temperature trend, however all three trends together displayed a very similar range, and similar variations within that range, at different magnifications (Figure 4.4). The trends displayed for the Jacovec Cavern and Antechamber 1 produced trends that were particularly close in similarity. There is an overall increasing trend for all three chambers from month 1 (July 2015) to month 5 (November 2015), with some variation for Antechamber 2 in month 2 (August 2015) and month 3 (September 2015). The cave air temperatures then decrease from approximately month 5 to month 7 (January 2016), followed by a short increase from month 7 to month 8 (February 2016), and then a gradual decrease from month 8 until month 13 (July 2016). A Pearson product-moment correlation test was conducted in PAST v3.14 software (Hammer et al., 2001) on the measured cave air temperature for the three chambers, and produced correlation values (r) of 0.66 to 0.87, showing strong positive correlations between the three data sets. Values for p averaged 0.0068 at a 90% confidence level (See Appendix B). These p values are within the confidence level of 90%, indicating that the results are statistically significant and therefore may be interpreted further.

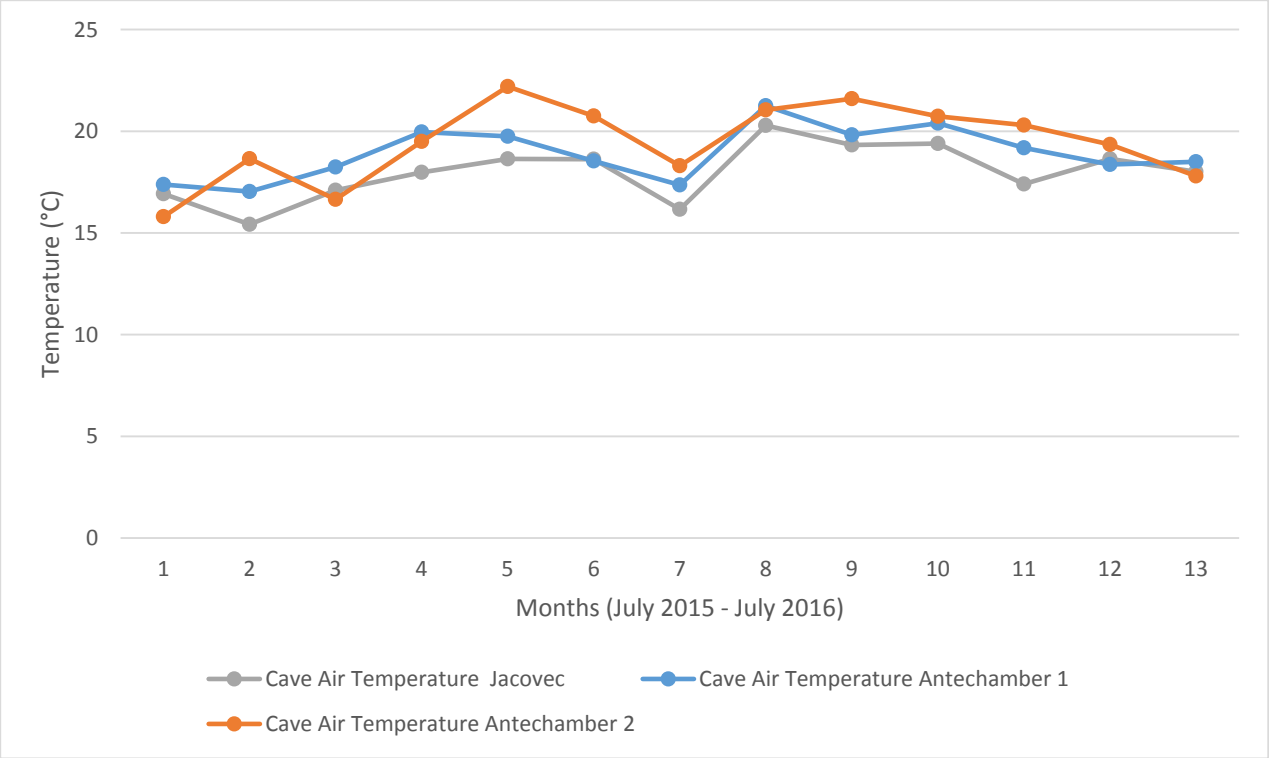

Fig. 4.4: Line graph displaying the cave air temperature trends measured from the Jacovec Cavern, Antechamber 1 and Antechamber 2.

Overall, the measured cave air temperatures reflect very similar trends to that displayed by the measured average atmospheric temperatures (Figure 4.5). The measured cave air temperatures show almost exactly the same increasing and decreasing trends, but slightly delayed compared to that of the measured average atmospheric temperature. The measured cave air temperatures are also consistently approximately 3°C to 4°C lower than that of the measured average atmospheric temperatures, which is to be expected in a karst environment. Pearson product-moment correlation tests were conducted in PAST v3.14 software (Hammer et al., 2001) on the measured cave air temperatures for the three chambers, and the average monthly atmospheric temperatures. A correlation value (*r*) of 0.19 was produced for the measured cave air temperatures from the Jacovec Cavern and the average monthly atmospheric temperatures, showing a weak positive correlation between the two data sets. The value for p was 0.54 at a 90% confidence level. A correlation value (*r*) of 0.38 was produced for the measured cave air temperatures from Antechamber 1 and the average monthly atmospheric temperatures, showing a weak to intermediate positive correlation between the two data sets. The value for p was 0.20 at a 90% confidence level. A correlation value (*r*) of 0.41 was produced for the measured cave air temperatures from Antechamber 2 and the average monthly atmospheric rainfall, showing an intermediate positive correlation between the two data sets. The value for

p was 0.16 at a 90% confidence level (See Appendix B). None of these p values however are within the confidence level of 90%, indicating that the results are not statistically significant and therefore may not be an accurate representation of the data.

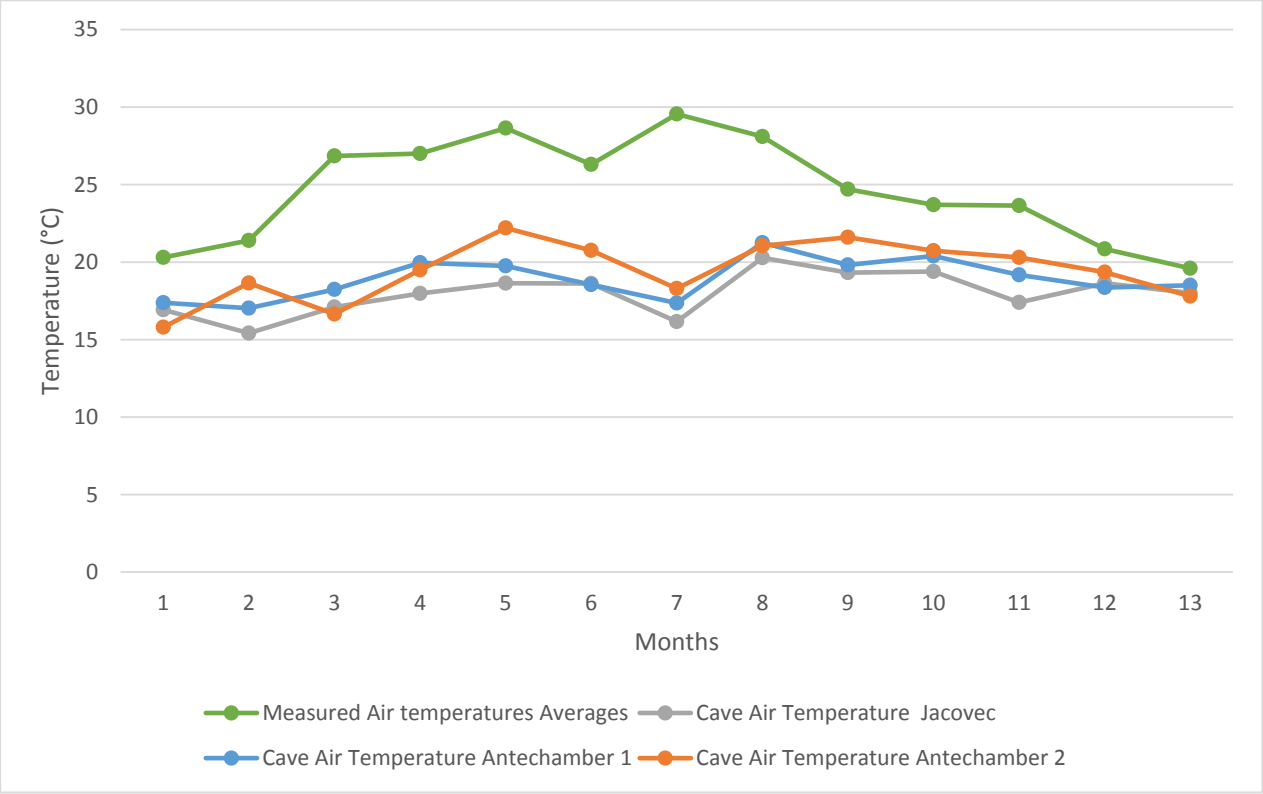

Fig. 4.5: Comparison of the measured cave air temperatures to the measured average atmospheric temperatures.

4.2.2 Humidity

The humidity of all three chambers remained intermediate to relatively high, ranging from 50% to 93% (Figure 4.6). The Jacovec Cavern and Antechamber 2 display the most variable humidity, with individual ranges of 50% to 93% and 52% to 89% respectively. This large range may be due to the differing locations of individual samples within the chambers, as those located deeper within the chambers produced higher individual humidity's, and those closer towards the entrances produced lower humidity's. The range of humidity for Antechamber 1 remained relatively high, varying between 69% and 93%. Overall, the humidity of each chamber increased from month 7 (December 2015) to months 10 to 11 (March to April 2016), and then began to decrease gradually until July 2016. The Jacovec Cavern and Antechamber 2 increased sharply between month 7 and 8 (December 2015 to January 2016), whereas Antechamber 1 increased gradually from month 5 (October 2015) up until month 10 (March 2016) (Figure 4.6). The Jacovec Cavern and Antechamber 2 also start to decrease towards

August 2016 slightly later than that of Antechamber 1, during months 11 to 12 (May to June 2016) A Pearson product-moment correlation test was conducted in PAST v3.14 software (Hammer et al., 2001) on the measured relative humidity for the three chambers, and produced correlation values (*r*) of 0.61 to 0.82, showing strong positive correlations between the three data sets. Values for p averaged 0.011 at a 90% confidence level (See Appendix B). These p values are within the confidence level of 90%, indicating that the results are statistically significant and therefore may be interpreted further.

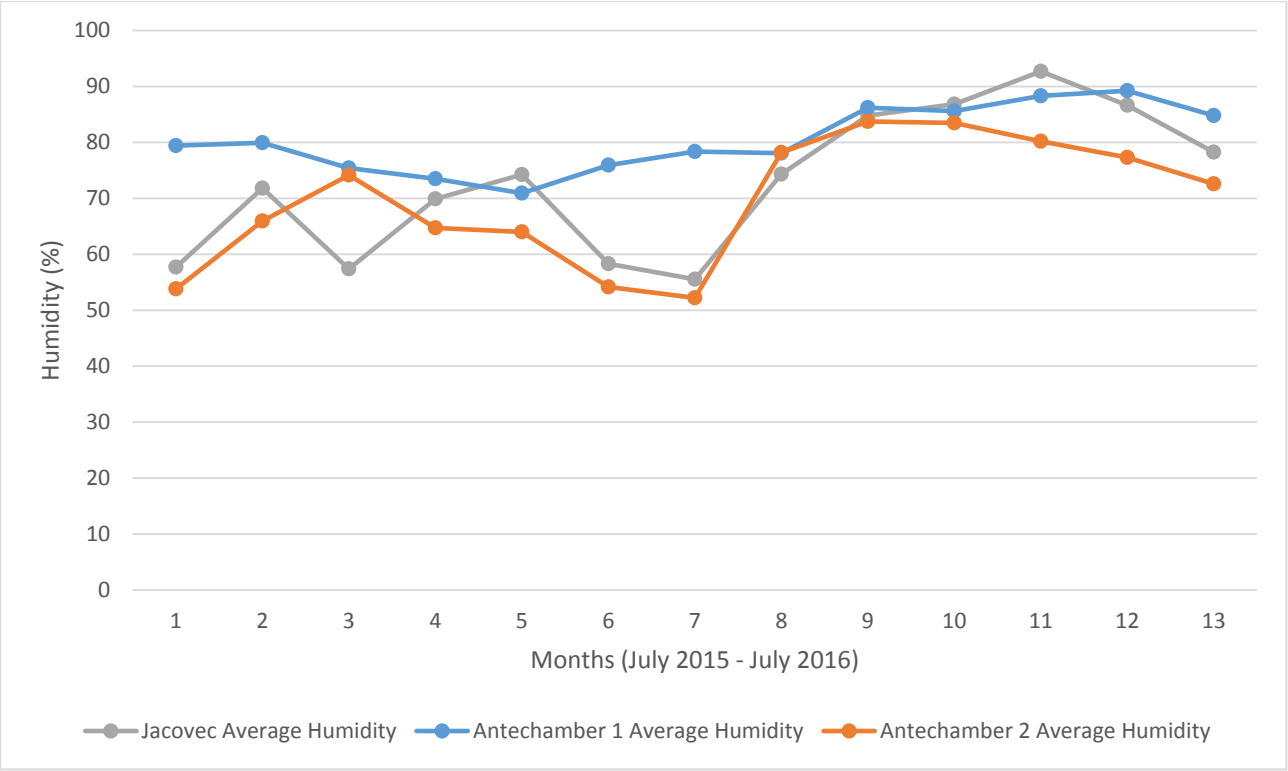

Fig. 4.6: Line graph displaying the humidity trends measured from the Jacovec Cavern, Antechamber 1 and Antechamber 2.

4.2.3 Cave Atmospheric Pressure

The atmospheric pressure for all three chambers varied very slightly throughout the duration of measurement (Figure 4.7). The range for the atmospheric pressure is 855 hPa to 867 hPa, which is a relatively small range. Variations occurring within the measured atmospheric pressure are mirrored by all three chambers, and are most probably influenced by smaller climatic events occurring on the exterior environment of the cave system. The atmospheric pressure seems to decrease slightly from July 2015 to December 2016 (fortnights 1 to 11), then gradually increase from January 2016 to August 2016 (fortnights 12 to 26). A Pearson product-

moment correlation test was conducted in PAST v3.14 software (Hammer et al., 2001) on the measured cave atmospheric pressure for the three chambers, and produced correlation values (*r*) of 0.991 to 0.997, showing very strong positive correlations between the three data sets. Values for p averaged 8.57 x 10^{-23} at a 90% confidence level (See Appendix B). These p values are within the confidence level of 90%, indicating that the results are statistically significant and therefore may be interpreted further.

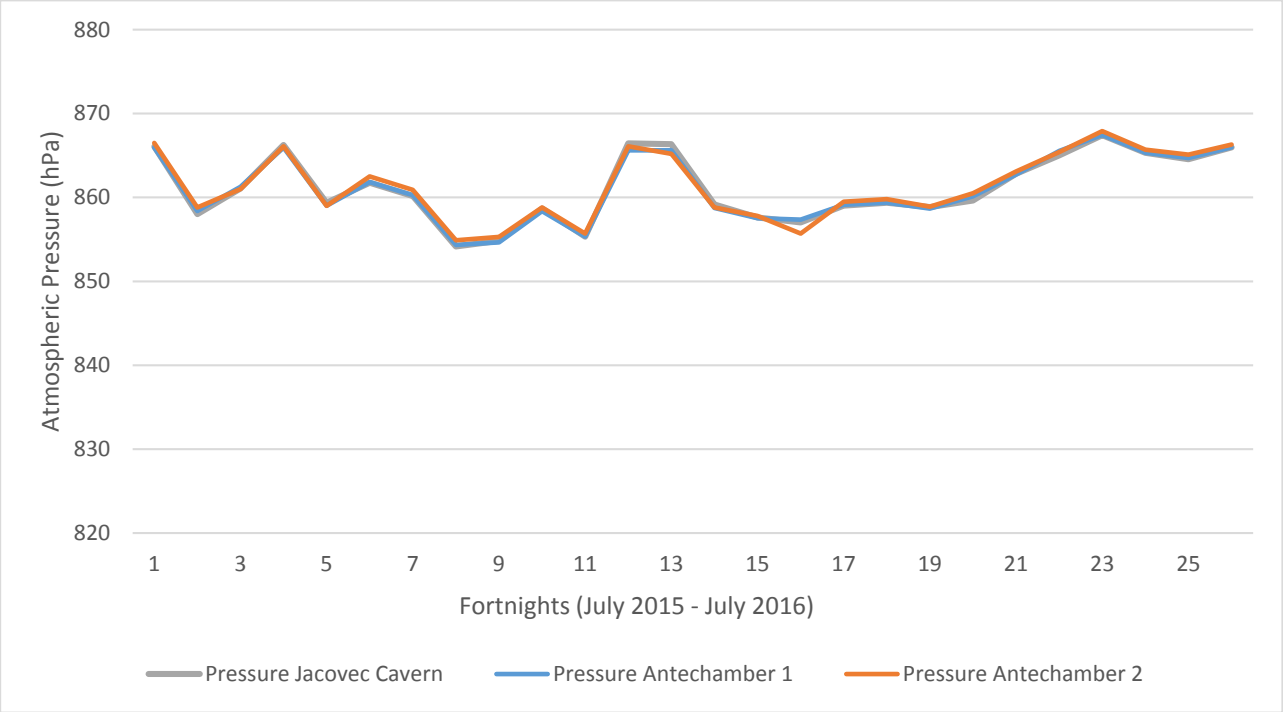

Fig.4.7: Line Graph showing the atmospheric pressure measured for the Jacovec Cavern, Antechamber 1 and Antechamber 2.

4.2.4 Vegetation

A general overview of the modern vegetation which currently exists above the Sterkfontein Caves system was conducted, in order to establish the distribution of different vegetation types in the modern environment (Figure 4.8A, B). In general, the observed vegetation types consisted of a large quantity of C_4 grasses, as well as some shrubs, trees and herbaceous plants. Grasses and small shrubs appeared to dominate the environment, with numerous trees dominating a few of the cave entrances and shafts. Some CAM succulents also occur, especially above the Jacovec Cavern area, but only in a very small percentage. The overall percentage of observed vegetation in the environment above the Sterkfontein Caves area is 75% C_4 vegetation, 24.5% C_3 vegetation and 0.5% CAM vegetation. Due to the combined

distribution of grasses, shrubs and trees, the environment can be described as a mosaic environment comprising mostly grasslands with patches of open woodland and shrubs.

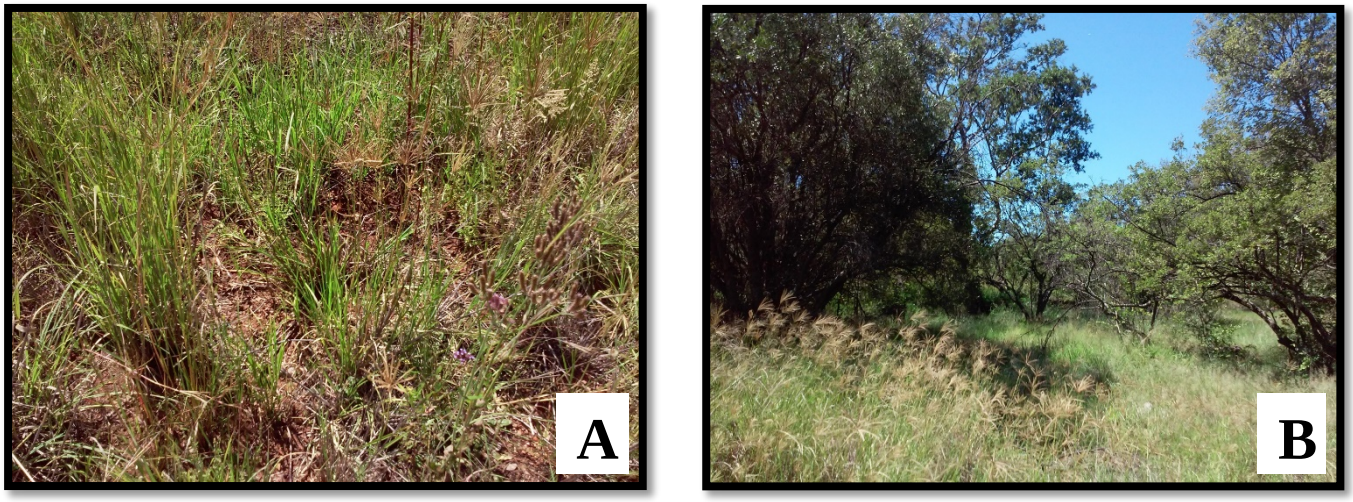

Fig. 4.8: (A) Photograph of some of the grasses and herbaceous plants present at the Sterkfontein site. (B)Overall view of some of the typical shrubs, grasses and trees present at Sterkfontein.

4.3 Speleothem Isotopes

Carbon and oxygen stable light isotope analysis was performed on the 16 modern speleothem samples (see Appendix C), in order to determine the degree to which kinetic fractionation has played a role during the precipitation of the speleothems, and to produce temperature and vegetation data regarding the surrounding environment above the Sterkfontein Caves system. This data was then compared to the modern environmental conditions outside Sterkfontein Caves, in order to determine the reliability of the modern speleothems as proxies of environmental data. Samples were collected at an altitude ranging from approximately 1441 m to 1453 m.

Figure 4.9 shows the spread of carbon and oxygen stable light isotope results for the speleothem samples from Sterkfontein Caves. These isotope results plot randomly and have no obvious linear trend; therefore it appears that kinetic fractionation has not played a great role during the precipitation of the calcium carbonate of the speleothems. This implies that kinetic fractionation has played no part in skewing the results and producing isotope results that cannot be used for palaeoenvironmental analysis, and that these isotope results are a fair representation of the environmental conditions outside the cave environment.

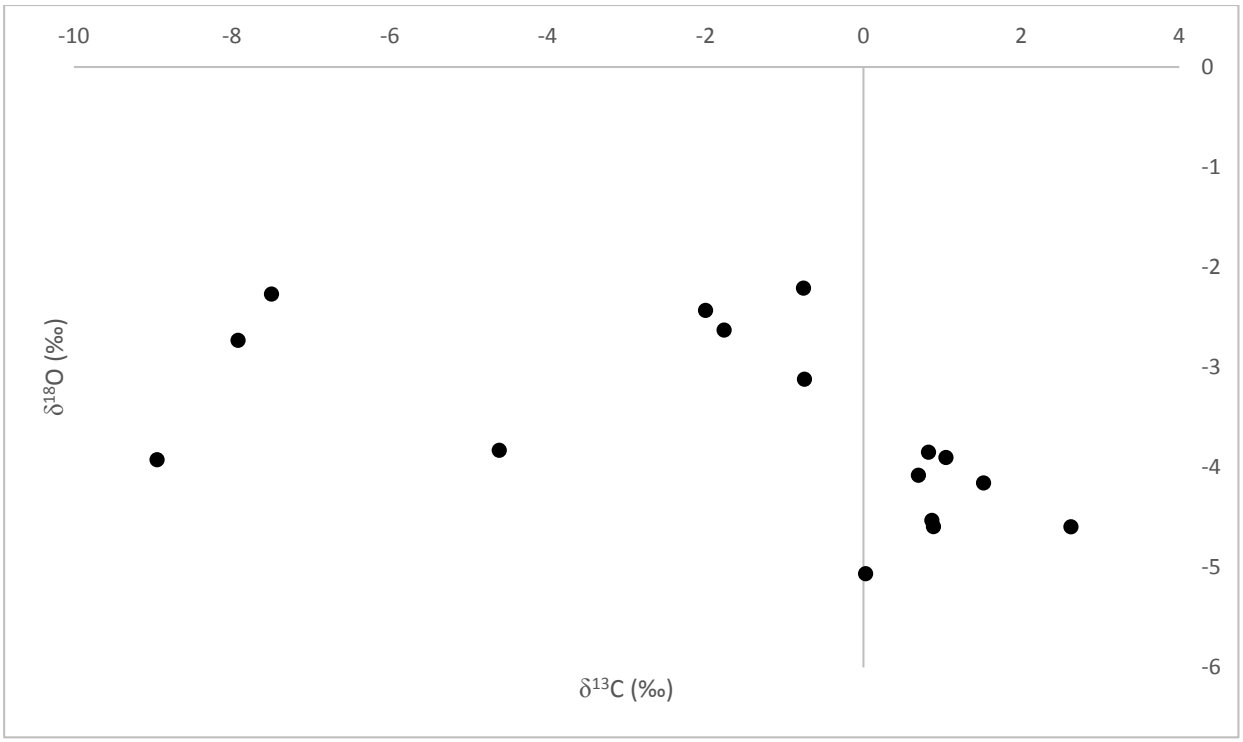

Fig. 4.9: $\delta^{13}C$ versus $\delta^{18}O$ for modern speleothem samples from the Sterkfontein Caves system.

4.3.1 Carbon Isotopes

Carbon stable light isotope analysis of speleothems provides detailed information regarding the distribution of C_3 and C_4 vegetation from the environment above the cave system. This distribution of vegetation is important to analyse as it reveals information regarding the climatic conditions of the exterior environment during the precipitation of the speleothems. Lower $\delta^{13}C$ values indicate an environment dominated by C_3 vegetation, which implies a warmer, wetter environment, while higher $\delta^{13}C$ values indicate an environment progressively dominated by C_4 vegetation, which implies cooler, drier overall climatic conditions. The vegetation distribution information produced from the carbon stable light isotope analysis of modern speleothems may also be compared to the current observed vegetation in the environment above the cave system, and therefore provide important information with regards to the accuracy with which carbon stable light isotope analysis of speleothems compares to the observed modern vegetation distribution. This therefore is a measure of the reliability of speleothems as palaeoclimate proxies.

In general, the carbon isotope results from the modern speleothem samples are within a range of -2‰ to 2‰, except for the Silberberg Grotto samples, which are significantly depleted compared the other samples, with a range of -4.61‰ to -8.95‰. The overall average $\delta^{13}C$ value for the modern speleothem samples is -1.61‰ (Figure 4.10).

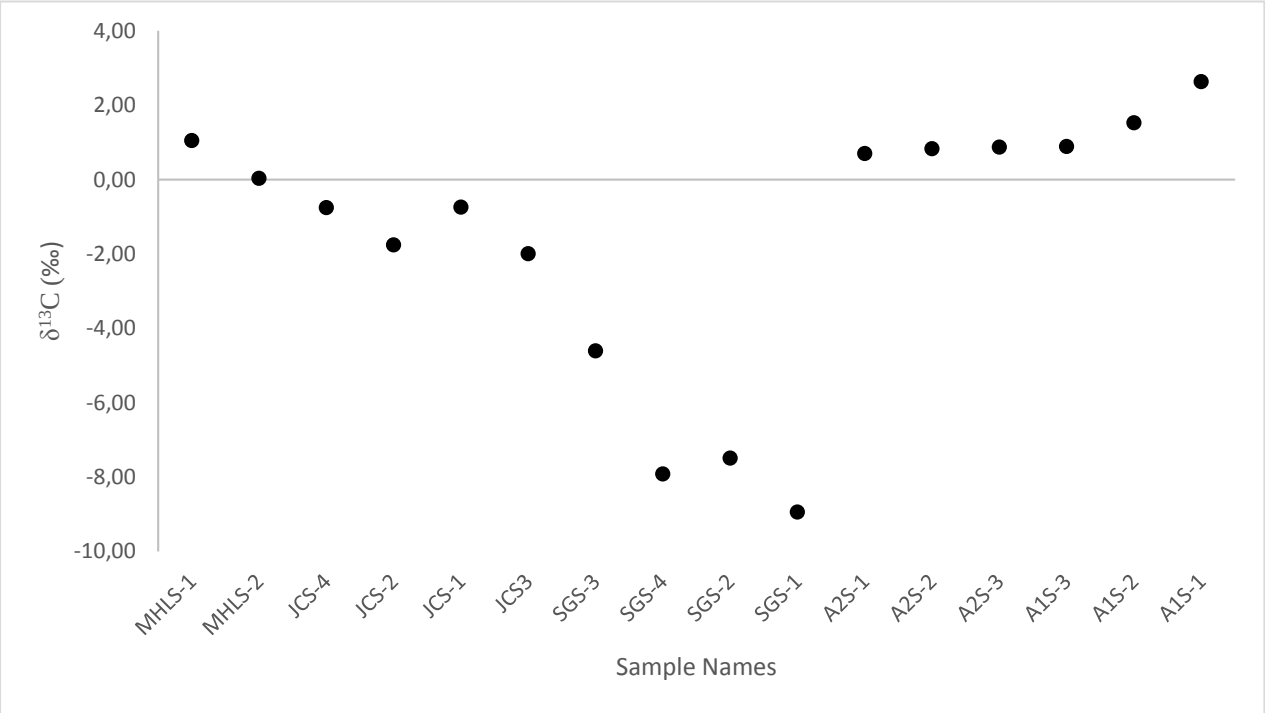

Fig. 4.10: $\delta^{13}C$ values for modern speleothem samples from Sterkfontein Caves.

Each modern speleothem sampled from the Sterkfontein Caves system underwent carbon stable light isotope analysis (see Appendix C) in order to establish the distribution of vegetation for the modern environment above the Sterkfontein Caves system, as dictated by the stable light isotopes. The estimation of the percentage of vegetation types for the environment above the Sterkfontein Caves system was calculated using Talma and Vogel's (1992) method for calculating vegetation types using $\delta^{13}C$ values (see Chapter 3, section 3.6.3).

Figure 4.11 shows the percentage C_3 and C_4 vegetation per speleothem sample, with the blue bars representing C_4 vegetation, and the red bars representing C_3 vegetation. C_4 vegetation is the dominant vegetation type for most of the speleothem samples with a range of 75% to 98%, except for the SGS-1 to SGS-4 samples, which are from the Silberberg Grotto in the Sterkfontein Caves system. The Silberberg Grotto speleothem samples display an average of 29.28% C_4 vegetation, which is considerably lower than that of the other modern speleothem samples, which have an average C_4 vegetation value of 92.05%. The average percentage of C_3 vegetation produced from the Silberberg Grotto speleothem samples is also considerably higher than that of the other samples, being 63.98%. The raw $\delta^{13}C$ values also display a very strong positive correlation in comparison to the distribution of C_4 vegetation, with a Pearson's *r* value of 1, and a very strong inverse relationship with the distribution of C_3 vegetation, with a

Pearson's *r* value of -0.99. The p values for these statistical correlations were both within the 90% confidence level, indicating that the correlation is statistically significant.

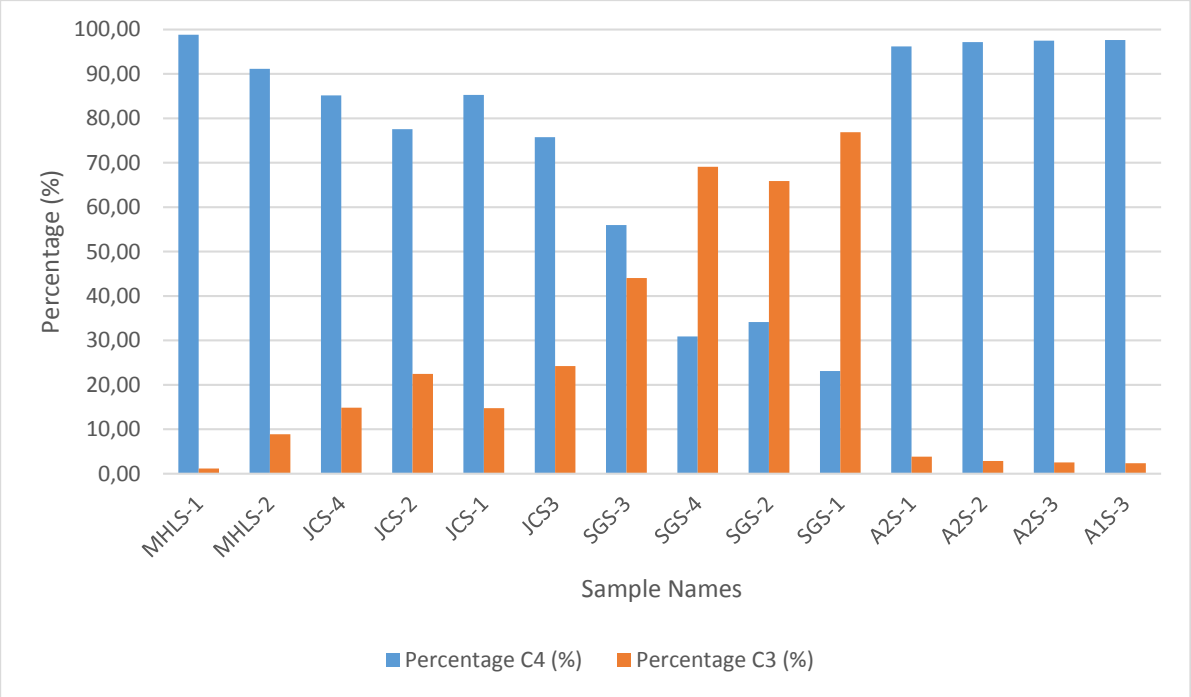

Fig. 4.11: Bar graph showing the percentage distribution of C_3 and C_4 vegetation for each speleothem sample, calculated using the carbon isotope data from the speleothem samples.

Figure 4.12 shows the overall average percentage C_3 and C_4 vegetation for the environment above the Sterkfontein Caves system, with C_4 vegetation being the overall dominant vegetation type at 78%. C_3 vegetation comprises 22% of the environment above the Sterkfontein Caves system. Overall, carbon isotopes are enriched, with an average of -1.61‰, which according to Talma and Vogel's (1992) method (see Chapter 3, section 3.6.3) for calculating vegetation types according to $\delta^{13}C$ equates to approximately 80% C_4 vegetation cover. This is also reflected by and in agreement with the overall average C_4 vegetation calculated from each speleothem samples' $\delta^{13}C$ signature, which is 78% C_4 vegetation as opposed to 22% C_3 vegetation for the environment above the Sterkfontein caves system. This would signify an environment with predominantly grasses, but with a significant amount of shrubs and open woodland trees as well. The carbon isotopes from speleothem samples taken from the Silberberg Grotto are significantly depleted compared to the other speleothem samples, and reflect 40% to 78% C_3 vegetation, whereas all of the other speleothem samples reflect between 75% to 98% C_4 vegetation.

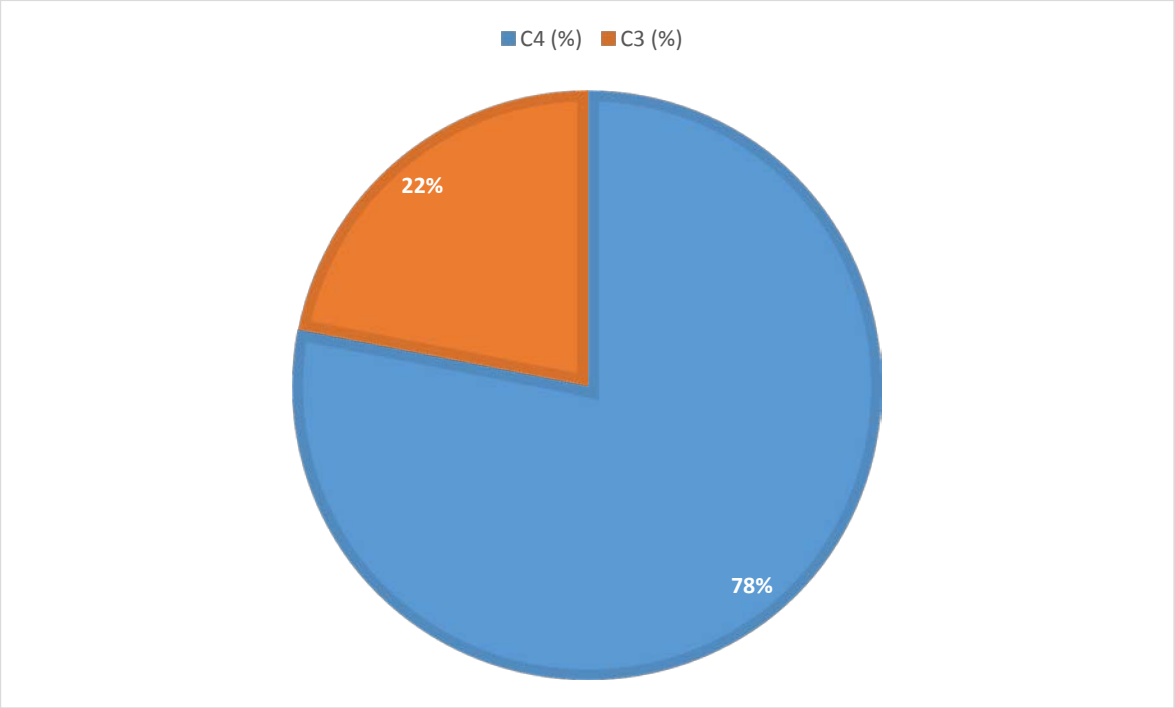

Fig. 4.12: Pie chart showing the overall average percentage distribution of C_3 and C_4 vegetation for the environment above the Sterkfontein Caves system, deduced from the $\delta^{13}C$ values.

The overall percentage of observed vegetation in the environment above the Sterkfontein Caves is also in agreement with the carbon stable light isotope analysis results, which came to average values of 78% C_4 vegetation and 22% C_3 vegetation, whereas the observed vegetation exhibited 75% C_4, 24.5% C_3 and 0.5% CAM. Due to the overall combined distribution of grasses, shrubs and trees, the environment can be described as a mosaic environment comprising mostly grasslands with patches of open woodland and shrubs.

3.2 Oxygen isotopes

Oxygen stable light isotope analysis of speleothems provides information with regard to precipitation and temperature climatic conditions present in the exterior environment during the precipitation of these speleothems. The temperature and precipitation data produced from oxygen stable light isotope analysis allows for detailed climatic reconstructions to be produced, which may then be compared to the current temperature and precipitation climatic conditions above the cave system. This may therefore provide important information with regards to the accuracy with which oxygen stable light isotope analysis of speleothems compares to the observed modern climatic conditions. This therefore is again a measure of the reliability of speleothems as palaeoclimate proxies.

Figure 4.13. displays the oxygen isotope results for the speleothem samples (see Appendix C). Depleted, more negative oxygen isotope values reflect drier conditions with less rainfall, while less depleted, more positive values reflect wetter conditions with an increase in warm, frequent rainfall. The oxygen isotopes produced from the modern speleothem samples are reasonably negative with an average of -3.6‰, signifying cooler and drier conditions during speleothem growth.

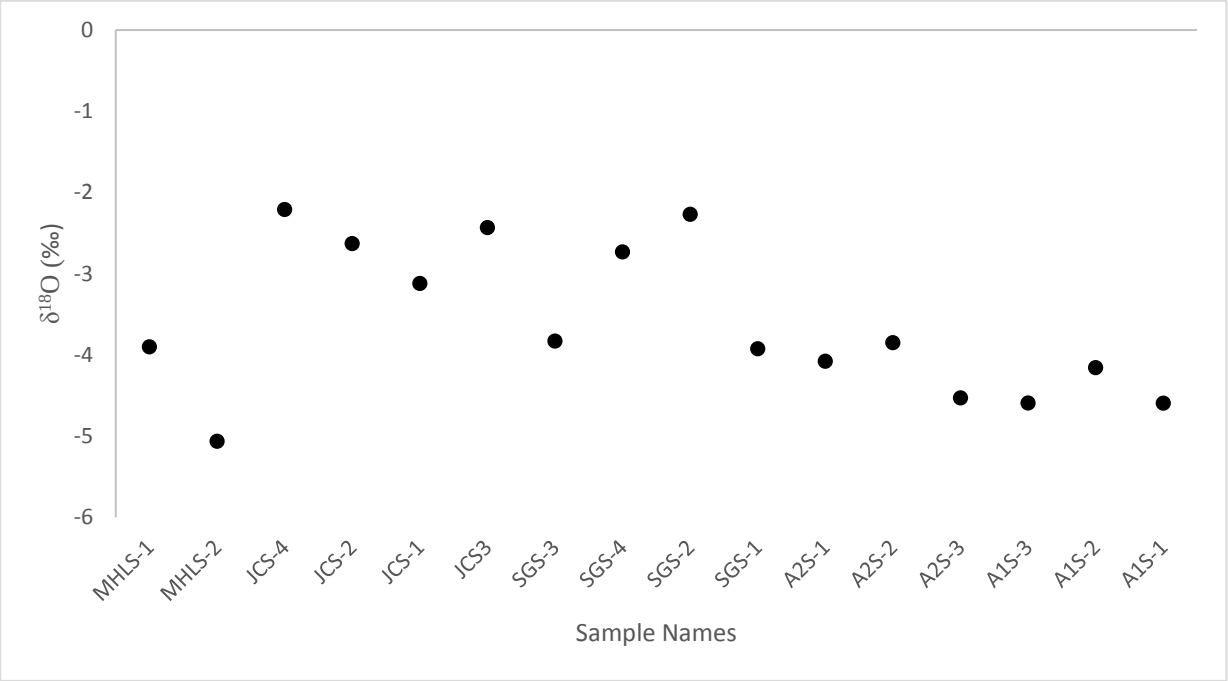

Fig. 4.13: $\delta^{18}O$ values from modern speleothem samples from the Sterkfontein Caves system.

Two different equations were used in order to determine and compare temperature results produced from the speleothem oxygen isotopes. These two equations include the empirical equation,

$T℃ = 16.9 - 4.2(\delta_c - \delta_w) + 0.13\ (\delta_c - \delta_w)^2$ (equation 1) (Epstein et al., 1953; Kim & O'Neil, 1997; Schwarcz, 2007; Lachniet, 2009; Feng et al., 2014),

and the experimental equation,

$10^3 \ln\alpha = 2.78(10^6 T^{-2}) - 2.89$ (equation 2) (Epstein et al., 1953; Kim & O'Neil, 1997; Schwarcz, 2007; Lachniet, 2009; Feng et al., 2014).

The temperatures produced using these two equations are ideal temperatures, as no fractionation was taken into consideration. Equation 1 produces a warm temperature trend, whereas equation 2 produces a trend approximately 7°C cooler (Figure 4.14).

The temperatures produced by the experimental equation were then compared to the measured cave air temperatures within the Sterkfontein Caves system (Figure 4.14). The experimental equation produced a range of temperatures that are fairly close in range with the measured cave air temperatures, producing a chi-squared value of 0.503, where p = 1, with variations of 1.75°C and 1.73°C between the idealised temperature and cave air temperature for sample JCS-2 and JCS-1 respectively, variations of 0.66°C for sample SGS-4, 0.64°C for samples SGS-3 and SGS-2, and 0.65°C for sample SGS-1, and variations of 2.24°C and 2.25°C for samples A1S-2 and A1S-1 respectively.

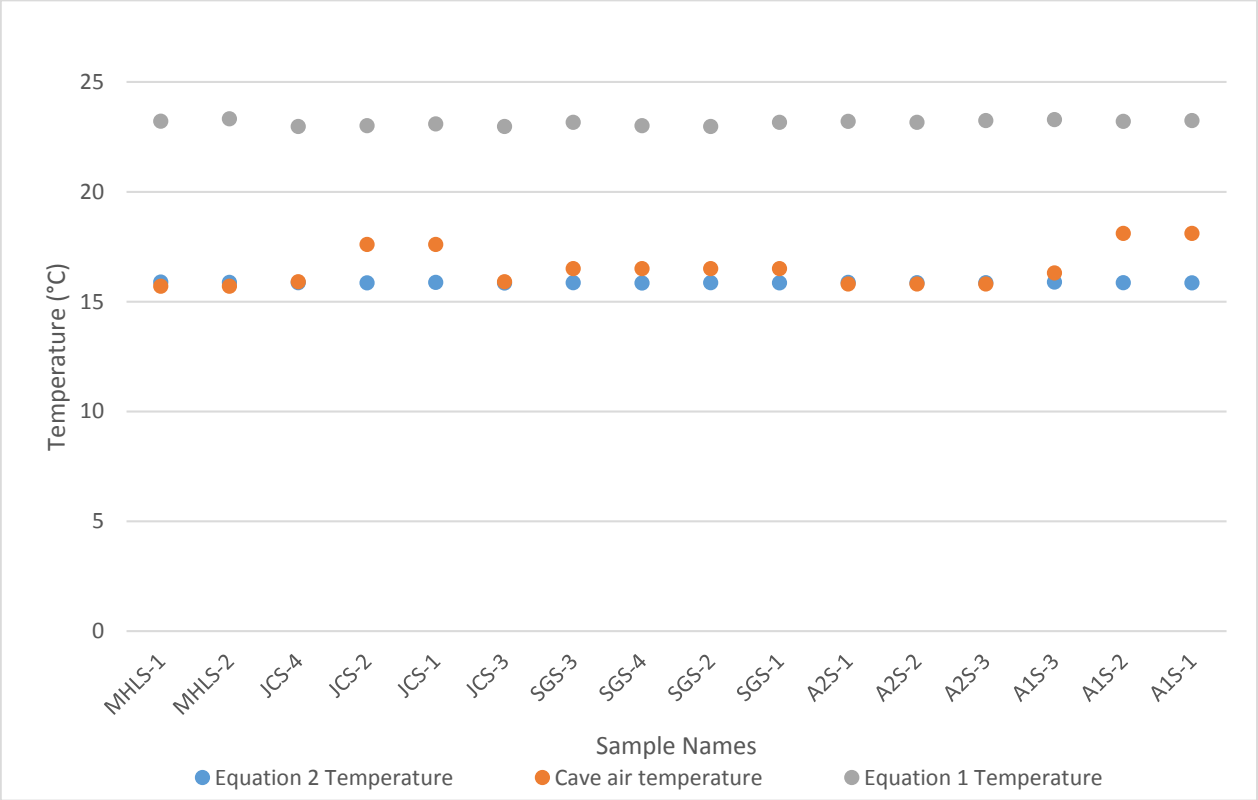

Fig. 4.14: Comparison of ideal temperatures produced using the empirical and experimental equations for deriving temperatures from speleothems, and the measured air temperatures in the cave system.

4.4 Drip Water

4.4.1 Oxygen Isotopes

328 drip water samples from the Jacovec Cavern, Antechamber 1 and Antechamber 2 were collected on a bi-monthly scale, for 14 months from July 2015 to August 2016. These samples underwent oxygen stable light isotope analysis (see Appendix C), in order for temperature calculations to be made with regards to these oxygen isotopes and the oxygen isotopes produced from the speleothem samples, and for any trends with regards to precipitation to be made by comparing the stable oxygen isotope trends to the rainfall measured in the area during

the period of collection. All the drip water samples were analysed for oxygen stable light isotopes and δ^2H, in order for a comparison to be made with regards to the global meteoric water line to establish the validity of the data produced from the isotope analysis (Figure 4.15, see Appendix C). 92.07% of the samples displayed $\delta^{18}O$ values of below zero, indicating less evaporative fractionation effects than that associated with positive $\delta^{18}O$ results. These few positive results were disregarded during data analysis compilation (See Chapter 3, section 3.6.1).

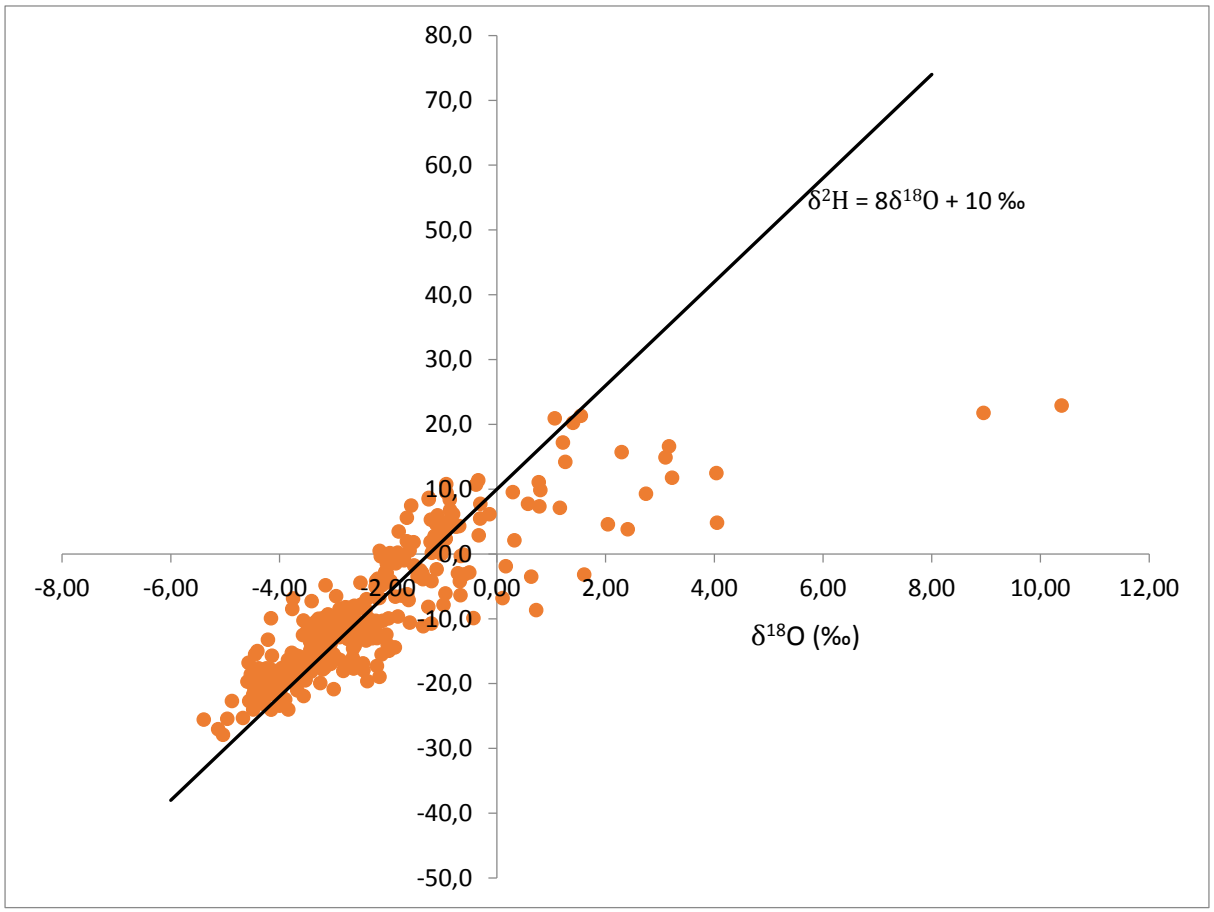

Fig. 4.15: Comparison of $\delta^{18}O$ data from 328 drip water samples with the global meteoric water line.

The $\delta^{18}O$ results from the drip water samples from the Jacovec Cavern display an irregular saw-tooth pattern, and include four outlier results, (see Chapter 3, section 3.6.1) which exhibited significantly higher $\delta^{18}O$ values than any of the other samples, and were thus disregarded (Figure 4.16A, B). The range of $\delta^{18}O$ values for the Jacovec Cavern is -0.14‰ to -5.39‰, which is a sufficiently large range of values displaying minimal flattening effects due to kinetic fractionation. This therefore indicates that the $\delta^{18}O$ values may be assumed to produce reliable temperatures (Kluge & Affek, 2012). The average $\delta^{18}O$ value for the Jacovec

Cavern is -2.83‰, disregarding the outlier samples. Drip water samples from JDW-3 showed the greatest range of values from -0.14‰ to -5.39‰, which incorporates both the minimum and maximum range values for the Jacovec Cavern. The most positive average originates from the JDW-1 samples, while the most negative average originates from the JDW-4 samples. Gaps in the $\delta^{18}O$ trends for these samples show where no drip water was present for that particular week.

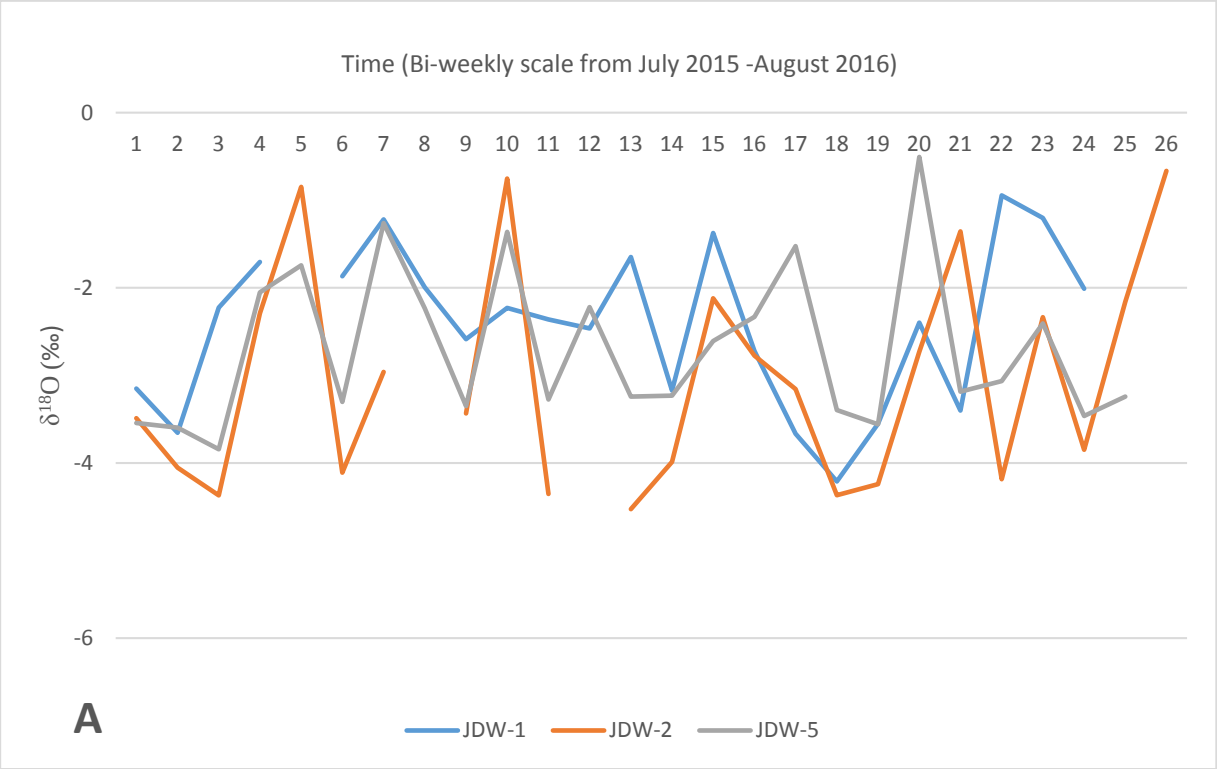

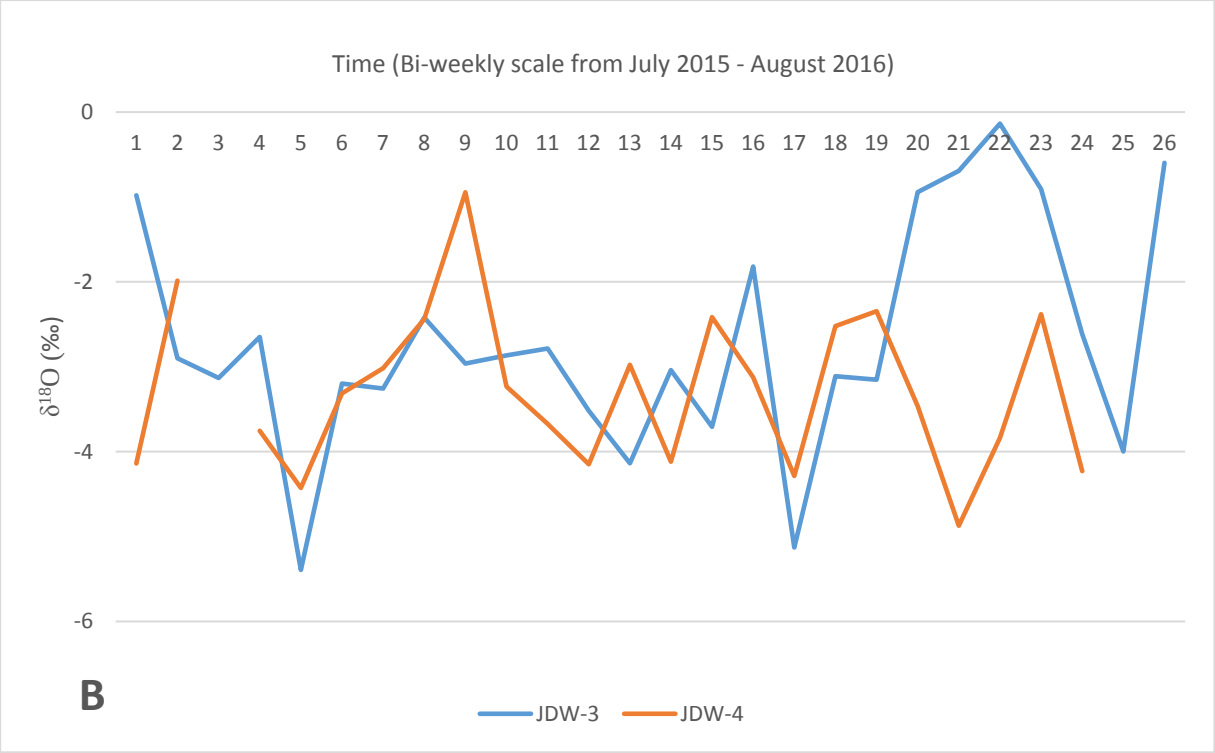

Fig. 4.16A, B: $\delta^{18}O$ results from the Jacovec Cavern, without the four outlier samples for 26 weeks.

The $\delta^{18}O$ results from the drip water samples from Antechamber 1 also display an irregular saw-tooth pattern, and includes 14 outlier results, which exhibited significantly high $\delta^{18}O$ values, and were also thus disregarded (Figure 4.17A, B). The range of $\delta^{18}O$ values for Antechamber 1 is -0.33‰ to -4.96‰, which is a sufficiently large range of values displaying minimal flattening effects due to kinetic fractionation. This therefore indicates that the $\delta^{18}O$ values may be assumed to produce reliable temperatures (Kluge & Affek, 2012). The average $\delta^{18}O$ value for Antechamber 1 is -2.77‰, disregarding the outlier samples. $\delta^{18}O$ values for the A1DW-3 and A1DW-4 samples show the greatest variability, with values varying between a range of -0.83‰ to -4.27‰ within a single month and -2.49‰ to -2.62‰ within a single month as well for A1DW-3 samples. A1DW-4 samples vary between a range of -0.33‰ to -4.06‰ within a single month, and -1.11‰ to -1.15‰ within another month. Gaps in the $\delta^{18}O$ trends for these samples show where no drip water was present for that particular week. Drip water samples from A1DW-5 show the greatest overall range, with a range of -1.00‰ to -4.59‰. The most positive average originates from A1DW-4 samples, which lies at -1.69‰, and the most negative average originates from A1DW-2 samples, which lies at -3.35‰.

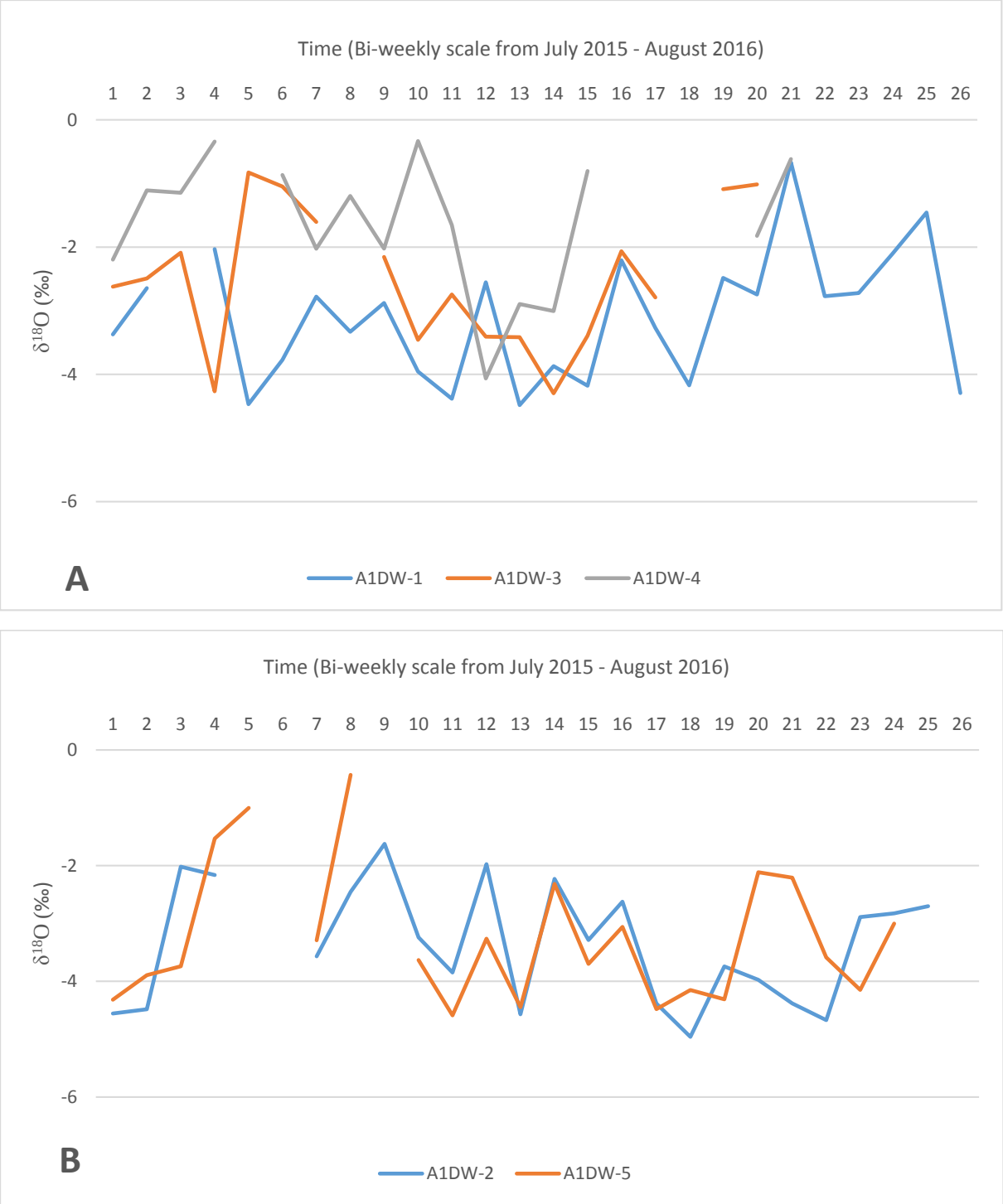

Fig. 4.17A, B: $\delta^{18}O$ trends for Antechamber 1 for 26 weeks. The 14 outlier samples have been disregarded.

The $\delta^{18}O$ results from the drip water samples from Antechamber 2 also display an irregular saw-tooth pattern, which becomes less pronounced between fortnights 10 and 20 (Figure 4.18). These $\delta^{18}O$ results include eight outlier results, which exhibited significantly high $\delta^{18}O$ values, and were also thus disregarded. The range of $\delta^{18}O$ values for Antechamber 2 is -0.30‰ to -5.04‰, which is a sufficiently large range of values displaying minimal flattening effects due

to kinetic fractionation. This therefore indicates that the $\delta^{18}O$ values may be assumed to produce reliable temperatures (Kluge & Affek, 2012). The average $\delta^{18}O$ value for Antechamber 2 is -2.59‰, disregarding the outlier samples. $\delta^{18}O$ values for all the Antechamber 2 samples show great variability. Gaps in the $\delta^{18}O$ trends for these samples show where no drip water was present for that particular week. Drip water samples from A2DW-1 show the greatest range, with a range of -0.31‰ to -5.04‰. The most positive average originates from A2DW-2 samples, and the most negative average originates from A2DW-3 samples. However, the samples from A2DW-3 are not reliable, as only four samples were produced, and two of those four samples were outlier samples. Most of the $\delta^{18}O$ trends for Antechamber 2 seem to decrease significantly between weeks 10 and 20 again, from an overall average of -1.70‰ to -2.80‰.

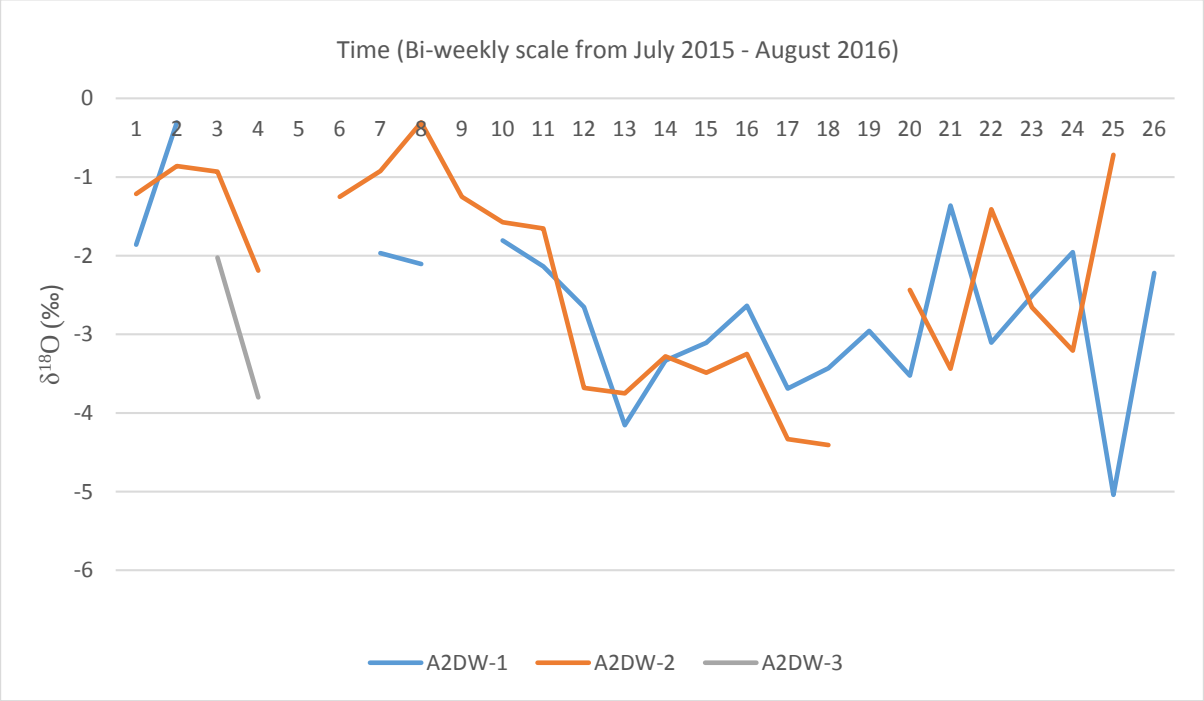

Fig. 4.18: $\delta^{18}O$ results for Antechamber 2 for 26 weeks. The eight outlier samples have been disregarded.

The $\delta^{18}O$ values for the Jacovec Cavern, Antechamber 1 and Antechamber 2 were averaged, removing all the outlier values, and single monthly average values were calculated for each chamber (Figure 4.19). These values produce a much less pronounced saw-tooth pattern, but still with a considerable range of -0.22‰ to -3.92‰. All three trends show a decreasing trend from September 2015 to approximately March/April 2016, where all three trends increase again. The trend for Antechamber 2 decreases from July 2015, as opposed to the other two trends, which show a sharp increase from July 2015 to September 2015. A Pearson product-

moment correlation test was conducted in PAST v3.14 software (Hammer et al., 2001) on the $\delta^{18}O$ values for the three chambers, and produced correlation values (*r*) of 0.44 to 0.60, showing intermediate to strong positive correlations between the three data sets. Values for p averaged 0.066 at a 90% confidence level (see Appendix B). These p values are within the confidence level of 90%, indicating that the results are statistically significant and may be interpreted further. This may also indicate a reliable correlation interpretation, and minimal fractionation effects.

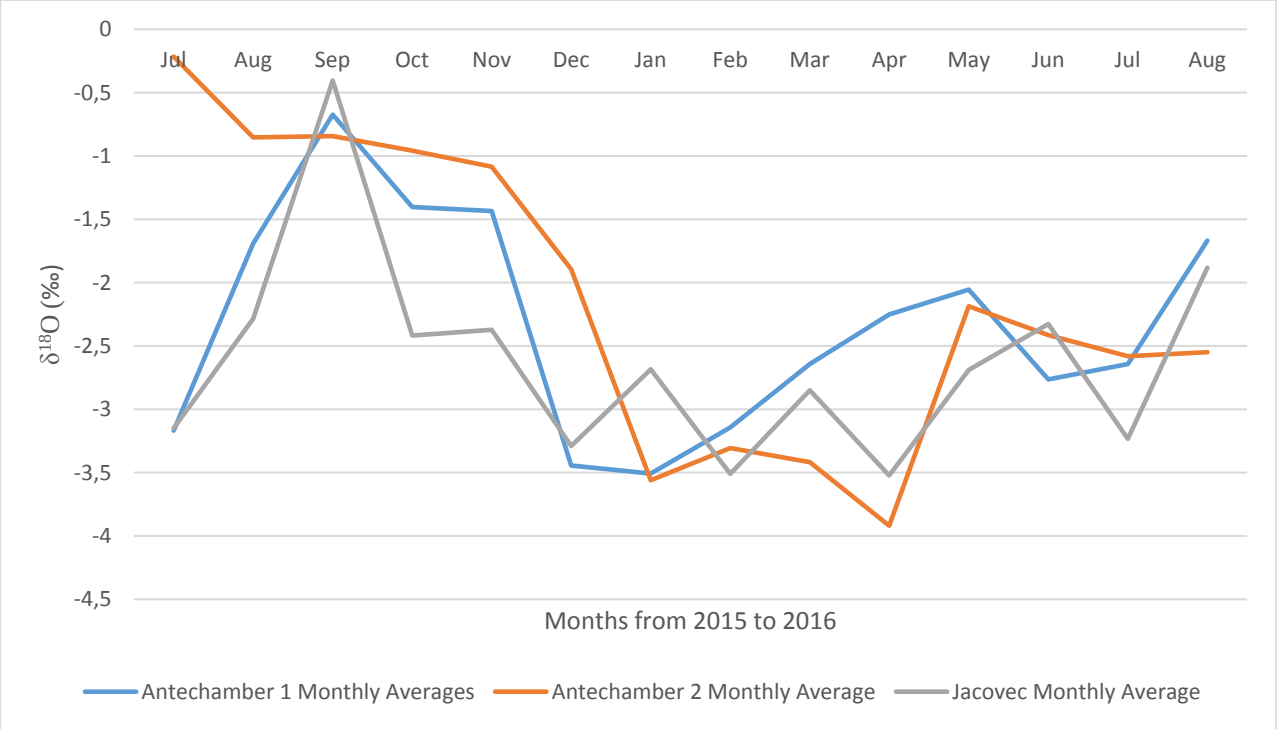

Fig 4.19: Monthly average $\delta^{18}O$ values for the Jacovec Cavern, Antechamber 1 and Antechamber 2.

4.4.2 Temperature

Using the $\delta^{18}O$ monthly average values for each cavern and the corresponding speleothem $\delta^{18}O$ results, temperatures were calculated for each month from each chamber. These temperatures were calculated twice, using the empirical equation for calculating temperatures from speleothems (equation 1) (Epstein et al., 1953; Kim & O'Neil, 1997; Schwarcz, 2007; Lachniet, 2009; Feng et al., 2014) and the experimental equation for calculating temperatures from speleothems (equation 2) (Epstein et al., 1953; Kim & O'Neil, 1997; Schwarcz, 2007; Lachniet, 2009; Feng et al., 2014) (see Chapter 3, section 3.6.1). In each case, the calculated temperatures were compared to the measured atmospheric temperatures for the period of collection of the drip water samples.

The average atmospheric temperatures produced from weather stations from Krugersdorp and Johannesburg Botanical Gardens vary from 18.6°C to 29.5°C. These temperatures increase from 19.5°C in July 2015 to 29.5°C in December 2015, and then decrease to 18.6°C in July 2016, and start increasing again from August 2016. This trend correlates well with seasonal temperature changes, with lower temperatures representing winter and autumn months and higher temperatures during spring and summer months.

The average monthly temperatures produced from the drip water and speleothem $\delta^{18}O$ for the Jacovec Cavern using equation 1 reflect a similar trend, increasing from 20.03°C in July 2015 to 22.86°C in November 2015, then decreasing from 21.13°C in December 2015 to March 2016, where a short increase to 23.36°C is observed (Figure 4.20). The temperatures then continue decreasing to 18.4°C in April 2016, and then slightly increase again shortly to 22.63°C in June 2016, decrease slightly to 19.43°C in July 2016, and then increase significantly to 26.61°C in August 2016. The warmer seasonal period however appears not to increase as much as the atmospheric temperatures do, and the calculated temperatures only increase slightly, producing an overall flatter increasing and decreasing curve, with much less significant variations as opposed to the average atmospheric measured temperatures. The calculated temperatures seem to correspond better with the average atmospheric measured temperatures, when these temperatures are lower. A Pearson product-moment correlation test was conducted in PAST v3.14 software (Hammer et al., 2001) on the temperatures calculated using equation 1 for the Jacovec Cavern and the average measured atmospheric temperatures, and produced a correlation value (r) of 0.04, showing a very weak positive correlation between the two data sets. The value for p was 0.9 at a 90% confidence level (see Appendix B). This p value however is not within the confidence level of 90%, indicating that the results are not statistically significant and therefore may not be an accurate representation of the data. This could indicate a weak correlation between the two data sets, and could also be due to kinetic fractionation effects, resulting in unreliable statistical results.

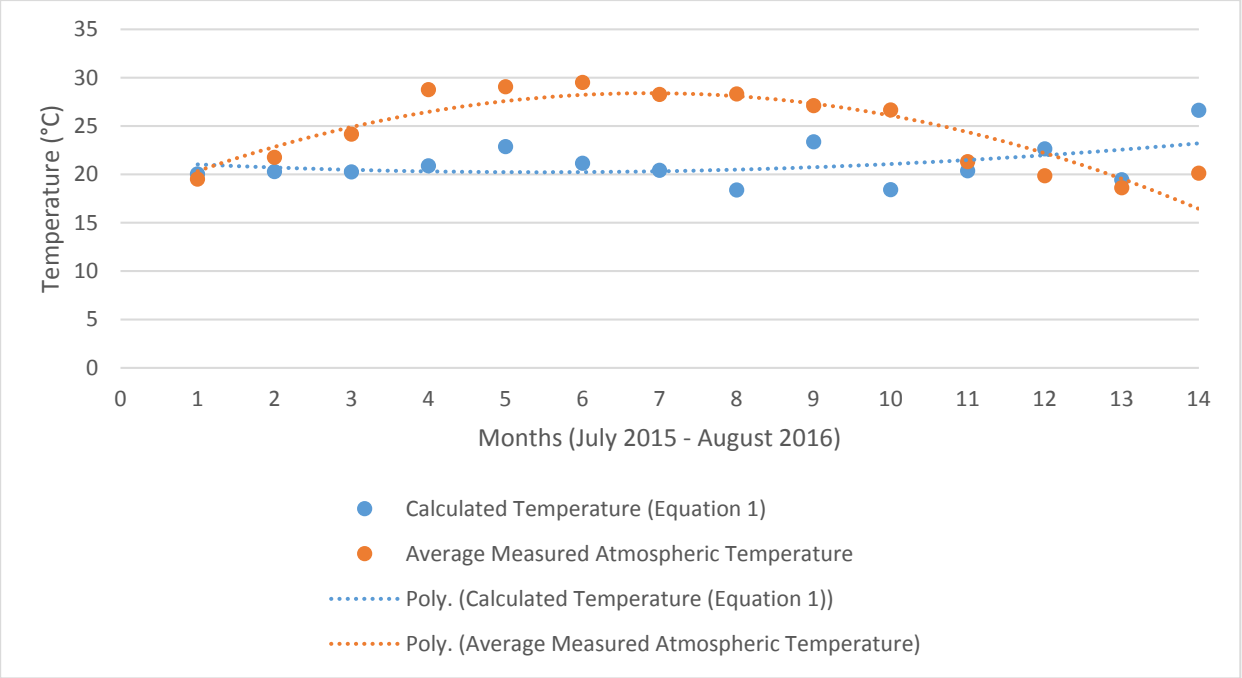

Fig. 4.20: Temperatures calculated from the Jacovec Cavern average $\delta^{18}O$ values using equation 1, and compared to the average measured atmospheric temperatures.

The average monthly temperatures produced from the drip water and speleothem $\delta^{18}O$ from Antechamber 1 using equation 1 reflect a similar trend, increasing from 23.5°C in July 2015 to 30.81°C in November 2015, then decreasing sharply to 20.78°C in December 2015 (Figure 4.21). Temperatures increase again to 28.3°C in February 2016, and then decrease again to 22.45°C in April 2016. A short increase to 26.69°C in May 2016 is observed. The temperatures then continue decreasing to 20.95°C in August 2016, with a very slight increase and subsequent decrease in June 2016. The warmer seasonal period appears to increase more correspondingly (as opposed to the temperatures produced from the Jacovec Cavern) with regards to the average measured atmospheric temperatures, producing an overall curve that seems to correspond reasonably well to the average measured atmospheric temperatures, displaying a Pearson's *r* value of 0.65. The decrease in calculated temperatures from Antechamber 1 does not decrease as steeply as that of the average measured atmospheric temperatures however, producing a slight departure between the two curves from April 2016 to July 2016. The higher calculated temperatures for Antechamber 1 correspond well with the higher average measured atmospheric temperatures in this case. A Pearson product-moment correlation test was conducted in PAST v3.14 software (Hammer et al., 2001) on the temperatures calculated using equation 1 for Antechamber 1 and the average measured atmospheric temperatures, and produced a correlation value (*r*) of 0.65, showing an intermediate to strong positive correlation between the two data sets. The value for p was 0.012 at a 90% confidence level (see Appendix

B). This p value is within the confidence level of 90%, indicating that the results are statistically significant and may be interpreted further. This may also indicate a reliable and strong correlation between the two data sets, and minimal fractionation effects.

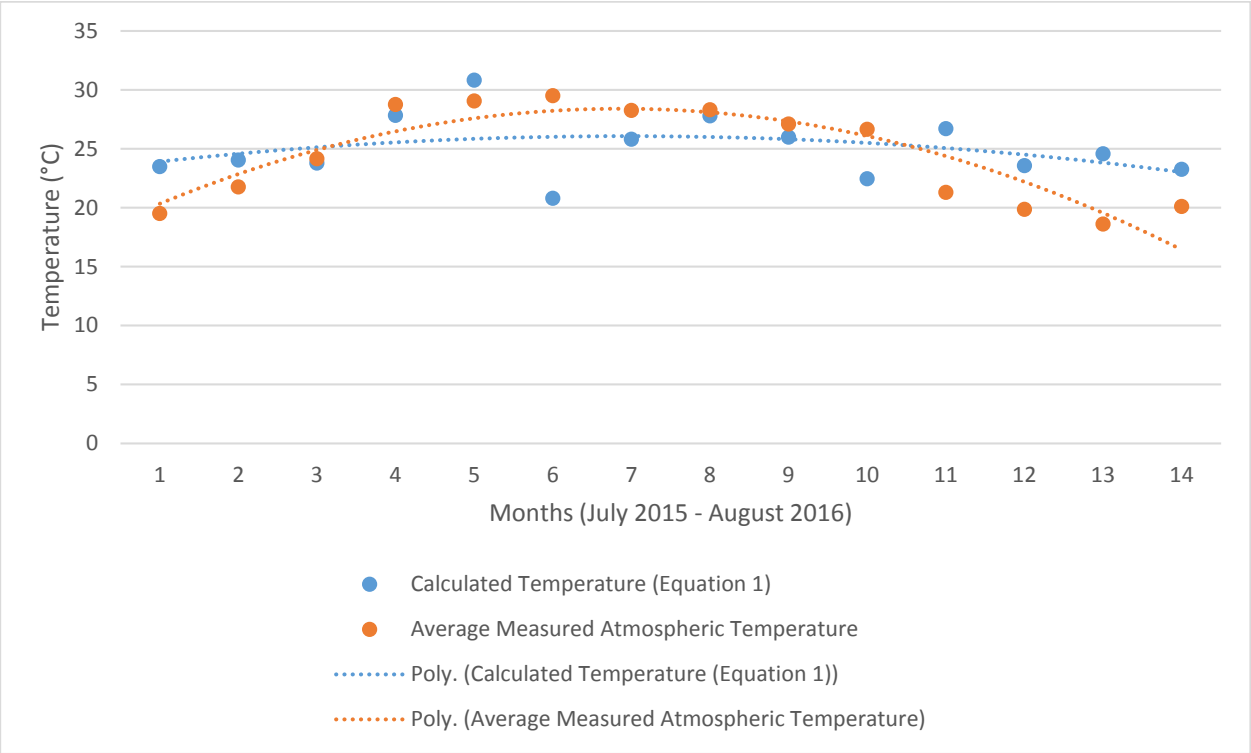

Fig, 4.21: Temperatures calculated from the Antechamber 1 average $\delta^{18}O$ values using equation 1, and compared to the average measured atmospheric temperatures.

The average monthly temperatures produced from the drip water and speleothem $\delta^{18}O$ from Antechamber 2 using equation 1 reflect a similar trend, increasing from 14.8°C in August 2015 to 32.74°C in November 2015, and decreasing very slightly to 32.24°C in December 2015 (Figure 4.22). Temperatures then decrease to 24.93°C in January 2016, increase slightly to 26.04°C in March 2016, and then decrease significantly again to 15.09°C in July 2016, with a sharp increase in May 2016 to 26.99°C, and sharp subsequent decrease. Temperatures then increase again to 17.62°C in August 2016. The temperatures produced from Antechamber 2 drip water $\delta^{18}O$ values show a significant decrease in temperatures from July 2015 to August 2015, at the beginning of the graph. Other than this anomaly, the calculated temperatures from Antechamber 2 and the average measured atmospheric temperatures seem to correspond well. Both the cooler and warmer seasonal periods appear to increase more correspondingly (as opposed to the temperatures produced from the Jacovec Cavern and Antechamber 1) with

regards to the average measured atmospheric temperatures, producing an overall curve that seems to correspond reasonably well to the average measured atmospheric temperatures. A Pearson product-moment correlation test was conducted in PAST v3.14 software (Hammer et al., 2001) on the temperatures calculated using equation 1 for Antechamber 2 and the average measured atmospheric temperatures, and produced a correlation value (*r*) of 0.68, showing an intermediate to strong positive correlation between the two data sets. The value for p was 0.01 at a 90% confidence level (see Appendix B). This p value is within the confidence level of 90%, indicating that the results are statistically significant and may be interpreted further. This may also indicate a reliable correlation interpretation, and minimal fractionation effects.

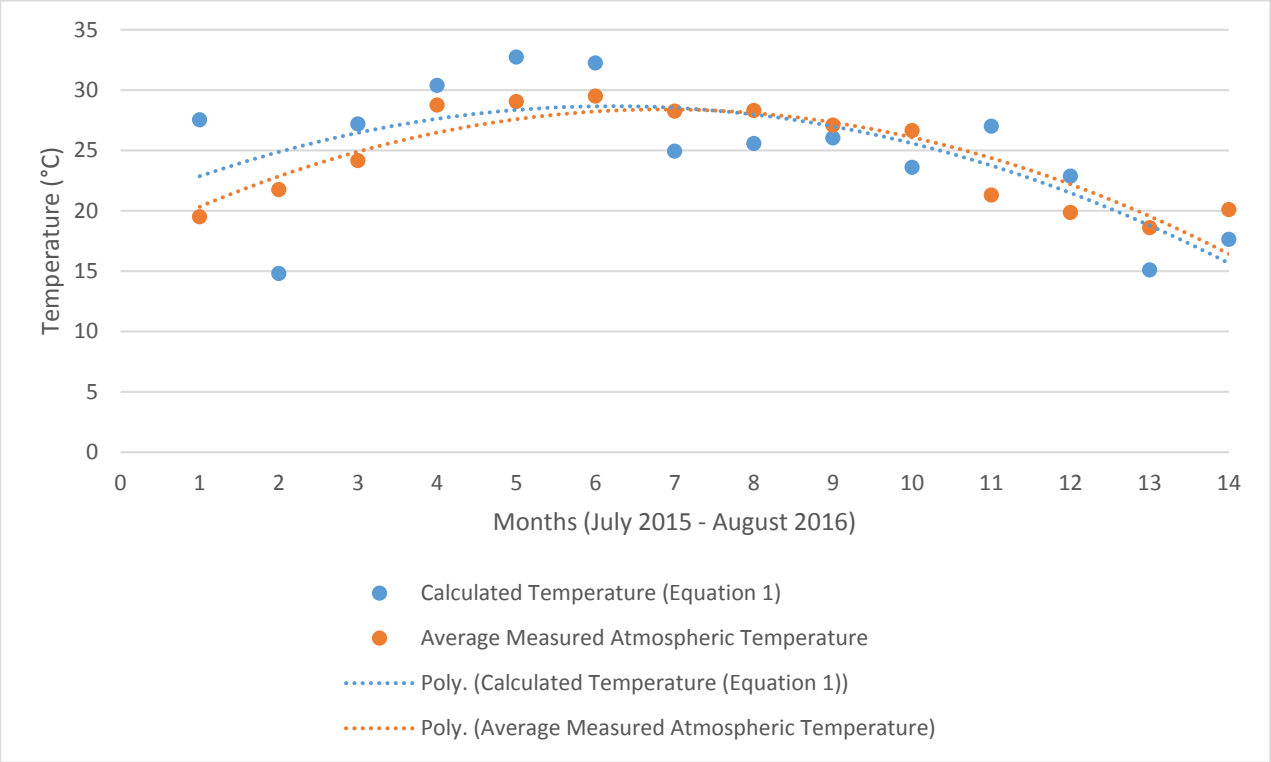

Fig. 4.22: Temperatures calculated from the Antechamber 2 average $\delta^{18}O$ values using equation 1, and compared to the average measured atmospheric temperatures.

A comparison of the measured cave air temperatures during the period of collection of drip water samples to the calculated temperatures using equation 1 from each chamber shows that the trends for each data set do correspond to a certain degree to one another (Figure 4.23). Both the measured cave air temperatures and the calculated temperatures for the chambers display an increasing trend from July 2015 to approximately November 2015, however the measured cave air temperatures display a much more gradual increase as opposed to the calculated temperatures from each chamber, which show a much steeper increase. All the trends for the

respective data sets then display a decreasing trend from November 2015 to January 2016, apart from the calculated temperatures from Antechamber 1, which start to increase again from December 2015 to February 2016, slightly earlier than the other data trends. All the other data trends begin to increase again from January 2016 to approximately March 2016.

The calculated temperatures from the Jacovec Cavern display a slight decrease and subsequent increase in February 2016. From March 2016, the measured cave air temperatures show a definite decreasing trend towards August 2016. The calculated temperatures display an overall very gradual and very irregular decrease in overall temperatures towards August 2016, but do not follow the exact same trend as that of the measured cave air temperatures. Overall, the data sets display similar overall increasing and decreasing trends, but the trends of the calculated temperatures are a lot more irregular and varied than that of the measured cave air temperature, and display steeper increasing and decreasing curves. These calculated temperatures are also slightly higher than that of the measured cave air temperatures, with calculated temperatures from Antechamber 1 and Antechamber 2 being distinctly higher than that of the measured cave air temperatures. The calculated temperatures from the Jacovec Cavern seem to reflect the measured cave air temperatures to a better degree.

Pearson product-moment correlation tests were conducted in PAST v3.14 software (Hammer et al., 2001) on the calculated temperatures for the three chambers and the average measured cave air temperatures. A correlation value (r) of 0.03 was produced for the calculated temperatures and the measured cave air temperatures from the Jacovec Cavern, showing a very weak positive correlation between the two data sets. The value for p was 0.92 at a 90% confidence level. A correlation value (r) of 0.44 was produced for the calculated temperatures and the measured cave air temperatures from Antechamber 1, showing a weak to intermediate positive correlation between the two data sets. The value for p was 0.13 at a 90% confidence level. A correlation value (r) of 0.34 was produced for the calculated temperatures and the measured cave air temperatures from Antechamber 2, showing a weak positive correlation between the two data sets. The value for p was 0.25 at a 90% confidence level (see Appendix B). None of these p values however are within the confidence level of 90%, indicating that the results are not statistically significant and therefore may not be an accurate representation of the data. This may also indicate unreliable and weak correlation between the data sets, and may be due to the large range of calculated temperatures with regard to the measured cave air temperatures, as well as the significant variation present in the calculated temperatures. This

large range and variability could result in a weaker correlation between the calculated temperatures and the cave air temperatures.

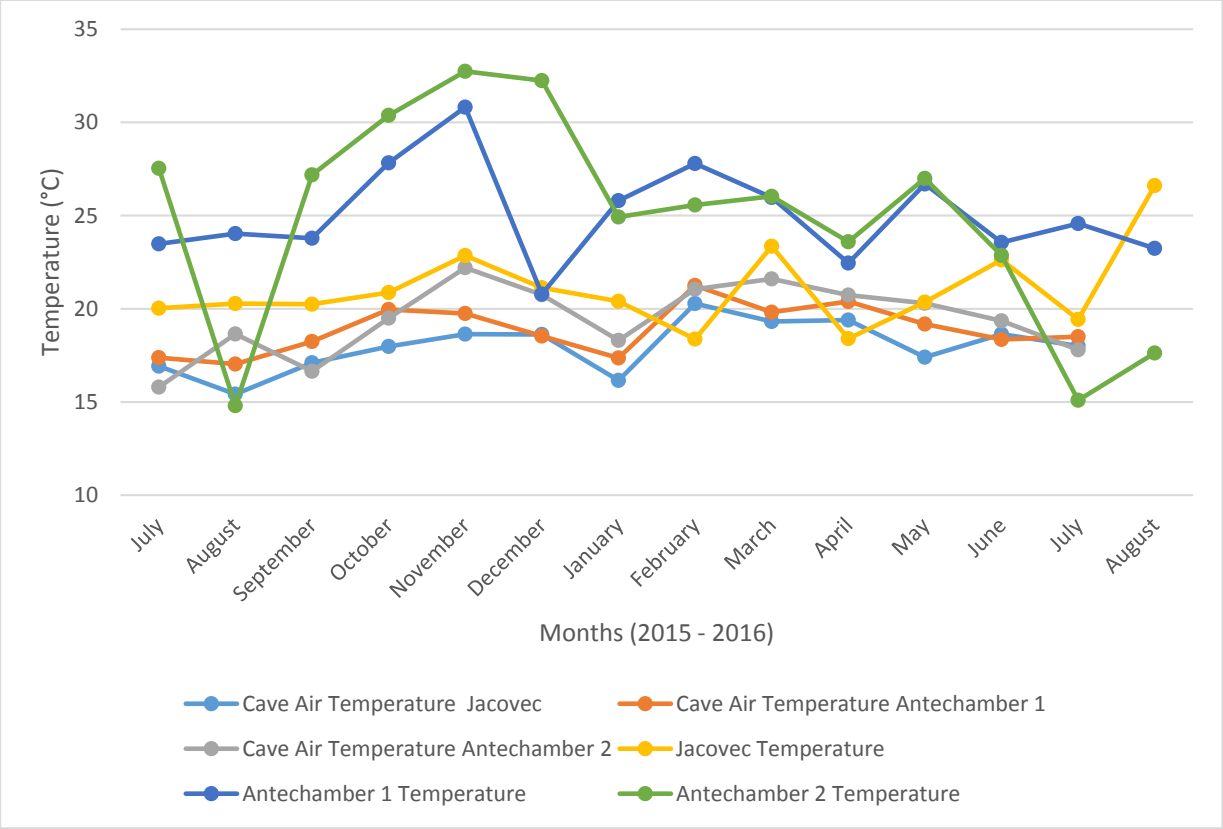

Fig. 4.23: Measured cave air temperatures versus the temperatures calculated from the Jacovec Cavern, Antechamber 1 and Antechamber 2 using equation 1.

Average monthly temperatures were produced from the drip water and speleothem $\delta^{18}O$ using equation 2, and were compared again to the average measured atmospheric temperature. The average monthly temperatures produced for the Jacovec Cavern using equation 2 reflect a very flat trend compared to that of the average measured atmospheric temperatures (Figure 4.24). Calculated temperatures increase from 11.61°C in July 2015 to 16.7°C in December 2015, with one significant decrease to 11.03°C in November 2015 and subsequent increase to the December 2015 temperature. The calculated temperatures then decrease to 11.02°C in January 2016, and increase again to 12.9°C in February 2016. The temperatures then decrease again to 10°C in March 2016, followed by an increase in temperatures to 17.18°C in June 2016, and then a slight decrease again to 15.55°C in July. This trend for the calculated temperatures for the Jacovec Cavern appears to be almost inversely proportional to the average measured atmospheric temperatures during the warmer seasons, and all of the calculated temperatures

are at least 2°C lower than the average measured atmospheric temperatures. The calculated temperatures only increase slightly, producing an overall flatter increasing and decreasing curve, with much less significant variations as opposed to the average atmospheric measured temperatures. A Pearson product-moment correlation test was conducted in PAST v3.14 software (Hammer et al., 2001) on the temperatures calculated using equation 2 for the Jacovec Cavern and the average measured atmospheric temperatures, and produced a correlation value (*r*) of -0.32, showing a weak negative correlation between the two data sets. The value for p was 0.29 at a 90% confidence level (see Appendix B). This p value however is not within the confidence level of 90%, indicating that the results are not statistically significant and therefore may not be an accurate representation of the data. This may indicate an unreliable and weak correlation, as well the presence of fractionation effects. This statistical unreliability could also be due to the weak inverse relationship between the two data sets, as well as a flatter trend for the calculated temperatures from the Jacovec Cavern.

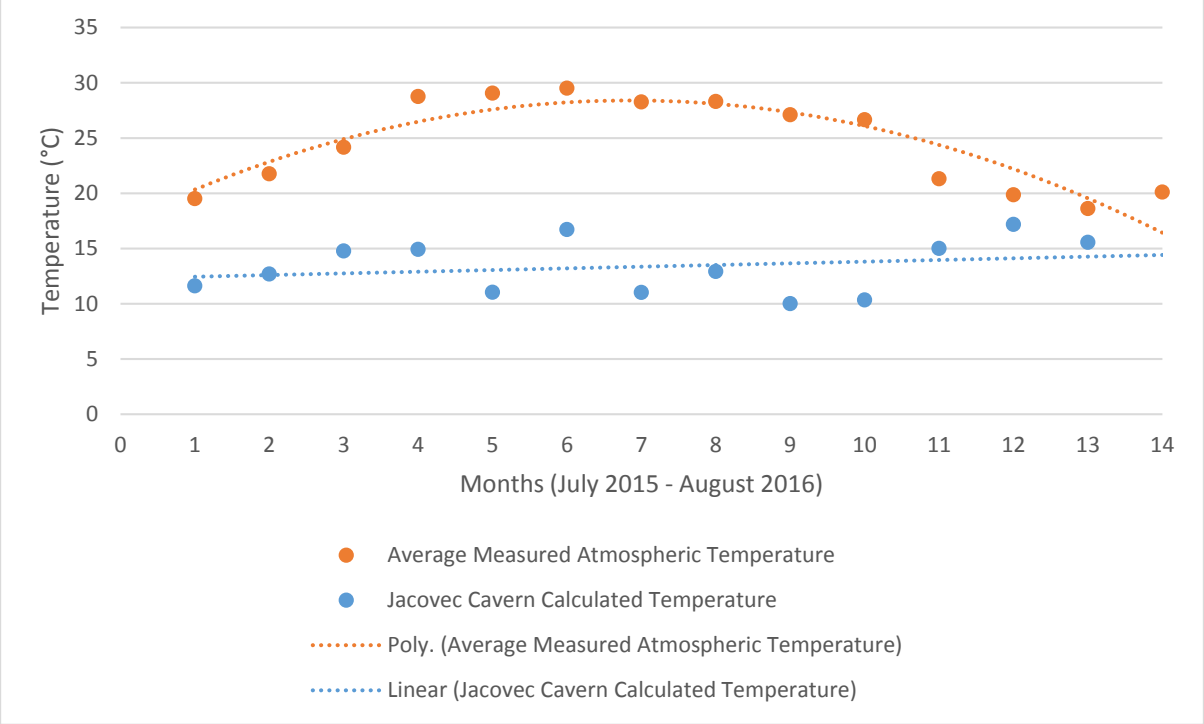

Fig. 4.24: Temperatures calculated from the Jacovec Cavern average $\delta^{18}O$ values using equation 2, and compared to the average measured atmospheric temperatures.

The average monthly temperatures produced for Antechamber 1 using equation 2 reflect a trend that corresponds slightly better to the average measured atmospheric temperatures than that of the Jacovec Cavern, but is still very irregular in comparison to the average measured atmospheric temperatures (Figure 4.25). Calculated temperatures increase from 20.5°C in July

2015 to 26.07°C in October 2015. Calculated temperatures then decrease to 16.86°C in February 2016, with one increase in January 2016 to 20.9°C, and subsequent decrease. The calculated temperatures then increase to 21.62°C in March 2016, and decrease again to 18.09°C in May 2016. The temperatures then increase again to 22°C in June 2016, followed by a decrease in temperatures to 19.72°C in July 2016, and then another increase to 22.07°C in August 2016. This trend for the calculated temperatures for Antechamber 1 appears to decrease a lot more drastically and a lot earlier during the summer to autumn months than that of the average measured atmospheric temperatures. The calculated temperatures correspond much better in the winter months to the average measured atmospheric temperatures, as opposed to the temperatures calculated during the summer to autumn months. A Pearson product-moment correlation test was conducted in PAST v3.14 software (Hammer et al., 2001) on the temperatures calculated using equation 2 for Antechamber 1 and the average measured atmospheric temperatures, and produced a correlation value (*r*) of -0.02, showing a very weak negative correlation between the two data sets. The value for p was 0.95 at a 90% confidence level (see Appendix B). This p value however is not within the confidence level of 90%, indicating that the results are not statistically significant and therefore may not be an accurate representation of the data. This may indicate an unreliable and weak correlation interpretation, as well the presence of fractionation effects. This statistical unreliability could also be due to inverse relationship between the two data sets.

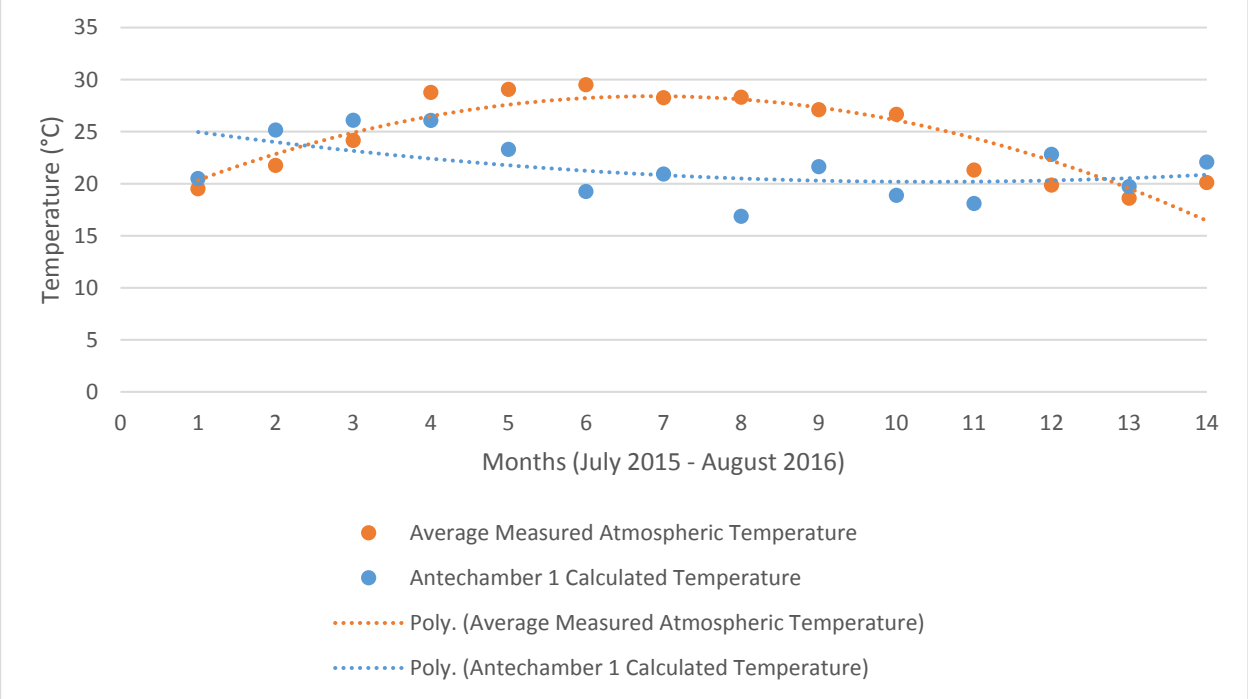

Fig. 4.25: Temperatures calculated from the Antechamber 1 average $\delta^{18}O$ values using equation 2, and compared to the average measured atmospheric temperatures.

The average monthly temperatures produced for Antechamber 2 using equation 2 reflect a trend that is also still very irregular in comparison to the average measured atmospheric temperatures, with more pronounced decreases which start a lot earlier in the summer months as opposed to the average measured atmospheric temperatures (Figure 4.26). Calculated temperatures decrease from 27.69°C in July 2015 to 26.17°C in August 2015, as opposed to the corresponding increase in the average measured atmospheric temperatures. Calculated temperatures then increase to 29.3°C in September 2015, and decrease sharply to 14.42°C in February 2016. The calculated temperatures then increase to 17.78°C in March 2016, and decrease again to 14.18°C in April 2016. The temperatures then increase sharply again to approximately 20°C in May 2016, and this temperature is then maintained until August 2016. This trend for the calculated temperatures for Antechamber 2 appears to decrease a lot more drastically and a lot earlier during the summer to autumn months than that of the average measured atmospheric temperatures, as it did with the temperatures calculated from Antechamber 1. The calculated temperatures do not seem to particularly correspond in any way to the average measured atmospheric temperatures. Although some decreasing or increasing trends do seem correspond to the average measured atmospheric temperature trend, they are either short-lived, or much more drastic and irregular than that of the average measured atmospheric temperature trend. A Pearson product-moment correlation test was conducted in PAST v3.14 software (Hammer et al., 2001) on the temperatures calculated using equation 2 for Antechamber 2 and the average measured atmospheric temperatures, and produced a correlation value (r) of -0.1, showing a very weak negative correlation between the two data sets. The value for p was 0.72 at a 90% confidence level (see Appendix B). This p value however is not within the confidence level of 90%, indicating that the results are not statistically significant and therefore may not be an accurate representation of the data. This may indicate an unreliable and weak correlation interpretation, as well the presence of fractionation effects. This statistical unreliability could also be due to inverse relationship between the two data sets.

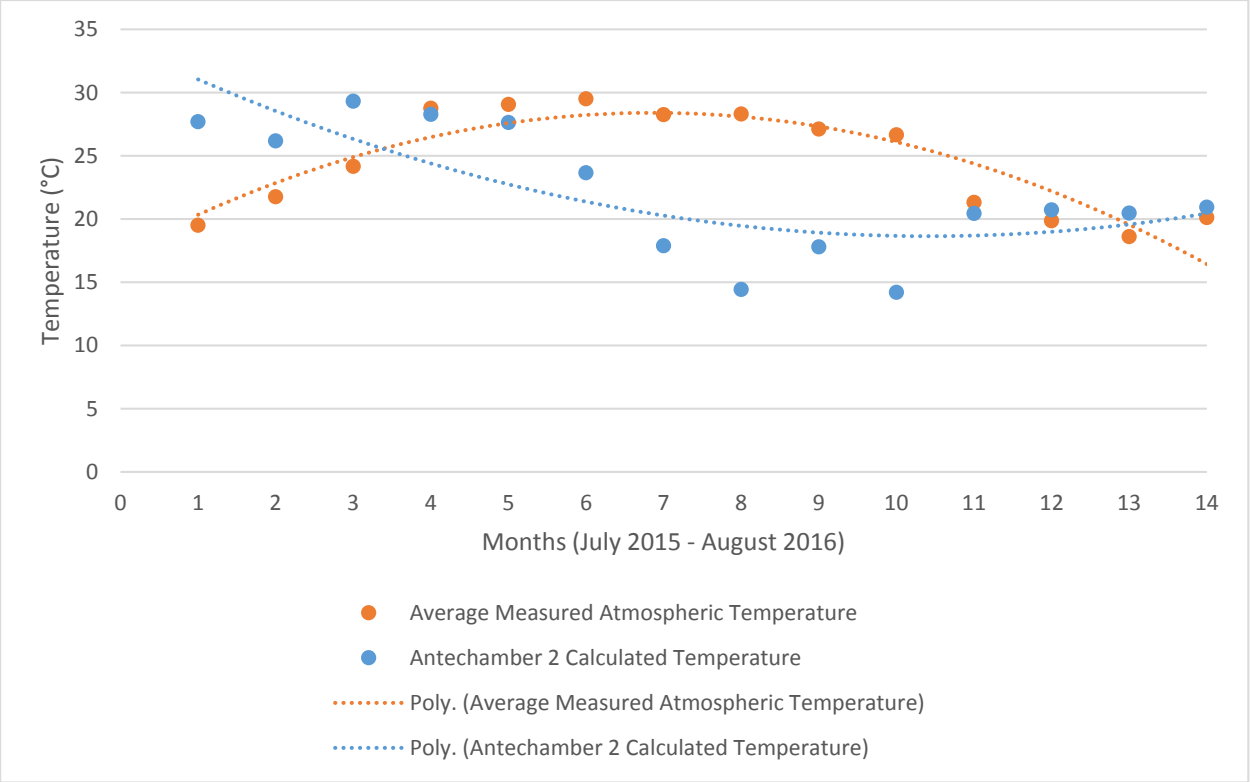

Fig. 4.26: Temperatures calculated from the Antechamber 2 average $\delta^{18}O$ values using equation 2, and compared to the average measured atmospheric temperatures.

A comparison of the measured cave air temperatures during the period of collection of drip water samples to the calculated temperatures using equation 1 from each chamber shows that the trends for each data set do correspond to a certain degree to one another (Figure 4.27). Both the measured cave air temperatures and the calculated temperatures for the chambers display an increasing trend from July 2015 to approximately October/November 2015, however the measured cave air temperatures display a much more gradual increase as opposed to the calculated temperatures from each chamber, which show a much steeper increase. All the trends for the respective data sets then display a decreasing trend from October/November 2015 to January 2016, apart from the calculated temperatures from Antechamber 1, which show a slight increase again and subsequent decrease in January 2016, and the calculated temperatures for the Jacovec Cavern, which show a sharp increase and subsequent decrease in December 2015. The measured cave air temperatures increase from January 2016 to February 2016, and then show a decreasing trend from March 2016. The calculated temperatures for Antechamber 1 show a decreasing trend until March 2016, and then display an overall increasing trend until August 2016. The calculated temperatures from Antechamber 2 show approximately the same overall trend as for Antechamber 1, with some occasional monthly increases and decreases in temperatures within the overall trend. The calculated temperatures for the Jacovec Cavern show

a very erratic trend, but a slight overall decreasing trend may be observed from December 2015 to April 2016, which is then followed by an increase towards August 2016. The calculated temperatures display an overall very gradual and very irregular decrease in overall temperatures towards February/March 2016, but show a much more pronounced and varied decreasing trend as that of the measured cave air temperatures.

Overall, the data sets display similar overall increasing and decreasing trends, with the exception of the winter months in 2016, as the measured cave air temperatures decrease, while the calculated temperatures display an increasing trend. The trends of the calculated temperatures are a lot more irregular and varied than that of the measured cave air temperature, and display steeper increasing and decreasing curves. These calculated temperatures also slightly higher than that of the measured cave air temperatures, with calculated temperatures from Antechamber 1 and Antechamber 2 being distinctly higher than that of the measured cave air temperatures during the late winter/spring and summer months. The calculated temperatures seem to match those of the measured cave air temperatures better during the autumn to early winter months.

Pearson product-moment correlation tests were conducted in PAST v3.14 software (Hammer et al., 2001) on the calculated temperatures for the three chambers and the average measured cave air temperatures. A correlation value (r) of -0.02 was produced for the calculated temperatures and the measured cave air temperatures from the Jacovec Cavern, showing a very weak negative correlation between the two data sets. The value for p was 0.94 at a 90% confidence level. A correlation value (r) of -0.34 was produced for the calculated temperatures and the measured cave air temperatures from Antechamber 1, showing a weak negative correlation between the two data sets. The value for p was 0.25 at a 90% confidence level. A correlation value (r) of -0.42 was produced for the calculated temperatures and the measured cave air temperatures from Antechamber 2, showing a weak to intermediate negative correlation between the two data sets. The value for p was 0.15 at a 90% confidence level (see Appendix B). None of these p values however are within the confidence level of 90%, indicating that the results are not statistically significant and therefore may not be an accurate representation of the data. This may indicate an unreliable and weak correlation interpretation, as well the presence of fractionation effects. This statistical unreliability could also be due to the very large range and variability of the calculated temperatures with regard to the cave air temperatures.

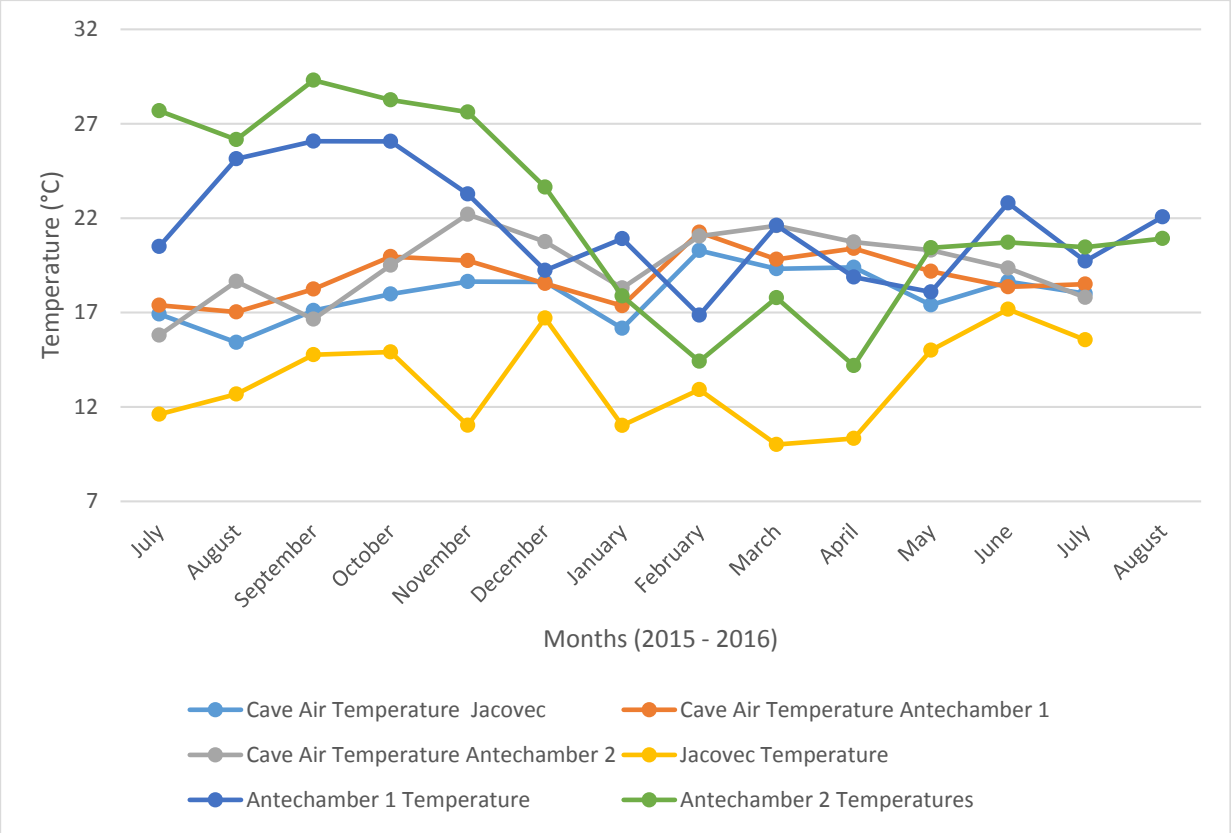

Fig. 4.27: Measured cave air temperatures versus the temperatures calculated from the Jacovec Cavern, Antechamber 1 and Antechamber 2 using equation 2.

4.4.3 Fractionation

The calculated temperatures using equation 1 from the Jacovec Cavern, Antechamber 1 and Antechamber 2 were compared to the idealised temperatures produced also using equation 1 from the $\delta^{18}O$ values of the speleothem samples from the respective chambers (Figure 4.28). These idealised temperatures did not take any fractionation into account, as opposed to the calculated temperatures which made use of the speleothem and drip water $\delta^{18}O$ values, which could display fractionation effects. The calculated temperatures using equation 1 display average values of approximately 21°C, 25°C and 24°C, which is very similar to the average idealised temperature value, which is approximately 23°C. Variations of the calculated temperatures from the idealised temperatures do however occur, with Antechamber 2 values ranging 10°C higher at its highest point and 8°C lower at its lowest point than that of the idealised temperatures. The calculated temperatures from Antechamber 2 show the greatest variations with regards to the idealised temperatures. Calculated temperatures from Antechamber 1 are approximately 7°C higher at its highest point and approximately 3°C lower at its lowest point than the idealised temperatures, which also shows some variation, but to a lower degree than that of the calculated temperatures from Antechamber 2. These calculated

temperature variations also only occur at three very distinctive points for Antechamber 1, whereas the variations in calculated temperatures for Antechamber 2 occur much more regularly, at approximately six points, compared to the idealised temperatures. The calculated temperatures for the Jacovec Cavern display variations that are only within 5°C lower and 3°C higher than the idealised temperatures, and the calculated temperatures only occur higher than the idealised temperatures at one point. Most of the calculated temperatures for the Jacovec Cavern remain lower than the idealised temperatures, within an average of approximately 2°C lower than that of the idealised temperatures. The calculated temperatures from the Jacovec Cavern therefore are closest to the idealised temperatures, with the calculated temperatures from Antechamber 1 coming in second, and those from Antechamber 2, third.

Overall, the calculated temperatures produced from equation 1 for the three chambers reflect averages which very closely reflect the idealised temperatures calculated also using equation 1, and the lower calculated temperatures seem to reflect the idealised temperatures to a better degree, with less variation. Pearson product-moment correlation tests were conducted in PAST v3.14 software (Hammer et al., 2001) on the calculated temperatures for the three chambers and the idealised temperatures calculated using equation 1. A correlation value (r) of 0.1 was produced for the calculated temperatures and the calculated idealised temperatures from the Jacovec Cavern, showing a very weak positive correlation between the two data sets. The value for p was 0.73 at a 90% confidence level. A correlation value (r) of -0.24 was produced for the calculated temperatures and the calculated idealised temperatures from Antechamber 1, showing a weak negative correlation between the two data sets. The value for p was 0.4 at a 90% confidence level. None of these p values however are within the confidence level of 90%, indicating that the statistical results are not significant and therefore may not be an accurate representation of the data. A correlation value (r) of -0.74 was produced for the calculated temperatures and the calculated idealised temperatures from Antechamber 2, showing a strong negative correlation between the two data sets. The value for p was 0.0027 at a 90% confidence level (see Appendix B). This p value is within the confidence level of 90%, indicating that the results are statistically significant and therefore may be interpreted further. Overall, however, the range and variability of the calculated temperatures in comparison with the calculated idealised temperatures indicates the unreliability of these statistical correlations.

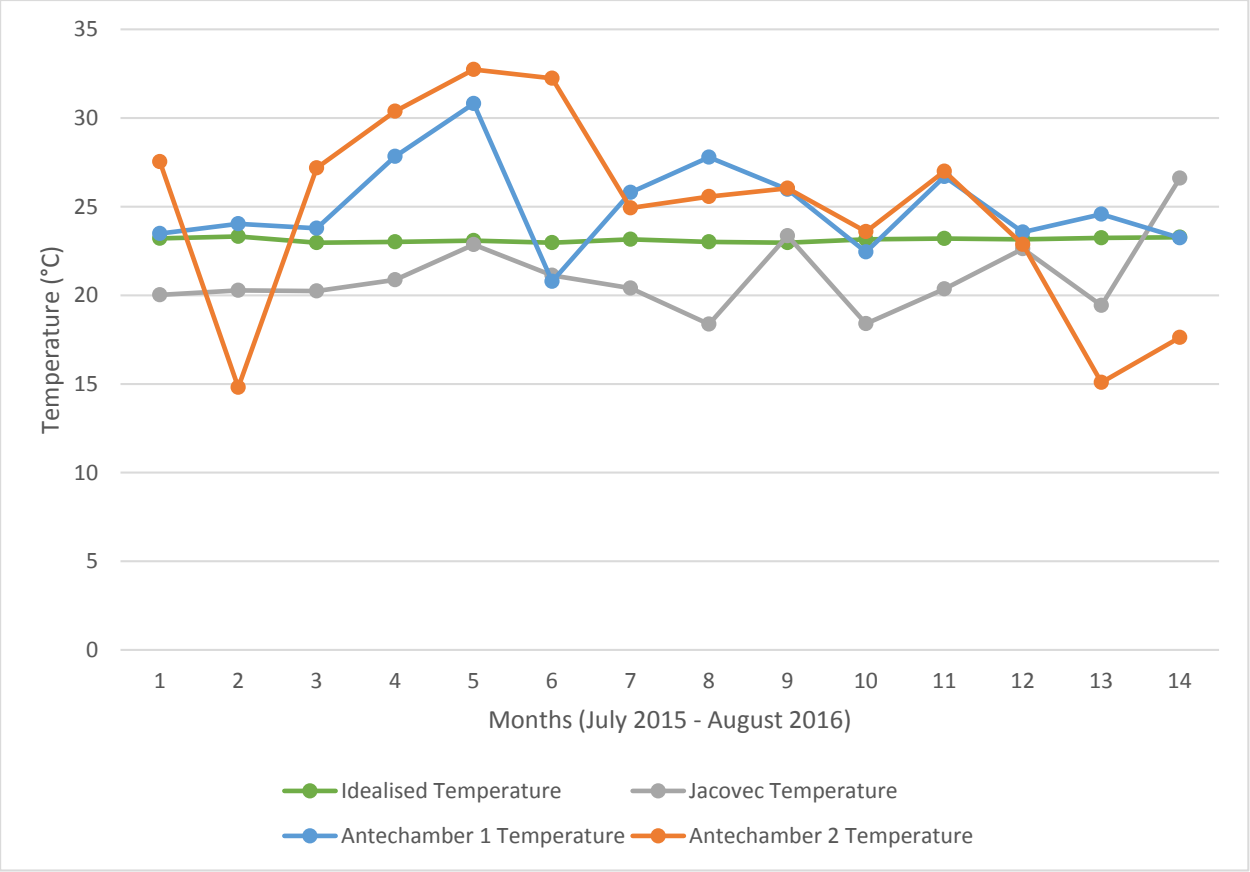

Fig. 4.28: Comparison between the idealised temperatures calculated using equation 1, and the temperatures calculated from the three chambers using equation 1.

The calculated temperatures using equation 2 from the Jacovec Cavern, Antechamber 1 and Antechamber 2 were compared to the idealised temperatures produced also using equation 2 from the $\delta^{18}O$ values of the speleothem samples from the respective chambers (Figure 4.29). These idealised temperatures did not take any fractionation into account, as opposed to the calculated temperatures which made use of the speleothem and drip water $\delta^{18}O$ values, which could display fractionation effects. The calculated temperatures using equation 2 display average values of approximately 13°C, 21.5°C and 22°C, which is approximately 2°C lower and 7°C higher than that of the average idealised temperature value, which is approximately 15°C. Variations of the calculated temperatures from the idealised temperatures occur on a large scale, with Antechamber 2 values ranging 14°C higher at its highest point and 1°C lower at its lowest point than that of the idealised temperatures. The calculated temperatures from Antechamber 2 show the greatest variations with regards to the idealised temperatures. Calculated temperatures from Antechamber 1 are approximately 11°C higher at its highest point and approximately 1°C higher at its lowest point than the idealised temperatures, which also shows some variation, but to a lower degree than that of the calculated temperatures from

Antechamber 2, especially with regards to the higher calculated temperatures. These calculated temperature variations also occur at ten distinctive points for Antechamber 1, whereas the variations in calculated temperatures for Antechamber 2 occur much more regularly, at approximately 11 points, compared to the idealised temperatures. The calculated temperatures for the Jacovec Cavern display variations that are only within 2°C higher and approximately 5°C lower than the idealised temperatures, and the calculated temperatures only occur higher than the idealised temperatures at two points. Most of the calculated temperatures for the Jacovec Cavern remain lower than the idealised temperatures, within an average of approximately 2°C lower than that of the idealised temperatures. The calculated temperatures from the Jacovec Cavern therefore are closest overall to the idealised temperatures, with the calculated temperatures from Antechamber 1 coming in second, and those from Antechamber 2, third.

Overall, the calculated temperatures produced from equation 2 for the three chambers reflect averages which vary significantly from the idealised temperatures calculated also using equation 2, in comparison to the idealised temperatures calculated using equation 2 and the equation 2 calculated temperatures. The lower calculated temperatures seem to reflect the idealised temperatures to a better degree, with less variation in comparison to the higher calculated temperatures. In general, the equation 1 calculated temperatures reflect the equation 1 idealised temperatures more closely than that of equation 2.

Pearson product-moment correlation tests were conducted in PAST v3.14 software (Hammer et al., 2001) on the calculated temperatures for the three chambers and the idealised temperatures calculated using equation 2. A correlation value (r) of -0.27 was produced for the calculated temperatures and the calculated idealised temperatures from the Jacovec Cavern, showing a weak negative correlation between the two data sets. The value for p was 0.37 at a 90% confidence level. A correlation value (r) of 0.22 was produced for the calculated temperatures and the calculated idealised temperatures from Antechamber 1, showing a weak positive correlation between the two data sets. The value for p was 0.46 at a 90% confidence level. A correlation value (r) of 0.35 was produced for the calculated temperatures and the calculated idealised temperatures from Antechamber 2, showing a weak to intermediate positive correlation between the two data sets. The value for p was 0.22 at a 90% confidence level (see Appendix B). None of these p values however are within the confidence level of 90%, indicating that the results are not statistically significant and therefore may not be an accurate representation of the data. Overall again, the large range and variability of the

calculated temperatures in comparison to the calculated idealised temperatures indicates the overall unreliability of these statistical correlations and interpretations.

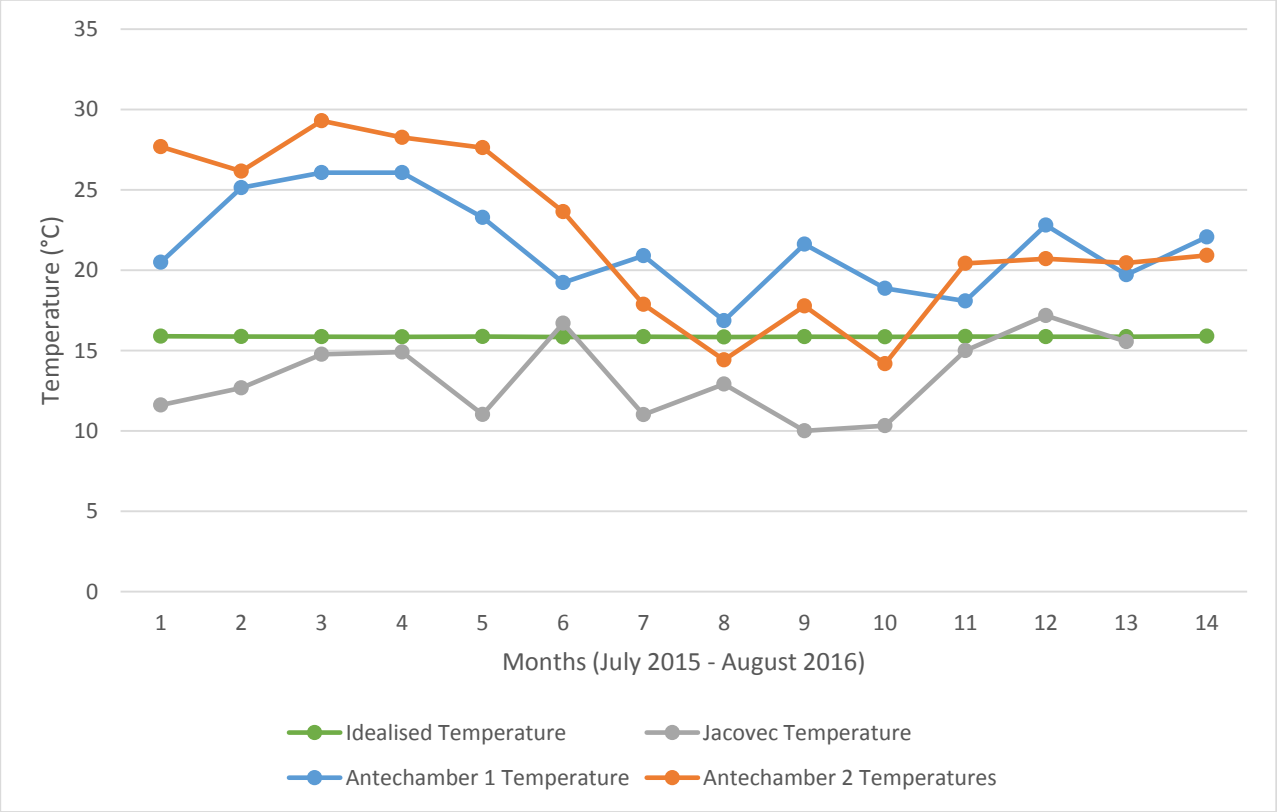

Fig. 4.29: Comparison between the idealised temperatures calculated using equation 2, and the temperatures calculated from the three chambers using equation 2.

4.4.4 Drip Rate and Precipitation

The drip rate monitored during the collection of the drip water samples shows a similar trend for all three chambers (Figure 4.30). Antechamber 2 shows an overall much lower drip rate than that of the other two chambers, with the Jacovec Cavern showing the highest drip rate, and Antechamber 1 showing a slightly lower drip rate, but quite close to that of the Jacovec Cavern. All three chambers show an increasing trend from July 2015 to September 2015, followed by a decreasing trend from September 2015 to November 2015. The Jacovec drip rate then settles into a steady value from November 2015 to March 2016, with one slight increase and decrease. The drip rate increases in April 2016, then decreases in May 2016, and then increases very sharply in June 2016. Antechamber 1 drip rates increase from November 2015 to December 2015, and then decrease gradually to February 2016. The drip rate then increases gradually until April 2016, with a short decrease in May 2016, and a sharp increase in June 2016. The Antechamber 2 drip rates also show slight increase from November 2015 to December 2015, and then decrease very gradually to April 2016, with a very slight increase in

April 2016. The drip rate then decreases slightly in May 2016, and begins to increase again in June 2016. All three data sets reflect a very similar increasing and decreasing trend, with slight variations. The trend for Antechamber 2 is observed to be very much flatter than that of the other two data sets. A Pearson product-moment correlation test was conducted in PAST v3.14 software (Hammer et al., 2001) on the drip rate values for the three chambers, and produced correlation values (*r*) of 0.5 to 0.85, showing strong positive correlations between the three data sets. Values for p averaged 0.036 at a 90% confidence level (see Appendix B). These p values are within the confidence level of 90%, indicating that the results are statistically significant and therefore may be interpreted further. This may also indicate a reliable correlation interpretation, and minimal fractionation effects.

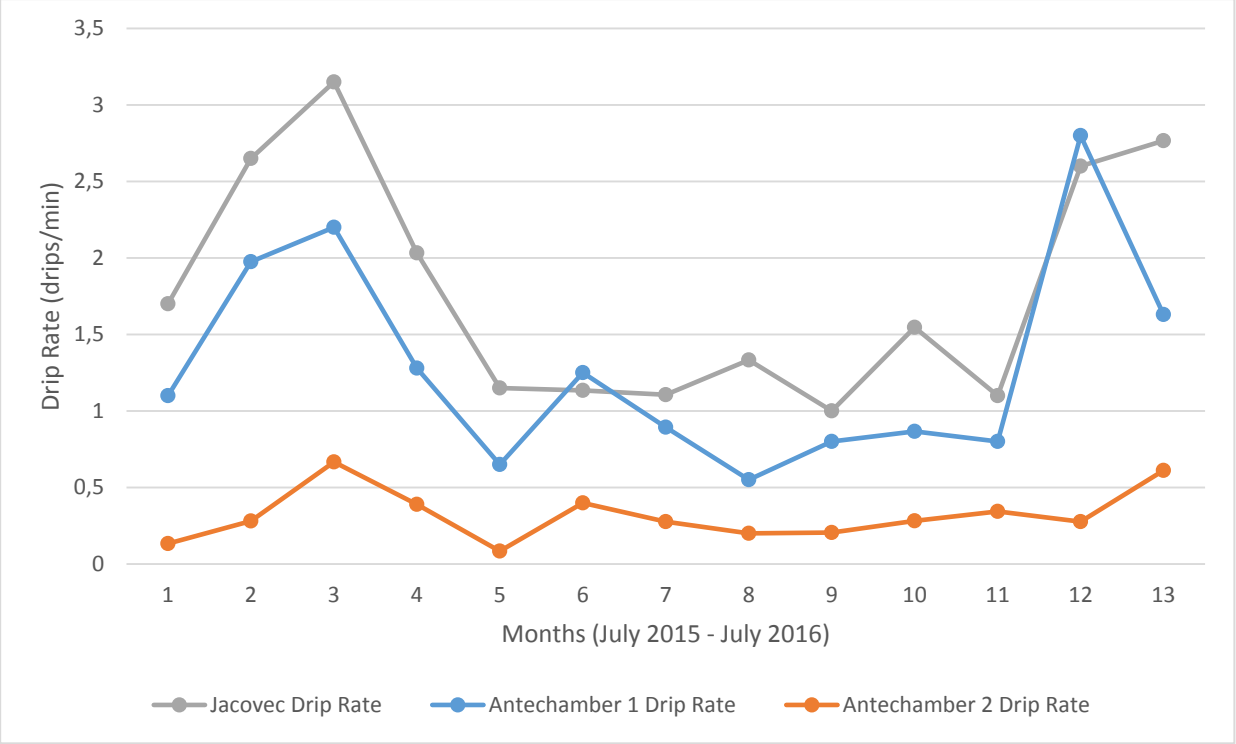

Fig. 4.30: Drip Rate for Jacovec Cavern, Antechamber 1 and Antechamber 2, from July 2015 to August 2016.

The drip rate of the three chambers displays a delayed trend in comparison to the measured precipitation for the area, where the drip rate peaks during the late winter and spring months, while the measured average rainfall peaks in the mid-summer months, and then decreases again (Figure 4.31). The drip rates show a much lower peak at its highest than that of the average measured rainfall, and much less varied, more gradual trend than that of the average measured rainfall. The Antechamber 2 drip rate trend is observed to be much flatter than that of the other

two chambers, or that of the average measured rainfall. Pearson product-moment correlation tests were conducted in PAST v3.14 software (Hammer et al., 2001) on the drip rates for the three chambers and the average measured monthly rainfall. A correlation value (*r*) of -0.45 was produced for the drip rates from the Jacovec Cavern and the average measured monthly rainfall, showing an intermediate negative correlation between the two data sets. The value for p was 0.12 at a 90% confidence level. A correlation value (*r*) of -0.34 was produced for the drip rates from Antechamber 1 and the average measured monthly rainfall, showing an intermediate negative correlation between the two data sets. The value for p was 0.25 at a 90% confidence level. A correlation value (*r*) of -0.14 was produced for the drip rates from Antechamber 2 and the average measured monthly rainfall, showing a very weak negative correlation between the two data sets. The value for p was 0.64 at a 90% confidence level (see Appendix B). None of these p values however are within the confidence level of 90%, indicating that the results are not statistically significant and therefore may not be an accurate representation of the data. This however may be due to the lag effect between the average measured monthly rainfall, and the drip rates, indicating that these correlations may not be accurate. The lag effect needs to be considered with regard to variations in drip rate in order to obtain accurate correlations.

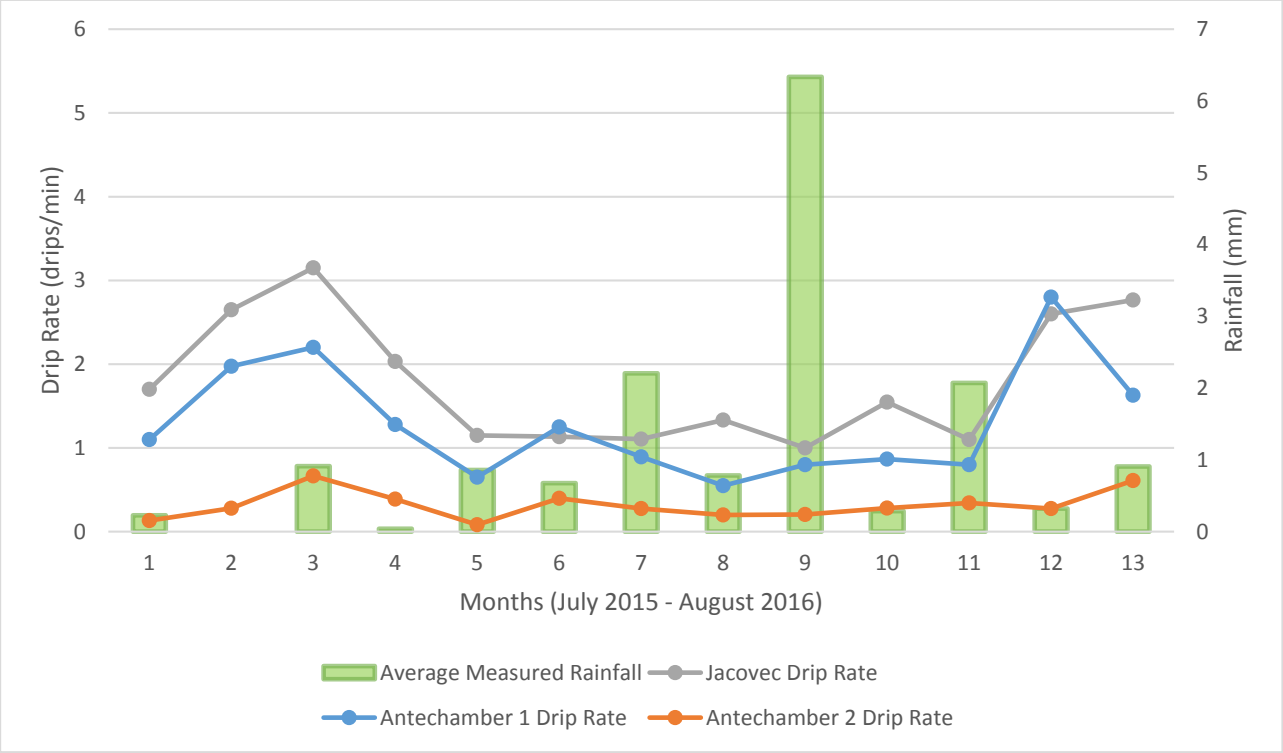

Fig. 4.31: Drip rate for the Jacovec Cavern, Antechamber 1 and Antechamber 2 in comparison to the average measured rainfall for July 2015 to August 2016.

The drip rate trends for the Jacovec Cavern, Antechamber 1 and Antechamber 2 also seem to reflect the average monthly $\delta^{18}O$ values for the drip water collected during which the drip rate was measured reasonably well (Figure 4.32). The data sets all increase from July 2015 to September 2015, and then decrease from September 2015 to November 2015 for the drip rate trends, after which they seem to settle into an approximately constant value until February 2016, when the drip rates start to gradually increase again until August 2016. The $\delta^{18}O$ values decrease from September 2015 to January 2016, after which they begin to increase in general very gradually towards August 2016, with a sharper increase in August 2016. These trends reflect each other well, with some variations with regards a shorter period of decrease, and a much flatter, gradual increase towards August 2016 compared to the $\delta^{18}O$ values, with the exception of a sharper increase towards August 2016 from April/May 2016.

Pearson product-moment correlation tests were conducted in PAST v3.14 software (Hammer et al., 2001) on the drip rates for the three chambers and the average monthly $\delta^{18}O$ drip water values. A correlation value (*r*) of 0.57 was produced for the drip rates and average monthly $\delta^{18}O$ drip water values from the Jacovec Cavern, showing an intermediate positive correlation between the two data sets. The value for p was 0.04 at a 90% confidence level. This p value is within the confidence level of 90%, indicating that the statistical results are significant and therefore may be interpreted further. A correlation value (*r*) of 0.26 was produced for the drip rates and average monthly $\delta^{18}O$ drip water values from Antechamber 1, showing a weak positive correlation between the two data sets. The value for p was 0.39 at a 90% confidence level. A correlation value (*r*) of 0.2 was produced for the drip rates and average monthly $\delta^{18}O$ drip water values from Antechamber 2, showing a weak positive correlation between the two data sets. The value for p was 0.51 at a 90% confidence level (see Appendix B). These two p values however are not within the confidence level of 90%, indicating that the results are not statistically significant and therefore may not be an accurate representation of the data. Overall however, the large range between the average monthly $\delta^{18}O$ drip water values and the drip rates may result in statistically unreliable correlations. The different units applicable to the drip rates and the $\delta^{18}O$ monthly values as well as the large amount of variability within data sets may also distort the correlation results, thereby leading to statistically unreliable correlations.

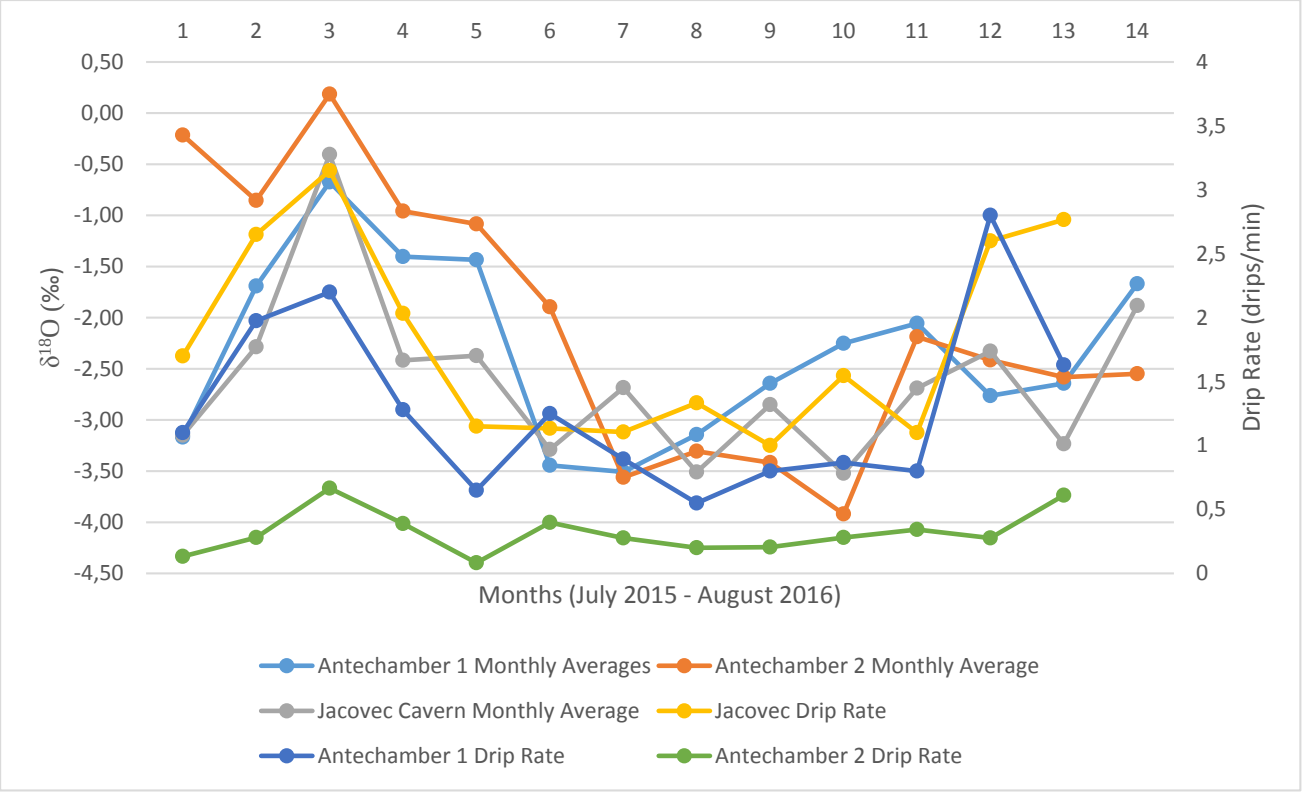

Fig. 4.32: Drip rate trends from the Jacovec Cavern, Antechamber 1 and Antechamber 2 compared to the $\delta^{18}O$ values measured from the drip water of the three chambers.

For precipitation interpretative purposes, the drip water $\delta^{18}O$ values were also compared to the monthly average measured rainfall from Krugersdorp, Johannesburg Botanical Gardens and Lanseria weather stations. The drip water $\delta^{18}O$ results display a distinctive inverse relationship with the rainfall measured in the area during the collection of the drip water samples. This is observed in figure 4.33, where higher measured rainfall corresponds to a decrease in drip water $\delta^{18}O$ values, and vice versa. Pearson product-moment correlation tests were conducted in PAST v3.14 software (Hammer et al., 2001) on the average monthly $\delta^{18}O$ drip water values for the three chambers and the average monthly measured rainfall. A correlation value (*r*) of -0.09 was produced for the average monthly $\delta^{18}O$ drip water values from the Jacovec Cavern and the average monthly measured rainfall, showing a very weak negative correlation between the two data sets. The value for p was 0.76 at a 90% confidence level. A correlation value (*r*) of -0.20 was produced for the average monthly $\delta^{18}O$ drip water values from Antechamber 1 and the average monthly measured rainfall, showing a weak negative correlation between the two data sets. The value for p was 0.48 at a 90% confidence level. A correlation value (*r*) of -0.39 was produced for the average monthly $\delta^{18}O$ drip water values from Antechamber 2 and the average monthly measured rainfall, showing a weak to intermediate negative correlation between the two data sets. The value for p was 0.17 at a 90% confidence level (see Appendix B). None of

these p values however are within the confidence level of 90%, indicating that the results are statistically not significant and therefore may not be an accurate representation of the data. This however may be due to the lag effect between the average measured monthly rainfall, and the drip rates, indicating that these correlations may not be accurate. The lag effect needs to be considered with regard to variations in drip rate in order to obtain accurate correlations. The different units of measurement between the two data sets could also result in inaccurate statistical correlations.

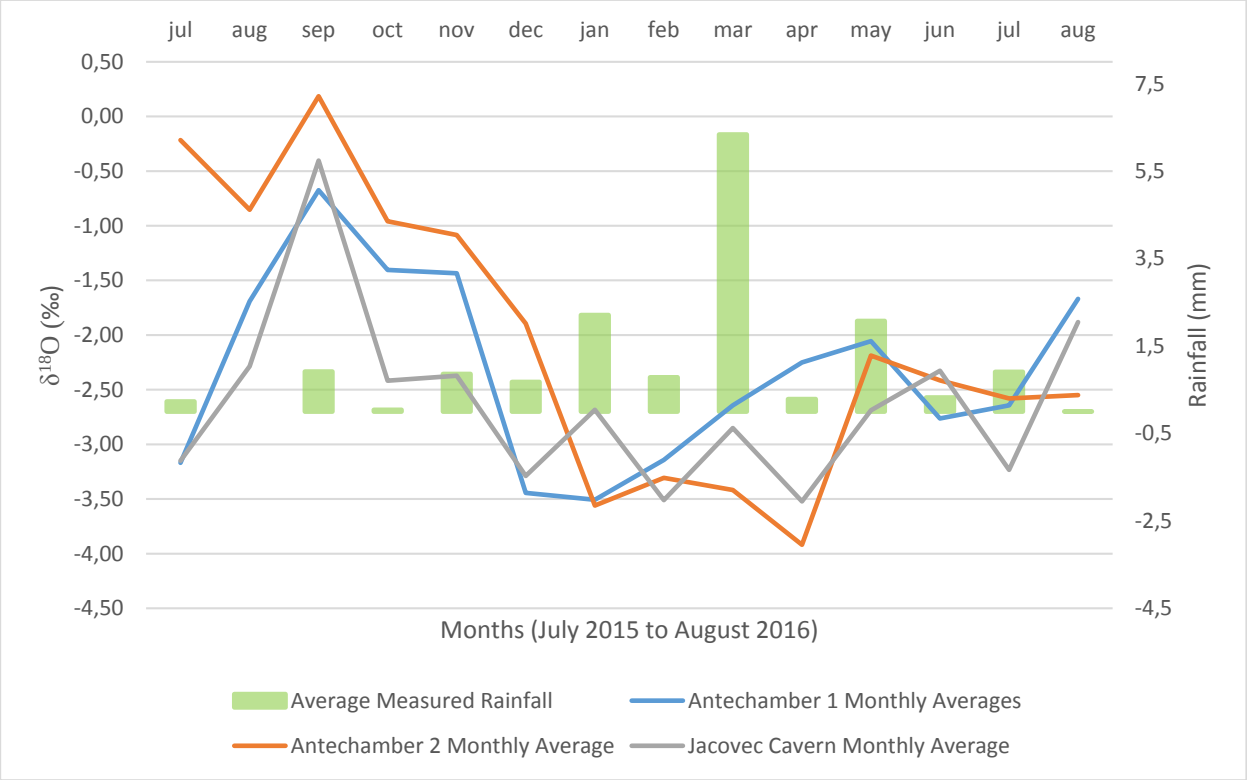

Fig. 4.33: Average monthly measured rainfall compared to the $\delta^{18}O$ values from drip water.

4.5 Hydrochemistry

4.5.1 Electro-conductivity

In general, the electro-conductivity of the cave drip water ranged from approximately 200 µS/cm to approximately 350 µS/cm (Figure 4.34). The electro-conductivity for individual drip water samples fluctuated between this range for the duration of the year. No clear trends can be observed between individual sample fluctuations. The electro-conductivity between samples within the same caverns or antechambers seemed to remain within a similar range to one another. Antechamber 1 samples are observed to have in general a slightly higher electro-conductivity than any of the other caverns, with an average range between 272.3 µS/cm and

309.9 µS/cm. Samples from the Jacovec Cavern follow closely, with an average range between 249.7 µS/cm and 282.5 µS/cm. The samples from antechamber 2 have the lowest average range of electro-conductivity values, ranging from 220.1 µS/cm to 208.1 µS/cm. The sample taken from the Milner Lake produced a much higher electro-conductivity of 668 µS/cm.

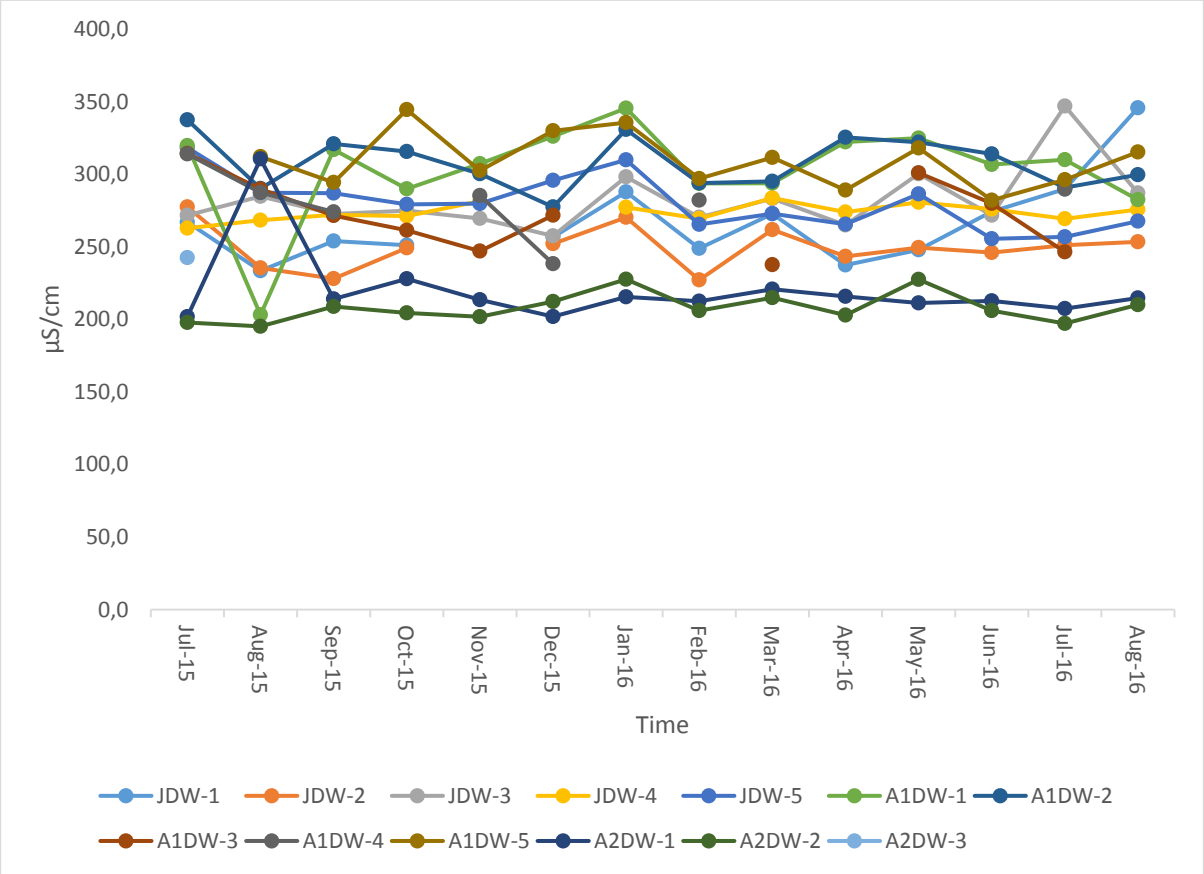

Fig. 4.34: Electro-conductivity results for the modern drip water samples.

4.5.2 pH

pH remained fairly constant between all the samples, ranging from approximately 7.7 to 8, with five outlier samples (Figure 4.35). This shows that the drip water samples were leaning towards a slightly more alkaline pH, in the range for groundwater pH (6 to 8.5). A sample from the Milner Lake was also analysed, in order to compare the pH values, and produced a pH of 7.76, which is slightly alkaline.

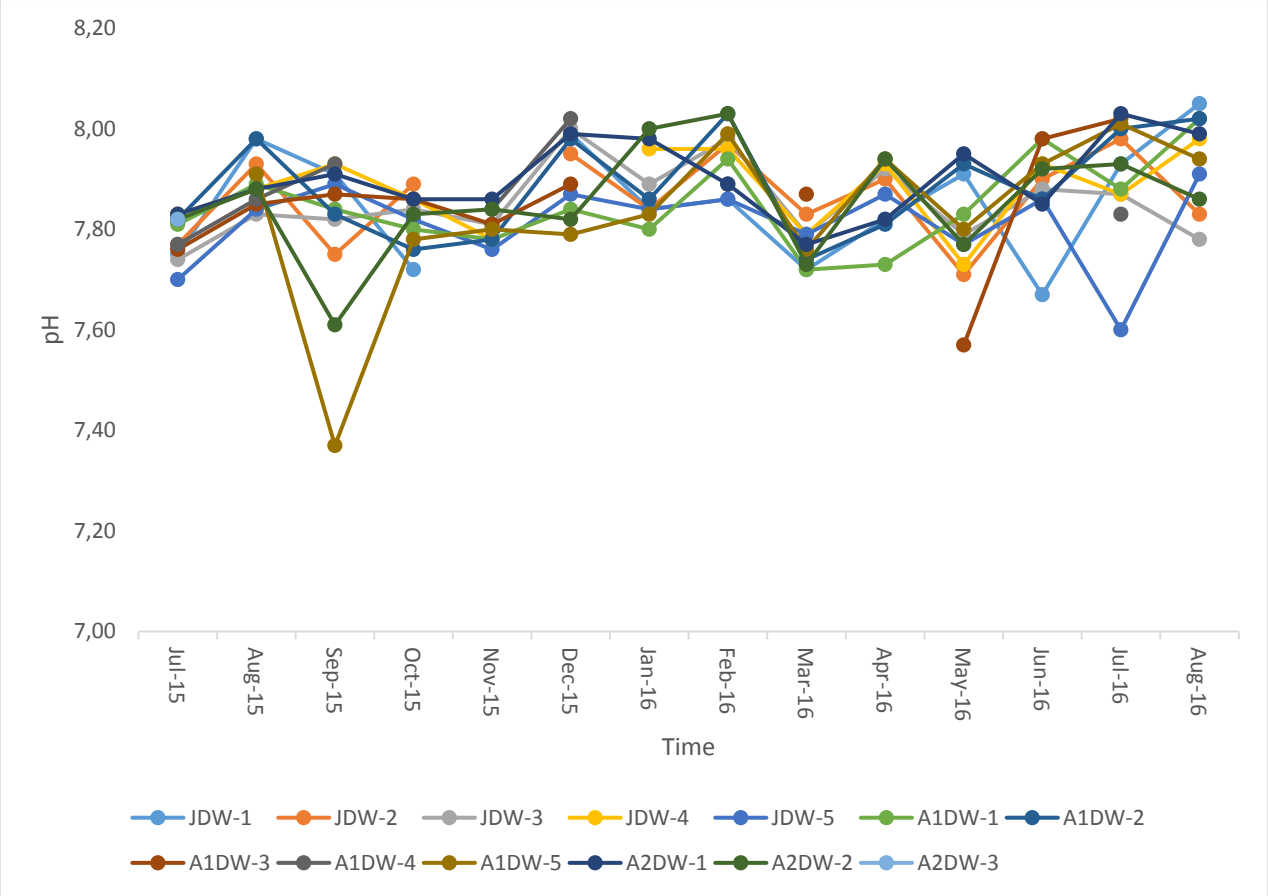

Fig. 4.35: pH results for the modern drip water samples from Sterkfontein Caves.

4.6 Summary

The overall climatic data presented for the area surrounding Sterkfontein displays regular seasonal trends, with average temperatures increasing slightly over the 10 year record. The cave air temperatures, humidity and atmospheric pressure constrain the climatic conditions within the Sterkfontein Caves environment well, and exhibit an environment with intermediate to high humidity, and relatively stable air temperatures and pressures. The vegetation distribution results of the carbon stable light isotope analysis correlate with the observed distribution of vegetation on the exterior environment, exhibiting a mosaic environment with open grasslands interspersed with shrubs and open woodland trees. The results of the oxygen isotope analysis of the modern speleothem and drip water samples reveals a wide range of temperatures which, to a certain degree, do exhibit relationships and similarities to the exterior temperatures, but also demonstrate that kinetic fractionation has played a role in skewing the results. The oxygen isotope values from the drip water samples mirror the rainfall cycles measured by the weather stations well, and display effects of ground water residence time,

recharge, and lag effects. The drip rate measured from the drip water samples also corresponds very well to the oxygen isotope values and rainfall data from the weather stations. The hydrochemistry of the drip water samples reveals electro-conductivity results which vary within a reasonable range, and may be comparable to drip rates and atmospheric pressure, as well as the exterior temperatures.

Chapter 5
Discussion

5.1 Vegetation

5.1.1 Modern Speleothem Carbon Isotopes

Raw carbon isotopic signatures produced from the carbon stable light isotope analysis of the modern speleothems reveal an enriched trend, with an average of -1.61‰ and a range of -2‰ to 2‰, with the exception of the Silberberg Grotto. Depending on the route taken by the drip water to ultimately precipitate these modern speleothems, this enrichment of $\delta^{13}C$ values in the modern speleothems may be attributed to a combination of factors which have a significant effect on the level of enrichment of the carbon isotope signature. These factors include; the isotopic composition of the dissolved HCO_3, the isotopic composition of the precipitated $CaCO_3$, kinetic fractionation present in the hydro-carbonate system within the cave, the percentage of saturation with regards to $CaCO_3$, the rate of exchange with gaseous phases within the cave system, and the ultimate rate of precipitation of the speleothem (Richards & Dorale, 2003). An increase in the percentage saturation with regards to $CaCO_3$ and the progressive precipitation of $CaCO_3$ both result in enriched $\delta^{13}C$ values, as well as progressive transformation of HCO_3 to CO_2 and the subsequent degassing thereof (Polag et al., 2010). The enrichment of the carbon isotopic signature of the modern speleothems therefore may reflect the degree to which these process and factors have affected the $\delta^{13}C$ signature.

The degassing of CO_2, and subsequent precipitation of $CaCO_3$ structures may occur under closed or open system conditions, which also ultimately influence the $\delta^{13}C$ signal produced from the speleothems (Hendy 1971; Dorale et al., 2002; Fairchild et al., 2006; Noah, 2010). If the cave system is of an open nature, the solution percolating through the soil and host rocks has access to a very large source of soil CO_2 (Hendy, 1971; Noah, 2010). This ultimately contributes to the isotopic signature of the dissolved HCO_3 in the cave system, and produces a $\delta^{13}C$ signature which primarily represents the soil CO_2, and therefore the vegetation growing above the cave environment (Hendy, 1971). This is the case with respect to the Sterkfontein Caves, as this cave system is regarded as an open cave system, with respect to the locations where the speleothem samples were collected. Due to the open nature of the cave system, the carbon isotope results of the speleothem samples are expected to be a reflection of the $\delta^{13}C$

signature primarily from soil CO_2, which would provide a good indication of the distribution of vegetation on the ground surface. In contrast, the solution percolating through a cave system of a closed nature has a very limited source of CO_2, which is degassed during entry into the cave system (Hendy, 1971). This therefore results in the $\delta^{13}C$ signature of the $CaCO_3$ structures precipitated under these circumstances to represent a mixture of the soil CO_2 as well as carbon from the dissolution of the $CaCO_3$ rich host rocks (Hendy, 1971; Noah, 2010). In order to produce reliable correlations with regards to ground surface vegetation distribution, it is therefore preferable to collect speleothem samples for stable carbon isotopic analysis from open caves.

Overall, the enriched $\delta^{13}C$ values from the modern speleothems correlate well with a drier, more arid environment dominated by C_4 vegetation. Carbon stable light isotope analysis of speleothems provides detailed information regarding the distribution of C_3 and C_4 vegetation from the environment above the cave system. This distribution of vegetation is important to analyse as it reveals information regarding the climatic conditions of the exterior environment during the precipitation of the speleothems. The raw $\delta^{13}C$ values also display a very strong positive correlation in comparison to the distribution of C_4 vegetation, with a Pearson's *r* value of 1, and a very strong inverse relationship with the distribution of C_3 vegetation, with a Pearson's *r* value of -0.99. The p values for these statistical correlations were both within the 90% confidence level, indicating that the correlation is statistically significant. These correlations are also in agreement with the average approximate value of 80% C_4 vegetation cover calculated from the average raw $\delta^{13}C$ signature, according to Talma and Vogel's (1992) method for calculating vegetation types and distribution.

Carbon isotopes from the modern speleothem samples produced vegetation trends with C_4 vegetation dominating approximately 78% of the predicted environment above the Sterkfontein Cave system, and C_3 vegetation occupying approximately 22% of the environment above the cave system. These distributions were calculated using Talma and Vogel's (1992) method for determining C_4 and C_3 vegetation distribution. CAM plants, such as succulents, are known to conserve water, and therefore may vary between C_3 and C_4 signatures (Raven & Johnson, 1989; van der Merwe, 1982). The degree to which CAM vegetation produces either a C_3 or C_4 signature is usually dependent on species, but may also be influenced by the overall local climatic conditions, such as seasonality, temperature, rainfall and fire cycles (Proches et al., 2006). CAM vegetation thriving in primarily hot and dry conditions has been noted to usually produced $\delta^{13}C$ values in the range of C_4 vegetation (Keeley & Rundel, 2003). However, CAM

vegetation thriving in more moderate, moisture rich environments tend to display $\delta^{13}C$ values in the intermediate range towards C_3 vegetation (Mooney et al., 1977). Due to the fact that the CAM carbon isotopic signature is very difficult to distinguish from the C_4 carbon isotopic signature, CAM vegetation cannot be adequately estimated, and therefore has been assumed to form a part of the C_4 carbon isotopic signature, for reasons of simplicity (Zech et al., 2009).

The average carbon isotope value produced from stable light isotope analysis of the modern speleothem samples equates to approximately 80% C_4 vegetation, which is in agreement with the overall C_4 vegetation percentage dominance. These values imply a mosaic modern environment above the Sterkfontein Caves site, dominated by grasses interspersed with larger shrubs and open woodland trees. This environment would coincide with a slowly aridifying modern environment, with warmer, arid seasonal summer rainfall (Vogel, 1993), where a more C_3 enriched, closed woodland environment is developing into a progressively more open, grassland dominated environment, thereby producing a mosaic environment with both C_4 and significant amounts of C_3 vegetation. A C_4 dominated environment, which is implied by the carbon isotopic signatures of the speleothems, suggests an environment controlled more by seasonal rainfall, high radiation and more arid conditions during the growth of the C_4 plants (Vogel, 1993). These conditions have also been attributed to interglacial periods, which are dominated by C_4 vegetation (Vogel, 1993; Lourens et al., 1996).

C_4 vegetation has also been documented to out-compete C_3 vegetation during periods when CO_2 levels within the atmosphere are particularly low (Cerling et al., 1997). It can therefore be assumed to a certain degree, that a dominance of C_4 produced from the isotopic signatures of modern speleothems indicates a decrease in atmospheric CO_2, as well as the seasonality of rainfall, and greater variation in temperature conditions. Smaller variations within the $\delta^{13}C$ values for the modern speleothem samples may also be related to seasonality, where carbon isotope values increase during summer and decrease again during the winter (Richards & Dorale, 2003), as well as due to the numerous factors which may affect the ultimate $\delta^{13}C$ signature of the modern speleothem samples. These interpretations are consistent with other faunal, floral and isotopic studies conducted within the Cradle of Humankind, which also revealed that a mosaic environment existed in the area during the early to middle Pleistocene, which included patches of open grasslands and woodlands hosting both C_3 and C_4 vegetation, revealing an aridifying environment where C_4 vegetation was slowly beginning to dominate

over C_3 vegetation (Reed, 1996; Sponheimer & Lee-Thorp, 2003; Reynolds, 2007; Reynolds & Kibii, 2011).

The analysis of the Member 4 deposits in the Sterkfontein cave site also revealed that a mosaic environment existed during the deposition of these sediments (Bamford, 1999; Kibii, 2004; Reynolds & Kibii, 2011), and habitat reconstructions of the Sterkfontein Valley are also consistent with a mosaic environment interpretation, indicating that the area was characterised by a medium density forest interspersed with an open savannah environment (Vrba, 1985, 1988; Benefit & McCrossin, 1990; Mckee, 1991; Clarke & Tobias, 1995; Berger & Tobias, 1996; Reed, 1996; Potts, 1998; Bamford, 1999; Reynolds & Kibii, 2011). These results and interpretations correlate well with the enriched $\delta^{13}C$ values from the modern speleothems, which indicate a drier, more arid environment dominated by C_4 vegetation, and are also consistent with the average approximate value of 80% C_4 vegetation cover calculated from the average raw $\delta^{13}C$ signature.

The carbon isotope data obtained from the Silberberg Grotto however were severely depleted in comparison to the rest of the modern speleothem carbon isotope results, with a range of -4.61‰ to -8.95‰, and displaying values of 40%-78% C_3 vegetation. This implies an area particularly more concentrated in C_3 woodland trees and shrubs above the cave system, near the Silberberg Grotto. This can possibly be explained by the fact that the Silberberg Grotto is in close proximity to a major entrance to the cave system. Groups of trees characteristically mark the entrances and shafts into cave systems in the Cradle of Humankind, and these trees may have influenced the C_3 dominated carbon isotope values for samples from the Silberberg Grotto. Percolating meteoric water through the karst system may have also influenced the significant concentration of carbon isotopes producing C_3 values, as descending meteoric water near the Silberberg Grotto is constrained in the area by numerous faults, joints and channels (Martini et al., 2003), and the Grotto lies quite close to the surface, where direct vertical water seepage may have affected the carbon isotope values of the precipitated speleothems (Partridge, 1978). The Silberberg Grotto also lies directly next to a swallow hole, where surface water may very easily percolate downwards towards the Grotto (Pickering et al., 2011), and provide a direct route for carbon isotopes to be transported from the surface to the precipitating speleothems within the Silberberg Grotto (Holland et al., 2010). This shows how the geomorphology and resulting hydrological systems within the karst environment may also play a role in skewing any carbon isotopic signatures produced from the speleothem samples.

Meteoric water flowing through soil from areas concentrated in trees and shrubs may have also influenced the Silberberg Grotto samples significantly. In order to precipitate and grow, speleothems need an increase in effective precipitation (Ayliffe et al., 1998), which holds true for C_3 vegetation as well (Vogel, 1993), therefore it would make sense for the Silberberg Grotto to hold a predominately C_3 signature, as there are no actively dripping modern speleothems within this chamber at the moment. The correlation between the significantly depleted, C_3 $\delta^{13}C$ signature from the Silberberg Grotto and the current environmental conditions and vegetation cover directly influencing the signature of the $\delta^{13}C$ values again indicates the reliability of using $\delta^{13}C$ trends from modern speleothems to determine current vegetation type and distribution on the overlying surface, as this depleted trend accurately represents the current vegetation existing specifically above the Silberberg Grotto.

5.1.2 Observed Vegetation

The current vegetation observed above the Sterkfontein Caves system exhibits approximately 75% C_4 vegetation consisting of numerous grasses and particular small shrubs, 24.5% C_3 vegetation consisting of woodland trees, shrubs and small herbaceous plants, and approximately 0.5% CAM vegetation, in the form of a few succulents occurring particularly above the Jacovec Cavern area (Figure 5.1). These observed approximate percentages are in agreement with the percentages calculated using the modern speleothem carbon isotopes and this displays a consistency between the vegetation results obtained from the carbon isotopes of the modern speleothem samples, and the current observed vegetation that exists above the Sterkfontein Caves system (Figure 5.1). The observed vegetation also included a clustering of trees and shrubs around the entrances of the Sterkfontein Cave system, which supports the possibility that the proximity of the Silberberg Grotto to one of the cave entrances could have influenced the significance of the C_3 value from the modern speleothem carbon isotopes (Figure 5.1). The strong correlation between the observed vegetation currently existing above the Sterkfontein Caves system and the overall C_3 and C_4 vegetation distribution calculated from the $\delta^{13}C$ values from the modern speleothems substantiate the use of $\delta^{13}C$ trends from speleothems as paleoclimate proxies for vegetation type and distribution.

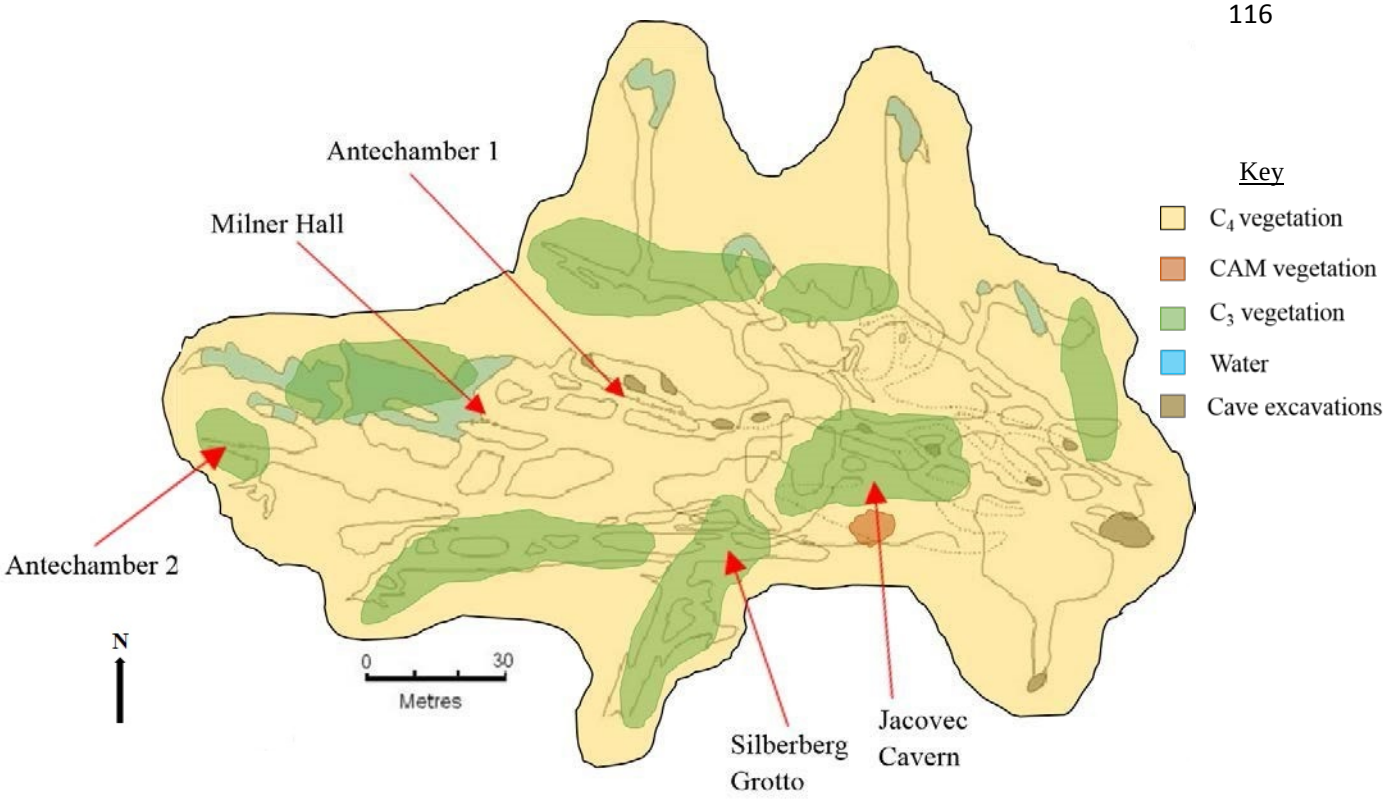

Fig. 5.1: Diagram showing the vegetation cover in relation to the cave chambers. Adapted from Reynolds et al. (2003).

5.1.3 Overall Vegetation Distribution

Overall, the carbon isotope vegetation data produced from the modern speleothems coincides very well with the observed vegetation currently existing above the cave environment, and therefore substantiates the reliability of environmental analysis using speleothems due to the similarity of the two results. This however also indicates that certain conditions need to be met in order for the carbon isotopic signature to accurately reflect the vegetation distribution on the ground surface.

The carbon isotope results from the modern speleothem samples at Sterkfontein display an environment dominated by C_4, but intertwined with C_3 vegetation distribution. This is in agreement with the actual observed vegetation distribution of the surface environment above the Sterkfontein Caves system. The strong positive correlation obtained from the Pearson product-moment test also confirms that this relationship is statistically significant. This correlation substantiates the overall reliability of using $\delta^{13}C$ values from speleothems as proxies from vegetation type and distribution, and consequently as palaeoclimate proxies, due to the implication of certain environmental and climatic conditions as a result of the distribution and type of vegetation indicated on the ground surface by the $\delta^{13}C$ trends.

5.2 Temperature

5.2.1 Modern Speleothem Oxygen Isotopes

The oxygen isotopes produced from the modern speleothem samples are reasonably negative with an average of -3.6‰, signifying overall long term cooler temperatures and drier conditions during speleothem growth, with seasonal rainfall. Temperatures deduced from the oxygen stable light isotope analysis of the modern speleothem samples reveal a very variable saw tooth pattern, with more depleted, negative oxygen isotope values reflecting drier periods with less rainfall, while less depleted, more positive values reflecting wetter conditions with an increase in warm, frequent rainfall.

There is variation in the spread of oxygen isotopes but the majority of the oxygen isotopes reflect more depleted values, therefore a general cooler, drier trend. Oxygen isotope values from modern speleothem samples from the Jacovec Cavern are slightly more enriched compared to the other modern speleothem samples in other caverns. This could be due to the fact that the Jacovec Cavern is more isolated from cave entrances or shafts, and the presence of a broad range of humidities compared to other areas within the cave system. With respect to the Milner Hall Lake modern speleothem samples, these samples are exposed to a number of air flow passages from various nearby cave shafts and entrances, exposing the speleothems to more evaporative overall conditions, thereby explaining the much more depleted oxygen isotope values produced by these samples. These variations in the oxygen isotope values from particular caverns therefore reflect current short term climatic and environmental variations between different chambers within the cave system at a local scale, therefore indicating the reliability of the oxygen isotopes produced from the analysis of the modern speleothems to reflect current climatic and environmental conditions within the cave system. These short term palaeoclimatic variations within the chambers may therefore also be inferred reliably using ancient speleothems.

Different conditions on which the speleothems were precipitated seemed to have differing effects on the values of the oxygen isotopes produced. Speleothem samples precipitated over older dolomite host rocks, as is the case with samples JCS-3 and MHLS-1, did not produce similar oxygen isotope results, showing no correlations within the data sets, and therefore no visible relationship.

Silberberg Grotto samples all precipitated over older speleothem. Samples SGS-1 and SGS-3 show much more depleted oxygen isotope values compared to samples SGS-2 and SGS-4.

Sample SGS-2 was collected directly below sample SGS-4, and shows a much more enriched oxygen isotope value compared to sample SGS-4. This might be a result of the movement of oxygen isotopes within drip water towards the bottom of the flow of the speleothem, thereby resulting in an enrichment of oxygen isotopes in comparison to a sample taken higher up in the flow.

Speleothem samples from Antechamber 1 and 2 were mostly precipitated over a combination of older speleothem material and older breccia. This may explain the fairly uniform trend in oxygen isotope values between these samples, only varying by approximately 0.7‰.

In general, the slight oxygen isotope variations due to chemically different flow paths through the host rocks did not significantly alter the idealised temperatures produced, as the graph produced from the calculated temperatures displayed a smooth, linear trend. As no fractionation was taken into account in the calculation of these temperatures, it could be assumed that some variations in $\delta^{18}O$ results could be due to differing formation conditions of the modern speleothem samples. These differing formation conditions would therefore have possibly affected the fractionation present in the samples to a certain degree. This can be seen when temperatures are calculated using oxygen isotopes from both the modern speleothem samples and the drip water samples, as well as in the statistical correlations produced from these calculated temperatures. If any drip water or speleothem samples had been collected from aragonite sources, this would have significantly influenced the $\delta^{18}O$ values produced, and a different equation would have been used to calculated temperatures, specific to aragonitic speleothems.

Idealised temperatures for the environment above the Sterkfontein Caves system were calculated using two different equations for calculating temperatures from speleothem samples, namely the experimental equation and the empirical equation. During the calculation of these temperatures it was assumed that fractionation did not play a role in affecting the oxygen isotopes from the modern speleothem samples. Therefore, it can be assumed that the cave air temperatures are similar in value to the calculated idealised temperatures using the speleothem samples. The use of these idealised temperatures and their comparison to the measured cave air temperatures allows for the amount fractionation that has occurred during the precipitation of the speleothem samples to be deduced, and therefore for possible methods to be obtained in order to work around this fractionation. When the calculated idealised temperatures were compared to the actual cave air temperatures, it was found that the idealised temperatures calculated from the experimental equation were much closer in value to the measured air

temperatures within the cave system than that of the idealised temperatures calculated using the empirical equation. These idealised temperatures calculated using the experimental equation could thus better predict air temperatures outside the cave environment. This could be due to the experimental nature of the calculation, which would more closely represent natural conditions of speleothem growth and precipitation.

The idealised temperatures calculated from the modern speleothem samples compared to the measured cave air temperature observed when the speleothems were collected show a close range of only approximately 2°C between the two data sets, but do show some large variations with regard to range, with some data set points being very closely situated, and other approximately 2°C apart. These variations could possibly be due to seasonal atmospheric temperature variations, or large climatic events on a local scale. The average cave air temperature is only 0.66°C higher than the idealised temperatures. This slight difference between the average cave air temperature and the idealised temperatures may also reflect the reliability of the modern speleothems as proxies for the current atmospheric temperatures, as this difference could possibly be due to the fact that fractionation was not taken into consideration for calculating the idealised temperatures, and possibly due to the relatively high humidity and low cave ventilation effects. This would therefore indicate that the modern speleothems would be reliable sources of temperature data. The idealised temperatures produced from the speleothem samples were then compared to the cave air temperature and the average atmospheric air temperature for the latter half of June 2015 (June 15th to June 30th) (Figure 5.2) in order to determine how close the relationship was between the three data sets. The cave air temperature varies around the atmospheric air temperature, with an average of 16.52°C, only 0.2°C less than that of the atmospheric air temperature, while the idealised temperatures from the experimental equation produce values slightly less than that of the atmospheric air temperature, but only by 0.89°C. Again this difference could be due to the fact that no fractionation or interference was taken into account, the effects of variations in humidity from intermediate to relatively high values, as well the fact that these idealised temperatures could possibly represent the average of a much greater range of atmospheric air temperatures than that of just June 2015 in combination with any smaller climatic events which may have been in effect during the precipitation of the speleothems. Variations between the average atmospheric temperatures, the idealised calculated temperatures and the cave air temperatures, however, indicate that significant kinetic fractionation effects have played a role in skewing the calculated temperatures from both equations. This occurs to a lesser degree in the narrower, smaller antechambers than in the Jacovec Cavern, which is quite large. This is due to higher

overall humidity in the antechambers, especially Antechamber 1, in comparison to the Jacovec Cavern, which displayed the greatest range of variations in humidity. To this extent, the idealised temperatures may indicate that the modern speleothems would be a reliable source of current temperature data, as the differences between the idealised temperatures and the cave air temperatures and atmospheric air temperatures do not differ by a significant degree, and may be explained by fractionation and climatic effects present in the cave system.

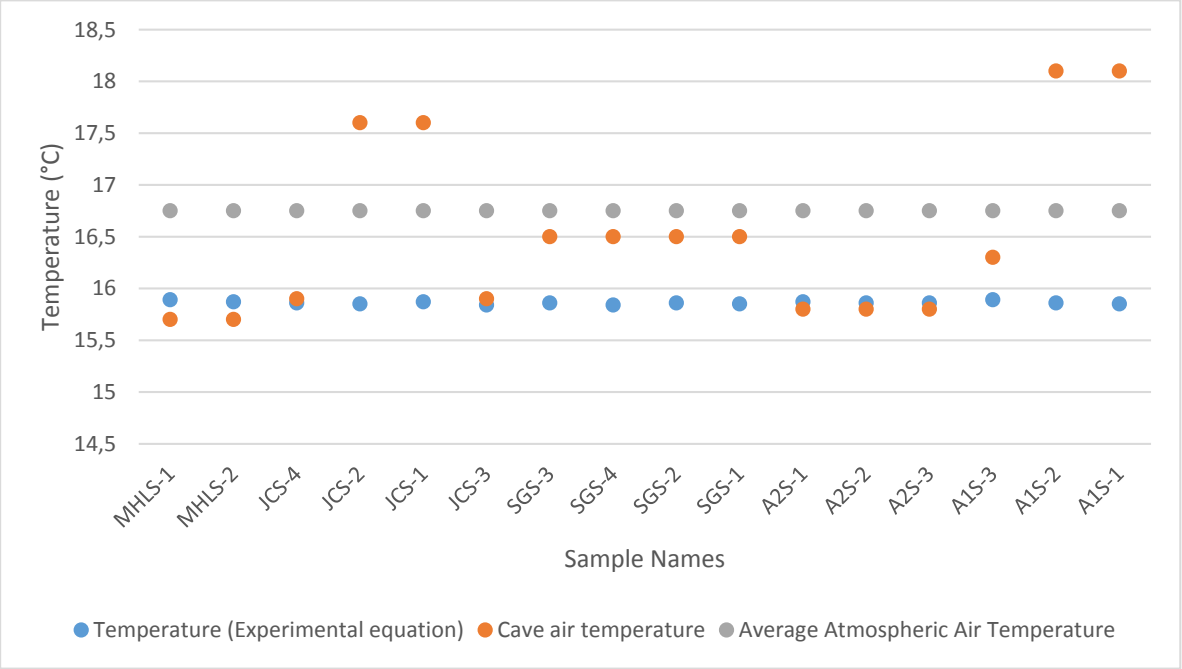

Fig. 5.2: Comparison of the idealised temperatures produced from the modern speleothem samples using the experimental equation for calculating temperature from speleothems, the measure cave air temperature and the average atmospheric air temperature during the period in which the samples were taken and cave air temperature measured.

5.2.2 Drip Water Oxygen Isotopes

The $\delta^{18}O$ values produced from the drip water samples collected from July 2015 to August 2016 reflect an irregular saw-tooth pattern of predominately negative, depleted oxygen isotope values. This is particularly observed during December 2015 to August 2016, during which there is a pronounced decrease in $\delta^{18}O$ values, which increase gradually towards August 2016. This decrease is reflected by both the cave air temperature and relative humidity measured within the cave system. These depleted $\delta^{18}O$ values represent progressively cooler and drier conditions, which corresponds to a certain degree to the seasons in which the $\delta^{18}O$ values decrease, which includes late summer, autumn and winter months. This correlation between the $\delta^{18}O$ trends and seasonal variations indicates the reliability of the $\delta^{18}O$ trends from the drip

water and speleothem samples to produce accurate climatic data. The $\delta^{18}O$ values also display a large range of values; possibly indicating that very little flattening of the $\delta^{18}O$ trends has occurred as a result of evaporative or kinetic fractionation.

The $\delta^{18}O$ values produced from the drip water samples may have been affected by numerous local, regional and temporal scale factors, resulting in variations within the $\delta^{18}O$ signatures (see Chapter 2, section 2.4.2). These variations may be attributed to fractionation effects, which indicate physical or chemical processes which have resulted in variations in the isotopic ratios of a phase or compound (Noah, 2010) (see Chapter 2, section 2.4.2). Kinetic fractionation plays a very important role in the interpretation of $\delta^{18}O$ values from speleothems and drip water, due to the fact that this process results in the irreversible enrichment of ^{18}O isotopes in the isotopic signature (White, 2004). Further effects of kinetic fractionation are bound to steps within the hydrological cycle (Noah, 2010). Variations within the $\delta^{18}O$ values produced from the drip water samples may therefore by attributed to kinetic fractionation effects, and may account for any abnormally enriched $\delta^{18}O$ outlier samples.

The amount of precipitation and the atmospheric air temperatures may also have contributed to fractionation effects with regards to the $\delta^{18}O$ signatures produced from the drip water samples, and are related to Rayleigh distillation, which takes place during the course of the hydrological cycle, and within the cave system (Noah, 2010) (see Chapter 2, section 2.4.2). In order to preserve calcite supersaturation, gaseous CO_2 is removed at a constant rate from the drip water solution. However, this results in the enrichment of ^{18}O in the drip water solution, and may therefore account for the abnormally enriched $\delta^{18}O$ values produced from the drip water samples. With regards to the hydrological cycle, fractionation caused by Rayleigh distillation usually occurs during the evaporation or condensation of water (Fairchild et al., 2006), and the effects thereof are usually determined by the amount of precipitation, leading to a gradual depletion of ^{18}O isotopes in the drip water samples during heavy rainfall events (White, 2004; Noah, 2010). This may be observed in the $\delta^{18}O$ trends produced from the analysis of the modern drip water and speleothem samples, and as a result, variations within the trends produced may be attributed to fractionation effects taking place in the cave environment.

Fractionation of $\delta^{18}O$ isotopes may also occur in the event that water accumulates and subsequently evaporates before entering the cave system (Harmon et al., 2004; van Beynen & Febbroriello, 2006). Cave air ventilation and low humidity may also result in kinetic fractionation (Wigley & Brown, 1976), caused by the evaporation of cave drip water (van Beynen & Febbroriello, 2006; Mattey et al., 2008). In general, low humidity of 25% to 70%

enhance the evaporation of drip water, and leads to increased kinetic fractionation (Noah, 2010). This effect may be observed in the $\delta^{18}O$ values produced from cave chambers which experienced lower overall humidity, such as in Antechamber 2. Kinetic fractionation effects can be observed in the $\delta^{18}O$ values produced from the drip water samples from Antechamber 2, as the values are either abnormally enriched or depleted, indicating the presence of significant kinetic fractionation effects. Overall, these fractionation effects have a significant effect on the $\delta^{18}O$ trends produced from drip water and speleothems, and influence the climatic information produced by analysing the $\delta^{18}O$ values. It is therefore important to understand these effects, in order to accurately interpret climatic data produced from the analysis of $\delta^{18}O$ trends from drip water and speleothems samples, as well as the statistical correlations exhibited between these climatic data.

The 26 outlier samples, which were significantly more positive than the other $\delta^{18}O$ values may possibly be explained by fractionation effects related to fracture flow and heat transport processes, as well as general kinetic fractionation associated with higher ambient temperatures, which all significantly increase the $\delta^{18}O$ values, resulting in significantly higher calculated temperatures, which do not accurately represent the current climatic conditions (Cuthbert et al., 2014). These fractionation effects may also include large variations in cave air ventilation, which alters the pCO_2 for the respective chambers, particularly close to chamber entrances, and in chambers close to ventilation shafts or the main tourist routes within the Sterkfontein Cave system. This may therefore significantly alter the $\delta^{18}O$ values produced from the drip water samples from these chambers. Evaporation in high humidity chambers may also result in an enrichment in $\delta^{18}O$ values in the remaining drip water for speleothems, and therefore result in higher calculated temperatures (Lachniet, 2009). A slower drip rate could also indicate a longer residence time of the drip water on the speleothem, and therefore increase the $\delta^{18}O$ values produced from the drip water, and ultimately increase the temperatures produced. This can possibly be seen with temperatures produced from Antechamber 2 samples, which include numerous outliers with the highest calculated temperatures, as well as some of the slowest drip rates within the cave system. The rate of degassing of CO_2 from drip water from the modern speleothems used may also alter the $\delta^{18}O$ values, and in some cases may result in abnormally high temperatures calculated from the speleothem and drip water $\delta^{18}O$ values, where an abnormal enrichment of ^{18}O isotopes has occurred during rapid CO_2 degassing. There is also the possibility that these outliers could have come about due to varied $\delta^{18}O$ values from drip water produced from a mix of water from differing origins and hydrological sources, as well as a mix of waters of differing ages.

The measured relative humidity and air pressure within the cave environment also exhibited climatic conditions within the cave system conducive to very little evaporative effects, and as a result potentially climatically reliable $\delta^{18}O$ values. As a result, it may be assumed thus far that the $\delta^{18}O$ values produced from the modern drip water and speleothem samples would produce reliable climate data with respect to temperature and precipitation. This would indicate that overall, speleothems are reliable palaeoclimate proxies.

A comparison between the calculated idealised temperatures, the measured cave air temperatures and measured atmospheric air temperatures all produced similar trends and values. This relationship may be explained by the fact that the oxygen isotopes produced from the drip water samples feeding the modern speleothem deposits may produce temperatures which resemble the ambient cave temperature, as well as a range of temperatures which resemble variations of the mean annual temperature on the surface above the cave environment (Nordhoff, 2005; Mandice et al., 2013) (see Chapter 2, section 2.4.2). The correlation between the raw oxygen isotope trends produced from the modern drip water samples and seasonal variations observed from measured atmospheric temperatures and precipitation indicate that the oxygen isotopes from the drip water samples may provide insight with regard to seasonality. This may also be due to the fact that the oxygen isotope values of meteoric precipitation, represented by the average drip water oxygen isotope values, vary depending on seasonal changes in temperature and precipitation (Nordhoff, 2005).

The temperatures calculated from the analysis of the oxygen stable light isotopes of drip water samples are dependent on numerous factors (see Chapter 2, section 2.4.2). These factors influence the degree to which the temperatures produced from the $\delta^{18}O$ values from the drip water samples represent modern atmospheric temperatures, and therefore the reliability of the drip water samples as climate proxies. These include evaporative cooling, fracture flow and heat transport process, and cave air ventilation processes (Cuthbert et al., 2014). The effect of evaporative cooling can be seen in abnormally low temperatures produced from the drip water and speleothem $\delta^{18}O$ trends in comparison to other temperatures from the same chamber, at the same time period. This may be due to the fact that cooling effects result in more negative, depleted oxygen isotope values, and therefore lower overall calculated temperatures. This makes the temperature data calculated from the drip water samples unreliable when comparing them to the mean temperature data from the ground surface (Cuthbert et al., 2014). Recording the humidity, cave air pressure and corresponding cave ventilation may assist in determining the degree to which evaporative cooling has played a role in altering the $\delta^{18}O$ signatures, as

chambers with lower humidities such as Antechamber 2 would result in more depleted $\delta^{18}O$ signatures. This would therefore account for the abnormally low temperatures calculated from the drip water samples from Antechamber 2. Fracture flow and heat transport process may also be observed in the temperatures produced from the drip water and speleothem $\delta^{18}O$ trends which are abnormally high. These processes may also be accompanied by higher humidity would indicate the presence of less evaporative effects. Recording these environmental factors may also assist in determining which chambers to sample, in order to produce the most accurate climate data from $\delta^{18}O$ trends.

Temperatures produced from the drip water and speleothem $\delta^{18}O$ trends, which were lower than normal may have been produced by the $\delta^{18}O$ values from samples located closer to chamber entrances, especially in chambers such as Antechamber 1, which are close to very large, main chambers or ventilation shafts, and thus more susceptible to cave air ventilation effects. These effects may alter the drip water temperatures by changing the relative humidity within the cave environment, which in turn controls the rate of evaporation, and therefore the rate of cooling of the drip water. This can result in drip water temperatures which are much lower due to a larger concentration of more negative, depleted oxygen isotope values, and therefore the temperatures produced would not represent the mean temperatures on the ground surface (Cuthbert et al., 2014). Cave air ventilation variations may also be related to temperature fluctuations between the cave interior and the exterior environment (Mattey et al., 2008; Noah, 2010), but these have the greatest effect in areas closest to cave entrances (Fairchild et al., 2006) (see Chapter 2, section 2.4.3). This may also account for large variations in the calculated temperatures from chambers and drip water samples located closest to chamber entrances or cave shafts.

The temperatures calculated using both the drip water $\delta^{18}O$ values and the speleothem $\delta^{18}O$ values were calculated using two equations, namely the empirical equation for calculating temperatures from speleothems (equation 1) and the experimental equation for calculating temperatures from speleothems (equation 2). The experimental equation (equation 2) leads to values which are 0.3‰ to 0.8‰ higher than those produced from the empirical equation (equation 1), and this is thought to provide a better indication of equilibrium fractionation within the speleothem calcite-drip water system as compared to the results produced from the empirical equation (Wackerbath et al., 2012). Values produced from the experimental equation have also been observed to produce more consistent results with respect to measured values, and as a result, values produced from the experimental equation are regarded as the best

representation of the fractionation occurring between isotopes during the precipitation of calcite in natural cave environments (McDermott et al., 2005). However, as the experimental equation cannot apply all fractionation effects and variations to the $\delta^{18}O$ values obtained, it should be used with some caution (Wackerbath et al., 2012). The empirical equation (equation 1) has a temperature range of 5° to 15°C, and produces more accurate temperatures from drip water and speleothems precipitated under cooler conditions, whereas equation 2 has a temperature range of 5° to 30°C, producing more accurate temperatures from drip water and speleothems precipitated under warmer conditions, as well as encompassing a greater range of temperatures than that of equation 1. The experimental equation however has in the past seen to produce temperatures that are too low compared to the measured atmospheric air temperature, by approximately 4°C. However, in order to produce the most accurate results, an examination of the cave environmental conditions needs to be taken into account, and the equations applied on this basis (Demeny et al., 2010). Earlier empirical equations however have been observed to reflect temperatures closer to that of the measured atmospheric temperatures, partly due to the fact that these equations made use of mixed calcite-aragonite mineralogies. These equations however may also not accurately reflect data taken from calcite speleothems, due to the inclusion of aragonite mineralogies (McDermott et al., 2006).

The temperatures produced from July 2015 to August 2016 using equation 1 displayed similar trends and temperatures to that of the average measured atmospheric temperatures, with the exception of the temperatures produced from the Jacovec Cavern, which displayed significant variation from the atmospheric temperatures during periods when the atmospheric temperatures were at their warmest. The significant decrease of the calculated temperatures from the Jacovec Cavern during higher seasonal atmospheric temperatures may also be interpreted as a result of evaporative cooling and less kinetic fractionation due to higher ambient temperatures and higher humidity, producing more negative, depleted $\delta^{18}O$ values, and cooler calculated temperatures (Nordhoff, 2005; Cuthbert et al., 2014). These fractionation effects may also include large variations in cave air ventilation, which alters the pCO_2 for the respective chambers, therefore significantly altering the $\delta^{18}O$ values produced from the drip water samples from these chambers and consequently the temperatures calculated from these oxygen isotopes. A slower rate of degassing of CO_2 from drip water from the modern speleothems may also have altered the $\delta^{18}O$ values from the Jacovec Cavern, producing lower temperatures than expected. All of these factors may also have affected the statistical correlation between the measured temperatures and the calculated temperatures.

This decrease in $\delta^{18}O$ values and subsequent decrease in calculated temperatures may also be a result of global glacial-interglacial changes in ocean oxygen isotope values (Richards & Dorale, 2003). The $\delta^{18}O$ values obtained from speleothems and drip water are affected by local meteoric precipitation $\delta^{18}O$ values, which in turn is affected by ocean water $\delta^{18}O$ values as meteoric water is derived from oceanic water, as demonstrated by the hydrological cycle (Schwarzc, 2007). Therefore, any variations in the $\delta^{18}O$ values of oceanic water as a result of global climatic events such as changes in ice volumes due to glacial or interglacial climatic periods may ultimately also affect the $\delta^{18}O$ values of local meteoric precipitation. This would result in these global glacial-interglacial induced variations in oceanic $\delta^{18}O$ values being ultimately reflected in the $\delta^{18}O$ values produced from speleothems and drip water (Schwarzc, 2007).

As equation 1 is best used in environments with lower ambient temperatures, it may be assumed that the resemblance of the calculated temperatures from Antechamber 1, Antechamber 2 and the Jacovec Cavern to the atmospheric temperatures may be due to this fact.

The temperatures produced using equation 1 from Antechamber 1 and Antechamber 2 show considerably higher temperatures than that of the ambient cave air temperature, while the calculated temperatures from the Jacovec Cavern seem to represent the ambient cave temperatures to a better degree. This could be due to kinetic fractionation effects, as well as cave air ventilation effects which alters the chambers' pCO_2 values, and consequently, the $\delta^{18}O$ values produced from the drip water samples. This would affect the ultimate temperatures produced from the $\delta^{18}O$ drip water values. Rapid degassing of CO_2 in the drip water from Antechamber 1 and 2 may also account for calculated temperatures higher than that of the cave air temperatures. These factors may also have affected the statistical correlations produced between the measured atmospheric temperatures, the cave air temperatures, and the calculated temperatures.

Overall, all three calculated data trends display similar overall increasing and decreasing trends to that of the ambient cave air temperature, but the trends of the calculated temperatures are a lot more irregular and varied than that of the measured cave air temperature, and display steeper increasing and decreasing curves. This indicates the presence of kinetic fractionation effects, which may be responsible for variations within $\delta^{18}O$ values from the drip water and speleothem samples, and as a result, the calculated temperatures. The variations within the calculated temperature trends may be attributed to evaporative cooling, variations in cave air ventilation, and variations in humidity, with lower humidity being associated with an increase in $\delta^{18}O$

values, and higher humidity with a decrease in $\delta^{18}O$ (Noah, 2010), during which the calculated temperatures would decrease with respect to the ambient cave air temperature.

A decrease in $\delta^{18}O$ values and subsequent decrease in calculated temperatures may also be a result of global glacial-interglacial changes in ocean oxygen isotope values, as any variations in the $\delta^{18}O$ values of oceanic water as a result of global climatic events may ultimately also affect the $\delta^{18}O$ values of local meteoric precipitation (Richards & Dorale, 2003). Significant increases in temperature or significantly higher temperatures than that of the ambient cave air temperature may be explained by fracture flow and heat transport processes, which may significantly increase the calculated temperatures from drip water $\delta^{18}O$, or by fractionation effects and variations in humidity, which are usually inversely proportional to the ambient temperatures (Nordhoff, 2005). These effects however may also represent variations in changing cave climatic conditions, which would not be as prominently displayed in the measured cave air temperatures. As a result of this, the fact that these small variations are evident in the temperatures calculated from the drip water and speleothem samples but do not significantly alter the overall trends in comparison to the cave air temperatures reveals that the speleothems may produce reliable temperatures, and may be considered reliable palaeotemperature proxies. The overall resemblance of the cave air temperature to a certain degree is in accordance with the expected relationship between the calculated temperatures from the drip water and speleothem $\delta^{18}O$, and the ambient cave air temperature (Nordhoff, 2005).

The equation 1 calculated temperatures from the speleothem and drip water $\delta^{18}O$ values were also compared to the standard increase in deduced temperatures with calcite using calcite-water fractionation factors ($1000\ln\alpha$) (Kim & O'Neil, 1997; Lachniet, 2009). The calculated temperatures produce fractionation values below that of the average values for calcite-water fractionation, exhibiting $1000\ln\alpha$ fractionation factors 1 unit higher than that of the standard fractionation factors for calcite-water. This reveals the definite presence of kinetic fractionation effects present in the $\delta^{18}O$ isotopic signature for the drip water samples, and this would account for the variations observed in the calculated temperature trends (Kim & O'Neil, 1997; Lachniet, 2009). This could be a result of evaporation effects during the flow or collection of the drip water samples, as well as variations in cave ventilation, which result in variations in evaporative conditions, and variations in humidity, which also affect the evaporation of the water.

The temperatures produced from July 2015 to August 2016 using equation 2 do not display very similar trends and temperatures to that of the average measured atmospheric temperatures, and instead display significant variation from the atmospheric temperatures during periods when the atmospheric temperatures were at their warmest. During cooler periods, the calculated temperatures seem to represent the atmospheric temperatures to a much greater degree. As equation 2 is best used in environments with much higher ambient temperatures, it may be assumed that the dissimilarity of the calculated temperatures from Antechamber 1, Antechamber 2 and the Jacovec Cavern to the atmospheric temperatures may be due to this fact. The significant variations of the calculated temperatures from the three chambers during higher atmospheric temperatures may be interpreted as a result of evaporative cooling and less kinetic fractionation due to higher ambient temperatures and higher humidity, producing more negative, depleted $\delta^{18}O$ values, and cooler calculated temperatures (Nordhoff, 2005; Cuthbert et al., 2014). Variations in cave air ventilation may also alter the pCO_2 of the cave chambers, which may lead to variations in the $\delta^{18}O$ values produced from the drip water samples, and as a result, altered calculated temperature values. Slower degassing of CO_2 within the drip water samples during these periods may also result in depleted $\delta^{18}O$ values, and as a result, cooler calculated temperatures as compared to the cave air temperatures and atmospheric air temperatures. Faster drip rates during this period may also be responsible for a decrease in $\delta^{18}O$ values, and thus lower calculated temperatures. This correlates well with the drip rates measured, as faster drip rates are associated with increased precipitation, meteoric water flow, and groundwater recharge, characteristic of warmer seasonal periods, taking a lag period into account. A decrease in $\delta^{18}O$ values and subsequent decrease in calculated temperatures may also be a result of global glacial-interglacial changes in ocean oxygen isotope values, as any variations in the $\delta^{18}O$ values of oceanic water as a result of global climatic events may ultimately also affect the $\delta^{18}O$ values of local meteoric precipitation (Richards & Dorale, 2003). These fractionation effects associated with variations in the calculated temperatures may have become more pronounced in the calculating of the temperatures from drip water from the three chambers using equation 2. As equilibrium fractionation effects are inversely proportional to the atmospheric air temperatures, it would therefore be possible for the temperatures calculated from the drip water samples and speleothem samples to decrease during an increase in atmospheric temperatures, due to a decrease in evaporative and kinetic fractionation, and to increase during a decrease in atmospheric temperatures, due to an increase in evaporative and kinetic fractionation (Nordhoff, 2005). The calculated temperatures from the three chambers resemble this inversely proportional relationship very well with regards to equation 2. Taking

this system into account along with the fractionation effects responsible for variations in the calculated temperatures, the calculated temperatures overall may be correlated well with the atmospheric air temperatures, exhibiting the reliability of using speleothems as palaeotemperature proxies.

The temperatures produced using equation 2 show much higher temperatures than that of the ambient cave air temperatures during the late winter to early summer months, and show more of an inverse relationship with regards to the ambient cave air temperature during this period. Kinetic fractionation effects may be responsible for this variation, as well as cave air ventilation effects which alters the chambers' pCO_2 values, and consequently, the $\delta^{18}O$ values produced from the drip water samples. This would affect the ultimate temperatures produced from the $\delta^{18}O$ drip water values. Rapid degassing of CO_2 in the drip water from Antechamber 1 and 2 may also account for calculated temperatures higher than that of the cave air temperatures. Higher humidity during this period could also affect the value of the calculated temperatures. However, from approximately December 2015/January 2016, the calculated temperature trends from equation 2 resemble the ambient cave air temperatures quite well, as well as matching the overall increasing trend in ambient cave air temperatures during this period. The calculated temperatures for the Jacovec Cavern however remain consistently much lower than the ambient cave air temperatures, and this may signify the influence of evaporative cooling effects, as well as cave air ventilation effects, rapid degassing of CO_2 from drip water, and slower drip rates. They do however resemble the overall trend of the ambient cave temperatures towards the end of the sampling period. This shows that overall, the calculated temperatures do resemble the cave air temperature trends to a certain degree, but significant fractionation factors need to be taken into consideration, particularly the inverse relationship between evaporative and kinetic fractionation and air temperatures, as these factors would affect the strength of the statistical correlation between the two data sets.

The equation 2 calculated temperatures from the speleothem and drip water $\delta^{18}O$ values were also compared to the standard increase in deduced temperatures with calcite using calcite-water fractionation factors ($1000\ln\alpha$) (Kim & O'Neil, 1997; Lachniet, 2009). As with equation 1, the calculated temperatures produced values below that of the calcite-water fractionation values, exhibiting $1000\ln\alpha$ fractionation factors generally higher than that of the standard fractionation factors for calcite-water. This reveals the definite presence of kinetic fractionation effects present in the $\delta^{18}O$ isotopic signature for the drip water samples and this could account for the variations observed in the calculated temperature trends (Kim & O'Neil, 1997; Lachniet, 2009).

This could be a result of evaporation effects during the flow or collection of the drip water samples, as well as variations in cave ventilation, which result in variations in evaporative conditions, and variations in humidity, which also affect the evaporation of the water.

The temperatures calculated from the Jacovec Cavern, Antechamber 1 and Antechamber 2 using equation 1 were compared to the idealised temperatures produced also using equation 1, and were found to average these idealised temperatures very well. Variations of the calculated temperatures with respect to the idealised temperatures may be explained by numerous factors, including evaporative cooling effects which may be responsible for a decrease in calculated temperatures below the idealised temperatures, as well as short periods of intensified rainfall and seasonal rainfall patterns which may also result in a decrease in calculated temperatures with regards to the idealised temperatures (Richards & Dorale, 2003). Significant increases in the calculated temperatures with regards to the idealised temperatures may be a result of fracture flow and heat transport processes through the cave system affecting the path of flow of the drip water samples, as well as exterior temperature changes, and variations in humidity and cave air ventilation, which may also vary the calculated temperatures. However, most of these variations do not range further than approximately 3°C from the idealised temperatures, with the exception of some large variations in temperatures calculated from Antechamber 2, and one or two variations from Antechamber 1. The calculated temperatures from the Jacovec Cavern remain approximately 2°C lower than that of the idealised temperatures, which may be a result of significant and constant evaporative cooling effects. Overall, the close resemblance of these calculated temperatures to the idealised temperatures indicates that the temperatures calculated from the drip water and speleothem samples are reliable, and that speleothems in general in these cave climatic conditions are reliable palaeotemperature proxies.

The temperatures calculated from the Jacovec Cavern, Antechamber 1 and Antechamber 2 using equation 2 were also compared to the idealised temperatures produced using equation 2, and did not resemble the idealised temperatures from equation 2 as well as the equation 1 calculated temperatures resembled the equation 1 idealised temperatures. The temperature trends for the three chambers only match the idealised temperatures once they have decreased to their minimum temperature range. This might indicate that these idealised temperatures calculated using equation 2 only represent the ideal lowest temperature for the calculated temperatures. These calculated temperatures also seem to be greatly affected by exterior temperature variations, and show an inversely proportional relationship in comparison to the measured atmospheric temperatures. This could therefore explain the degree of variation in the

calculated temperatures with regard to the equation 2 idealised temperatures. As with the equation 1 calculated and idealised temperatures, the equation 2 calculated temperatures for the Jacovec Cavern consistently remain below the idealised temperatures, which again may be a result of significant and constant evaporative cooling effects. With regards to the correlation between the temperatures calculated using equation 2 and the idealised temperatures calculated using equation 2, the inverse relationship between fractionation effects and resulting temperatures needs to be taken into consideration before the reliability of the calculated temperatures and the strength of statistical correlations between temperature data sets may be assessed. When taken into account, these calculated temperatures do correlate well with the atmospheric air temperatures to a certain degree, indicating their reliability, however they do not reflect a correlation as reliable as that of the temperatures calculated using equation 1.

Overall, it can be said that the temperatures calculated using equation 1, the empirical equation, represent current temperature conditions to a better degree as compared to the temperatures calculated using equation 2 (the experimental equation). This may be due to a narrower range of temperatures represented by the empirical equation, which fits in with the range of atmospheric and cave air temperatures obtained for the Sterkfontein Caves system. It also may represent the overall mineralogy of the speleothems to a better extent that that of the experimental equation. The empirical equation may also have produced more reliable temperatures by taking more fractionation effects into account, and taking into account the variation produced by these effects. This would result in a temperature trend which closely resembles the cave air and atmospheric temperatures, with smaller variations within the trend accounting for fractionation effects.

5.3 Precipitation

5.3.1 Modern Speleothems

Oxygen isotopes produced from the modern speleothem samples do not reveal much with regards to the precipitation conditions outside the cave environment, as the values are stand-alone values and do not produce a trend which can be used to interpret precipitation. However, changes in humidity may reflect somewhat on the precipitation conditions during the formation of the speleothems and collection of the drip water samples, and slight changes in the humidity may indicate wetter conditions or drier conditions with regards to precipitation. These variations in humidity within the cave system seem to be related to seasonality with regards to

wetter or drier conditions, with lower relative humidity during June 2015 to September 2015, and a subsequent increase in humidity from September 2015 to April 2016.

5.3.2 Drip Water

Variations of $\delta^{18}O$ in the drip water samples may be related to temporal variations of $\delta^{18}O$ in precipitation, which may be affected by latitude, atmospheric temperatures and wind effects (van Beynen & Febbroriello, 2006), as well as due to the mixing of water from differing sources and of differing ages. Latitudinal effects are related to differential heating of the earth's surface, where increasing latitude results in progressively lower temperatures and lower relative humidity, and as a result, higher evaporation rates. This is due to the fact that the angle at which solar radiation strikes the earth decreases with increasing latitude. This effect results in precipitation which is progressively more depleted in $\delta^{18}O$ with increasing latitude (Noah, 2010). As a result of this effect, precipitation in northern South Africa is less depleted in $\delta^{18}O$ than rainfall at higher latitudes, as South Africa occupies the lower portion of the mid-latitudes. In contrast to latitudinal effects, winds are produced by pressure variations linked to insolation (Noah, 2010). As a result of this, low pressure climatic systems which develop due to warm air that is rising, usually produce precipitation which is depleted with respect to ^{18}O (Noah, 2010). With regards to atmospheric temperatures, precipitation which forms in warmer climates is usually enriched in ^{18}O values, as opposed to cooler climates (Craig, 1961; White, 2004). This again results in less depleted, more enriched overall $\delta^{18}O$ values in rainfall in South Africa, as a result of a warmer climate. These enriched $\delta^{18}O$ values for South African precipitation may affect the $\delta^{18}O$ values produced from drip water and speleothems, as drip water $\delta^{18}O$ is greatly influenced by the $\delta^{18}O$ values of meteoric precipitation.

The drip rate measured during the collection of the drip water samples showed a distinctive trend in drip rate for all three chambers, where high drip rates were observed to increase from July, with a maximum in August until October, where drip rates started to decreases. This trend of drip rate is very similar to the trend for precipitation from Krugersdorp, however the drip water rates peak in the late winter to spring months, which seems to correspond to rainfall that occurred approximately four to six months prior to the collection of the drip water, in the mid-summer months, displaying a typical lag effect (Cruz et al., 2005; Mattey et al., 2008; Lachniet, 2009). This lag effect may be due to the residence time of meteoric water feeding the karst environment, with rainfall $\delta^{18}O$ effects only reaching the cave drip waters four to six months after the event, due to the residence time of the groundwater containing water from that particular rainfall event. It may also be attributed to the mixing of water of differing origins

and ages in the karst system. The presence of this lag effect within the drip rate measurements provides evidence for the reliability of these drip rates representing the precipitation occurrence and variations for the Sterkfontein Caves area. Small variations in drip rate may be attributed to small climatic events within the area, such as short bursts of intense rainfall. Heavy rainfall events may be responsible for short increases in drip rate, followed by sudden decreases as the drip rate returns to base levels soon after the conclusion of the rainfall event. This spiking in response to rainfall events seems to occur independently of any seasonality (Smith et al., 2015). These variations reflected in the drip rates measured from the Sterkfontein Caves system provides evidence for the drip rates as proxies for modern precipitation occurrence, amount and variations.

Groundwater recharge to the Sterkfontein karst environment is only approximately 15% with regards to precipitation in the area (Martini et al., 2003), due to high evapo-transpiration rates. This slow recharge rate responsible for the significant lag effect displayed by the drip water $\delta^{18}O$ values and drip rates may be accounted for by fracture flow of meteoric water within the karst system, as well as diffuse seepage flow (Lachniet, 2009). This slow recharge rate suggests that climatic studies conducted within the Sterkfontein Caves system with regards to speleothems would better represent longer term climatic events than short term events (Lachniet, 2009).

The drip rate trends for the Jacovec Cavern, Antechamber 1 and Antechamber 2 seem to reflect the average monthly $\delta^{18}O$ values for the drip water collected during which the drip rate was measured reasonably well (see figure 4.26). These trends reflect each other well, with some variations with regards a shorter period of decrease, and a much flatter, gradual increase towards August 2016 compared to the $\delta^{18}O$ values. This indicates only a small amount of kinetic fractionation present, as the $\delta^{18}O$ values and the drip rate match reasonably well with one another.

Positive variations in drip water $\delta^{18}O$ may be related to evaporative effects in caverns with low relative humidity and low air ventilation, which results in a concentration of ^{18}O within the drip water (Lachniet, 2009). The humidity trends for the Jacovec Cavern, Antechamber 1 and Antechamber 2 remain relatively high throughout the year however, and the drip water $\delta^{18}O$ values reflect the relative humidity trends of the Jacovec Cavern and Antechamber 2, with overall increasing and decreasing trends in humidity being reflected by the $\delta^{18}O$ results. The humidity for Antechamber 1 stays approximately constant, increasing during September 2015

to April 2016, as do the other two chambers. The variations in humidity can be accounted for by various climatic events.

Overall negative variations in drip water $\delta^{18}O$ values may be attributed to variations in the ocean water $\delta^{18}O$ during glacial-interglacial transition periods, which affect $\delta^{18}O$ values in meteoric precipitation and as a result, affect the $\delta^{18}O$ values of drip water resulting from meteoric precipitation. Negative variations may also be attributed to the amplification of rainfall patterns, and the seasonality of rainfall (Richards & Dorale, 2003). This reflection of rainfall seasonality within the $\delta^{18}O$ drip water trends indicates the accuracy of the $\delta^{18}O$ values in representing current precipitation conditions, and may indicate that speleothem drip water $\delta^{18}O$ values may produce reliable interpretations with regards to precipitation events and intensity, as well as resulting climatic interpretations. A study of the isotopic signature of the T8 stalagmite from Makapansgat by Holmgren et.al. (2003) also concluded that variations within the $\delta^{18}O$ signature of the stalagmite represent variations in the different types of precipitation occurring within that area during the precipitation of the stalagmite. In this case, lower, more depleted $\delta^{18}O$ values may have represented drier, increasingly arid overall long term climatic conditions, and more enriched $\delta^{18}O$ values may have represented overall long term wetter, warmer environments (Holmgren et al., 2003). This has also been observed in the $\delta^{18}O$ values of the drip water and speleothem samples, as these precipitation event interpretations coincide with climatic and temperature data deduced from the $\delta^{18}O$ values. With regard to temperature interpretations, it has also been concluded that depleted $\delta^{18}O$ values represent cooler, drier conditions, while enriched $\delta^{18}O$ values represent warmer, wetter conditions. This may be reflected in the $\delta^{18}O$ trends with respect to drip rate and ultimately precipitation events and intensity as well. Variations within the drip water $\delta^{18}O$ trends are a result of variations in the frequency between persistent mid-altitude rainfall events, and intense convective higher altitude precipitation events (Holmgren et al., 2003), and the variations in the drip water $\delta^{18}O$ trends may thus be interpreted accordingly. Higher altitude precipitation events, which increase in frequency during dry summers (Harrison, 1986), are characterised by more depleted $\delta^{18}O$ values in the drip water $\delta^{18}O$ trends (Rozanski et al., 1993). Northern summer rainfall areas in southern Africa are characterised by drier and more arid conditions, due to the expansion of the atmospheric circumpolar vortex towards the equator (Tyson, 1986; Tyson & Preston-Whyte, 2000). The expansion of the tropical circulation towards the poles, accompanied by a contraction of the atmospheric vortex produces the opposite result, and is associated with warmer and wetter climates (Tyson, 1986; Tyson & Preston-Whyte, 2000). Due to this, Holmgren et al. (2003) interpreted lower, more depleted $\delta^{18}O$ values to represent

drier periods with a decrease in average annual rainfall, in comparison to wetter years which are characterised by an increase in heavy precipitation events, as well as in the amount of rainfall produced in a single event. These interpretations may also be extended to the $\delta^{18}O$ trends produced from the drip water samples with regards to precipitation events and intensity, and coincide with interpretations made regarding cooler and drier conditions associated with depleted $\delta^{18}O$ values, and warmer, wetter conditions associated with enriched $\delta^{18}O$ values with respect to the temperatures calculated from the drip water and speleothem $\delta^{18}O$ values. As a result, it is evident that the correlation between the temperature and precipitation information produced from the drip water and speleothem $\delta^{18}O$ values reliably represent current environmental and climatic conditions and variations.

In general, any flatness in the curve of the $\delta^{18}O$ trend for the drip water may be a result of the passage of meteoric water through the host rocks, mixing of meteoric water and groundwater, and the residence time of the groundwater above the cave system. During this time, the original $\delta^{18}O$ signal produced from the rainfall may be varied or removed completely. Talma and Vogel (1992) attributed the flatness of the oxygen isotope trend produced from the Cango Caves stalagmite to this factor. This may also account for some flatter portions of the $\delta^{18}O$ trend from the drip water samples from Sterkfontein Caves, however the overall trend does not display a great deal of flatness.

The drip water $\delta^{18}O$ values display a very distinctive inverse relationship with regards to the average monthly measured rainfall, where decreases in $\delta^{18}O$ values are accompanied by increases in the average monthly rainfall. This inverse relationship however may be due to the fact that the $\delta^{18}O$ values of the drip water are representing rainfall periods four to six months prior to the displayed $\delta^{18}O$ values, which is also observed when comparing the drip rate to the average monthly measured rainfall. This inverse relationship between drip water $\delta^{18}O$ values and average monthly rainfall may however also be explained by the amount effect, which is characterised by higher $\delta^{18}O$ values being correlated with lower rainfall patterns, and vice versa (Fleitmann et al., 2004; Lachniet et al., 2004; Lachniet, 2009; Scholl et.al., 2009). This effect is more common in tropical areas, where the drip water $\delta^{18}O$ values would increase due to the evaporation of drip water during periods of lower rainfall or slow infiltration rates, in a similar manner described by the amount effect (Fleitmann et al., 2004; Lachniet et al., 2004; Lachniet, 2009). The $\delta^{18}O$ drip waters measured from Sterkfontein Caves may represent this amount effect to a certain degree, but variably, as the overall climate is not tropical. Evaporation effects within the Sterkfontein Caves system may result in a decrease in $\delta^{18}O$ values during high

temperature or high humidity events associated with high rainfall, due to the high humidity within the cave system. Due to these factors and potential interpretations, the interpretation observed by Holmgren et al. (2003) may also to a certain, more long term extent be applicable to the $\delta^{18}O$ results from the modern speleothem and drip water samples from the Sterkfontein Caves.

Variations between rainfall recorded at the different weather stations may also have affected correlations between the $\delta^{18}O$ values of the drip water samples in the Sterkfontein Caves system and the measured rainfall from the weather stations. Differences between the rainfall trends recorded by the two stations have possibly been attributed to the distance between them (see Chapter 3, section 3.6.1). As the Krugersdorp weather station is situated closer to the Sterkfontein Caves site, the rainfall patterns from this weather station, especially for 2015 and 2016, should reflect the rainfall conditions at the Sterkfontein Caves site more accurately, and may be reflected in the $\delta^{18}O$ values produced from the modern drip water and speleothems, as well as the drip rates measured. However, differences in altitude between the weather stations and the cave site may account for variations between the drip water $\delta^{18}O$ values and the recorded rainfall at the weather stations. Wind effects may also have varied the frequency and intensity of precipitation events between the weather stations and the cave site, due to the distance between them. This in turn may have resulted in variations in correlations between the $\delta^{18}O$ values produced from the drip water samples, and the rainfall trends produced from the weather stations. Due to the distance between the weather stations and the Sterkfontein Caves site, the climatic data produced by the weather stations might be an average trend which would be more useful in determining longer term variations in climate, and as a result, might not reflect smaller climatic variations exhibited by variations in the $\delta^{18}O$ values and drip rates of the drip water samples. The location of the weather stations with regards to the surrounding environment would also be at prime locations to capture weather data with minimal influences, whereas numerous influences such as wind activity, human activity and the influence of surrounding low-lying vegetation and topography might affect the climatic conditions experienced by the Sterkfontein Cave site. These effects may therefore be represented to a certain degree by the $\delta^{18}O$ signatures of the speleothems and drip water within the cave system. Overall, these factors may account for the variability between the recorded precipitation and temperature data from the weather stations, and the ultimate climatic data produced from the speleothem and drip water $\delta^{18}O$ trends.

Overall, the correlation between the $\delta^{18}O$ values from the drip water samples, the drip rate and the average precipitation for the area is very good, providing evidence that the $\delta^{18}O$ values from the drip water samples are reliable indicators of current precipitation conditions, and therefore would be reliable palaeoprecipitation proxies.

5.4 Hydrochemistry

5.4.1 Electro-conductivity

Three major trends occur within the electro-conductivity results of the drip water samples. Samples from Antechamber 1 occupy the highest range of electro-conductivity values, the Jacovec Cavern occupy the middle range of values, and Antechamber 2 occupy the lowest range of values. The electro-conductivity value for the Milner Lake sample was significantly higher than any of the other samples, signifying a higher concentration of ions and total dissolved solids within the lake water. As this lake is static (Martini et al., 2003), an enrichment of ions and total dissolved solids (Smith et al., 2015) would be expected, as these ions and solids are not being transported in a flow of water from the lake, and instead collect and pool within the lake.

The electro-conductivity of drip water within karst environments is assumed to be controlled by the air pressure of carbon dioxide (pCO_2) within the soil gas and the processes accompanying dissolution of the bedrock (Smith et al., 2015). Electro-conductivity values may vary from different drip locations, based on the ground water residence time within a nearby aquifer (Miorandi et al., 2010; Sherwin & Baldini, 2011; Smith et al., 2015), the extent of groundwater mixing within the aquifer (Genty & Deflandre, 1998), as well as any prior calcite precipitation which may have occurred (Fairchild et al., 2000; Fairchild et al., 2006; Sherwin & Baldini, 2011). Numerous studies in the past have noted strong relationships between the speleothem drip rate and the electro-conductivity of the drip water, which has been attributed to the associated karst hydrology. Negative relationships between electro-conductivity and drip rate have been noted by Borsato (1997) and Miorandi et al. (2010) in reference to Ernesto Cave in Italy, as well as in Crag Cave in Ireland during the summer season, which was described by Sherwin and Baldini (2011). In the Ernesto Cave in Italy, it was discovered that under dry conditions associated with low drip rates, the electro-conductivity of the drips produced was seen to increase. This was attributed to increased karst water residence time, as well as enhanced bedrock dissolution (Borsato, 1997; Miorandi et al., 2010). During periods of increased moisture and drip rates, the electro-conductivity values were observed to decrease

rapidly, which was attributed to the possible dilution of karst water (Miorandi et al., 2010; Sherwin & Baldini, 2011; Smith et al., 2015). This can be seen to a certain degree with regards to the drip rate for the Jacovec Cavern samples, Antechamber 1 samples, and Antechamber 2 samples, and the electro-conductivity of these samples. This relationship only seems to be slightly proportional, however it is still noticeable in the data trends. This may to a certain degree indicate the reliability of the electro-conductivity of the drip water samples in representing current cave conditions. However, the opposite result has also been observed by Genty and Deflandre, (1998) and Fernandez-Cortes et al. (2007), where electro-conductivity values were observed to increase during periods of enhanced hydraulic pressure, and therefore during periods of increased drip rates. These results have been explained by the activation and drainage of a second, high electro-conductivity aquifer in the karst system due to the storage of water within micro-fissures in the aquifer (Smith et al., 2015).

Electro-conductivity of drip water has however very rarely been discussed on a sub-seasonal scale in terms of carbonate saturation states aided and produced by the cave air pCO_2 (Sherwin & Baldini, 2011; Smith et al., 2015). The degassing of carbon dioxide from drip water produced from karst water entering the cave system is driven by the cave air pCO_2 (Spotl et al., 2005; Baldini et al., 2008; Tremaine et al., 2011; Wong et al., 2011). As the cave air pCO_2 increases, it decreases the normal rate of carbon dioxide degassing from drip water, and therefore constrains the supersaturation of water flowing through the karst system (Smith et al., 2015). This in turn therefore constrains the potential for calcium carbonate precipitation, and thereby increases the electro-conductivity values in the drip water (Sherwin & Baldini, 2011; Smith et al., 2015). However, this control has been observed to be secondary in nature to the hydrological mechanism, and mainly operates during winter (Sherwin & Baldini, 2011; Smith et al., 2015).

As electro-conductivity may be related to changes in pCO_2 within the cave, and therefore may also be affected by cave ventilation (Smith et al., 2015), this may suggest that the differing trends observed with regards to electro-conductivity for the three chambers may be attributed to changes in cave air ventilation (Sherwin & Baldini, 2011). Changes in external pressures and temperatures result in a corresponding change in pressure and air density and thus, as a result, ventilation within the cave, as air enters the cave system in differing ventilation patterns in order to balance with external pressure changes. This may also in turn be related to short term changes in temperature associated with decreases or increases in external pressure. If external temperatures fall below the average temperature measured within the cave system, air

from the outside environment with a low pCO_2 enters the cave system, and increases the deposition of speleothem carbonate, and thereby reduced the electro-conductivity values measured within the resulting drip water samples (Sherwin & Baldini, 2011; Smith et al., 2015). When the external air pressure decreases, it results in a similar decreases within the cave air pressure, which increases the drawdown of air into the cave system, thereby increasing the pCO_2 within the cave system and resultantly, the electro-conductivity values of the drip water samples (Sherwin & Baldini, 2011; Smith et al., 2015). Comparing the electro-conductivity of the three chambers within the Sterkfontein Caves system to variations in the external air temperature with regards to the average cave air temperature, only the Jacovec Cavern and Antechamber 1 show a slight trend with decreasing electro-conductivity when exterior temperatures decrease below the average cave air temperature. Antechamber 2 only shows a sharp peak in electro-conductivity from June 2015 to August 2015, and then decreases and maintains an overall flat trend for the rest of the year. Comparing the three chambers to one another however, it would suggest then that Antechamber 1 has the highest ventilation and pCO_2 of the three chambers, with Jacovec Cavern having a slightly lower pCO_2 and cave ventilation, and antechamber 2 having the lowest pCO_2 and cave ventilation. This, however, is in contrast to the observed ventilation of the three chambers. As the observed trends between decreasing exterior temperatures and electro-conductivity is only very slight, it may be assumed that this is not a reliable measure of air ventilation within the three chambers with respect to electro-conductivity. This is in keeping with the fact that there is very little statistically significant correlation between the exterior temperatures and interior cave temperatures (see Chapter 4), indicating that the exterior temperatures had a minimal effect on the hydrochemistry within the cave system. In addition, the slight trends observed here may have been affected by the constant movement of people along the tourist path within Sterkfontein Caves. This would affect Antechamber 1 the greatest, as Antechamber 1 is closest to, and has to the best access to the tourist path within the cave system.

Smaller variations within each chamber's range of electro-conductivity values may be attributed to small climatic changes occurring exterior to the cave environment, and the resulting pressure and ventilation variations being recorded within the electro-conductivity values from the drip water samples. Reduced electro-conductivity values within each range may suggest a decrease in external air temperatures, and vice versa. This gives an indication of the climate dynamics of the environment outside the cave system, recorded within the drip water produced from the modern speleothems.

The total range of electro-conductivity values produced display typical values associated with ground water permeating cave systems, and indicates no significant intrusions by any group of specific ions (Smith et al., 2015). The three differing trends may also indicate differing levels of total dissolved solids, which may be affected by the path of the drip water through the host rocks, and the CO_2 diffusion to and from the water.

Slight correlation between atmospheric cave pressure and electro-conductivity does exist, but it does not seem strong enough to state that the results are related to one another, especially not for the lower electro-conductivity trends. This may be due to the fact that the cave air pressure remained almost constant for the entire sampling period.

5.4.2 pH

The overall pH across all the samples remained fairly constant, only varying slightly between 7.7 and 8. Five samples produced outlier results, but these samples still produced similar results, with their pH ranging between 7.3 and 7.7. The sample from the Milner Lake also produced a pH within the range of 7.7 and 8, corresponding to the values produced by the other samples. This sample is representative of the ambient groundwater present in the Sterkfontein Caves system. These pH results display a slightly alkaline trend, which is very typical of most groundwater pH. The fact that there is only slight variation within the pH of the drip water samples and the Milner Lake sample shows that the drip water samples have retained the pH derived from the groundwater system which feeds the drip water collection points. This indicates the reliability of the drip water samples for further climatic analysis, as it demonstrates that very little exterior influences have affected the drip water samples. The groundwater system feeding into the Sterkfontein Caves system has been found to be slightly alkaline due to the dolomitic, karst-dominated terrain through which the water flows. (Hobbs, 2011)

The overall variation in the pH of the samples may reflect climatic changes, with pH increasing during periods of low cave air CO_2 concentrations and low pCO_2, and vice versa. This has implications for calcite saturation values, as these values follow a similar trend with respect to the measured pH and cave air CO_2 (Wang et al., 2015). These variations in the pH may also therefore reflect changing climatic conditions in the cave system with regards to cave pCO_2 and cave air ventilation, which in turn reflect climatic conditions and events in the exterior environment (Wang et al., 2015). A definite relationship exists between the pH produced from the drip water samples and the measured atmospheric pressure, with pH values increasing with atmospheric pressure, and vice versa. This reveals the climatic controls on the pH of the drip

water samples, particularly with regard to the cave pCO_2 and cave air CO_2 values, which can be interpreted with regard to temperature and precipitation variations in the exterior environment. This correlation again reveals the reliability of the drip water samples in representing current cave climatic conditions accurately with respect to the hydrochemical composition of the drip water. A comparison of the pH values of the drip water samples, the atmospheric pressure in the cave system and the measured cave air temperatures shows a very definite inverse relationship, with pH and atmospheric pressure increasing during a period of decreasing cave air temperatures. This reveals the manner in which the pH values of the drip water samples may vary seasonally, and therefore reflect subsequent climatic variations on the exterior environment reliably.

Overall, the hydrochemical composition and analysis of the drip water samples indicates the reliability of using drip water and speleothems as paleoclimate proxies, as the hydrochemistry indicates very little exterior influence on the drip water samples, and thus implies that the climatic data produced from the analysis of the drip water samples would prove to be accurate with regards to current climatic conditions.

Chapter 6
Conclusions

6.1 Modern Environment

The overall current observed vegetation above the Sterkfontein Caves system was replicated by the $\delta^{13}C$ vegetation trends calculated from the modern speleothem samples. Both data sets reflected an environment dominated by C_4 vegetation in the form of numerous grass species and particular small shrub-like species, with a smaller distribution of C_3 vegetation, consisting of woodland trees, large shrubs and small herbaceous plants. A small percentage of CAM vegetation was observed for the current environment above the Sterkfontein Caves system, but could not be accurately determined through the $\delta^{13}C$ analyses because the CAM carbon isotopic signature is very difficult to distinguish from the C_4 carbon isotopic signature. The CAM signature was therefore assumed to form part of the C_4 signature calculated from the $\delta^{13}C$ values of the modern speleothems, which was slightly higher than the observed vegetation. The unexpectedly low $\delta^{13}C$ values deduced from speleothem samples from the Silberberg Grotto may be explained in reference to the current environment above the Silberberg Grotto and the location of the Grotto with regards to the cave entrance, and therefore displays a greater resolution of the speleothem $\delta^{13}C$ with regard to the calculated vegetation in comparison to the current modern distribution of vegetation above the Sterkfontein Caves system.

Carbon isotope systems however, are complex to interpret, due to numerous factors which influence isotope values. The soil, roof rocks and host rocks through which the meteoric water flows to form drip water affects its' carbon isotope value. Therefore, the C_3 and C_4 values obtained from the carbon isotopes and the interpretations associated with them should be treated cautiously and not as absolute values.

The distribution of vegetation deduced from both the $\delta^{13}C$ values and the observed vegetation above the Sterkfontein Caves system both imply a mosaic environment dominated by grasses interspersed with larger shrubs and open woodland trees. Overall, the carbon isotope vegetation data produced from the modern speleothems coincides with the observed vegetation currently existing above the cave environment. This study substantiates the reliability of environmental analysis using speleothems.

The temperatures produced from the analysis of the $\delta^{18}O$ values from the modern speleothem samples and the corresponding drip water samples show great variation with respect to the equation used to calculate the temperatures, and in comparison to the measured atmospheric air temperatures for the area, the measured cave air temperatures, to a lesser degree, and the idealised temperatures calculated from the speleothem $\delta^{18}O$, without taking fractionation into consideration. The temperatures produced using the empirical equation (equation 1) displayed much better direct correlation to the measured atmospheric temperatures and measured cave air temperatures than that of the temperatures produced using the experimental equation (equation 2). However, these temperatures did show variations, particularly during periods of higher atmospheric temperatures, which is indicative of evaporative cooling effects affecting the $\delta^{18}O$ signature of the drip water samples (see chapter 5). The temperatures calculated using the experimental equation (equation 2) display an almost inversely proportional relationship to the measured atmospheric temperatures, with calculated temperatures reflecting the measured atmospheric temperatures better during cooler atmospheric temperatures. As equilibrium fractionation usually also displays an inverse relationship to temperature, this relationship between the temperatures calculated using equation 2 and the measured atmospheric temperatures may be a result of equilibrium fractionation. In this regard, it may be better to compare the measured atmospheric temperatures to a combination of calculated temperatures using both equations, which could constrain the data better in terms of relationships between the calculated temperatures and measured atmospheric temperatures being reflected more accurately. This theory should be tested further however with a larger data pool sampled over a longer period of time in order to increase the resolution of the data, which would assist in ascertaining its' validity.

The overall variations that are present between the calculated temperature data, the measured atmospheric temperature, the measured cave temperatures and the idealised temperatures reveal that significant kinetic fractionation effects have played a role in skewing the calculated temperatures from both the empirical and experimental equations. This occurs to a lesser degree in the narrower, smaller antechambers than in the Jacovec Cavern, which is quite large. This may be due to higher overall humidity in the antechambers, especially Antechamber 1, in comparison to the Jacovec Cavern, which displayed the greatest range of variations in humidity. Cave air ventilation also played a role in encouraging evaporative fractionation effects, as more air flow through the chambers would result in further fractionation of the $\delta^{18}O$ values produced from the drip water samples. As Sterkfontein Caves is frequently visited by tourists, which pass close by these chambers, it may have affected the cave air ventilation and

therefore the fractionation processes affected the drip water and consequently speleothem $\delta^{18}O$ signatures. The calculated temperatures and equilibrium fractionation factors from the three chambers compared to the expected temperatures and corresponding equilibrium fractionation factors for calcite showed the calculated temperatures to correspond to higher equilibrium fractionation factors overall, again exhibiting skewness resulting from kinetic fractionation effects. Due to these factors, the overall temperatures produced from the analysis of the $\delta^{18}O$ values from the modern speleothem and drip water samples are not reliable estimations of the current atmospheric temperature trends, and should be treated with caution. The overall trends displayed by the calculated temperatures however may reflect similar or related trends in the short term measured atmospheric temperature data.

Overall however, the $\delta^{18}O$ trends without further analysis displayed more depleted values, with an average of -3.6‰, signifying cooler, drier and more arid climatic conditions, which is also exhibited by the $\delta^{13}C$ trends.

The $\delta^{18}O$ values from the modern drip water samples and the drip rate measured during the collection of the drip water samples correspond well with one another, reflecting the same general trends during the period of drip water collection. Small variations in $\delta^{18}O$ values compared to the drip rates may be a result of slight kinetic fractionation, but not enough to offset any of the trends. Both data sets exhibit a lag period of approximately 4 to 6 months in relation to the average monthly rainfall for the area. This coincides well with the residence time of meteoric water flowing into the Sterkfontein Caves system, and the low recharge rate of groundwater into the karst environment (Martini et al., 2013). Another interpretation of the relationship between the drip rates and $\delta^{18}O$ values, and the average measured rainfall is that it may represent an inverse relationship with the average monthly rainfall, due to the ‘amount effect’. However, as this effect is most common in tropical environments, it is assumed that the drip water $\delta^{18}O$ values and the drip rate represent a lag effect with regards to the monthly average rainfall, as there is more evidence to support this theory. Variations in the $\delta^{18}O$ values may be assumed to represent short periods of intense rainfall or other climatic events, or due to evaporative effects associated with high temperatures, high humidity, and high rainfall. Due to these factors, lower, more depleted $\delta^{18}O$ values of the drip water have been interpreted to represent drier periods with a decrease in average annual rainfall, in comparison to higher, more enriched $\delta^{18}O$ values which have been interpreted to represent wetter periods, characterised by an increase in heavy precipitation events, as well as in the amount of rainfall produced in a single event.

The hydrochemistry of the Sterkfontein Caves system seems to be linked with climatic conditions within the cave system, as well as to the exterior climate. Variations in electro-conductivity of drip water has been related to drip rates, where faster drip rates are accompanied by lower electro-conductivities and vice versa (see chapter 5). This, in turn, may be related to precipitation events, as the drip rates reflect local monthly rainfall events, despite a lag period. The electro-conductivity therefore may be analysed in terms of precipitation, and in this case reveals trends that match with increasing or decreasing drip rates, and as a result, increasing and decreasing periods of rainfall. As a result, electro-conductivity values from drip water may provide valuable insight as to the degree to which precipitation has affected the cave system, and how well it has been represented by the drip water samples. However, as the relationship between drip rates and the electro-conductivity of the drip water samples only displays a slight relationship, other factors have also been taken into account, which may explain the variations in the drip water electro-conductivity to a better degree. The electro-conductivity of the drip water samples has also been related to variations in air ventilation, which are controlled by changing pCO_2 conditions within the cave system as a result of changes in external pressures and temperatures. As external air pressure decreases, it results in similar decreases within the cave air pressure, which increases the drawdown of air into the cave, thereby increasing the pCO_2 within the cave system and consequently, the electro-conductivity values of the drip water samples. In this way, the electro-conductivity values from the drip water samples may be able to provide insight into pressure and temperature changes occur in the exterior environment, and therefore provide clues as to the current climatic conditions. This relationship however is only exhibited to a small degree in the electro-conductivity values from the drip water samples. Overall however, the differing electro-conductivity trends for the three chambers provide insight as to the differing conditions with regards to air ventilation, which is important to understand when sampling speleothems and drip water affected by the least amount of kinetic fractionation.

The pH values produced from the drip water samples all remain within a small range that reflects the pH measured of the groundwater within the cave system. Variations within the pH values may reflect changing CO_2 and pCO_2 conditions within the cave system (see chapter 5), and therefore subsequent variations in climatic factors such as the exterior pressure systems, which may affect cave pCO_2 and CO_2 conditions, as well as the saturation of calcite during the precipitation of speleothems. The pH values also display an inverse relationship with regard to the measured cave air temperature, which reveals the extent to which the pH values may represent changing climatic conditions on the exterior environment. These small variations in

the drip water pH therefore may also add insight as to the overall exterior climatic conditions, as well as to the saturation of calcite with regard to the precipitation of speleothems.

6.2 Implications for Palaeo-environmental Analysis

The corresponding vegetation distribution reflected by the calculated $\delta^{13}C$ values from the modern speleothem samples and the current observed vegetation distribution display the reliability of using carbon isotope signatures from speleothems from the Sterkfontein Caves system in reconstructing the distribution of vegetation in the exterior environment. It can therefore be assumed to a certain degree that using the $\delta^{13}C$ values of ancient speleothems as environmental proxies for vegetation distribution during the period of precipitation of the speleothems would be reliable. The carbon isotope system with regards to speleothem precipitation is very complex due to the numerous factors which may influence the $\delta^{13}C$ signature. Speleothem samples need to be selected and sampled very carefully in order to avoid any fractionation which might have influenced the $\delta^{13}C$ signature during precipitation of the speleothems (see chapter 5). With regard to this, it is suggested that the interpretations associated with the $\delta^{13}C$ analysis of the speleothems be treated cautiously, and placed in context with regard to the length of sampling period and sampling localities within the cave system. Overall however, these values do provide reliable estimates with regard to the overlying vegetation at the Sterkfontein Caves.

The temperatures calculated from the $\delta^{18}O$ values of the modern speleothem and corresponding drip water samples display trends which may be related to the measured atmospheric temperatures to a certain degree, however the kinetic fractionation which has skewed the calculated temperature results may have affected the temperatures to such a degree that climatic interpretations based on the calculated temperatures would not be accurate. The trends displayed by the calculated temperatures may be used in the future in reconstructing long term palaeo-temperatures from ancient speleothems, but should be used with caution. In general, in order to fully determine the reliability of these calculated temperatures, a greater resolution with regards to sampling over a longer period of time should be used. Overall, the $\delta^{18}O$ values from the modern speleothem and drip water samples both display aridifying trends, as is displayed by the $\delta^{13}C$ trends from the modern speleothem samples, and these trends may be used to establish general climatic patterns from speleothem and drip water samples as palaeoclimate proxies.

The drip water $\delta^{18}O$ trends and the drip rate trends seem to reflect the average monthly rainfall well, exhibiting a lag period between rainfall events and the results thereof on the $\delta^{18}O$ values and drip rates. This lag period, as previously mentioned, has been attributed to groundwater residence time and recharge period. Due to this, drip water $\delta^{18}O$ values and drip rate may be used to establish general short term rainfall patterns for palaeoclimatic reconstructions to a certain degree, however it is recommended to collect a higher resolution of $\delta^{18}O$ and drip rate data before this can be confidently assumed.

The hydrochemistry results produced from the drip water samples show definite relationships with regard to variations in the cave climate, and therefore may be reliably used (especially with regard to the pH values produced from the drip water samples) in deducing climatic conditions within the cave system and consequently the exterior environment. These hydrochemistry results reveal the reliability of the speleothems and drip water in the Sterkfontein Caves system to replicate current environmental conditions above the cave environment to a certain degree.

Ideally, using speleothems and drip water samples to provide palaeoclimate reconstructions should be performed at a higher resolution, which can be achieved by sampling over a longer period with regards to the collection of drip water and monitoring of drip rate and climatic data. This would produce a larger pool of data to be analysed, and therefore trends may be more accurately interpreted with regards to the modern environment. This would result in data of a higher resolution, which would produce more accurate analyses. This is particularly important for samples collected at Sterkfontein Caves, as samples analysed from this cave system would produce more reliable long term palaeoclimatic interpretations, as opposed to the short term results produced by this study. The location of samples should also be chosen very carefully, as a unique set of climatic conditions within the cave system are conducive to producing $\delta^{18}O$ trends from speleothems and drip water which have been influenced the least by kinetic fractionation. Closed cave systems with high humidity and little cave air ventilation influence should be prioritised as prime locations for speleothem and drip water sampling to take place, especially for longer term studies. Drip water which displays the shortest flow time from source to collection should ideally be chosen for sampling.

The use of speleothems and drip water as palaeoclimate proxies may produce reliable reconstructions, but should be used with caution due to the complex interplay of factors which affect the precipitation of speleothems from drip water, and which may affect the $\delta^{18}O$ values through kinetic fractionation.

Overall, the modern speleothem and drip water samples reflect the modern environment well with regards to vegetation and precipitation, and these interpretations are supported by previous studies in the area (see chapter 5). The hydrochemistry of the drip water samples provides insight into general climatic trends in the current exterior environment, and reflects the overall reliability of the cave system in replicating climatic conditions on the environment above the cave system. The temperatures calculated from the modern speleothem and drip water samples do reflect relationships and similarities to the short term, measured atmospheric temperatures and the measured cave air temperatures. These interpretations and conclusions suggest that the speleothems in the Sterkfontein Caves system may be reliable palaeoclimate proxies, with respect to vegetation and precipitation, and may provide reliable short term relationships with regards to modern temperatures.

Future research with regard to the reliability of speleothems as palaeoclimate proxies could possibly include a longer period of sampling and data collection with respect to the cave climatic conditions, as well as sampling from a larger range of speleothem specimens, which could include a more diverse range of formation conditions. A more detailed examination of the hydrochemical aspects of the cave system and the manner in which this influences oxygen and carbon isotopic signatures in the drip water and speleothems may also be pursued. Cave systems with differing cave climatic conditions could also be examined to determine the effects thereof on the isotopic signature of drip water and speleothem samples, and therefore the environmental and climatic data produced from the drip water and speleothems, as opposed to the outside environment. Cave systems occupied by a larger abundance of organisms such as bats may also be examined with respect to the effects organisms may have on CO_2 concentrations, humidity and pH, and how this may, in turn, effect speleothem and drip water isotopic signatures. A weather station set up at Sterkfontein Caves, or any particular cave system that is being studied would provide the best replication of current climatic data directly related to the cave system area, therefore ensuring the accuracy and reliability of results. For a comparative function, artificially precipitating calcium carbonate under ideal or replicated circumstances may provide additional data and insight into the precipitation mechanisms involved which constrain the isotopic signatures of drip water and speleothems. This would allow for severe kinetic fractionation effects in natural speleothems to be identified and further constrained.

The aims of this study were to ascertain the reliability of speleothems in representing precipitation, temperature and vegetation data with regard to the modern environment and

climate, and thus to ascertain whether speleothems would be reliable palaeoclimate proxies for future studies. These aims were achieved, as the modern climatic and environmental data produced by the carbon and oxygen isotope analysis of modern speleothems and drip water correlates to a certain degree with the vegetation, precipitation and temperature data with regard to the modern environment. This therefore ascertains the reliability of speleothems as palaeoclimate proxies.

References

Aggarwal, P. K., Aráguas-Aráguas, L., Gröning, M., Kulkarni, K.M., Kurttas, T., Newman, B.D. & Tanweer, A. (2009) Laser spectroscopic analysis of liquid water samples for stable hydrogen and oxygen isotopes. *Training course series no. 35*, AIEA Pub.

Avery, D.M., 2001. The Plio-Pleistocene vegetation and climate of Sterkfontein and Swartkrans, South Africa, based on micromammals. *Journal of Human Evolution*, **41**, 113-132.

Ayliffe, L.K., Marinelli, P.C., Moriarty, K.C., Wells, R.T., McCulloch, M.T., Mortimer, G.E. & Hellstrom, J.C. (1998) 500 Ka precipitation record from south- eastern Australia: Evidence for interglacial relative aridity. *Geology*, **26** (2), 147-150.

Baker, A., Ito, E., Smart, P. L. & McEwan, R. F. (1997) Elevated and variable values of ^{13}C in speleothems in a British cave system. *Chemical Geology*, **136**, 263-270.

Baldini, J.U.L., McDermott, F., Hoffmann, D.L., Richards, D.A. & Clipson, N. (2008) Very high- frequency and seasonal cave atmosphere P-CO_2 variability: Implications for stalagmite growth and oxygen isotope-based paleoclimate records. *Earth and Planetary Science Letters*, **272**, 118-129.

Bamford, M. (1999) Pliocene woods from an early hominid cave deposit, Sterkfontein, South Africa. *South African Journal of Science*, **95**, 231-237.

Bassinot, F.C., Labeyrie, L.D., Vincent, E., Quidelleur, X., Shackleton, N.J. & Lancelot, Y. (1994) The astronomical theory of climate and the age of the Brunhes- Matuyama magnetic reversal. *Earth and Planetary Science Letters*, **126**, 91-108.

Bates, J.R. (1973) The intertropical convergence zone and the atmospheric circulation – A study using the primitive equations. *Proceedings of the Royal Irish Academy*, **73A**, 227-254.

Behrensmeyer, A.K. (2006) Climate change and human evolution. *Science*, **311**, 476-478.

Benefit, B.R. & McCrossin, M.L. (1995) Miocene hominoids and hominid origins. *Annual Review of Anthropology*, **24**, 1-592.

Berger, L.R. & Tobias, P.V. (1994) New discoveries at the early hominin site of Gladysvale, South Africa. *South African Journal of Science*, **90**, 223-226.

Berger, L.R. & Tobias, P.V. (1996) A chimpanzee-like tibia from Sterkfontein, South Africa and its implications for interpretations of bipedalism in *Australopithecus africanus*. *Journal of Human Evolution*, **30**, 343-350.

Berger, L.R., Lacruz, R.S. & De Ruiter, D.J. (2002) Brief communication: revised age estimates of *Australopithecus* bearing deposits at Sterkfontein, South Africa. *American Journal of Physical Anthropology*, **119**, 192-197.

Berger, L.R., De Ruiter, D.J., Churchill, S.E., Schmid, P., Carlson, K.J., Dirks, P.H.G.M. & Kibii, J.M. (2010) *Australopithecus sediba*: a new species of homo-like *Australopith* from South Africa. *Science*, **328**, 195-204.

Blackwell, B. & Schwarcz, H.P. (1995) The Uranium Series Disequilibrium Dating Methods, In: Rutter, N.W. & Catto, N.R. (1995) *Dating methods for Quaternary deposits.* Newfoundland, Canada: Geological Association of Canada.

Blyth, A.J., Asrat, A., Baker, A., Gulliver, P., Leng, M.J. & Genty, D. (2007) A new approach to detecting vegetation and land-use change using high-resolution lipid biomarker records in stalagmites. *Quaternary Research*, **68**, 314-324.

Blumenschine, R.J. (1987) Characteristics of an early hominid scavenging niche. *Current Anthropology*, **28**, 383-407.

Bobe, R., Behrensmeyer, A.K. & Chapman, R.E. (2002) Faunal change, environmental variability and late Pliocene hominin evolution. *Journal of Human Evolution*, **42**, 475-497.

Bobe, R. & Behrensmeyer, A.K. (2004) The expansion of grassland ecosystems in Africa in relation to mammalian evolution and the origin of the genus *Homo*. *Palaeogeography, Palaeoclimatology, Palaeoecology*, **207**, 399-420.

Bobe, R. (2006) The evolution of arid ecosystems in eastern Africa. *Journal of Arid Environments*, **66**, 564-584.

Boggs, S. (2001) *Principles of Sedimentology and Stratigraphy (3rd Ed.)*. Prentice Hall, New Jersey.

Bonnefille, R. (1995) A reassessment of the Plio-Pleistocene pollen record of East Africa. In: Vrba, E.S., Denton, G.H., Partridge, T.C. & Burckle, L.H. (Eds.) *Paleoclimate and Evolution, with Emphasis on Human Origins*. Yale University Press, New Haven, 299-310.

Borsato, A. (1997) Dripwater monitoring at Grotta di Ernesto (NE-Italy): a contribution to the understanding of karst hydrology and the kinetics of carbonate dissolution. *Proceedings of the 12th International Congress of Speleology*, **2**, 57-60.

Brain, C.K. (1958) The Transvaal Ape-Man Bearing Cave Deposits, Transvaal Museum, Pretoria: *Transvaal Museum Memoir* no. 11

Brain, C.K., 1981, *The hunters or the hunted? An introduction to African cave taphonomy*. Chicago University Press, Chicago.

Brain, C.K. (1993) Structure and stratigraphy of the Swartkrans Cave in the light of the new excavations. In: Brain, C.K. (Eds) *Swartkrans: A Cave's Chronicle of Early Man*, 23-33.

Brain, C.K. (1995) The Influence of climatic changes on the completeness of the early hominin record in southern African caves, with particular reference to Swartkrans. In: Vrba, E.S. (Ed) *Palaeoclimate and Evolution, with Emphasis on Human Origins*. Yale University Press, New Haven.

Broom, R. (1936) A new fossil anthropoid skull from South Africa. *Nature*, **138**, 486-488.

Broom, R. (1938) The Pleistocene anthropoid ages of apes of South Africa. *Nature,* **142**, 377-379.

Bruxelles, L., Clarke, R. J., Maire, R., Ortega, R., & Stratford, D (2014) Stratigraphic analysis of the Sterkfontein StW 573 *Australopithecus* skeleton and implications for its age. *Journal of Human Evolution*, **70**, 36-48.

Burckle, L.H. (1995) Current issues in Pliocene paleoclimatology. In: Vrba, E.S., Denton, G.H., Partridge, T.C., Burckle, L.H. (Eds.) *Paleoclimate and Evolution: with Emphasis on Human Origins*. Yale University Press, New Haven, 3-7.

Button, A. (1973). The stratigraphic history of the Malmani Dolomite in the eastern and north-eastern Transvaal. *Transactions of the Geological Society of South Africa*, **76**, 229-247.

Butzer, K.W. (1976) Lithostratigraphy of the Swartkrans Formation. *South African Journal of Science*, **72**, 136-141.

Cadman A., & Rayner R.J. (1989) Climatic change and the appearance of *Australopithecus africanus* in the Makapansgat sediments. *Journal of Human Evolution*, **18**, 107-113.

Cane, M.A. & Molnar, P. (2001) Closing of the Indonesian seaway as a precursor to east African aridification around 3–4 million years ago. *Nature*, **411**, 157-162.

Cerling, T.E. (1992) Development of grasslands and savannas in East Africa during the Neogene. *Palaeogeography, Palaeoclimatology, Palaeoecology*, **97**, 241-247.

Cerling, T.E., Harris, J.M., Macfadden, B.J., Leakey, M.G., Quade, J., Eisenmann, V. & Ehleringer, J.R. (1997) Global vegetation changes through the Miocene/Pliocene boundary. *Nature*, **389**, 153-158.

Chappell, J. & Shackleton, N.J. (1986) Oxygen isotopes and sea level. *Nature*, 324.

Clarke, P.U., Alley, R.B. & Pollard, D. (1999) Northern hemisphere ice-sheet influences on

global climate change. *Science*, **286**, 1104-1111.

Clarke, R.J. (1985) Early Acheulean with *Homo habilis* at Sterkfontein. In: Tobias, P. V. (Ed.), *Hominid Evolution: Past, Present, and Future*. 287-298. Alan R. Liss, New York.

Clarke, R.J. (1994) On some new interpretations of Sterkfontein stratigraphy. *South African Journal of Science*, **90**, 211-214.

Clarke, R.J. & P.V. Tobias (1995). Sterkfontein Member 2 foot bones of the oldest South African hominid. *Science*, **269**, 521-524.

Clarke, R.J. (1998) First ever discovery of a well-preserved skull and associated skeleton of *Australopithecus*. *South African Journal of Science*, **94**, 460-463.

Clarke, R.J. (2006) A deeper understanding of the stratigraphy of Sterkfontein fossil hominid site: hominid studies. *Transactions of the Royal Society of South Africa*, **61** (2), 111-120.

Clarke, R. (2013). *Australopithecus* from Sterkfontein Caves, South Africa. In: K. E. Reed, J. G. Fleagle, & R. E. Leakey (Eds.) *The Paleobiology of Australopithecus: Vertebrate Paleobiology and Paleoanthropology*, 105-123.

Clemens, S.C. & Prell, W.J. (1991) One million year record of summer monsoon winds and continental aridity from the Owen Ridge (Site 722), Northwest Arabian Sea. In: Prell, W.J. & Niitsuma, N. (Eds.) *Proc. ODP*, **117**, 365-388.

Clemens, S.C., Murray, D.W. & Prell, W.L. (1996) Non-stationary phase of the Plio-Pleistocene Asian monsoon. *Science*, **274**, 943-948.

Cohen, A., Arrowsmith, R., Behrensmeyer, A.K., Campisano, C., Feibel, C., Fisseha, S., Johnson, R., Bedaso, Z.K., Lockwood, C., Mbua, E., Olago, D., Potts, R., Reed, K., Renaut, R., Tiercelin, J.J. & Umer, M. (2009) Understanding Palaeoclimate and Human Evolution through the Hominin Sites and Palaeolakes Drilling Project. *Scientific Drilling*, **10**, 60-65.

Cooke, H.B.S. (1938) The Sterkfontein bone breccia: a geological note. *South African Journal of Science*, **35**, 204-208.

Coplen, T.B. (1996) New guidelines for reporting stable hydrogen, carbon, and oxygen isotope-ratio data. *Geochimica et Cosmochimica Acta*, **60**, 3359-3360.

Coxall, H.K., Wilson, P.A., Palike, H., Lear, C.H. & Backman, J. (2005) Rapid stepwise onset of Antarctic glaciation and deeper calcite compensation in the Pacific Ocean. *Nature*, **433**, 53-57.

Craig, H. (1961) Isotopic variations in meteoric waters. *Science*, **133**, 1702-1703.

Craig, H. (1965) The measurement of oxygen isotope palaeotemperatures. In: Tongiorgi, E. (Ed.) *Stable Isotopes in Oceanographic Studies and Palaeotemperatures*. CNR, Pisa.

Cruz Jr., F.W., Karmann, I., Viana Jr., O., Burns, S.J., Ferrari, J.A., Vuille, M., Sial, A.N. & Moreira, M. Z. (2005) Stable isotope study of cave percolation waters in subtropical Brazil: Implications for palaeoclimate inferences from speleothems. *Chemical Geology*, **220**, 245-262.

Cruz, F.W., Burns, S.J., Karmann, I., Sharp, W.D., Vuille, M. & Ferrarri, J.A. (2006) A stalagmite record of changes in atmospheric circulation and soil processes in the Brazilian subtropics during the Late Pleistocene. *Quaternary Science Reviews*, **25**, 2749-2761.

Curnoe, D. (2010) A review of early *Homo* in southern Africa focusing on cranial, mandibular and dental remains, with the description of a new species (*Homo gautengensis* sp. nov.). *Journal of Comparative Human Biology*, **61**, 151-177.

Cuthbert, M.O., Rau, G.C., Andersen, M.S., Roshan, H., Rutlidge, H., Marjo, C.E., Markowska, M., Jex, C.N., Graham, P.W., Mariethoz, G., Acworth, R.I. & Baker, A. (2014). Evaporative cooling of speleothem drip water. *Scientific reports*, **4**, 51-62.

Dart, R.A. (1925) *Australopithecus africanus*: The man-ape of South Africa. *Nature*, **115**, 195-199.

De Cisneros, J.C. & Caballero, E. (2013) Paleoclimate reconstruction during MIS5a based on a speleothem from Nerja Cave, Málaga, South Spain. *Natural Science*, **5**, 533-540.

De Menocal, P.B., & Bloemendal, J. (1995) Plio-Pleistocene subtropical African climate variability and the paleoenvironment of hominid evolution: A combined data-model approach. In*:* Vrba, E., Denton, G., Burckle, L., & Partridge, T., (Eds.). *Paleoclimate and Evolution with Emphasis on Human Origins.* New Haven, Yale University Press, 262-288.

De Menocal, P.B. (1995) Plio–Pleistocene African climate. *Science*, **270**, 53-59.

De Menocal, P.B. (2004) African climate change and faunal evolution during the Pliocene-Pleistocene. *Earth and Planetary Science Letters*, **220**, 3-24.

Demeny, A., Kele, S. & Siklosy, Z. (2010) Empirical equations for the temperature dependence of calcite-water oxygen isotope fractionation from 10 to 70°C. *Rapid Communications in Mass Spectrometry*, **24**, 3521-3526.

Dirks, P.H.G.M., & Berger, L.R. (2012) Hominin-bearing caves and landscape dynamics in the Cradle of Humankind, South Africa. *Journal of African Earth Sciences*, **78**, 109-131.

Dominguez-Villar, D., Fairchild, I.J., Carrasco, R.M., Pedraza, J. & Baker, A. (2010) The effect of visitors in a touristic cave and the resulting constraints on natural thermal conditions for palaeoclimate studies (Eagle Cave, Central Spain). *Acta Carsological*, **39**, 491-502.

Dorale, J.A., Edwards, R.L., Ito, E. & González, L.A. (1998) Climate and Vegetation History of the Midcontinent from 75 to 25 Ka: A Speleothem Record from Crevie Cave, Missouri, USA. *Science*, **282**, 1871-1874.

Dorale, J.A., Edwards, R.L. & Onac, B.P. (2002) Stable isotopes as environmental indicators in speleothems. In: Yuan, D. (Ed.) *Karst processes and the carbon cycle*. Geological Publishing House, Beijing, 107-120.

Dupont, L.M. & Leroy, S.A.G. (1995) Steps toward drier climatic conditions in Northwestern

Africa during the Upper Pliocene. In: Vrba, E.S., Denton, G.H., Partridge, T.C., Burckle, L.H. (Eds.) *Paleoclimate and Evolution: with Emphasis on Human Origins*. Yale University Press, New Haven, 289-298.

Edwards, R.L., Chen J.H. & G.J. Wasserburg (1987) $^{238}U - ^{234}U - ^{230}Th - ^{232}Th$ systematics and the precise measurement of time over the past 500,000 years. *Earth and Planetary Science Letters*, **81**, 175-192.

Elderfield, H. & Ganssen, G. (2000) Past temperature and $\delta^{18}O$ of surface ocean waters inferred from foraminiferal Mg/Ca ratios. *Nature*, **405**, 442-445.

Eriksson, K.A. & Truswell, J.F. (1974) Stratotypes from the Malmani Dolomite, Transvaal, South Africa. *Sedimentary Geology*, **18**, 223-244.

Eriksson, P.G., Altermann, W. & Hartzer, F.J. (2006) The Transvaal Supergroup and its precursors. In: Johnson, M.R., Anhaeusser, C.R., Thomas, R.J. (Eds.) *The Geology of South Africa.* Geological Society of South Africa and Council for Geoscience Publication, Pretoria, 237-260.

Fairchild, I.J., Smith, C.L., Baker, A., Fuller, L., Spötl, C., Mattey, D., McDermott, F. & E.I.M.F. (2006) Modification and preservation of environmental signals in speleothems. *Earth-Science Reviews,* **75**, 105-153.

Fairchild, I.J., Borsato, A., Tooth, A.F., Frisia, S., Hawkesworth, C.J., Huang, Y., McDermott, F. & Spiro, B. (2000) Controls on trace element (Sr-Mg) compositions of carbonate cave waters: implications for speleothem climatic records. *Chemical Geology*, **166**, 255-269.

Faure, G. (1986) *Principles of Isotope Geology (2nd Edition)*. John Wiley & Sons, New York, 282-459.

Feakins, S.J., De Menocal, P.B. & Eglinton, T.I. (2005) Biomarker records of Late Neogene changes in northeast African vegetation. *Geology*, **33**(12), 977-980.

Feng, W., Casteel, R.C., Banner, J.L. & Heinze-Fry, A. (2014) Oxygen isotope variations in rainfall drip water and speleothem calcite from a well-ventilated cave in Texas, USA: Assessing a new speleothem temperature proxy. *Geochimica et Cosmochimica Acta*, **127**, 233-250.

Fernandez, M.H. & Vrba, E.S. (2006) Plio-Pleistocene climatic change in the Turkana Basin (East Africa): Evidence from large mammal faunas. *Journal of Human Evolution*, **50**, 595-626.

Fernández-Cortés A., Calaforra J.M., Sánchez-Martos F., & Gisbert J. (2007) Stalactite drip rate variations controlled by air pressure changes: an example of non-linear infiltration processes in the 'Cueva del Agua' (Spain). *Hydrological Processes*, **21**, 920-930.

Fletcher, B.J., Brentnall, S.J., Anderson, C.W., Berner, R.A. & Beerling, D.J. (2008) Atmospheric carbon dioxide linked with Mesozoic and Cenozoic climate change. *Nature Geoscience*, **1**, 43-48.

Fleitmann, D., Burns, S.J., Neff, U., Mudelsee, M., Mangini, A. & Matter, A. (2004) Palaeoclimatic interpretation of high-resolution oxygen isotope profiles derived from annually laminated speleothems from Southern Oman. *Quaternary Science Reviews*, **23**, 935-945.

Friedmann, I. & O'Neil, J.R. (1977) Compilation of stable isotope fractionation factors of geochemical interest. In: Fleischer, M. (Ed.) *Data of Geochemistry 6th Edition*. US Geological Survey Prof. Paper 440 KK, US Geological Survey, Washington.

Gascoyne, M. (1992) Palaeoclimate determination from cave calcite deposits. *Quaternary Science Reviews*, **11**, 609-632.

Genty, D. & Deflandre, G. (1998) Drip flow variations under a stalactite of the Pere Noel cave (Belgium). Evidence of seasonal variations and air pressure constraints. *Journal of Hydrology*, **211**, 208-232.

Gonfiantini, R., Stichler, W. & Rozanski, K. (1995) Standards and intercomparison materials distributed by the International Atomic Energy Agency for stable isotope measurements. In: *Reference and Intercomparison Materials for Stable Isotopes of Light Elements*, IAEA TEC-DOC 825, 13-29.

Granger, D.E., Gibbon, R.J., Kuman, K., Clarke, R.J., Bruxelles, L. & Caffee, M.W. (2015) New cosmogenic burial ages for Sterkfontein Member 2 Australopithecus and Member 5 Oldowan. *Nature*, **522**, 85-88.

Gray, J.R. (2004). Conductivity Analysers and Their Application. In: Down, R.D. & Lehr, H. (Eds) *Environmental Instrumentation and Analysis Handbook*. Wiley, 491-510.

Hammer, O., Harper, D.A.T., & Ryan, P.D. (2001) PAST: Paleontological Statistics Software Package for Education and Data Analysis. *Palaeontologia Electronica*, **4** (1), 9.

Harmon, R.S., Schwarcz, H.P., Gascoyne, M., Hess, J.W. & Ford, D.C. (2004) Palaeoclimate information from speleothems: the present as a guide to the past. In: Sasowsky, I. D. & Mylroie, J. (Eds) *Studies of cave sediments: physical and chemical records of palaeoclimate*. Kluwer, New York, 199-206.

Harrison, M.S.J. (1986) A Synoptic Climatology of South African Rainfall Variations. Ph.D. Thesis, University of the Witwatersrand.

Haug, G.H. & Tiedemann, R. (1998) Effect of the formation of the Isthmus of Panama on Atlantic Ocean thermohaline circulation. *Nature*, **393**, 673-676.

Haug, G.H., Hughen, K.A., Sigman, D.M., Peterson, L.C. & Rohl, U. (2001) Southward migration of the intertropical convergence zone through the Holocene. *Science*, **293**, 1304-1308.

Hendy, C.H. (1971) The isotopic geochemistry of speleothems: I. The calculation of the effects of different modes of formation on the isotopic composition of speleothems and their applicability as palaeoclimatic indicators. *Geochimica et Cosmochimica Acta*, **35**, 801-824.

Herries, A.I.R., Hopley, P.J., Adams, J.W., Curnoe, D. & Maslin, M.A. (2010) Geochronology and palaeoenvironments of Southern African hominin-bearing localities—A reply to Wrangham et al., 2009. "Shallow-water habitats as sources of fallback foods for hominins". *American Journal of Physical Anthropology*, **143** (4), 640-646.

Hilkert, A.W. & Avak, H. (2008) *Isotope Analysis of Water, Fruit Juice and Wine Using the Thermo Scientific GasBench II IRMS*. Thermo Fisher Scientific, Bremen, Germany.

Hill, C.A. (1995). Sulfur redox reactions, native sulfur, Mississippi Valley-type deposits and sulfuric acid karst, Delaware Basin, New Mexico and Texas. *Environmental Geology,* **25**, 16-23.

Hilton-Barber, B. & Berger, L.R. (2002) *The official guide to the Cradle of Humankind Sterkfontein, Swartkrans, Kromdraai and environs World Heritage Site.* Struik, Cape Town.

Hobbs, P.J. (2011) *Situation assessment of the surface water and groundwater resource environments in the Cradle of Humankind World Heritage Site*. Council for Scientific and Industrial Research, Department of Economic Development, 2011.

Holland, M.M., Bailey, D.A. & Vavrus, S. (2010) Inherent sea ice predictability in the rapidly changing Arctic environment of the Community Climate System Model, version 3. *Climate Dyrnamics,* **36**(7),1239-1253.

Holmgren, K., Lee-Thorpe, J.A., Cooper, G.R.J., Lundblad, K., Partridge, T.C., Scott, L., Sithaldeen, R., Talma, A.S. & Tyson, P.D. (2003) Persistent millennial-scale climatic variability over the past 25,000 years in Southern Africa. *Quaternary Science Reviews*, **22**, 2311-2326.

Hopley, P.J., Marshall, J.D., Weedon, G.P., Latham, A.G., Herries, A.I.R & Kuykendall, K.L. (2007) Orbital forcing and the spread of C_4 grasses in the Late Neogene: Stable isotope evidence from South African speleothems. *Journal of Human Evolution*, **53**, 620-634.

Hopley, P.J. & Maslin, M.A. (2010) Climate-averaging of terrestrial faunas: an example from the Plio-Pleistocene of South Africa. *Palaeobiology*, **36**, 32-50.

Horstmann, U.E. & Buhman, D. (1999) C and O isotopic composition of carbonates from the Pretoria Saltpan (Tswaing) reflecting environmental change. In: Partridge, T.C. (Ed.) 1999, *Investigations into the origin, age and palaeoenvironments of the Pretoria Saltpan*, Memoir 85, Council for Geosciences, Pretoria, 127-142.

Hughes, A.R. & Tobias, P.V. (1977) A fossil skull probably of the genus *Homo* from Sterkfontein, Transvaal. *Nature*, **265**, 310-312.

Imbrie, J., Hays, J.D., Martinson, D.G., McIntyre, A., Mix, A.C., Morley, J.J., Pisias, N.G., Prell, W.L. & Shackleton, N.J. (1984) The orbital theory of Pleistocene climate: support from a revised chronology of the marine D180 record. In: Berger, A.L., Imbrie, J., Hays, J., Kukla, G. & Salzman, B. (Eds.) *Milankovitch and Climate, Part 1*, Reidel Publishing Company, 269-305.

Keeley, J.E. & Rundel, P.W. (2003) Evolution of CAM and C_4 carbon-concentrating mechanisms. *International Journal of Plant Science*, **164**, S55-S57.

Kennett, J.P. (1995) A review of polar climatic evolution during the Neogene, based on the marine sediment record. In: Vrba, E.S., Denton, G.H., Partridge, T.C., Burckle, L.H. (Eds.) *Paleoclimate and Evolution, with Emphasis on Human Origins.* Yale University Press, New Haven, 49-64.

Kibii, J.M. (2000) *The macrofauna from Jacovec Cavern, Sterkfontein*. M.Sc. thesis, University of the Witwatersrand, Johannesburg.

Kibii, J.M. & Clarke, R.C. (2003) A reconstruction of the Stw 431 Australopithecus pelvis based on newly discovered fragments. *South African Journal of Science*, **99**, 225-226.

Kibii, J.M. (2004) *Comparative taxonomic, taphonomic and palaeoenvironmental analysis of 4-2.3 million year old australopithecine cave infills at Sterkfontein*. Unpublished Ph.D. dissertation, University of the Witwatersrand, Johannesburg.

Kibii, J.M., Clarke, R.C. & Tocheri, M.W. (2011) A hominin scaphoid from Sterkfontein, Member 4: Morphological description and first comparative phenetic 3D analyses. *Journal of Human Evolution*, **61** (4), 510-517.

Kim, S.T. & O'Neil, J. R. (1997) Equilibrium and non-equilibrium oxygen isotope effects in synthetic carbonates. *Geochimica et Cosmochimica Acta*, **61**, 3461-3475.

Kingston, J.D., Deino, A.L., Edgar, R.K. & Hill, A. (2007) Astronomically forced climate change in the Kenyan Rift Valley 2.7–2.55 Ma: implications for the evolution of early hominin ecosystems. *Journal of Human Evolution*, **53**,487-503.

Kluge, T., Marx, T., Scholz, D., Niggeman, S., Mangini, A. & Aeschbach-Hertig, W. (2008) A new tool for palaeoclimate reconstruction: Noble gas temperatures from fluid inclusions in speleothems. *Earth and Planetary Science Letters*, **269**(3-4), 408-415.

Kluge, T. & Affek, H.P. (2012) Quantifying kinetic fractionation in Bunker Cave speleothems using Δ_{47}. *Quaternary Science Reviews*, **49**, 82-94.

Kos, A.M. (2001) Stratigraphy, sedimentary development and palaeoenvironmental context of a naturally accumulated pitfall cave deposit from south- eastern Australia. *Journal of Earth Sciences*, **48**, 621-632.

Kramers, J.D. & Dirks, H.G.M. (2017) The age of fossil StW573 (’Little foot’): An alternative interpretation of 26Al/10Be burial data. *South African Journal Science*, **113** (3-4), 1-8.

Kuman, K. (1994a). The archaeology of Sterkfontein: preliminary findings on site formation and cultural change. *South African Journal of Science*, **90**, 215-219.

Kuman, K. (1994b). The archaeology of Sterkfontein–past and present. *Journal of Human Evolution*, **27**, 471-495.

Kuman, K. (1996) The Oldowan Industry from Sterkfontein: raw materials and core forms. In: Pwiti, G. & Soper, R. (Eds) *Aspects of African Archaeology: papers from the 10th Congress of the Pan African Association for Prehistory and Related Studies*. University of Zimbabwe Publications, Harare, 139-146.

Kuman, K. (1998) The earliest South African industries. In: Petraglia, M.D. & Korisettar, R. (Eds), *Early Human Behaviour in Global Context: The Rise and Diversity of the Lower Palaeolithic Record*. Routledge, London, 151-186.

Lachniet, M.S. (2009) Climatic and environmental controls on speleothem oxygen-isotope values. *Quaternary Science Reviews*, **28**, 412-432.

Lachniet, M.S., Burns, S.J., Piperno, D.R., Asmerom, Y., Polyak, V.J., Moy, C.M. & Christenson, K. (2004) A 1500 year El Nin˜o/Southern oscillation and rainfall history for the Isthmus of Panama from speleothem calcite. *Journal of Geophysical Research: Atmospheres*, **109** (D20).

Laporte, L.F. & Zihlman, A.L. (1983) Plates, climate and hominoid evolution. *South African Journal of Science*, **79**, 96-110.

Lear, C.H., Elderfield, H. & Wilson, P.A. (2000) Cenozoic deep-sea temperatures and global ice volumes from Mg/Ca in benthic foraminiferal calcite. *Science*, **287**, 269.

Li, W.X., Lundberg, J., Dickin, A.P., Ford, D.C., Schwarcz, H.P., McNutt, R. & Williams, D. (1989) High- precision mass-spectrometric uranium-series dating of cave deposits and implications for palaeoclimate studies. *Science*, **339,** 534-536.

Lourens, L.J., Antonarakou, A., Hilgen, F.J., Van Hoof, A.A.M., Vergnaud-Grazzini, C. & Zachariasse, W.J. (1996) Evaluation of the Plio-Pleistocene astronomical timescale. *Paleoceanography*, **11** (4), 391-413.

Magill, C.R., Ashley, G.M. &Freeman, K.H. (2013) Ecosystem variability and early human habitats in eastern Africa. *Proceedings of the National Academy of Sciences*, **110** (4), 1167-1174.

Mandice, M., Mihevc, A., Leis, A., Lojen, S., & Bronić, I. K. (2013). Mean residence time of drip water in Postojna Cave, Slovenia. *Waters in sensitive and protected areas*.

Martini, J.E.J., Wipplinger, P.E., Moen, H.F.G. & Keyser, A. (2003) Contribution to the speleology of Sterkfontein cave, Gauteng Province, South Africa. *International Journal of Speleology*, **32**, 43-69.

Mattey, D., Lowry, D., Duffet, J., Fisher, R., Hodge, E. & Frisia, S. (2008) A 53-year seasonally

resolved oxygen and carbon isotope record from a modern Gibraltar speleothem: reconstructed drip water and relationship to local precipitation. *Earth and Planetary Science Letters*, **269**, 80-95.

McDermott, F. (2004) Palaeo-climate reconstruction from stable isotope variations in speleothems: a review. *Quaternary Science Reviews*, **23**, 901-918.

McDermott, F., Schwarcz, H.P. & Rowe, P.J. (2006) Isotopes in speleothems. In: Leng, M.J. (Ed.) *Isotopes in palaeoenvironmental research*. Springer, Dordrecht, 185-226.

McKee, J.K. (1991) Palaeo-ecology of the Sterkfontein hominids: A review and synthesis. *Palaeontologia Africana*, **28**, 41-51.

McKee, J.K. (2001) Faunal turnover rates and mammalian biodiversity of the late Pliocene and Pleistocene of eastern Africa. *Palaeobiology*, **27**, 500-511.

Melis, R.T., Ghaleb, B., Boldrini, R. & Palombo, M.R. (2013) The Grotta dei Fiori (Sardinia, Italy) stratigraphical successions: A key for inferring palaeoenvironment evolution and updating the biochronology of the Pleistocene mammalian fauna from Sardinia. *Quaternary International*, **288**, 81-96.

Mickler, P.J., Banner, J.L., Stern, L., Asmerom, Y., Edwards, R.L., & Ito, E. (2004). Stable isotope variations in modern tropical speleothems: evaluating equilibrium vs. kinetic isotope effects. *Geochimica et Cosmochimica Acta*, **68**(21), 4381-4393.

Miller, K.G., Janecek, T.R., Katz, M.E. & Keil, D.J. (1987) Stable carbon and oxygen isotope record of benthic foraminifera from Paleocene-Eocene sediments. *Pangaea*. Supplement to: Miller, KG et al. (1987) Abyssal circulation and benthic foraminiferal changes near the Paleocene/Eocene boundary. *Paleoceanography*, **2**(6), 741-761.

Miorandi, R., Borsato, A., Frisia, S., Fairchild, I.J. & Richter, D.K. (2010) Epikarst hydrology and implications for stalagmite capture of climate changes at Grotta di Ernesto (NE Italy): results from long-term monitoring. *Hydrological Processes*, **24**, 3101-3114.

Mogg, A.O.D. (1975) *Important Plants of Sterkfontein*. The Natal Witness, University of the Witwatersrand, Johannesburg.

Mooney, H.A., Troughton, J.H. & Berry, J.A. (1977) Carbon isotope ratio measurements of succulent plants in southern Africa. *Oecologia,* **30**, 295-305.

Moriarty, K.C., McCulloch, T.M., Wells, R.T. & McDowell, M.C. (2000) Mid-Pleistocene cave fills, megafaunal remains and climate change at Naracoorte, South Australia: towards a predicative model using U-Th dating of speleothems, *Palaeogeography, Palaeoclimate, Palaeoecology,* **159**, 113-143.

Morgan, M.E., Kingston, J.D. & Marino, B.D. (1994) Carbon isotopic evidence for the emergence of C_4 plants in the Neogene from Pakistan and Kenya. *Nature*, **367**, 162-165.

Morley, R.J. & Richards, K. (1993) Gramineae cuticle: a key indicator of late Cenozoic climatic change in the Niger Delta. *Review of Palaeobotany and Palynology*, **77**, 119-127.

Noah, J.S. (2010) Reconstructing palaeoenvironments during the Middle Stone Age in the southern Cape, South Africa: stable isotope analysis of speleothems from the De Hoop Nature Reserve. MSc Thesis, University of the Witwatersrand.

Nordhoff, P. (2005) Stable isotope investigations on speleothems from different cave systems in Germany. PhD Thesis, University of Gottingen.

Obbes, A.M. (2000) *The structure, stratigraphy and sedimentology of the Black Reef Malmani-Rooihoogte succession of the Transvaal Supergroup southwest of Pretoria*. Council for Geoscience Bulletin 127, Pretoria.

Ogola, C. (2009) The Sterkfontein western breccias: stratigraphy, fauna and artefacts. PhD thesis, University of the Witwatersrand.

O'Leary, M.H. (1981) Carbon isotope fractionation in plants. *Phytochemistry,* **20**, 553-567.

O'Leary, M.H. (1993) Biochemical basis of carbon isotope fractionation. In: Ehleringer, J.R., Hall, A.E. & Farquhar, G.D. (Eds.) *Stable light isotope and plant carbon-water relations*. Academic Press, 19-28.

Ouelette, G.R. (2013) Late Holocene Paleoenvironmental Reconstruction in Barbados. MSc Thesis, Western Kentucky University.

Partridge, T.C. (1973) Geomorphological dating of cave opening at Makapansgat, Sterkfontein, Swartkrans and Taung. *Nature*, **246**, 75-79.

Partridge, T.C. (1978) Re-appraisal of lithostratigraphy of Sterkfontein hominin site. *Nature*, **275** (5678), 282-287.

Partridge, T.C. (1982) Some preliminary observations on the stratigraphy and sedimentology of the Kromdraai B hominid site. *Palaeoecology of Africa and the Surrounding Islands,* **15**, 3-12.

Partridge, T.C., De Menocal, P.B., Lorentz, S.A., Paiker, M.J. & Vogel, J.C. (1997) Orbital forcing of climate over South Africa: A 200 000-year rainfall record from the Pretoria saltpan. *Quaternary Science Reviews,* **16** (10), 1125-1133.

Partridge, T.C. (2000) Hominin-bearing cave and tufa deposits, In: Partridge, T.C. & Maud, R.R. (Eds.) (2000) *The Cenozoic of Southern Africa,* Oxford Monographs on Geology & Geophysics, no. 40, Oxford University Press, New York, 100-133.

Partridge, T.C. (2002) Were Heinrich Events forced from the southern hemisphere? *South African Journal of Science,* **98**, 43-36.

Partridge, T.C., Granger, D.E., Caffee, M.W. & Clarke, R.J. (2003) Lower Pliocene hominid remains from Sterkfontein. *Science*, **300** (5619), 607-612.

Partridge, T.C., Scott, L. & Schneider, R.R. (2004) Between Agulhas and Benguela: responses of southern African climates of the Late Pleistocene to current fluxes, orbital precession and the extent of the Circum-Antarctic vortex. In: Barrarbee, R.W., Gasse, F. & Stickling, C. (Eds.) *Past climate variability through Europe and Africa*. Kluwer Academic Publishers, The Netherlands.

Partridge, T.C. (2005) Dating of the Sterkfontein hominids: progress and possibilities. *Transactions of the Royal Society of South Africa*, **60** (2), 107-109.

Petit, J.R., Jouzel, J., Raynaud, D., Barkov, N.I., Barnola, J.M., Basile, I., Bender, M., Chappellaz, J., Davis, M., Delaygue, G. & Delmotte, M. (1999) Climate and atmospheric history of the past 420,000 years from the Vostok Ice Core, Antarctica. *Nature*, **399** (6735), 429-436.

Pickering, R. (2004) The stratigraphy, chronology and palaeoenvironment of the Pleistocene cave fill, Gladysvale Cave, South Africa. MSc thesis, University of the Witwatersrand.

Pickering, R., Kramers, J.D., Partridge, T.C. & Venneman, T.M. (2006) U–Pb dating of speleothems from Sterkfontein Cave, South Africa. *Goldschmidt Conference Abstracts*. 492.

Pickering, R. & Kramers, J.D. (2010) Re-appraisal of the stratigraphy and determination of new U–Pb dates for the Sterkfontein hominin site, South Africa. *Journal of Human Evolution*, **59**, 70-86.

Pickering, R., Kramers, J.D. & Partridge, T.C. (2010) U–Pb dating of calcite– aragonite layers in speleothems from hominin sites in South Africa by MC-ICP-MS. *Quaternary Geochronology*, **5**(5), 544-558.

Polag, D., Scholz, D., Muhlinghaus, C., Spotl, C., Schroder-Ritzrau, A., Segl, M. & Mangini, A. (2010) Stable isotope fractionation in speleothems: Laboratory experiments. *Chemical Geology*, **279**, 31-39.

Polyak, V.J. & Asmerom, Y. (2001) Late Holocene climate and cultural changes in the southwestern United States. *Science*, **294**, 148-151.

Potts, R. (1996) Evolution and climate variability. *Science*, **273**, 922-923.

Potts, R. (1998) Environmental hypotheses of hominin evolution. *Yearbook of Physical Anthropology*, **41**, 93-136.

Potts, R., (2007) Environmental hypotheses of Pliocene human evolution. In: Bobe, R., Alemseged, Z., Behrensmeyer, A.K. (Eds.) *Hominin Environments in the East African Pliocene: an Assessment of the Faunal Evidence*. Springer, New York, 25-50.

Procheş, S., Cowling, R.M., Goldblatt, P., Manning, J.C. & Snijman, D.A. (2006) An overview of Cape geophytes. *Biological Journal of the Linnaean Society,* **87**, 27-43.

Raven, P.H. & Johnson, G.B. (1989) *Biology*. Missouri: Times Mirror/Mosby College Publishing.

Raymo, M.E., Ruddiman, W.F., Shackleton, N.J. & Oppo, D.W. (1990) Evolution of Atlantic-Pacific N13C gradients over the last 2.5 m.y. *Earth and Planetary Science Letters*, **97**, 353-368.

Rayner, R.J., Moon, B.P. & Masters, J.C. (1993) The Makapansgat Australopithecine environment. *Journal of Human Evolution,* **24**, 219-231.

Reed, K. (1996) Early hominid evolution and ecological change through the African Plio-Pleistocene. *Journal of Human Evolution,* **32,** 289-322.

Reynolds, S.C., Vogel, J.C., Clarke, R.J. & Kuman, K.A. (2003) Preliminary results of excavations at Lincoln Cave, Sterkfontein, South Africa. *South African Journal of Science,* **99**, 286-288.

Reynolds, S.C. (2007) Mammalian body size changes and Plio–Pleistocene environmental shifts: implications for understanding hominin evolution in eastern and southern Africa. *Journal of Human Evolution*, **53**, 528-548.

Reynolds, S.C. & Kibii, J.M. (2011) Sterkfontein at 75: review of the palaeoenvironments, fauna and archaeology from the hominin site of Sterkfontein (Gauteng, South Africa). *Palaeontologica Africana*, **46**, 59-88.

Richards, D.A. & Dorale, J.A. (2003) Uranium-series Chronology and Environmental Applications of Speleothems, in Uranium-series Geochemistry. *Reviews in Mineralogy and Geochemistry,* **52**, 407-460.

Robinson, J.T. (1953) *Meganthropus, Australopithecus* and hominids. *American Journal of Physical Anthropology*, **11**, 1-38.

Robinson, J.T. (1954) The genera and species of the *Australopithecinae.* American *Journal of Physical Anthropology*, **12**, 181-200.

Robinson, J.T. (1962) Sterkfontein stratigraphy and the significance of the Extension Site. *South African Archaeological Bulletin*, **17**, 87-107.

Rozanski, K., Araguas-Araguas, L. & Gonfiantini, R. (1993) Isotopic patterns in modern global precipitation. In: Swart, P.P., Lohmann, K.C., McKenzir, J. & Savin, S. (Eds) Climate change in Continental Isotopic Records. *American Geophysical Union, Geophysical Monograph*, **78**, 1-36.

Ruddiman, W.F. & Janecek, T. (1989) Pliocene-Pleistocene biogenic and terrigenous fluxes at equatorial Atlantic Sites 662, 663, and 664. In: Ruddiman, W.F., Sarnthein, M. et al. (Eds.) *Proc. ODP Science. Results*, **108**, 211-240.

Scholl, M.A., Shanley, J.B., Zegarra, J.P. & Coplen, T.B. (2009) The stable isotope amount effect: New insights from NEXRAD echo tops, Luquillo Mountains, Puerto Rico. *Water Resources Research*, **45** (12), 1-14.

Schwarcz, H.P. (1989) Uranium series dating of Quaternary deposits. *Quaternary International*, **1**, 7-17.

Schwarcz, H.P. & Latham, A.G. (1989) Dirty calcite: uranium-series dating of contaminated calcite using leachates alone. *Chemical Geology (Isotope Geoscience Section)*, **80**, 35-43.

Schwarcz, H.P. (1992) Uranium series dating in Palaeoanthropology. *Evolutionary Anthropology*, **1**, 56-62.

Schwarcz, H.P. (2007) Speleothems. In: Elias, S. & Mock, C. *Encyclopedia of Quaternary Science*, Elsevier, 290-300.

Shackleton, N.J. & Kennett, J.P. (1975) Paleotemperature history of the Cenozoic and the initiation of Antarctic glaciation: oxygen and carbon isotope analyses in DSDP sites 277, 279, and 281. *Deep Sea Drilling Project 29*, **17**, 743-755.

Shackleton, N.J. & Opdyke, N.D. (1973) Oxygen isotope and palaeomagnetic stratigraphy of Equatorial Pacific core V28-238: oxygen isotope temperatures and ice volumes on a 105 and 106 year scale. *Quaternary Research*, **3**, 39-55.

Shackleton, N.J., Backman, J., Zimmerman, H., Kent, D.V., Hall, M., Roberts, D.G., Schnitker, D., Baldauf, J.G., Desprairies, A., Homrighausen, R., Huddlestun, P., Keene, J.B., Kaltenbach, A.J., Krumsieck, K.A.O., Moston, A.C., Murray, J.W., & Westberg-Smith, J. (1984) Oxygen isotope calibration of the onset of icerafting and history of glaciation in the North Atlantic region. *Nature*, **307**, 620-623.

Shackleton, N.J., Berger, A. & Peltier, W.J. (1990) An alternative astronomical calibration of the lower Pleistocene timescale based on OPD site 677. *Transactions of the Royal Society of Edinburgh*, **81**, 251-26.

Shackleton, N.J. (1995) New data on the evolution of Pliocene climatic variability. In: Vrba, E.S., Denton, G.H., Partridge, T.C. & Burckle, L.H. (Eds.) *Paleoclimate and Evolution: with Emphasis on Human Origins.* Yale University Press, New Haven, 242-248.

Sherwin C.M., & Baldini J.U.L. (2011) Cave air and hydrological controls on prior calcite precipitation and stalagmite growth rates: Implications for palaeoclimate reconstructions using speleothems. *Geochimica et Cosmochimica Acta*, **75**, 3915-3929.

Smith, A.C., Wynn, P.M., Barker, P.A. & Leng, M.J. (2015) Drip water electrical conductivity as an indicator of cave ventilation at the event scale. *The Science of the Total Environment*, **532**, 517-527.

Sponheimer, M. & Lee-Thorpe, J. (2003) Using carbon isotope data of fossil bovid communities for palaeoenvironmental reconstruction. *South African Journal of Science*, **99**, 273-275.

Spötl, C., Fairchild, I.J., & Tooth, A.F. (2005). Cave air control on dripwater geochemistry, Obir Caves (Austria): Implications for speleothem deposition in dynamically ventilated caves. *Geochimica et Cosmochimica Acta*, **69** (10), 2451-2468.

Stiles, D. & Partridge, T.C. (1979) Results of recent archaeological and palaeoenvironmental studies at the Sterkfontein Extension Site. *South African Journal of Science,* **75,** 346-352.

Stratford, D.J. (2011) *The underground central deposits of the Sterkfontein Caves, South Africa*. PhD thesis, University of the Witwatersrand.

Stratford, D., Granger, D.L., Bruxelles, L., Clarke, R.J., Kuman, K. & Gibbon, R.J. (2017) Comments on 'The age of fossil StW573 ('Little Foot'): An alternative interpretation of 26Al/10Be burial data'. *South African Journal Science*, **113** (5-6), 1-3.

Street, F.A. (1981) Tropical palaeoenvironments. *Progress in Physical Geography*, **5** (2), 157-185.

Sundqvist, H.S., Seibert, J. & Holmgren, K. (2007) Understanding conditions behind speleothem formation in Korallgrottan, northwestern Sweden. *Journal of Hydrology*, **347**, 13-22.

Talma, A.S. & Vogel, J.C. (1992) Late Quaternary Palaeotemperatures Derived from a Speleothem from Cango Caves, Cape Province, South Africa, *Quaternary Research*, **37**, 203-213.

Tan, M., Liu, T., Hou, J., Qin, X., Zhang, H. & Li, T. (2003) Cyclic rapid warming on centennial-scale revealed by a 2650-year stalagmite record of warm season temperature. *Geophysical Research Letters*, **30** (12), 19.1-19.4.

Tan, M., Baker, A., Genty, O., Smith, C. & Esper, J. (2006) Applications of stalagmite laminae to palaeoclimate reconstructions: comparison with dendrochronology/climatology. *Quaternary Science*, **25** (17- 18), 2103-2117.

Thermo Electron Corporation (2004) *Finnigan GasBench II: Operating Manual*. Thermo

Electron Corporation, Germany, Bremen.

Thermo-Fischer Scientific (2014) *Measuring pH in Surface Water*. In: USGS National Field Manual: pH Method, Chapter 6.4; Version 1.3, January 2006.

Tiedemann, R., Sarnthein, M., and Shackleton, N.J. (1994) Astronomic timescale for the Pliocene Atlantic $\delta^{18}O$ and dust flux records of Ocean Drilling Program site 659. *Paleoceanography,* **9**, 619-638.

Tipple, B.J. (2013) Capturing climate variability during our ancestors' earliest days. *Proceedings of the National Academy of Sciences,* **110** (4), 1144-1145.

Tobias, P.V., & Hughes, A. R. (1969) The new Witwatersrand University Excavation at Sterkfontein. *South African Archaeological Bulletin,* **24**, 158-169.

Tobias, P.V. (1973) New developments in hominid palaeontology in South and East Africa. *Annual Review of Anthropology*, **2,** 311-334.

Tobias, P.V. & Hughes, A.R. (1977) A fossil skull probably of the genus *Homo* from Sterkfontein, Transvaal. *Nature,* **265**, 310-312.

Tobias, P.V. (2000) The fossil hominids. In: Partridge, T.C. and Maud, R.R. (Eds) *The Cenozoic of South Africa.* Oxford University Press, Oxford, 252-276.

Traverse, A. (1982) Response of world vegetation to Neogene tectonic and climatic events. *Alcheringa: An Australasian Journal of Palaeontology*, **6** (3), 197-209.

Trauth, M.H., Larrasoana, J.C. & Mudelsee, M. (2009) Trends, rhythms and events in Plio-Pleistocene African climate. *Quarternary Science Reviews*, **28**, 399-411.

Tremaine D.M., Froelich P.N. & Wang Y. (2011) Speleothem calcite farmed in situ: Modern calibration of $\delta^{18}O$ and $\delta^{13}C$ palaeoclimate proxies in a continuously-monitored natural cave system. *Geochimica et Cosmochimica Acta,* **75**, 4939-4950.

Tyson, P.D. (1986) *Climate change and variability in Southern Africa*. Oxford University Press, Oxford.

Tyson, P.D. & Preston-Whyte, R.A. (2000) *The weather and climate of southern Africa*. Oxford University Press, Cape Town, southern Africa.

Vaks, A., Bar-Matthews, M., Ayalon, A. & Schilman, B. (2003) Paleoclimate reconstruction based on the timing of speleothem growth and oxygen and carbon isotope composition in a cave located in the rain shadow in Israel. *Quaternary Science*, **59** (2), 182-193.

Van Beynen, P. & Febbroriello, P. (2006) Seasonal isotopic variability of precipitation and cave drip water at Indian Oven Cave, New York. *Hydrological Processes*, **20** (8), 1793-1803.

Van der Merwe, N.J. (1982) Carbon isotopes, photosynthesis and archaeology. *American Scientist,* **70**, 596-606.

Van Valen, L. (1973) A new evolutionary law. *Evolutionary Theory*, **1**, 1-30.

Van Zinderen Bakker, E.M. & Mercer, J.H. (1986) Major late Cainozoic climatic events and palaeoenvironmental changes in Africa viewed in a worldwide context. *Palaeogeography, Palaeoclimatology, Palaeoecology*, **56** (3-4), 217-235.

Vogel, J.C. (1993) Variability of carbon isotope fractionation during photosynthesis, In: Ehleringer, J.R., Hall, A.E. & Farquhar G.D. (Eds.) *Stable light isotopes and plant carbon-water relations*, Academic Press, San Diego, 29-38.

Vrba, E.S. (1974) Chronological and ecological implications of the fossil Bovidae at the Sterkfontein *Australopithecine* site. *Nature*, **250**, 19-23.

Vrba, E.S. (1975) Some evidence of chronology and palaeoecology of Sterkfontein, Swartkrans and Kromdraai from the fossil Bovidae. *Nature*, **254**, 301-304.

Vrba, E.S. (1980) Evolution, species and fossils: how does life evolve? *South African Journal of Science*, **76**, 61-84.

Vrba, E.S. (1982) *South African hominid-associated assemblages: biostratigraphy, chronology and evolutionary pulses*. Address to 1982 Congres International de Paleontologie Humaine, Union Internationale des Sciences Prehistoriques et Protohistoriques: Nice, France.

Vrba, E.S. (1985) Ecological and adaptive changes associated with early hominid evolution. In: Delson, E. (Ed.) *Ancestors, the Hard Evidence*. Alan R. Liss, New York, 63-71.

Vrba, E.S. (1988) Late Pliocene climatic events and hominid evolution. In: Grine, F.E. (Ed.) *The Evolutionary History of the ‘‘Robust’’ Australopithecines.* Aldine Publishing Company, New York, 405-426.

Vrba, E.S. (1995) The fossil record of the African antelopes (Mammalia, Bovidae) in relation to human evolution and paleoclimate. In: Vrba, E.S., Denton, G.H., Partridge, T.C. & Burckle, L.H. (Eds.) *Paleoclimate and Evolution with emphasis on human origins*. Yale University Press, Boston, 385-424.

Walker, J., Cliff, R.A. & Latham, A.G. (2004) *Research into U-Pb dating of ‘Little Foot’*. Geoscience Africa 2004 (Abstract Volume). University of the Witwatersrand, Johannesburg, 684.

Walker, J., Cliff, R.A. & Latham, A.G. (2006) U-Pb isotopic age of the StW573 hominid from Sterkfontein, South Africa. *Science*, **314**, 1592-1594.

Wang, X., Wu, Y. & Shen, L. (2015) Influences of air CO_2 on hydrochemistry of drip water and implications for paleoclimate study in a stream-developed cave, SW China. *Acta Geochimica*, **35** (2), 172-183.

Wara, M.W., Ravelo, A.C. & Delaney, M.L. (2005) Permanent El Niño-like conditions during the Pliocene Warm Period. *Science*, **309**, 758-761.

White, W.B. (2004) Palaeoclimate records from speleothems in limestone caves. In: Sasowsky, I.D. & Mylroie, J. (Eds) *Studies of cave sediments: physical and chemical records of palaeoclimate*. Kluwer Academic, New York, 135-175.

Wigley, T.M.L & Brown, M.C. (1976) *The Science of Speleology*. Cullingford, C.H.D & Ford, T.D. (Eds). Academic Press, London.

Wilkinson, M.J. (1973) *Sterkfontein cave system: evolution of a karst form*. M.A. thesis, University of the Witwatersrand, Johannesburg.

Wilkinson, M.J. (1983) Geomorphic perspectives on the Sterkfontein *Australopithecine* breccias. *Journal of Archaeological Science,* **10**, 515-529.

Wilkinson, M.J. (1985) Lower-lying and possibly older fossilferous deposits at Sterkfontein. In: P. V. Tobias (Ed.) *Hominid Evolution: Past, Present and Future*. Alan R. Liss, New York, 165-170.

Wolfe, J.A. (1985) Distribution of Major Vegetational Types During the Tertiary. In: Sundquist, E.T. & Broecker, W.S. (Eds) *The Carbon Cycle and Atmospheric CO: Natural Variations Archean to Present*. American Geophysical Union, Washington, D. C.

Wong, C.I., Banner, J.L. & Musgrove, M. (2011) Seasonal dripwater Mg/Ca and Sr/Ca variations driven by cave ventilation: Implications for modelling of speleothem palaeoclimate records. *Geochimica et Acta*, **75**, 3514-3529.

Woodruff, F., Savin, S.M. & Douglas, R.G. (1981) Miocene stable isotope record: A detailed deep Pacific Ocean study and its palaeoclimatic implications. *Science,* **212**, 665-668.

Wynn, J.G. (2004) Influence of Plio-Pleistocene aridification on human evolution: Evidence from paleosols of the Turkana Basin, Kenya. *American Journal of Physical Anthropology*, **123** (2), 106-118.

Wynn, J.G., Bird, M.I. & Wong, V.N.L. (2005) Rayleigh distillation and the depth profile of 13C/12C ratios of soil organic carbon from soils of disparate texture in Iron Range National Park, far north Queensland, Australia. *Geochimica et Cosmochimica Acta*, **69**, 1961-1973.

Wynn, P.M., Fairchild, I.J., Baker, A., Frisia, S., Borsato, A., Baldini, J. & McDermott, F. (2008). Isotopic archives of sulphur in speleothems. *Geochimica et Cosmochimica Acta*, **72**, 2465-2477.

Zachos, J., Pagani, M., Sloan, L., Thomas, E. & Billups, K. (2001) Trends, rhythms, and aberrations in global climate 65 Ma to present. *Science*, **292**, 686-693.

Zech, M., Zech, R., Morrás, H., Moretti, L., Glaser, B. & Zech, W. (2009) Late Quaternary environmental changes in Misiones, subtropical NE Argentina, deduced from multi-proxy geochemical analyses in a palaeosol-sediment sequence. *Quaternary International*, **196**, 121-136.

Appendix A

Speleothem Sample Total Station Co-ordinates

Sample Name	X-co-ordinate (m)	Y-co-ordinate (m)	Z-co-ordinate (m)
JCS-1	2 878 782,552	-73 573,270	1 446,280
JCS-2	2 878 783,683	-73 574,253	1 444,358
JCS-3	2 878 783,671	-73 574,193	1 444,255
JCS-4	2 878 780,330	-73 562,818	1 445,990
MHLS-1	2 878 781,868	-73 458,769	1 440,092
MHLS-2	2 878 781,377	-73 459,024	1 440,827
SGS-1	2 878 796,000	-73 528,000	1462,304
SGS-2	2 878 796,000	-73 527,000	1461,171
SGS-3	2 878 796,000	-73 528,100	1462,059
SGS-4	2 878 796,000	-73 528,000	1462,502
A1S-1	2 878 766,731	-73 500,164	1 448,098
A1S-2	2 878 766,877	-73 499,399	1 448,199
A1S-3	2 878 766,857	-73 492,455	1 447,332
A2S-1	2 878 809,000	-73 397,700	1448,727
A2S-2	2 878 810,000	-73 413,900	1443,623
A2S-3	2 878 808,000	-73 412,100	1443,199

Drip Water Sample Total Station Co-ordinates

Sample Name	X-co-ordinate (m)	Y-co-ordinate (m)	Z-co-ordinate (m)
JDW-1	2 878 778,192	-73 563,782	1 444,876
JDW-2	2 878 780,449	-73 571,813	1 444,243
JDW-3	2 878 784,125	-73 574,219	1 443,868
JDW-4	2 878 784,435	-73 573,767	1 443,815
JDW-5	2 878 780,476	-73 567,137	1 444,489
A1DW-1	2 878 766,225	-73 500,020	1 446,660
A1DW-2	2 878 766,061	-73 496,226	1 447,136
A1DW-3	2 878 766,890	-73 490,854	1 444,724
A1DW-4	2 878 766,925	-73 489,855	1 444,355
A1DW-5	2 878 766,166	-73 496,017	1 447,088
A2DW-1	2 878 808,000	-73 405.300	1443,623
A2DW-2	2 878 807,000	-73 405.900	1445,312
A2DW-3	2 878 808,000	-73 412.100	1441,749

Appendix B

Statistics

1. Pearson's product-moment correlation test

Statistic values are represented in the bottom left hand corner of the tables, p values are represented on the top right hand corner of the tables.

Measured Cave Air Temperatures (see Chapter 4, fig. 4.4)

	Cave Air Temperature Jacovec	Cave Air Temperature Antechamber 1	Cave Air Temperature Antechamber 2
Cave Air Temperature Jacovec		0,00010628	0,014161
Cave Air Temperature Antechamber 1	0,87097		0,0061047
Cave Air Temperature Antechamber 2	0,65967	0,71413	

Measured Cave Air Temperatures versus Average Measured Air Temperatures (see Chapter 4, fig. 4.5)

	Cave Air Temperature Jacovec	Cave Air Temperature Antechamber 1	Cave Air Temperature Antechamber 2	Measured Air temperatures Averages
Cave Air Temperature Jacovec		0,00010628	0,014161	0,53995
Cave Air Temperature Antechamber 1	0,87097		0,0061047	0,20496
Cave Air Temperature Antechamber 2	0,65967	0,71413		0,16085
Measured Air temperatures Averages	0,18735	0,37638	0,4129	

Measured Average Cave Humidity (see Chapter 4, fig. 4.6)

	Jacovec Average Humidity	Antechamber 1 Average Humidity	Antechamber 2 Average Humidity
Jacovec Average Humidity		0,0060685	0,00059508
Antechamber 1 Average Humidity	0,71448		0,026801
Antechamber 2 Average Humidity	0,82018	0,61013	

Measured Average Cave Atmospheric Pressure (see Chapter 4, fig. 4.7)

	Jacovec Cavern	Antechamber 1	Antechamber 2
Jacovec Cavern		5,9064E-28	2,4858E-22
Antechamber 1	0,99686		8,5692E-24
Antechamber 2	0,99075	0,99302	

Vegetation Distribution (see Chapter 4, fig. 4.11)

	$\delta^{13}C$	Percentage C_4 (%)	Percentage C_3 (%)
$\delta^{13}C$		4,3124E-54	1,0645E-15
Percentage C4 (%)	1		1,0679E-15
Percentage C3 (%)	-0,99545	-0,99545	

$\delta^{18}O$ Monthly Average Values (see Chapter 4, fig. 4.19)

	Antechamber 1 Monthly Averages	Antechamber 2 Monthly Average	Jacovec Cavern Monthly Average
Antechamber 1 Monthly Averages		0,11739	0,023117
Antechamber 2 Monthly Average	0,43784		0,058637
Jacovec Cavern Monthly Average	0,60066	0,51648	

Jacovec Cavern Equation 1 Temperatures versus Monthly Average Temperatures (see Chapter 4, fig.4.20)

	Calculated Temperature (Equation 1)	Average Measured Atmospheric Temperature
Calculated Temperature (Equation 1)		0,9023
Average Measured Atmospheric Temperature	0,039785	

Antechamber 1 Equation 1 Temperatures versus Monthly Average Temperatures (see Chapter 4, fig. 4.21)

	Calculated Temperature (Equation 1)	Average Measured Atmospheric Temperature
Calculated Temperature (Equation 1)		0,012144
Average Measured Atmospheric Temperature	0,64835	

Antechamber 2 Equation 1 Temperatures versus Monthly Average Temperatures (see Chapter 4, fig. 4.22)

	Calculated Temperature (Equation 1)	Average Measured Atmospheric Temperature
Calculated Temperature (Equation 1)		0,010942
Average Measured Atmospheric Temperature	0,67755	

Cave Air Temperatures versus Equation 1 Calculated Temperatures (see Chapter 4, fig. 4.23)

	Cave Air Temp Jacovec	Cave Air Temp Antechamber 1	Cave Air Temp Antechamber 2	Jacovec Temp	Antechamber 1 Temp	Antechamber 2 Temp
Cave Air Temperature Jacovec		0,00010628	0,014161	0,91584	0,60213	0,28262
Cave Air Temperature Antechamber 1	0,87097		0,0061047	0,71831	0,1278	0,24591
Cave Air Temperature Antechamber 2	0,65967	0,71413		0,28481	0,1675	0,25477
Jacovec Temperature	0,032586	-0,11091	0,32105		0,94712	0,86814
Antechamber 1 Temperature	0,15976	0,44476	0,40701	0,019548		0,25429
Antechamber 2 Temperature	0,32244	0,34664	0,34062	-0,048903	0,32668	

Jacovec Cavern Equation 2 Temperatures versus Average Monthly Temperatures (see Chapter 4, fig. 4.24)

	Average Measured Atmospheric Temperature	Jacovec Cavern Calculated Temperature
Average Measured Atmospheric Temperature		0,28528
Jacovec Cavern Calculated Temperature	-0,32076	

Antechamber 1 Equation 2 Temperatures versus Average Monthly Temperatures (see Chapter 4, fig. 4.25)

	Average Measured Atmospheric Temperature	Antechamber 1 Calculated Temperature
Average Measured Atmospheric Temperature		0,95253
Antechamber 1 Calculated Temperature	-0,017545	

Antechamber 2 Equation 2 Temperatures versus Average Monthly Temperatures (see Chapter 4, fig. 4.26)

	Average Measured Atmospheric Temperature	Antechamber 2 Calculated Temperature
Average Measured Atmospheric Temperature		0,71678
Antechamber 2 Calculated Temperature	-0,10662	

Cave Air Temperatures versus Equation 2 Calculated Temperatures (see Chapter 4, fig. 4.27)

	Cave Air Temp Jacovec	Cave Air Temp Antechamber 1	Cave Air Temp Antechamber 2	Jacovec Temp	Antechamber 1 Temp	Antechamber 2 Temp
Cave Air Temperature Jacovec		0,00010628	0,014161	0,93961	0,11237	0,069888
Cave Air Temperature Antechamber 1	0,87097		0,0061047	0,60145	0,25353	0,12344
Cave Air Temperature Antechamber 2	0,65967	0,71413		0,53788	0,34828	0,15055

Jacovec Temperature	-0,023365	-0,16005	-0,18829		0,7839	0,40391
Antechamber 1 Temperature	-0,46154	-0,34145	-0,28329	0,084432		0,0028703
Antechamber 2 Temperatures	-0,51783	-0,44937	-0,42232	0,2532	0,73281	

Idealised Temperatures Equation 1 versus Equation 1 Calculated Temperatures (see chapter 4, fig. 4.28)

	Equation 1 Idealised Temperature	Jacovec Temperature	Antechamber 1 Temperature	Antechamber 2 Temperature
Equation 1 Idealised Temperature		0,7325	0,39659	0,002673
Jacovec Temperature	0,10049		0,94712	0,86814
Antechamber 1 Temperature	-0,23625	0,019548		0,25429
Antechamber 2 Temperature	-0,73633	-0,048903	0,32668	

Idealised Temperatures Equation 2 versus Equation 2 Calculated Temperatures (see Chapter 4, fig.4.29)

	Idealised Temperature Equation 2	Jacovec Temperature	Antechamber 1 Temperature	Antechamber 2 Temperatures
Idealised Temperature Equation 2		0,36595	0,45697	0,22379
Jacovec Temperature	-0,27348		0,7839	0,40391
Antechamber 1 Temperature	0,21662	0,084432		0,0028703
Antechamber 2 Temperatures	0,34726	0,2532	0,73281	

Drip Rates (see Chapter 4, fig. 4.30)

	Jacovec Drip Rate	Antechamber 1 Drip Rate	Antechamber 2 Drip Rate
Jacovec Drip Rate		0,00021403	0,018021
Antechamber 1 Drip Rate	0,85246		0,089102
Antechamber 2 Drip Rate	0,64189	0,49009	

Drip Rates versus Average Monthly Rainfall (see Chapter 4, fig. 4.31)

	Jacovec Drip Rate	Antechamber 1 Drip Rate	Antechamber 2 Drip Rate	Average Measured Rainfall
Jacovec Drip Rate		0,00021403	0,018021	0,11977
Antechamber 1 Drip Rate	0,85246		0,089102	0,24969
Antechamber 2 Drip Rate	0,64189	0,49009		0,64338
Average Measured Rainfall	-0,45332	-0,34406	-0,14207	

Drip Rates versus $\delta^{18}O$ Monthly Averages (see Chapter 4, fig. 4.32)

	Jacovec Drip Rate	Antechamber 1 Drip Rate	Antechamber 2 Drip Rate	Antechamber 1 Monthly Averages	Antechamber 2 Monthly Average	Jacovec Cavern Monthly Average
Jacovec Drip Rate		0,00021403	0,018021	0,099086	0,096056	0,04324
Antechamber 1 Drip Rate	0,85246		0,089102	0,38833	0,19245	0,050371
Antechamber 2 Drip Rate	0,64189	0,49009		0,27199	0,50752	0,12636
Antechamber 1 Monthly Averages	0,47728	0,26139	0,32925		0,052284	0,0020552
Antechamber 2 Monthly Average	0,48107	0,38618	0,20227	0,52802		0,032281
Jacovec Cavern Monthly Average	0,56715	0,5522	0,44627	0,74888	0,57279	

$\delta^{18}O$ Monthly Averages versus Average Monthly Rainfall (see Chapter 4. Fig. 4.33)

	Antechamber 1 Monthly Averages	Antechamber 2 Monthly Average	Jacovec Cavern Monthly Average	Average Measured Rainfall
Antechamber 1 Monthly Averages		0,052284	0,0020552	0,48067
Antechamber 2 Monthly Average	0,52802		0,032281	0,16646
Jacovec Cavern Monthly Average	0,74888	0,57279		0,76204
Average Measured Rainfall	-0,20562	-0,39134	-0,089072	

Measured Drip Water Electro-Conductivity versus Drip Rate (see Chapter 5, section 4.1)

	Jacovec Drip Rate	Antechamber 1 Drip Rate	Antechamber 2 Drip Rate	Jacovec	Antechamber 1	Antechamber 2
Jacovec Drip Rate		0,00021403	0,018021	0,44718	0,26301	0,66431
Antechamber 1 Drip Rate	0,85246		0,089102	0,4884	0,3255	0,61899
Antechamber 2 Drip Rate	0,64189	0,49009		0,81554	0,63133	0,57189
Jacovec	-0,23124	-0,21127	-0,071858		0,19371	0,70193
Antechamber 1	-0,33512	-0,29636	-0,14719	0,36935		0,72884
Antechamber 2	0,13325	0,15247	-0,17302	-0,11244	-0,10191	

Measured Drip Water Electro-Conductivity versus Average Measured Air Temperatures (see Chapter 5, section 4.1)

	Jacovec	Antechamber 1	Antechamber 2	Ave Measured Temps
Jacovec		0,19371	0,70193	0,3267
Antechamber 1	0,36935		0,72884	0,73138
Antechamber 2	-0,11244	-0,10191		0,92862
Ave Measured Temps	-0,28311	-0,10092	0,0264	

Measured Drip Water Electro-Conductivity versus Measured Average Cave Atmospheric Pressure (see Chapter 5, section 4.1)

	Jacovec Atmos Pressure	Antechamber 1 Atmos Pressure	Antechamber 2 Atmos Pressure	Jacovec EC	Antechamber 1 EC	Antechamber 2 EC
Jacovec Atmos Pressure		3,5557E-13	1,2074E-10	0,092332	0,069836	0,69323
Antechamber 1 Atmos Pressure	0,99645		1,0989E-11	0,11747	0,086466	0,76158
Antechamber 2 Atmos Pressure	0,98973	0,99337		0,13316	0,096402	0,66606
Jacovec EC	0,48584	0,45583	0,43926		0,19371	0,70193
Antechamber 1 EC	0,51792	0,49363	0,48064	0,36935		0,72884
Antechamber 2 EC	-0,12122	-0,093373	-0,13252	-0,11244	-0,10191	

Measured Cave Atmospheric Pressure versus Measured Drip Water pH (see Chapter 5, section 4.2)

	Jacovec pH	Antechamber 1 pH	Antechamber 2 pH	Jacovec	Antechamber 1	Antechamber 2
Jacovec pH		0,0074262	0,041723	0,75504	0,69598	0,68189
Antechamber 1 pH	0,68024		0,0044033	0,63812	0,63287	0,58636
Antechamber 2 pH	0,54968	0,71048		0,31837	0,37687	0,34447
Jacovec	-0,096008	0,1443	0,30056		3,5557E-13	1,2074E-10
Antechamber 1	-0,12008	0,14653	0,26753	0,99645		1,0989E-11
Antechamber 2	-0,12591	0,16664	0,28545	0,98973	0,99337	

Appendix C

Oxygen and Carbon Stable light Isotope Results

Speleothem Samples

Laboratory Number	Sample Identification		$d^{13}C$ (‰)	$d^{18}O$ (‰)	$d^{13}C$ Average (‰)	$d^{18}O$ Average (‰)
ESI 001	1a	MHLS-1	+1,02	-3,96	1,05	-3,90
ESI 001	1b	MHLS-1	+1,07	-3,85		
ESI 002	2a	MHLS-2	+0,05	-5,05	0,03	-5,06
ESI 002	2b	MHLS-2	+0,01	-5,07		
ESI 003	3a	JCS-4	-0,75	-2,21	-0,76	-2,21
ESI 003	3b	JCS-4	-0,77	-2,22		
ESI 004	4a	JCS-2	-1,81	-2,67	-1,76	-2,63
ESI 004	4b	JCS-2	-1,71	-2,58		
ESI 005	5a	JCS-1	-0,70	-3,07	-0,75	-3,12
ESI 005	5b	JCS-1	-0,80	-3,17		
ESI 006	6a	JCS-3	-2,01	-2,41	-2,00	-2,43
ESI 006	6b	JCS-3	-1,99	-2,45		
ESI 007	7a	SGS-3	-4,58	-3,82	-4,61	-3,83
ESI 007	7b	SGS-3	-4,65	-3,84		
ESI 008	8a	SGS-4	-7,92	-2,78	-7,92	-2,73
ESI 008	8b	SGS-4	-7,92	-2,68		
ESI 009	9a	SGS-2	-7,43	-2,23	-7,50	-2,27
ESI 009	9b	SGS-2	-7,56	-2,31		
ESI 010	10a	SGS-1	-8,99	-3,98	-8,95	-3,93
ESI 010	10b	SGS-1	-8,91	-3,87		
ESI 011	11a	A2S-1	+0,67	-4,14	0,70	-4,08
ESI 011	11b	A2S-1	+0,73	-4,02		
ESI 012	12a	A2S-2	+0,83	-3,83	0,82	-3,85
ESI 012	12b	A2S-2	+0,82	-3,87		
ESI 013	13a	A2S-3	+0,82	-4,58	0,87	-4,53
ESI 013	13b	A2S-3	+0,91	-4,48		
ESI 014	14a	AIS-3	+0,81	-4,60	0,89	-4,59
ESI 014	14b	AIS-3	+0,96	-4,59		
ESI 015	15a	AIS-2	+1,15	-4,22	1,52	-4,16
ESI 015	15b	AIS-2	+1,90	-4,10		
ESI 016	16a	AIS-1	+2,62	-4,62	2,63	-4,60
ESI 016	16b	AIS-1	+2,64	-4,57		

Drip Water Samples

Sample Name	δ2H (‰)	± 2H StDev	δ 18O (‰)	± 18O StDev
A1DW-1	-17,7	0,29	-3,68	0,11
A1DW-3	-8,5	0,29	-3,76	0,09
JDW-3	-11,9	0,32	-3,25	0,04
JDW-2	-16,8	0,67	-3,33	0,10
A2DW-2	12,5	0,82	4,04	0,19
JDW-4	-18,8	0,87	-4,01	0,10
A2DW-1	-4,2	0,43	-0,68	0,06
JDW-5	-13,6	0,49	-3,31	0,06
A1DW-5	-15,5	0,25	-3,00	0,04
A1DW-2	-14,4	0,31	-3,29	0,04
JDW-1	-11,4	1,16	-3,13	0,10
JDW-1 17-09-15	-12,8	0,28	-2,89	0,04
A1DW-2 17-09-15	-3,2	0,28	1,61	0,26
JDW-4 17-09-15	-14,4	0,36	-1,88	0,07
JDW-2 17-09-15	-16,0	0,33	-3,26	0,03
JDW-3 17-09-15	-13,9	0,24	-3,06	0,14
A1DW-3 17-09-15	-0,5	0,46	-1,71	0,07
A1DW-4 17-09-15	1,1	0,10	-1,12	0,03
A1DW-5 17-09-15	-17,5	0,72	-3,46	0,16
A2DW-1 17-09-15	4,6	0,42	-1,12	0,06
A1DW-1 17-09-15	-17,4	1,91	-3,33	0,13
JDW-5 17-09-15	-10,6	0,26	-1,60	0,06
A2DW-2 17-09-15	10,7	1,11	-0,38	0,19
A2DW-1 14-07-16	-4,2	0,58	-1,95	0,05
A1DW-5 14-07-16	-20,9	0,45	-3,00	0,01
A1DW-3 14-07-16	0,0	0,67	-1,02	0,07
JDW-2 14-07-16	-19,7	0,26	-3,85	0,09
JDW-3 14-07-16	-14,2	0,39	-2,62	0,04
A1DW-2 14-07-16	-18,1	0,45	-2,82	0,08
JDW-5 14-07-16	-13,4	0,32	-2,41	0,06
JDW-4 14-07-16	-24,0	2,75	-3,84	0,21
A1DW-4 14-07-16	-0,1	0,59	-0,62	0,14
JDW-1 14-07-16	-4,2	0,18	-1,20	0,05
A2DW-2 14-07-16	-12,6	0,18	-2,66	0,08
A1DW-1 14-07-16	-10,3	0,37	-2,10	0,12
A1DW-4 19-05-16	11,8	0,61	3,22	0,14
A1DW-1 19-05-16	-12,2	0,88	-2,75	0,18
A2DW-2 19-05-16	-1,9	0,44	0,17	0,13
JDW-2 19-05-16	-16,9	0,38	-2,73	0,11
JDW-4 19-05-16	-11,6	0,17	-2,35	0,06
JDW-1 19-05-16	-22,0	4,00	-3,55	0,38
A1DW-2 19-05-16	-19,9	0,28	-3,97	0,07

A1DW-5 19-05-16	-4,8	0,58	-2,11	0,17
JDW-3 19-05-16	2,3	0,33	-0,94	0,11
A1DW-3 19-05-16	-11,4	0,49	-2,79	0,08
A1DW-4 19-05-16	-9,5	0,23	-2,63	0,07
A2DW-1 19-05-16	-19,5	0,46	-3,52	0,06
A1DW-2 20-08-15	-6,8	0,19	-2,16	0,14
JDW-3 20-08-15	-16,0	0,33	-2,65	0,12
JDW-2 20-08-15	-13,0	0,23	-2,29	0,10
JDW-5 20-08-15	-2,8	0,28	-2,05	0,06
A1DW-3 20-08-15	-21,4	0,09	-4,27	0,03
JDW-4 20-08-15	-16,6	0,73	-3,75	0,06
A2DW-1 20-08-15	-8,7	0,17	0,72	0,12
A1DW-5 20-08-15	1,8	0,26	-1,53	0,07
A1DW-1 20-08-15	-12,5	0,38	-2,03	0,03
JDW-1 20-08-15	-1,0	0,26	-1,71	0,04
A1DW-4 20-08-15	11,4	0,47	-0,34	0,04
A2DW-2 20-08-15	-3,8	0,40	-2,19	0,06
A2DW-1 25-08-16	-4,2	0,80	-2,22	0,09
A1DW-3 25-08-16	20,9	1,86	1,06	0,21
A2DW-3 25-08-16	-18,0	0,41	-3,80	0,06
JDW-5 25-08-16	-14,2	0,35	-3,24	0,07
A2DW-2 25-08-16	-3,0	0,28	-0,72	0,04
A1DW-5 25-08-16	-12,8	0,43	-2,91	0,04
A1DW-1 25-08-16	-23,2	0,95	-4,29	0,10
JDW-4 25-08-16	-21,9	0,21	-4,23	0,07
JDW-2 25-08-16	-0,3	0,15	-0,66	0,12
JDW-3 25-08-16	-3,2	0,22	-0,60	0,08
A1DW-2 25-08-16	7,7	0,35	0,57	0,21
JDW-1 25-08-16	-18,0	2,07	-2,45	0,31
JDW-2 17-03-16	-10,9	0,11	-2,77	0,09
A2DW-1 17-03-16	-17,7	0,33	-2,64	0,08
JDW-4 17-03-16	-8,6	0,17	-2,41	0,01
A1DW-3 17-03-16	-18,2	0,20	-3,42	0,12
A1DW-5 17-03-16	-17,0	0,21	-3,06	0,12
A1DW-2 17-03-16	-10,4	0,18	-2,62	0,14
A2DW-2 17-03-16	-19,9	0,53	-3,25	0,18
A1DW-1 17-03-16	-13,0	0,33	-2,21	0,18
JDW-5 17-03-16	-11,2	0,12	-2,33	0,04
JDW-3 17-03-16	-9,7	3,15	-1,82	0,23
JDW-1 17-03-16	-2,9	0,36	-1,37	0,07
A1DW-3 07-01-16	-13,1	0,36	-2,74	0,06
JDW-1 07-01-16	-16,9	0,34	-2,46	0,06
JDW-4 07-01-16	-21,1	0,21	-3,67	0,08
JDW-2 07-01-16	4,6	0,65	2,04	0,14

A2DW-2 07-01-16	-19,3	0,76	-3,68	0,14
A1DW-1 07-01-16	-10,6	0,25	-2,55	0,02
JDW-5 07-01-16	-5,2	0,44	-2,22	0,06
A2DW-1 07-01-16	-11,7	0,26	-2,65	0,03
JDW-3 07-01-16	-19,4	3,43	-3,52	0,34
A1DW-5 07-01-16	-16,7	0,22	-3,26	0,07
A1DW-2 07-01-16	-4,4	0,15	-1,97	0,06
A1DW-4 07-01-16	-21,4	0,58	-4,06	0,18
JDW-2 04-08-16	-19,0	0,33	-2,16	0,09
A1DW-2 04-08-16	-13,2	0,10	-2,70	0,07
A2DW-2 04-08-16	-17,8	0,26	-3,21	0,07
JDW-5 04-08-16	-17,5	0,34	-3,46	0,06
JDW-3 04-08-16	-23,4	0,12	-4,00	0,05
JDW-4 04-08-16	-19,6	0,47	-2,38	0,08
A1DW-5 04-08-16	7,3	0,43	0,78	0,05
JDW-1 04-08-16	-14,0	0,63	-2,01	0,03
A1DW-1 04-08-16	-3,5	0,39	-1,46	0,05
A2DW-1 04-08-16	-27,9	0,76	-5,04	0,12
A1DW-2 31-03-16	-22,3	0,26	-4,39	0,11
JDW-2 31-03-16	-14,7	0,28	-3,16	0,09
JDW-5 31-03-16	-1,8	0,34	-1,52	0,10
A1DW-3 31-03-16	-21,5	0,41	-4,30	0,05
JDW-4 31-03-16	-12,1	0,26	-3,12	0,09
JDW-3 31-03-16	-27,0	0,40	-5,13	0,10
A1DW-5 31-03-16	-21,7	0,60	-4,48	0,03
A1DW-1 31-03-16	-12,3	0,27	-3,27	0,05
A2DW-1 31-03-16	-15,7	0,23	-3,69	0,02
A2DW-2 31-03-16	-19,8	0,16	-4,33	0,05
JDW-1 31-03-16	-17,4	0,33	-2,72	0,08
A2DW-2 03-09-15	17,2	0,80	1,21	0,08
A1DW-2 03-09-15	15,7	0,16	2,29	0,04
A2DW-1 03-09-15	5,5	0,29	-0,84	0,11
A1DW-3 03-09-15	6,1	0,29	-0,83	0,05
A1DW-1 03-09-15	-20,6	0,82	-4,47	0,08
A1DW-5 03-09-15	0,9	2,41	-1,00	0,21
JDW-1 03-09-15	22,9	0,80	10,39	0,26
JDW-2 03-09-15	4,3	0,59	-0,85	0,24
A1DW-4 03-09-15	-3,5	0,64	0,63	0,11
JDW-5 03-09-15	-6,5	0,30	-1,74	0,06
JDW-3 03-09-15	-25,6	0,49	-5,39	0,08
JDW-4 03-09-15	-20,8	0,18	-4,43	0,07
A1DW-4 02-06-16	11,1	0,41	0,77	0,04
JDW-3 02-06-16	4,3	0,19	-0,69	0,08
JDW-1 02-06-16	-7,0	0,33	-2,40	0,05

JDW-5 02-06-16	-2,9	0,18	-0,51	0,04
JDW-4 02-06-16	-18,0	0,57	-3,46	0,14
A2DW-1 02-06-16	-3,2	0,39	-1,36	0,05
JDW-2 02-06-16	-11,2	0,25	-1,36	0,04
A1DW-5 02-06-16	-17,3	0,13	-2,21	0,14
A2DW-2 02-06-16	-12,3	0,10	-2,43	0,12
A1DW-1 02-06-16	-6,4	0,29	-0,67	0,07
A1DW-2 02-06-16	-20,6	0,27	-4,38	0,05
A1DW-3 02-06-16	14,2	0,87	1,26	0,13
A1DW-4 10-12-15	1,9	0,36	-1,66	0,10
A2DW-2 10-12-15	5,6	0,46	-1,65	0,12
A2DW-1 10-12-15	-0,4	0,46	-2,14	0,09
A1DW-5 10-12-15	-19,7	0,67	-4,59	0,04
JDW-1 10-12-15	-10,0	0,30	-2,36	0,22
A1DW-3 10-12-15	-16,1	0,23	-3,46	0,10
JDW-2 10-12-15	-19,0	0,34	-4,35	0,09
A1DW-1 10-12-15	-17,7	0,11	-4,38	0,06
JDW-5 10-12-15	-11,0	0,09	-3,27	0,11
JDW-3 10-12-15	-8,2	0,18	-2,78	0,18
A1DW-2 10-12-15	-18,4	0,34	-3,85	0,10
JDW-4 22-01-16	-17,9	0,44	-4,15	0,06
JDW-5 22-01-16	-10,8	0,15	-3,24	0,11
A1DW-1 22-01-16	-18,5	1,00	-4,48	0,12
JDW-2 22-01-16	-18,6	0,29	-4,53	0,07
A1DW-3 22-01-16	-7,3	0,17	-3,41	0,08
JDW-3 22-01-16	-15,7	0,25	-4,14	0,05
A2DW-2 22-01-16	-6,9	1,33	-3,75	0,17
A2DW-3 22-01-16	-2,9	2,05	-2,03	0,15
A2DW-1 22-01-16	-9,9	0,27	-4,16	0,06
A1DW-5 22-01-16	-15,5	0,27	-4,45	0,06
A1DW-2 22-01-16	-16,8	0,27	-4,57	0,07
A1DW-2 05-05-16	-18,4	0,11	-3,74	0,06
A2DW-1 05-05-16	-6,5	0,22	-2,96	0,05
A1DW-1 05-05-16	-12,5	0,54	-2,48	0,11
A2DW-2 05-05-16	-15,0	0,16	-4,41	0,06
JDW-1 05-05-16	-13,3	0,17	-4,21	0,07
JDW-4 05-05-16	-12,8	0,06	-2,52	0,06
A1DW-4 05-05-16	6,1	0,40	-0,80	0,10
JDW-2 05-05-16	-17,7	0,55	-4,24	0,05
JDW-3 05-05-16	-4,8	0,30	-3,15	0,05
A1DW-5 05-05-16	-20,7	0,42	-4,31	0,08
JDW-5 05-05-16	-10,3	0,38	-3,56	0,03
A1DW-3 05-05-16	-0,5	2,56	-2,07	0,19
JDW-3 30-06-16	4,8	0,35	-0,91	0,06

A1DW-1 30-06-16	-8,3	0,42	-2,72	0,07
ADW-4 30-06-16	-10,8	0,17	-1,20	0,05
A1DW-4 30-06-16	0,2	0,27	-1,82	0,03
JDW-2 30-06-16	-12,8	0,34	-2,33	0,06
A1DW-3 30-06-16	5,9	0,93	-1,09	0,19
JDW-1 30-06-16	2,3	1,23	-0,94	0,10
A2DW-2 30-06-16	-2,5	0,13	-1,41	0,03
JDW-5 30-06-16	-11,0	0,20	-3,06	0,03
A2DW-1 30-06-16	-4,4	0,95	-2,51	0,10
A1DW-5 30-06-16	-21,6	0,48	-4,15	0,03
A1DW-2 30-06-16	-16,4	0,10	-2,89	0,04
A2DW-1 18-02-16	-10,5	0,25	-3,33	0,17
A2DW-2 18-02-16	-10,0	0,18	-3,28	0,10
JDW-2 18-02-16	-21,4	2,89	-3,99	0,18
JDW-3 18-02-16	-10,2	0,18	-3,04	0,07
JDW-1 18-02-16	-6,2	0,20	-1,65	0,12
JDW-4 18-02-16	-15,9	0,36	-2,98	0,07
JDW-5 18-02-16	-11,4	0,05	-3,23	0,06
A1DW-2 18-02-16	-11,2	0,12	-2,23	0,03
A1DW-4 18-02-16	-8,5	0,48	-2,89	0,07
A1DW-1 18-02-16	-18,2	0,29	-3,87	0,07
A1DW-5 18-02-16	-12,5	0,09	-2,32	0,08
JDW-5 03-03-16	-12,6	0,17	-2,61	0,10
A1DW-4 03-03-16	-10,2	0,18	-3,00	0,06
A2DW-1 03-03-16	-9,4	0,05	-3,11	0,08
JDW-3 03-03-16	-16,7	0,15	-3,71	0,18
A1DW-2 03-03-16	-15,3	0,04	-3,29	0,04
JDW-4 03-03-16	-19,2	0,25	-4,12	0,08
A1DW-1 03-03-16	-20,9	0,29	-4,18	0,04
JDW-2 03-03-16	-15,5	0,14	-2,12	0,06
A1DW-5 03-03-16	-17,6	0,17	-3,70	0,06
JDW-1 03-03-16	-17,6	0,14	-3,17	0,10
A2DW-2 03-03-16	-11,8	0,19	-3,49	0,05
A1DW-1 14-04-16	-20,7	0,32	-4,17	0,07
A2DW-1 14-04-16	-14,8	0,13	-3,43	0,05
JDW-5 14-04-16	-14,3	0,69	-3,40	0,09
A1DW-5 14-04-16	-24,0	0,37	-4,15	0,15
JDW-1 14-04-16	-17,0	0,20	-3,67	0,10
JDW-3 14-04-16	-11,9	0,22	-3,11	0,11
A1DW-2 14-04-16	-25,4	0,33	-4,96	0,08
JDW-2 14-04-16-	-21,2	0,13	-4,37	0,08
A1DW-2 14-04-16	-15,8	0,11	-3,39	0,06
JDW-4 14-04-16	-20,5	0,17	-4,29	0,09
A1DW-1 15-10-15	-10,3	0,88	-2,78	0,05

A1DW-3 15-10-15	0,5	0,23	-1,61	0,09
JDW-3 15-10-15	-11,1	0,35	-3,26	0,04
A2DW-2 15-10-15	9,4	0,63	-0,92	0,20
JDW-4 15-10-15	-13,1	0,67	-3,02	0,12
JDW-2 15-10-15	-16,2	0,26	-2,96	0,06
A1DW-5 15-10-15	-13,5	0,10	-3,29	0,06
A1DW-2 15-10-15	-12,5	0,34	-3,57	0,06
JDW-5 15-10-15	-8,2	0,54	-1,26	0,18
A2DW-1 15-10-15	0,1	0,22	-1,97	0,05
JDW-1 15-10-15	1,8	0,22	-1,22	0,06
A1DW-4 15-10-15	-0,4	0,17	-2,03	0,05
JDW-3 15-06-16	6,1	0,11	-0,14	0,04
A2DW-2 15-06-16	-13,4	0,51	-3,44	0,04
JDW-1 15-06-16	-13,9	0,11	-3,40	0,06
A1DW-1 15-06-16	-11,5	1,85	-2,77	0,16
A1DW-2 15-06-16	-25,3	0,37	-4,67	0,04
JDW-2 15-06-16	-20,9	0,15	-4,19	0,06
JDW-5 15-06-16	-13,3	0,19	-3,19	0,08
A1DW-5 15-06-16	-19,3	0,28	-3,59	0,03
JDW-4 15-06-16	-22,7	0,12	-4,87	0,05
A1DW-4 15-06-16	9,3	0,74	2,74	0,18
A2DW-1 15-06-16	-10,1	0,88	-3,11	0,10
A1DW-2 26-11-15	-12,3	0,64	-3,24	0,13
A1DW-2 26-11-15	7,4	1,12	-1,58	0,15
A1DW-3 26-11-15	0,5	0,25	-2,15	0,01
JDW-1 26-11-15	4,2	0,16	-0,75	0,08
A1DW-1 26-11-15	-17,6	0,61	-3,96	0,10
JDW-1 26-11-15	-5,0	0,44	-2,23	0,23
JDW-5 26-11-15	-3,9	0,09	-1,36	0,12
A2DW-1 26-11-15	3,5	0,24	-1,81	0,05
A1DW-5 26-11-15	-15,8	2,52	-3,63	0,26
A1DW-4 26-11-15	2,9	0,40	-0,33	0,06
JDW-4 26-11-15	-13,8	0,41	-3,23	0,10
JDW-3 26-11-15	-10,4	0,33	-2,87	0,06
A2DW-2 29-10-15	7,7	0,34	-0,30	0,11
A1DW-1 29-10-15	-13,8	0,17	-3,33	0,04
JDW-5 29-10-15	-10,8	0,07	-2,23	0,12
JDW-1 29-10-15	-10,0	0,14	-1,99	0,09
A1DW-4 29-10-15	0,2	0,18	-1,20	0,07
A1DW-3 29-10-15	7,1	0,11	1,16	0,08
JDW-2 29-10-15	2,1	0,17	0,32	0,04
A1DW-5 29-10-15	-9,9	0,39	-0,43	0,05
JDW-3 29-10-15	-10,5	0,59	-2,42	0,10
JDW-4 29-10-15	-11,6	0,61	-2,44	0,12

A1DW-2 29-10-15	-12,8	0,12	-2,45	0,09
A2DW-1 29-10-15	-4,1	3,55	-2,11	0,31
A2DW-1 23-07-15	5,5	0,42	-0,31	0,06
A1DW-3 23-07-15	-7,8	0,46	-2,49	0,04
JDW-2 23-07-15	-21,1	0,38	-4,05	0,08
A2DW-3 23-07-15	20,2	0,94	1,40	0,12
A2DW-2 23-07-15	6,8	0,37	-0,86	0,06
A1DW-5 23-07-15	-22,5	0,75	-3,89	0,06
JDW-5 23-07-15	-17,8	0,18	-3,60	0,08
A1DW-1 23-07-15	-14,6	0,15	-2,65	0,02
A1DW-4 23-07-15	-2,4	0,23	-1,11	0,07
JDW-3 23-07-15	-12,3	0,47	-2,90	0,11
A1DW-2 23-07-15	-24,0	0,60	-4,48	0,11
JDW-1 23-07-15	-18,1	0,19	-3,65	0,04
JDW-4 23-07-15	-15,0	0,15	-1,99	0,01
A1DW-5 12-11-15	21,8	1,18	8,96	0,28
A1DW-2 12-11-15	-7,1	0,15	-1,62	0,04
A1DW-4 12-11-15	-1,5	0,12	-2,02	0,05
JDW-1 12-11-15	-8,2	0,25	-2,59	0,02
JDW-3 12-11-15	-10,1	0,26	-2,96	0,06
A1DW-1 12-11-15	-12,2	0,15	-2,88	0,05
JDW-4 12-11-15	-6,1	0,20	-0,94	0,04
JDW-2 12-11-15	-13,6	0,30	-3,43	0,12
A2DW-1 12-11-15	9,5	0,57	0,29	0,06
A2DW-2 12-11-15	8,6	0,07	-1,25	0,08
JDW-5 12-11-15	-11,3	0,60	-3,35	0,08
A1DW-4 09-07-15	-6,8	0,10	-2,20	0,05
A1DW-3 09-07-15	-8,0	0,09	-2,62	0,05
JDW-1 09-07-15	-16,8	0,43	-3,15	0,07
A2DW-3 09-07-15	21,3	0,69	1,55	0,04
A1DW-1 09-07-15	-14,5	0,87	-3,37	0,09
JDW-3 09-07-15	-7,9	0,22	-0,98	0,06
A1DW-5 09-07-15	-22,9	0,44	-4,32	0,09
JDW-2 09-07-15	-16,9	0,37	-3,49	0,05
JDW-5 09-07-15	-16,7	0,08	-3,54	0,06
A2DW-1 09-07-15	-1,5	0,54	-1,86	0,10
JDW-4 09-07-15	-20,8	0,47	-4,14	0,08
MHLDW-1 09-07-15	-18,3	0,21	-3,49	0,14
A2DW-2 09-07-15	5,3	0,21	-1,21	0,05
A1DW-2 09-07-15	-22,7	0,69	-4,56	0,05
A1DW-4 06-08-15	2,8	0,56	-1,15	0,04
A2DW-1 06-08-15	14,9	1,32	3,10	0,21
JDW-4 06-08-15	16,6	0,95	3,17	0,08
A1DW-3 06-08-15	-12,7	0,92	-2,09	0,10

A1DW-2 06-08-15	-1,0	0,45	-2,02	0,08
JDW-2 06-08-15	-19,0	0,53	-4,37	0,04
JDW-1 06-08-15	-10,3	0,60	-2,23	0,13
A1DW-1 06-08-15	3,8	0,77	2,41	0,18
A1DW-5 06-08-15	-19,8	0,61	-3,74	0,09
A2DW-2 06-08-15	10,8	0,58	-0,93	0,11
JDW-3 06-08-15	-10,1	0,52	-3,13	0,04
JDW-5 06-08-15	-16,4	0,79	-3,84	0,08
A1DW-1 01-10-15	-15,3	0,10	-3,77	0,04
A1DW-3 01-10-15	3,7	0,34	-1,05	0,12
JDW-5 01-10-15	-11,9	0,88	-3,30	0,09
JDW-3 01-10-15	-9,9	0,11	-3,20	0,05
A2DW-1 01-10-15	9,8	2,17	0,80	0,24
JDW-2 01-10-15	-18,4	0,66	-4,11	0,11
JDW-4 01-10-15	-12,1	0,58	-3,31	0,07
A1DW-2 01-10-15	-6,8	0,34	0,10	0,09
A1DW-5 01-10-15	4,8	0,76	4,05	0,14
A2DW-2 01-10-15	8,4	0,17	-1,25	0,07
A1DW-4 01-10-15	8,4	0,16	-0,87	0,04
JDW-1 01-10-15	-6,6	0,83	-1,87	0,10

Appendix D

Measured Cave Climatic Parameters

Date	Sample Name	Atmospheric Temperature (°C)	Humidity (%)	Atmospheric Pressure (hPa)	Drip Rate (drips/min)
25/06/2015	JDW-3	17,6	57,5	866,1	2
	JDW-4	17,6	57,5	866,1	3
	JDW-2	17,6	57,5	866,1	2
	JDW-5	15,9	58	866	1
	JDW-1	15,9	58	866	0,5
	A1DW-1	18,1	79,7	865,9	1
	A1DW-2	18,1	79,7	865,9	3
	A1DW-3	16,3	79	866	1
	A1DW-4	16,3	79	866	0,25
	A1DW-5	18,1	79,7	865,9	0,25
	A2DW-1	15,8	53,8	866,5	0,2
	A2DW-2	15,8	53,8	866,5	0,2
	A2DW-3	15,8	53,8	866,5	0
09/07/2015	JDW-3	14,2	77,2	858,1	2
	JDW-4	14,2	77,2	858,1	3
	JDW-2	14,2	77,2	858,1	2
	JDW-5	15,9	77,3	857,9	2
	JDW-1	15,9	77,3	857,9	0,5
	A1DW-1	16,3	85,3	858,3	1
	A1DW-2	16,3	85,3	858,3	3
	A1DW-3	15,8	78,9	858,5	1
	A1DW-4	15,8	78,9	858,5	0,25
	A1DW-5	16,3	85,3	858,3	4
	A2DW-1	18,9	65,4	858,8	0,2
	A2DW-2	18,9	65,4	858,8	0,2
	A2DW-3	18,9	65,4	858,8	0,14
23/07/2015	JDW-3	16	64,5	861,1	3
	JDW-4	16	64,5	861,1	4
	JDW-2	16	64,5	861,1	2
	JDW-5	15,9	69,2	861	6
	JDW-1	15,9	69,2	861	2
	A1DW-1	18,4	80,1	861,1	1
	A1DW-2	18,4	80,1	861,1	3
	A1DW-3	17,3	72,7	861,5	1
	A1DW-4	17,3	72,7	861,5	0,5
	A1DW-5	18,4	80,1	861,1	5
	A2DW-1	18,4	66,5	861	0,5
	A2DW-2	18,4	66,5	861	0,5
	A2DW-3	18,4	66,5	861	0,14
06/08/2015	JDW-3	16,5	49,4	866,3	1
	JDW-4	16,5	49,4	866,3	5
	JDW-2	16,5	49,9	866,3	2
	JDW-5	16,9	53,1	866,2	8
	JDW-1	16,9	53,1	866,2	0
	A1DW-1	18,1	82,2	865,9	1
	A1DW-2	18,1	82,2	865,9	6
	A1DW-3	16,7	72,2	866	0,5
	A1DW-4	16,7	72,2	866	1
	A1DW-5	18,1	82,2	865,9	5

	A2DW-1	17,4	78,7	866,1	1
	A2DW-2	17,4	78,7	866,1	1
	A2DW-3	17,4	78,7	866,1	0
20/08/2015	JDW-3	17,3	66,7	859,4	1
	JDW-4	17,3	66,7	859,4	5
	JDW-2	17,3	66,7	859,4	2
	JDW-5	17,9	59,4	859,3	7
	JDW-1	17,9	59,4	859,3	0,5
	A1DW-1	18,5	78,1	858,9	1
	A1DW-2	18,5	78,1	858,9	2
	A1DW-3	19,6	64,4	859,2	1
	A1DW-4	19,6	64,4	859,2	0,5
	A1DW-5	18,5	78,1	858,9	4
	A2DW-1	15,9	69,6	859	1
	A2DW-2	15,9	69,6	859	1
	A2DW-3	15,9	69,6	859	0
03/09/2015	JDW-3	17,3	72,2	861,8	1
	JDW-4	17,3	72,2	861,8	3
	JDW-2	17,3	72,2	861,8	2
	JDW-5	15,5	71,4	861,7	6
	JDW-1	15,5	71,4	861,7	0,5
	A1DW-1	18,3	75,9	862,1	2
	A1DW-2	18,3	75,9	861	2
	A1DW-3	17,2	72,8	862	0,5
	A1DW-4	17,2	72,8	862	0,2
	A1DW-5	18,3	75,9	862,1	2
	A2DW-1	16,7	66,8	862,5	0,33
	A2DW-2	16,7	66,8	862,5	2
	A2DW-3	16,7	66,8	862,5	0
17/09/2015	JDW-3	17,7	71,8	860,2	1
	JDW-4	17,7	71,8	860,2	2
	JDW-2	17,7	71,8	860,2	1
	JDW-5	18,4	69,7	860,1	4
	JDW-1	18,4	69,7	860,1	1
	A1DW-1	20,2	79,2	860,2	0,5
	A1DW-2	20,2	79,2	860,2	2
	A1DW-3	19,9	64,9	860,4	0,5
	A1DW-4	19,9	64,9	860,4	0
	A1DW-5	20,2	79,2	860,2	4
	A2DW-1	18,5	72,9	860,9	0,2
	A2DW-2	18,5	72,9	860,9	0,33
	A2DW-3	18,5	72,9	860,9	0
01/10/2015	JDW-3	19,9	64,9	854,2	1
	JDW-4	19,9	64,9	854,2	3
	JDW-2	19,9	64,9	854,2	2
	JDW-5	18,6	69,7	854,1	1
	JDW-1	18,6	69,7	854,1	2
	A1DW-1	21,3	79,3	854,3	0,5
	A1DW-2	21,3	79,3	854,3	1
	A1DW-3	22,9	61,9	854,4	1
	A1DW-4	22,9	61,9	854,4	0
	A1DW-5	21,3	79,3	854,3	3
	A2DW-1	23,3	54,4	854,9	0,5
	A2DW-2	23,3	54,4	854,9	0,14
	A2DW-3	23,3	54,4	854,9	0
15/10/2015	JDW-3	18	71,3	854,8	2
	JDW-4	18,8	71,3	854,8	2
	JDW-2	18,8	71,3	854,8	0

	JDW-5	17	76,3	854,8	1
	JDW-1	17	76,3	854,9	0
	A1DW-1	22,2	67,7	854,6	1
	A1DW-2	22,2	67,7	854,6	1
	A1DW-3	19,2	70,2	854,7	0
	A1DW-4	19,2	70,2	854,7	0
	A1DW-5	22,2	67,7	854,6	1.5
	A2DW-1	21	65,2	855,3	0
	A2DW-2	21	65,2	855,3	0
	A2DW-3	21	65,2	855,3	0
29/10/2015	JDW-3	18,8	78,5	858,8	2
	JDW-4	18,8	78,5	858,8	1
	JDW-2	18,8	78,5	858,8	1
	JDW-5	20,2	70,2	858,5	1
	JDW-1	20,2	70,2	858,5	0,5
	A1DW-1	18,1	74,2	858,4	1
	A1DW-2	18,1	74,2	858,4	2
	A1DW-3	19,1	71,5	858,3	0
	A1DW-4	19,1	71,5	858,3	0
	A1DW-5	18,1	74,2	858,4	1
	A2DW-1	23,4	62,8	858,8	0,5
	A2DW-2	23,4	62,8	858,8	0
	A2DW-3	23,4	62,8	858,8	0
12/11/2015	JDW-3	21,6	59,2	855,4	2
	JDW-4	21,6	59,2	855,4	1
	JDW-2	21,6	59,2	855,4	0,5
	JDW-5	18,8	64,8	855,2	1
	JDW-1	18,8	64,8	855,2	1
	A1DW-1	20,7	70,4	855,3	2
	A1DW-2	20,7	70,4	855,3	1
	A1DW-3	20,7	70,4	855,3	1
	A1DW-4	19,5	78,7	855,4	0
	A1DW-5	19,5	78,7	855,4	1
	A2DW-1	24,1	54,9	855,7	0,25
	A2DW-2	24,1	54,9	855,7	0,14
	A2DW-3	24,1	54,9	855,7	0
26/11/2015	JDW-3	17,2	53,2	866,6	2
	JDW-4	17,2	53,2	866,6	3
	JDW-2	17,2	53,2	866,6	0,2
	JDW-5	16,1	58,1	866,2	0,5
	JDW-1	16,1	58,1	866,2	0,14
	A1DW-1	17,9	78,6	865,3	2
	A1DW-2	17,9	78,6	865,3	1
	A1DW-3	15,3	77,5	866,1	0,5
	A1DW-4	15,3	77,5	866,1	1
	A1DW-5	17,9	78,6	865,3	3
	A2DW-1	17,4	53,4	866,1	1
	A2DW-2	17,4	53,4	866,1	1
	A2DW-3	17,4	53,4	866,1	0
10/12/2015	JDW-3	16,8	53,9	866,5	2
	JDW-4	16,8	53,9	866,5	2
	JDW-2	16,8	53,9	866,5	0,33
	JDW-5	15,2	58	866,1	1
	JDW-1	15,2	58	866,1	0,2
	A1DW-1	18,8	79,2	866,1	1
	A1DW-2	18,8	79,2	866,1	1
	A1DW-3	16,4	77,1	864,9	0,33
	A1DW-4	16,4	77,1	864,9	0,14

	A1DW-5	16,4	79,2	866,1	2
	A2DW-1	18,3	52,2	865,2	0,33
	A2DW-2	18,3	52,2	865,2	0,5
	A2DW-3	18,3	52,2	865,2	0
07/01/2016	JDW-3	20,9	67,5	859,2	2
	JDW-4	20,9	67,5	859,2	1
	JDW-2	20,9	67,5	859,2	1
	JDW-5	19,4	76,2	859,1	1
	JDW-1	19,4	76,2	859,1	0,33
	A1DW-1	23,7	71,7	858,7	1
	A1DW-2	23,7	71,7	858,7	1
	A1DW-3	23,2	73,1	858,8	0
	A1DW-4	23,2	73,1	858,8	0
	A1DW-5	23,7	71,7	858,7	1
	A2DW-1	19,4	81,1	858,8	0,2
	A2DW-2	19,4	81,1	858,8	0,33
	A2DW-3	19,4	81,1	858,8	0,14
21/01/2016	JDW-3	19,1	78,6	857,7	2
	JDW-4	19,1	78,6	857,7	2
	JDW-2	19,1	78,6	857,7	2
	JDW-5	22	76,3	857,5	1
	JDW-1	22	76,3	857,5	1
	A1DW-1	18,8	83,5	857,4	1
	A1DW-2	18,8	83,5	857,4	0,5
	A1DW-3	19,3	84,5	857,7	0
	A1DW-4	19,3	84,5	857,7	0
	A1DW-5	18,8	83,5	857,4	1
	A2DW-1	22,7	75,3	857,8	0,2
	A2DW-2	22,7	75,3	857,8	0,33
	A2DW-3	22,7	75,3	857,8	0
04/02/2016	JDW-3	18	77,6	857,3	0,5
	JDW-4	18	77,6	857,3	1
	JDW-2	18	77,6	857,3	1
	JDW-5	23,1	75,5	856,6	0,5
	JDW-1	23,1	75,5	856,6	1
	A1DW-1	18,7	82,6	857,2	1
	A1DW-2	18,7	82,6	857,6	0,5
	A1DW-3	19,1	83,7	857,6	0
	A1DW-4	19,1	83,7	857,2	1
	A1DW-5	18,7	82,6	857,2	0,5
	A2DW-1	21,5	78,3	855,7	0,33
	A2DW-2	21,5	78,3	855,7	0,5
	A2DW-3	21,5	78,3	855,7	0
18/02/2016	JDW-3	18,2	93,5	859,1	1
	JDW-4	18,2	93,5	859,1	1
	JDW-2	18,2	93,5	859,1	2
	JDW-5	19,2	91,8	858,9	1
	JDW-1	19,2	91,8	858,9	1
	A1DW-1	19,5	89,2	859	1
	A1DW-2	19,5	83,7	859	1
	A1DW-3	22,7	97,9	859,3	1
	A1DW-4	22,7	97,9	859,3	0
	A1DW-5	19,5	83,7	859	2
	A2DW-1	21,7	89,2	859,5	0,2
	A2DW-2	21,7	89,2	859,5	0,2
	A2DW-3	21,7	89,2	859,5	0
03/03/2016	JDW-3	18,4	84,6	859,4	3
	JDW-4	18,4	84,6	859,4	3

	JDW-2	18,4	84,6	859,4	2
	JDW-5	19,9	84	859,3	1
	JDW-1	19,9	84	859,3	1
	A1DW-1	21,4	78,9	859,3	1
	A1DW-2	21,4	78,9	859,3	1
	A1DW-3	22,1	84,4	859,5	1
	A1DW-4	22,1	84,4	859,5	0
	A1DW-5	21,4	78,9	859,3	1
	A2DW-1	20,9	81,8	859,8	0,33
	A2DW-2	20,9	81,8	859,8	0,2
	A2DW-3	20,9	81,8	859,8	0
17/03/2016	JDW-3	22,1	88,5	858,9	2
	JDW-4	22,1	85,4	858,9	4
	JDW-2	22,1	85,4	858,9	1
	JDW-5	19	89,7	858,8	1
	JDW-1	19	89,7	858,8	1
	A1DW-1	19,5	88,5	858,6	2
	A1DW-2	19,5	88,5	858,6	1
	A1DW-3	19,5	95,4	858,8	0
	A1DW-4	19,1	95,4	858,8	0
	A1DW-5	19,1	88,5	858,6	1
	A2DW-1	20,7	88,8	858,9	0
	A2DW-2	20,7	88,8	858,9	0
	A2DW-3	20,7	88,8	858,9	0
31/03/2016	JDW-3	18,4	89,1	860	1
	JDW-4	18,4	89,1	860	1
	JDW-2	18,4	89,1	860	1
	JDW-5	18,2	88,9	859,1	1
	JDW-1	18,2	88,9	859,1	0,2
	A1DW-1	20,2	83,5	860,1	1
	A1DW-2	20,2	83,5	860,1	2
	A1DW-3	20,1	85,9	860,2	0
	A1DW-4	20,1	85,9	860,2	0
	A1DW-5	20,2	83,5	860,1	2
	A2DW-1	20,6	79,8	860,5	1
	A2DW-2	20,6	79,8	860,5	1
	A2DW-3	20,6	79,8	860,5	0
14/04/2016	JDW-3	17,6	92,2	862,9	1
	JDW-4	17,6	92,2	862,9	2
	JDW-2	17,6	92,2	862,9	0,5
	JDW-5	17,1	93,4	862,7	1
	JDW-1	17,1	93,4	862,7	1
	A1DW-1	19,1	88,6	862,7	1
	A1DW-2	19,1	88,6	862,7	1
	A1DW-3	19,3	87,9	862,8	0
	A1DW-4	19,3	87,9	862,8	0
	A1DW-5	19,1	88,6	862,7	2
	A2DW-1	92,2	80,2	863,1	0,5
	A2DW-2	20,3	80,2	863,1	0,33
	A2DW-3	20,3	80,2	863,1	0,2
05/05/2016	JDW-3	17,8	90,3	865,1	5
	JDW-4	17,8	90,3	865,1	3
	JDW-2	17,8	90,3	865,1	2
	JDW-5	18,8	87,2	864,9	2
	JDW-1	18,8	87,2	864,9	1
	A1DW-1	18,4	89,4	865,9	1
	A1DW-2	18,4	89,4	865,9	6
	A1DW-3	18,3	89,7	865	1

	A1DW-4	18,3	89,7	865	0
	A1DW-5	18,4	89,4	865,9	6
	A2DW-1	19,3	76,3	865,4	0,5
	A2DW-2	19,3	76,3	865,4	0,33
	A2DW-3	19,3	76,3	865,4	0
19/05/2016	JDW-3	18,4	84,4	867,5	
	JDW-4	19,4	84,4	867,5	
	JDW-2	19,4	84,4	867,5	
	JDW-5	18,6	83,9	867,3	
	JDW-1	18,6	83,9	867,3	
	A1DW-1	18,4	89,8	867,4	
	A1DW-2	18,4	89,8	867,4	
	A1DW-3	18,3	87,7	867,5	
	A1DW-4	18,3	87,7	867,5	
	A1DW-5	18,4	89,8	867,4	
	A2DW-1	19,4	78,3	867,9	
	A2DW-2	19,4	78,3	867,9	
	A2DW-3	19,4	78,3	867,9	
02/06/2016	JDW-3	19,5	80,5	865,4	8
	JDW-4	19,5	80,5	865,4	3
	JDW-2	19,5	80,5	865,4	2
	JDW-5	18,6	78,4	865,2	2
	JDW-1	18,6	78,4	865,2	1
	A1DW-1	18,7	78,9	865,2	1
	A1DW-2	18,7	78,9	865,5	5
	A1DW-3	17,9	69,5	865,5	0
	A1DW-4	17,9	69,5	865,2	0
	A1DW-5	18,7	78,9	865,2	5
	A2DW-1	19,9	68,2	865,7	1
	A2DW-2	19,9	68,2	865,7	1
	A2DW-3	19,9	68,2	865,7	0
15/06/2016	JDW-3	17,6	80,5	864,6	5
	JDW-4	17,6	80,5	864,6	3
	JDW-2	17,6	80,5	864,6	1
	JDW-5	18	79,6	864,5	1
	JDW-1	18	79,6	864,5	1
	A1DW-1	17,1	97,2	864,7	2
	A1DW-2	17,1	97,2	864,7	4
	A1DW-3	20	79,3	864,7	0
	A1DW-4	20	79,3	864,7	0,25
	A1DW-5	17,1	97,2	864,7	3
	A2DW-1	16,8	76,7	865,1	1
	A2DW-2	16,8	76,7	865,1	0,5
	A2DW-3	16,8	76,7	865,1	0
30/06/2016	JDW-3	17,2	77,7	866	5
	JDW-4	17,2	77,7	866	7
	JDW-2	17,2	77,7	866	0,5
	JDW-5	17	70,8	865,9	1
	JDW-1	17	70,8	865,9	1
	A1DW-1	18,7	94,2	865,9	0,5
	A1DW-2	18,7	94,2	865,9	2
	A1DW-3	19,1	81,8	866,1	0,5
	A1DW-4	19,1	81,8	866,1	0,2
	A1DW-5	18,7	94,2	865,9	1
	A2DW-1	16,7	72,8	866,3	1
	A2DW-2	16,7	72,8	866,3	1
	A2DW-3	16,7	72,8	866,3	0

Appendix E

Equation 1 and 2 Calculated Temperatures

Equation 1

Date	Sample Name	Drip water $\delta^{18}O$ (‰)	Calcite $\delta^{18}O$ (‰)	Calculated Temperature (°C)
09-07-15	A1DW-1	-3,37225	-4,59534	24,63236
23-07-15		-2,64556	-4,59534	8,908531
06-08-15		2,408735	-4,59534	62,04454
20-08-15		-2,03221	-4,59534	42,32646
03-09-15		-4,46725	-4,59534	20,81176
01-10-15		-3,77234	-4,59534	22,10305
15-10-15		-2,7788	-4,59534	32,01105
29-10-15		-3,3297	-4,59534	25,93693
12-11-15		-2,87853	-4,59534	33,89159
26-11-15		-3,9562	-4,59534	27,40916
10-12-15		-4,38348	-4,59534	16,35674
07-01-16		-2,5532	-4,59534	38,54351
22-01-16		-4,483	-4,59534	21,09414
18-02-16		-3,8694	-4,59534	27,22881
03-03-16		-4,17914	-4,59534	16,51577
17-03-16		-2,20647	-4,59534	36,01398
31-03-16		-3,26895	-4,59534	31,83134
14-04-16		-4,1713	-4,59534	17,74349
05-05-16		-2,48409	-4,59534	31,75964
19-05-16		-2,74525	-4,59534	21,08714
02-06-16		-0,66879	-4,59534	44,94474
15-06-16		-2,77183	-4,59534	29,50943
30-06-16		-2,72162	-4,59534	27,28725
14-07-16		-2,10279	-4,59534	29,16653
04-08-16		-1,4571	-4,59534	45,76223
25-08-16		-4,29315	-4,59534	27,38297
09-07-15	A1DW-2	-4,55684	-4,15753	21,35225
23-07-15		-4,48307	-4,15753	11,59928
06-08-15		-2,01894	-4,15753	31,31348
20-08-15		-2,16322	-4,15753	11,5141
03-09-15		2,294897	-4,15753	51,44151
01-10-15		0,104098	-4,15753	52,40986
15-10-15		-3,5678	-4,15753	20,70384
29-10-15		-2,45292	-4,15753	25,79974
12-11-15		-1,62443	-4,15753	38,74645
26-11-15		-3,23948	-4,15753	29,11734
10-12-15		-3,84686	-4,15753	16,49321

07-01-16		-1,97352	-4,15753	41,75514
22-01-16		-4,56899	-4,15753	11,78403
18-02-16		-2,22835	-4,15753	34,4651
03-03-16		-3,28563	-4,15753	23,6218
17-03-16		-2,62363	-4,15753	36,10292
31-03-16		-4,38521	-4,15753	24,742
14-04-16		-4,9603	-4,15753	14,9528
05-05-16		-3,74197	-4,15753	25,7266
19-05-16		-3,97474	-4,15753	25,59051
02-06-16		-4,38087	-4,15753	23,56402
15-06-16		-4,67153	-4,15753	13,72397
30-06-16		-2,88824	-4,15753	27,52928
14-07-16		-2,82431	-4,15753	27,50174
04-08-16		-2,70128	-4,15753	14,69075
25-08-16		0,572387	-4,15753	49,73655
09-07-15	A1DW-3	-2,6208	-4,59412	29,67382
23-07-15		-2,49229	-4,59412	28,93632
06-08-15		-2,08852	-4,59412	41,06265
20-08-15		-4,26552	-4,59412	10,03939
03-09-15		-0,82784	-4,59412	36,59121
01-10-15		-1,04831	-4,59412	37,3812
15-10-15		-1,60575	-4,59412	21,78746
29-10-15		1,159755	-4,59412	54,65308
26-11-15		-2,15483	-4,59412	37,18253
10-12-15		-3,45762	-4,59412	24,38846
07-01-16		-2,74462	-4,59412	32,59329
22-01-16		-3,40821	-4,59412	27,58968
17-03-16		-3,4164	-4,59412	31,22185
31-03-16		-4,29619	-4,59412	20,56594
14-04-16		-3,39188	-4,59412	22,04065
05-05-16		-2,06537	-4,59412	35,03427
19-05-16		-2,78978	-4,59412	12,65458
02-06-16		1,258346	-4,59412	50,8199
30-06-16		-1,0901	-4,59412	34,6086
14-07-16		-1,01596	-4,59412	26,39308
25-08-16		1,064846	-4,59412	54,21034
09-07-15	A1DW-4	-2,19637	-4,59412	27,01272
23-07-15		-1,10901	-4,59412	35,0234
06-08-15		-1,14659	-4,59412	31,37373
20-08-15		-0,34102	-4,59412	32,91328
03-09-15		0,63229	-4,59412	45,7861
01-10-15		-0,8674	-4,59412	40,41798
15-10-15		-2,0255	-4,59412	28,63133
29-10-15		-1,19575	-4,59412	38,08837

12-11-15		-2,02281	-4,59412	25,02931
26-11-15		-0,33342	-4,59412	42,57534
10-12-15		-1,65576	-4,59412	43,36553
07-01-16		-4,0638	-4,59412	20,30998
18-02-16		-2,895	-4,59412	29,76493
03-03-16		-3,00423	-4,59412	19,70056
05-05-16		-0,80454	-4,59412	18,81787
19-05-16		3,222291	-4,59412	69,4863
19-05-16		-2,63075	-4,59412	15,89302
02-06-16		0,771145	-4,59412	31,53519
15-06-16		2,744197	-4,59412	63,21935
30-06-16		-1,8235	-4,59412	27,67004
14-07-16		-0,61613	-4,59412	51,79659
09-07-15	A1DW-5	-4,31679	-4,59412	22,50969
23-07-15		-3,8935	-4,59412	25,1889
06-08-15		-3,73929	-4,59412	17,11341
20-08-15		-1,53072	-4,59412	31,40868
03-09-15		-1,00239	-4,59412	13,94707
01-10-15		4,050979	-4,59412	77,1039
15-10-15		-3,29086	-4,59412	15,95369
29-10-15		-0,43183	-4,59412	-2,66876
12-11-15		8,955172	-4,59412	103,5585
26-11-15		-3,63276	-4,59412	30,78352
10-12-15		-4,58893	-4,59412	17,69387
07-01-16		-3,262	-4,59412	33,03631
22-01-16		-4,44659	-4,59412	14,85433
18-02-16		-2,31591	-4,59412	37,00254
03-03-16		-3,69756	-4,59412	23,85151
17-03-16		-3,05794	-4,59412	34,73543
31-03-16		-4,48121	-4,59412	22,28751
14-04-16		-4,15127	-4,59412	25,56456
05-05-16		-4,30979	-4,59412	15,09297
19-05-16		-2,11442	-4,59412	32,22909
02-06-16		-2,20754	-4,59412	37,33047
15-06-16		-3,58521	-4,59412	29,30365
30-06-16		-4,14906	-4,59412	20,08488
14-07-16		-3,00096	-4,59412	13,06378
04-08-16		0,781532	-4,59412	55,36584
25-08-16		-2,91347	-4,59412	27,04958
09-07-15	A2DW-1	-1,86065	-4,07974	24,43523
23-07-15		-0,3073	-4,07974	21,31997
06-08-15		3,101744	-4,07974	53,69738
20-08-15		0,722996	-4,07974	44,97457
03-09-15		-0,84355	-4,07974	27,18758

01-10-15		0,80076	-4,07974	50,21724
15-10-15		-1,96716	-4,07974	31,19853
29-10-15		-2,10597	-4,07974	20,0797
12-11-15		0,29482	-4,07974	46,10641
26-11-15		-1,80605	-4,07974	32,52065
10-12-15		-2,13611	-4,07974	32,24063
07-01-16		-2,65433	-4,07974	34,63508
22-01-16		-4,15635	-4,07974	19,43997
18-02-16		-3,33348	-4,07974	24,99127
03-03-16		-3,1067	-4,07974	24,78
17-03-16		-2,63699	-4,07974	32,80689
31-03-16		-3,68962	-4,07974	23,56041
14-04-16		-3,43107	-4,07974	23,59485
05-05-16		-2,95568	-4,07974	29,67109
19-05-16		-3,52402	-4,07974	16,17815
02-06-16		-1,36318	-4,07974	39,84629
15-06-16		-3,10611	-4,07974	24,25372
30-06-16		-2,51061	-4,07974	26,48048
14-07-16		-1,95467	-4,07974	43,61344
04-08-16		-5,03978	-4,07974	7,584237
25-08-16		-2,21984	-4,07974	26,55857
09-07-15	A2DW-2	-1,21391	-3,84984	30,77285
23-07-15		-0,86116	-3,84984	33,63081
06-08-15		-0,93176	-3,84984	38,40247
20-08-15		-2,18932	-3,84984	14,80403
03-09-15		1,214421	-3,84984	49,39174
01-10-15		-1,25183	-3,84984	30,75891
15-10-15		-0,92387	-3,84984	30,54048
29-10-15		-0,30381	-3,84984	38,9568
12-11-15		-1,25194	-3,84984	33,49329
26-11-15		-1,5751	-3,84984	31,44838
10-12-15		-1,65446	-3,84984	39,3753
07-01-16		-3,68186	-3,84984	24,0782
22-01-16		-3,74959	-3,84984	21,5665
18-02-16		-3,2799	-3,84984	26,15233
03-03-16		-3,48768	-3,84984	23,51588
17-03-16		-3,24936	-3,84984	29,94151
31-03-16		-4,33284	-3,84984	21,60907
05-05-16		-4,40688	-3,84984	1,803808
19-05-16		0,16537	-3,84984	47,21315
02-06-16		-2,43467	-3,84984	32,47411
15-06-16		-3,4363	-3,84984	16,19967
30-06-16		-1,41086	-3,84984	36,87157
14-07-16		-2,6571	-3,84984	29,8083

04-08-16		-3,20692	-3,84984	15,08958
25-08-16		-0,71754	-3,84984	21,31257
09-07-15	A2DW-3	1,545257	-4,53084	42,05296
23-07-15		1,402202	-4,53084	55,53
22-01-16		-2,02549	-4,53084	39,36813
25-08-16		-3,80069	-4,53084	15,03202
30-06-16		-1,20453	-4,53084	48,67905
09-07-15	JDW-1	-3,15134	-3,12116	25,07504
23-07-15		-3,65488	-3,12116	15,00894
06-08-15		-2,22594	-3,12116	24,18405
20-08-15		-1,70517	-3,12116	-22,6056
03-09-15		10,38975	-3,12116	102,1469
01-10-15		-1,8676	-3,12116	24,90711
15-10-15		-1,21874	-3,12116	33,08762
29-10-15		-1,99415	-3,12116	29,67538
12-11-15		-2,58572	-3,12116	23,57454
26-11-15		-2,22929	-3,12116	26,91249
10-12-15		-2,36098	-3,12116	26,31544
07-01-16		-2,46291	-3,12116	22,09731
18-02-16		-1,64822	-3,12116	34,78963
03-03-16		-3,17243	-3,12116	15,33012
17-03-16		-1,37487	-3,12116	34,96498
31-03-16		-2,72085	-3,12116	28,54514
14-04-16		-3,6662	-3,12116	23,25754
05-05-16		-4,21183	-3,12116	16,0137
19-05-16		-3,55383	-3,12116	16,55007
02-06-16		-2,39739	-3,12116	29,97464
15-06-16		-3,40181	-3,12116	11,6741
30-06-16		-0,94359	-3,12116	31,81263
14-07-16		-1,20134	-3,12116	33,28282
04-08-16		-2,00955	-3,12116	29,00294
25-08-16		-2,45388	-3,12116	32,03016
09-07-15	JDW-2	-3,48967	-2,62964	22,0163
23-07-15		-4,05287	-2,62964	18,67712
06-08-15		-4,37072	-2,62964	7,271319
20-08-15		-2,2918	-2,62964	18,22276
03-09-15		-0,84791	-2,62964	43,07953
01-10-15		-4,10979	-2,62964	12,27845
15-10-15		-2,96081	-2,62964	7,947255
29-10-15		0,324077	-2,62964	48,89614
12-11-15		-3,43343	-2,62964	8,617652
26-11-15		-0,75265	-2,62964	44,81854
10-12-15		-4,35313	-2,62964	-10,7812
07-01-16		2,041817	-2,62964	65,53239

22-01-16		-4,52695	-2,62964	13,07192
18-02-16		-3,98817	-2,62964	9,763403
03-03-16		-2,11956	-2,62964	27,66968
17-03-16		-2,77351	-2,62964	24,07182
31-03-16		-3,15549	-2,62964	26,07485
14-04-16		-4,36812	-2,62964	15,48485
05-05-16		-4,24217	-2,62964	10,19567
19-05-16		-2,7298	-2,62964	16,86617
02-06-16		-1,35624	-2,62964	39,53403
15-06-16		-4,18611	-2,62964	9,009131
30-06-16		-2,33498	-2,62964	30,48678
14-07-16		-3,84934	-2,62964	11,09254
04-08-16		-2,16042	-2,62964	18,48749
25-08-16		-0,66391	-2,62964	32,17563
09-07-15	JDW-3	-0,98134	-2,43268	36,30276
23-07-15		-2,90072	-2,43268	22,15749
06-08-15		-3,13221	-2,43268	18,24354
20-08-15		-2,64983	-2,43268	33,67986
03-09-15		-5,39219	-2,43268	1,379369
01-10-15		-3,19744	-2,43268	20,25504
15-10-15		-3,25603	-2,43268	16,26924
29-10-15		-2,42157	-2,43268	25,31134
12-11-15		-2,96322	-2,43268	20,53055
26-11-15		-2,86588	-2,43268	20,9817
10-12-15		-2,7849	-2,43268	24,72279
07-01-16		-3,51933	-2,43268	21,3023
22-01-16		-4,13727	-2,43268	11,52251
18-02-16		-3,03977	-2,43268	23,44041
03-03-16		-3,70729	-2,43268	10,01151
17-03-16		-1,82092	-2,43268	39,16212
31-03-16		-5,12793	-2,43268	3,331409
14-04-16		-3,11234	-2,43268	20,51721
05-05-16		-3,15247	-2,43268	10,90621
19-05-16		-0,94236	-2,43268	27,32405
02-06-16		-0,69219	-2,43268	26,88788
15-06-16		-0,13661	-2,43268	34,27968
30-06-16		-0,90718	-2,43268	35,66885
14-07-16		-2,6153	-2,43268	28,0982
04-08-16		-3,99699	-2,43268	2,447267
25-08-16		-0,59745	-2,43268	45,37281
09-07-15	JDW-4	-4,13937	-2,21117	6,099902
23-07-15		-1,98544	-2,21117	2,173862
06-08-15		3,168541	-2,21117	68,75907
20-08-15		-3,755	-2,21117	19,60919

03-09-15		-4,42797	-2,21117	9,213699
01-10-15		-3,31398	-2,21117	17,36657
15-10-15		-3,01724	-2,21117	17,38431
29-10-15		-2,43829	-2,21117	15,82349
12-11-15		-0,94459	-2,21117	37,19371
26-11-15		-3,23356	-2,21117	20,78612
07-01-16		-3,67283	-2,21117	19,12186
22-01-16		-4,14768	-2,21117	10,1952
18-02-16		-2,97735	-2,21117	24,77031
03-03-16		-4,1189	-2,21117	8,077575
17-03-16		-2,41487	-2,21117	25,1698
31-03-16		-3,12494	-2,21117	24,25578
14-04-16		-4,28539	-2,21117	7,1043
05-05-16		-2,52102	-2,21117	21,03891
19-05-16		-2,34541	-2,21117	27,14982
02-06-16		-3,46326	-2,21117	23,92091
15-06-16		-4,87322	-2,21117	7,561809
14-07-16		-3,83662	-2,21117	10,33134
04-08-16		-2,38254	-2,21117	30,07117
25-08-16		-4,22994	-2,21117	11,87251
09-07-15	JDW-5	-3,54359	-2,21117	17,88723
23-07-15		-3,59619	-2,21117	18,48329
06-08-15		-3,84278	-2,21117	8,890616
20-08-15		-2,05189	-2,21117	22,27522
03-09-15		-1,74336	-2,21117	31,27213
01-10-15		-3,30337	-2,21117	10,07421
15-10-15		-1,26002	-2,21117	30,55458
29-10-15		-2,23242	-2,21117	27,58066
12-11-15		-3,34991	-2,21117	10,11242
26-11-15		-1,36104	-2,21117	34,14707
10-12-15		-3,2747	-2,21117	14,34755
07-01-16		-2,22092	-2,21117	27,22219
22-01-16		-3,24263	-2,21117	18,85328
18-02-16		-3,23049	-2,21117	16,33944
03-03-16		-2,60805	-2,21117	20,27388
17-03-16		-2,33108	-2,21117	19,11779
31-03-16		-1,52343	-2,21117	33,38991
14-04-16		-3,39624	-2,21117	18,95554
05-05-16		-3,55818	-2,21117	4,789396
02-06-16		-0,50667	-2,21117	40,33221
15-06-16		-3,18636	-2,21117	18,61935
30-06-16		-3,06405	-2,21117	16,86893
14-07-16		-2,40721	-2,21117	26,64908
04-08-16		-3,46245	-2,21117	17,08087

25-08-16		-3,24304	-2,21117	12,60044

Equation 2

Date	Sample Name	Drip Water $\delta^{18}O$ (‰)	Calcite $\delta^{18}O$ (‰)	Calculated Temperature (°C)
09-07-15	A1DW-1	-3,37225	-4,59534	19,827947
23-07-15	A1DW-1	-2,64556	-4,59534	23,171541
06-08-15	A1DW-1	2,408735	-4,59534	50,097042
20-08-15	A1DW-1	-2,03221	-4,59534	26,084496
03-09-15	A1DW-1	-4,46725	-4,59534	14,996921
01-10-15	A1DW-1	-3,77234	-4,59534	18,034778
15-10-15	A1DW-1	-2,7788	-4,59534	22,549912
29-10-15	A1DW-1	-3,3297	-4,59534	20,020611
12-11-15	A1DW-1	-2,87853	-4,59534	22,087158
26-11-15	A1DW-1	-3,9562	-4,59534	17,221657
10-12-15	A1DW-1	-4,38348	-4,59534	15,358099
07-01-16	A1DW-1	-2,5532	-4,59534	23,604738
22-01-16	A1DW-1	-4,483	-4,59534	14,929166
18-02-16	A1DW-1	-3,8694	-4,59534	17,604672
03-03-16	A1DW-1	-4,17914	-4,59534	16,244813
17-03-16	A1DW-1	-2,20647	-4,59534	25,248137
31-03-16	A1DW-1	-3,26895	-4,59534	20,296377
14-04-16	A1DW-1	-4,1713	-4,59534	16,27899
05-05-16	A1DW-1	-2,48409	-4,59534	23,930151
19-05-16	A1DW-1	-2,74525	-4,59534	22,706063
02-06-16	A1DW-1	-0,66879	-4,59534	32,880211
15-06-16	A1DW-1	-2,77183	-4,59534	22,582319
30-06-16	A1DW-1	-2,72162	-4,59534	22,816205
14-07-16	A1DW-1	-2,10279	-4,59534	25,744918
04-08-16	A1DW-1	-1,4571	-4,59534	28,895364
25-08-16	A1DW-1	-4,29315	-4,59534	15,749078
09-07-15	A1DW-2	-4,55684	-4,15753	12,696992
23-07-15	A1DW-2	-4,48307	-4,15753	13,007414
06-08-15	A1DW-2	-2,01894	-4,15753	23,995397
20-08-15	A1DW-2	-2,16322	-4,15753	23,31684
03-09-15	A1DW-2	2,294897	-4,15753	46,717297
01-10-15	A1DW-2	0,104098	-4,15753	34,551598
15-10-15	A1DW-2	-3,5678	-4,15753	16,944993
29-10-15	A1DW-2	-2,45292	-4,15753	21,968237
12-11-15	A1DW-2	-1,62443	-4,15753	25,874898
26-11-15	A1DW-2	-3,23948	-4,15753	18,397547
10-12-15	A1DW-2	-3,84686	-4,15753	15,727256
07-01-16	A1DW-2	-1,97352	-4,15753	24,209984
22-01-16	A1DW-2	-4,56899	-4,15753	12,645948

18-02-16	A1DW-2	-2,22835	-4,15753	23,012035
03-03-16	A1DW-2	-3,28563	-4,15753	18,192079
17-03-16	A1DW-2	-2,62363	-4,15753	21,182159
31-03-16	A1DW-2	-4,38521	-4,15753	13,420793
14-04-16	A1DW-2	-4,9603	-4,15753	11,016903
05-05-16	A1DW-2	-3,74197	-4,15753	16,183184
19-05-16	A1DW-2	-3,97474	-4,15753	15,174328
02-06-16	A1DW-2	-4,38087	-4,15753	13,439137
15-06-16	A1DW-2	-4,67153	-4,15753	12,216394
30-06-16	A1DW-2	-2,88824	-4,15753	19,975981
14-07-16	A1DW-2	-2,82431	-4,15753	20,266032
04-08-16	A1DW-2	-2,70128	-4,15753	20,826652
25-08-16	A1DW-2	0,572387	-4,15753	37,035328
09-07-15	A1DW-3	-2,6208	-4,59412	23,281614
23-07-15	A1DW-3	-2,49229	-4,59412	23,885589
06-08-15	A1DW-3	-2,08852	-4,59412	25,80746
20-08-15	A1DW-3	-4,26552	-4,59412	15,863557
03-09-15	A1DW-3	-0,82784	-4,59412	32,05712
01-10-15	A1DW-3	-1,04831	-4,59412	30,935863
15-10-15	A1DW-3	-1,60575	-4,59412	28,155084
29-10-15	A1DW-3	1,159755	-4,59412	42,759126
26-11-15	A1DW-3	-2,15483	-4,59412	25,489283
10-12-15	A1DW-3	-3,45762	-4,59412	19,436919
07-01-16	A1DW-3	-2,74462	-4,59412	22,703166
22-01-16	A1DW-3	-3,40821	-4,59412	19,659804
17-03-16	A1DW-3	-3,4164	-4,59412	19,622809
31-03-16	A1DW-3	-4,29619	-4,59412	15,730474
14-04-16	A1DW-3	-3,39188	-4,59412	19,733541
05-05-16	A1DW-3	-2,06537	-4,59412	25,918775
19-05-16	A1DW-3	-2,78978	-4,59412	22,493054
02-06-16	A1DW-3	1,258346	-4,59412	43,319716
30-06-16	A1DW-3	-1,0901	-4,59412	30,724705
14-07-16	A1DW-3	-1,01596	-4,59412	31,099593
25-08-16	A1DW-3	1,064846	-4,59412	42,222277
09-07-15	A1DW-4	-2,19637	-4,59412	25,290476
23-07-15	A1DW-4	-1,10901	-4,59412	30,629312
06-08-15	A1DW-4	-1,14659	-4,59412	30,439999
20-08-15	A1DW-4	-0,34102	-4,59412	34,577541
03-09-15	A1DW-4	0,63229	-4,59412	39,809741
01-10-15	A1DW-4	-0,8674	-4,59412	31,85499
15-10-15	A1DW-4	-2,0255	-4,59412	26,110775
29-10-15	A1DW-4	-1,19575	-4,59412	30,192882
12-11-15	A1DW-4	-2,02281	-4,59412	26,123783
26-11-15	A1DW-4	-0,33342	-4,59412	34,617364

10-12-15	A1DW-4	-1,65576	-4,59412	27,909332
07-01-16	A1DW-4	-4,0638	-4,59412	16,743472
18-02-16	A1DW-4	-2,895	-4,59412	22,005185
03-03-16	A1DW-4	-3,00423	-4,59412	21,50128
05-05-16	A1DW-4	-0,80454	-4,59412	32,176318
19-05-16	A1DW-4	3,222291	-4,59412	55,14802
19-05-16	A1DW-4	-2,63075	-4,59412	23,234996
02-06-16	A1DW-4	0,771145	-4,59412	40,578147
15-06-16	A1DW-4	2,744197	-4,59412	52,146814
30-06-16	A1DW-4	-1,8235	-4,59412	27,089359
14-07-16	A1DW-4	-0,61613	-4,59412	33,145583
09-07-15	A1DW-5	-4,31679	-4,59412	15,641156
23-07-15	A1DW-5	-3,8935	-4,59412	17,492657
06-08-15	A1DW-5	-3,73929	-4,59412	18,176099
20-08-15	A1DW-5	-1,53072	-4,59412	28,52493
03-09-15	A1DW-5	-1,00239	-4,59412	31,168376
01-10-15	A1DW-5	4,050979	-4,59412	60,552868
15-10-15	A1DW-5	-3,29086	-4,59412	20,191134
29-10-15	A1DW-5	-0,43183	-4,59412	34,102645
12-11-15	A1DW-5	8,955172	-4,59412	99,118996
26-11-15	A1DW-5	-3,63276	-4,59412	18,651005
10-12-15	A1DW-5	-4,58893	-4,59412	14,469325
07-01-16	A1DW-5	-3,262	-4,59412	20,322274
22-01-16	A1DW-5	-4,44659	-4,59412	15,080482
18-02-16	A1DW-5	-2,31591	-4,59412	24,720561
03-03-16	A1DW-5	-3,69756	-4,59412	18,361867
17-03-16	A1DW-5	-3,05794	-4,59412	21,254451
31-03-16	A1DW-5	-4,48121	-4,59412	14,931467
14-04-16	A1DW-5	-4,15127	-4,59412	16,360921
05-05-16	A1DW-5	-4,30979	-4,59412	15,671504
19-05-16	A1DW-5	-2,11442	-4,59412	25,683059
02-06-16	A1DW-5	-2,20754	-4,59412	25,23705
15-06-16	A1DW-5	-3,58521	-4,59412	18,863744
30-06-16	A1DW-5	-4,14906	-4,59412	16,370564
14-07-16	A1DW-5	-3,00096	-4,59412	21,516309
04-08-16	A1DW-5	0,781532	-4,59412	40,635855
25-08-16	A1DW-5	-2,91347	-4,59412	21,919797
09-07-15	A2DW-1	-1,86065	-4,07974	24,364648
23-07-15	A2DW-1	-0,3073	-4,07974	32,007427
06-08-15	A2DW-1	3,101744	-4,07974	51,08268
20-08-15	A2DW-1	0,722996	-4,07974	37,414021
03-09-15	A2DW-1	-0,84355	-4,07974	29,302819
01-10-15	A2DW-1	0,80076	-4,07974	37,833856
15-10-15	A2DW-1	-1,96716	-4,07974	23,861401

29-10-15	A2DW-1	-2,10597	-4,07974	23,209333
12-11-15	A2DW-1	0,29482	-4,07974	35,132436
26-11-15	A2DW-1	-1,80605	-4,07974	24,623616
10-12-15	A2DW-1	-2,13611	-4,07974	23,06833
07-01-16	A2DW-1	-2,65433	-4,07974	20,674859
22-01-16	A2DW-1	-4,15635	-4,07974	14,052205
18-02-16	A2DW-1	-3,33348	-4,07974	17,624169
03-03-16	A2DW-1	-3,1067	-4,07974	18,632261
17-03-16	A2DW-1	-2,63699	-4,07974	20,753992
31-03-16	A2DW-1	-3,68962	-4,07974	16,061939
14-04-16	A2DW-1	-3,43107	-4,07974	17,193553
05-05-16	A2DW-1	-2,95568	-4,07974	19,309397
19-05-16	A2DW-1	-3,52402	-4,07974	16,78521
02-06-16	A2DW-1	-1,36318	-4,07974	26,749483
15-06-16	A2DW-1	-3,10611	-4,07974	18,634866
30-06-16	A2DW-1	-2,51061	-4,07974	21,332806
14-07-16	A2DW-1	-1,95467	-4,07974	23,920283
04-08-16	A2DW-1	-5,03978	-4,07974	10,360143
25-08-16	A2DW-1	-2,21984	-4,07974	22,677659
09-07-15	A2DW-2	-1,21391	-3,84984	26,3248
23-07-15	A2DW-2	-0,86116	-3,84984	28,043635
06-08-15	A2DW-2	-0,93176	-3,84984	27,697254
20-08-15	A2DW-2	-2,18932	-3,84984	21,720841
03-09-15	A2DW-2	1,214421	-3,84984	38,79405
01-10-15	A2DW-2	-1,25183	-3,84984	26,141771
15-10-15	A2DW-2	-0,92387	-3,84984	27,735944
29-10-15	A2DW-2	-0,30381	-3,84984	30,820847
12-11-15	A2DW-2	-1,25194	-3,84984	26,14125
26-11-15	A2DW-2	-1,5751	-3,84984	24,594954
10-12-15	A2DW-2	-1,65446	-3,84984	24,218869
07-01-16	A2DW-2	-3,68186	-3,84984	15,069609
22-01-16	A2DW-2	-3,74959	-3,84984	14,778352
18-02-16	A2DW-2	-3,2799	-3,84984	16,81646
03-03-16	A2DW-2	-3,48768	-3,84984	15,909551
17-03-16	A2DW-2	-3,24936	-3,84984	16,950511
31-03-16	A2DW-2	-4,33284	-3,84984	12,306313
05-05-16	A2DW-2	-4,40688	-3,84984	11,99703
19-05-16	A2DW-2	0,16537	-3,84984	33,219252
02-06-16	A2DW-2	-2,43467	-3,84984	20,595803
15-06-16	A2DW-2	-3,4363	-3,84984	16,133031
30-06-16	A2DW-2	-1,41086	-3,84984	25,377822
14-07-16	A2DW-2	-2,6571	-3,84984	19,586922
04-08-16	A2DW-2	-3,20692	-3,84984	17,137058
25-08-16	A2DW-2	-0,71754	-3,84984	28,752009

09-07-15	A2DW-3	1,545257	-4,53084	44,5911
23-07-15	A2DW-3	1,402202	-4,53084	43,768855
22-01-16	A2DW-3	-2,02549	-4,53084	25,796806
25-08-16	A2DW-3	-3,80069	-4,53084	17,614479
30-06-16	ADW-4	-1,20453	-4,53084	29,821892
09-07-15	JDW-1	-3,15134	-3,12116	14,124006
23-07-15	JDW-1	-3,65488	-3,12116	12,000468
06-08-15	JDW-1	-2,22594	-3,12116	18,153529
20-08-15	JDW-1	-1,70517	-3,12116	20,497058
03-09-15	JDW-1	10,38975	-3,12116	98,343327
01-10-15	JDW-1	-1,8676	-3,12116	19,760008
15-10-15	JDW-1	-1,21874	-3,12116	22,73791
29-10-15	JDW-1	-1,99415	-3,12116	19,189632
12-11-15	JDW-1	-2,58572	-3,12116	16,566862
26-11-15	JDW-1	-2,22929	-3,12116	18,138644
10-12-15	JDW-1	-2,36098	-3,12116	17,554909
07-01-16	JDW-1	-2,46291	-3,12116	17,10556
18-02-16	JDW-1	-1,64822	-3,12116	20,756789
03-03-16	JDW-1	-3,17243	-3,12116	14,034128
17-03-16	JDW-1	-1,37487	-3,12116	22,013056
31-03-16	JDW-1	-2,72085	-3,12116	15,977563
14-04-16	JDW-1	-3,6662	-3,12116	11,953265
05-05-16	JDW-1	-4,21183	-3,12116	9,7057022
19-05-16	JDW-1	-3,55383	-3,12116	12,422872
02-06-16	JDW-1	-2,39739	-3,12116	17,394145
15-06-16	JDW-1	-3,40181	-3,12116	13,061813
30-06-16	JDW-1	-0,94359	-3,12116	24,028375
14-07-16	JDW-1	-1,20134	-3,12116	22,819016
04-08-16	JDW-1	-2,00955	-3,12116	19,120445
25-08-16	JDW-1	-2,45388	-3,12116	17,145283
09-07-15	JDW-2	-3,48967	-2,62964	10,586929
23-07-15	JDW-2	-4,05287	-2,62964	8,3007749
06-08-15	JDW-2	-4,37072	-2,62964	7,0346895
20-08-15	JDW-2	-2,2918	-2,62964	15,640659
03-09-15	JDW-2	-0,84791	-2,62964	22,106894
01-10-15	JDW-2	-4,10979	-2,62964	8,0727529
15-10-15	JDW-2	-2,96081	-2,62964	12,785221
29-10-15	JDW-2	0,324077	-2,62964	27,687364
12-11-15	JDW-2	-3,43343	-2,62964	10,818301
26-11-15	JDW-2	-0,75265	-2,62964	22,548913
10-12-15	JDW-2	-4,35313	-2,62964	7,1042815
07-01-16	JDW-2	2,041817	-2,62964	36,46993
22-01-16	JDW-2	-4,52695	-2,62964	6,4186044
18-02-16	JDW-2	-3,98817	-2,62964	8,5606018

03-03-16	JDW-2	-2,11956	-2,62964	16,389774
17-03-16	JDW-2	-2,77351	-2,62964	13,576075
31-03-16	JDW-2	-3,15549	-2,62964	11,970072
14-04-16	JDW-2	-4,36812	-2,62964	7,0449729
05-05-16	JDW-2	-4,24217	-2,62964	7,5446673
19-05-16	JDW-2	-2,7298	-2,62964	13,761597
02-06-16	JDW-2	-1,35624	-2,62964	19,781159
15-06-16	JDW-2	-4,18611	-2,62964	7,7679489
30-06-16	JDW-2	-2,33498	-2,62964	15,45378
14-07-16	JDW-2	-3,84934	-2,62964	9,1205505
04-08-16	JDW-2	-2,16042	-2,62964	16,211509
25-08-16	JDW-2	-0,66391	-2,62964	22,96252
09-07-15	JDW-3	-0,98134	-2,43268	20,561324
23-07-15	JDW-3	-2,90072	-2,43268	12,186
06-08-15	JDW-3	-3,13221	-2,43268	11,223574
20-08-15	JDW-3	-2,64983	-2,43268	13,240181
03-09-15	JDW-3	-5,39219	-2,43268	2,3121191
01-10-15	JDW-3	-3,19744	-2,43268	10,95413
15-10-15	JDW-3	-3,25603	-2,43268	10,712753
29-10-15	JDW-3	-2,42157	-2,43268	14,209532
12-11-15	JDW-3	-2,96322	-2,43268	11,925181
26-11-15	JDW-3	-2,86588	-2,43268	12,331672
10-12-15	JDW-3	-2,7849	-2,43268	12,671199
07-01-16	JDW-3	-3,51933	-2,43268	9,635598
22-01-16	JDW-3	-4,13727	-2,43268	7,1550598
18-02-16	JDW-3	-3,03977	-2,43268	11,606709
03-03-16	JDW-3	-3,70729	-2,43268	8,8741501
17-03-16	JDW-3	-1,82092	-2,43268	16,808067
31-03-16	JDW-3	-5,12793	-2,43268	3,3110917
14-04-16	JDW-3	-3,11234	-2,43268	11,305798
05-05-16	JDW-3	-3,15247	-2,43268	11,139792
19-05-16	JDW-3	-0,94236	-2,43268	20,739148
02-06-16	JDW-3	-0,69219	-2,43268	21,888062
15-06-16	JDW-3	-0,13661	-2,43268	24,488611
30-06-16	JDW-3	-0,90718	-2,43268	20,89987
14-07-16	JDW-3	-2,6153	-2,43268	13,386196
04-08-16	JDW-3	-3,99699	-2,43268	7,7124792
25-08-16	JDW-3	-0,59745	-2,43268	22,326703
09-07-15	JDW-4	-4,13937	-2,21117	6,2465876
23-07-15	JDW-4	-1,98544	-2,21117	15,100491
06-08-15	JDW-4	3,168541	-2,21117	40,2504
20-08-15	JDW-4	-3,755	-2,21117	7,7668319
03-09-15	JDW-4	-4,42797	-2,21117	5,1211747
01-10-15	JDW-4	-3,31398	-2,21117	9,542091

15-10-15	JDW-4	-3,01724	-2,21117	10,75571
29-10-15	JDW-4	-2,43829	-2,21117	13,169189
12-11-15	JDW-4	-0,94459	-2,21117	19,691966
26-11-15	JDW-4	-3,23356	-2,21117	9,8694585
07-01-16	JDW-4	-3,67283	-2,21117	8,0950462
22-01-16	JDW-4	-4,14768	-2,21117	6,2139841
18-02-16	JDW-4	-2,97735	-2,21117	10,920026
03-03-16	JDW-4	-4,1189	-2,21117	6,3269292
17-03-16	JDW-4	-2,41487	-2,21117	13,268128
31-03-16	JDW-4	-3,12494	-2,21117	10,313426
14-04-16	JDW-4	-4,28539	-2,21117	5,6754808
05-05-16	JDW-4	-2,52102	-2,21117	12,820562
19-05-16	JDW-4	-2,34541	-2,21117	13,562126
02-06-16	JDW-4	-3,46326	-2,21117	8,9374487
15-06-16	JDW-4	-4,87322	-2,21117	3,411326
14-07-16	JDW-4	-3,83662	-2,21117	7,4419414
04-08-16	JDW-4	-2,38254	-2,21117	13,404845
25-08-16	JDW-4	-4,22994	-2,21117	5,8919207
09-07-15	JDW-5	-3,54359	-2,21117	8,6136349
23-07-15	JDW-5	-3,59619	-2,21117	8,4022502
06-08-15	JDW-5	-3,84278	-2,21117	7,4174387
20-08-15	JDW-5	-2,05189	-2,21117	14,81466
03-09-15	JDW-5	-1,74336	-2,21117	16,149082
01-10-15	JDW-5	-3,30337	-2,21117	9,5852198
15-10-15	JDW-5	-1,26002	-2,21117	18,277424
29-10-15	JDW-5	-2,23242	-2,21117	14,042362
12-11-15	JDW-5	-3,34991	-2,21117	9,3962106
26-11-15	JDW-5	-1,36104	-2,21117	17,828716
10-12-15	JDW-5	-3,2747	-2,21117	9,7018409
07-01-16	JDW-5	-2,22092	-2,21117	14,091373
22-01-16	JDW-5	-3,24263	-2,21117	9,8324969
18-02-16	JDW-5	-3,23049	-2,21117	9,881978
03-03-16	JDW-5	-2,60805	-2,21117	12,455127
17-03-16	JDW-5	-2,33108	-2,21117	13,622926
31-03-16	JDW-5	-1,52343	-2,21117	17,111738
14-04-16	JDW-5	-3,39624	-2,21117	9,2084302
05-05-16	JDW-5	-3,55818	-2,21117	8,5549554
02-06-16	JDW-5	-0,50667	-2,21117	21,690388
15-06-16	JDW-5	-3,18636	-2,21117	10,062129
30-06-16	JDW-5	-3,06405	-2,21117	10,563244
14-07-16	JDW-5	-2,40721	-2,21117	13,300521
04-08-16	JDW-5	-3,46245	-2,21117	8,940699
25-08-16	JDW-5	-3,24304	-2,21117	9,8308257

Appendix F

Hydrochemistry

Electro-conductivity (µS/cm)														
	Jul-15	Aug-15	Sep-15	Oct-15	Nov-15	Dec-15	Jan-16	Feb-16	Mar-16	Apr-16	May-16	Jun-16	Jul-16	Aug-16
JDW-1	267,0	233,5	254,0	251,2		256,8	287,9	249,0	272,8	237,5	247,9	274,3	289,9	345,8
JDW-2	277,5	235,5	228,1	249,3		252,1	270,3	227,2	261,8	243,4	249,5	246,1	251,2	253,5
JDW-3	271,8	284,8	272,7	275,0	269,6	257,5	298,2	270,4	283,3	265,0	300,3	271,8	347,0	287,1
JDW-4	262,9	268,4	272,1	271,2	281,5		277,3	269,5	283,7	274,0	280,7	276,0	269,3	275,7
JDW-5	318,3	287,3	287,0	279,3	279,8	295,8	309,9	265,5	272,9	265,6	286,4	255,6	256,9	267,7
A1DW-1	319,8	203,2	317,0	290,0	307,3	326,2	345,6	293,7	293,8	322,3	324,9	306,7	310,1	282,5
A1DW-2	337,5	290,2	321,0	315,7	300,4	277,5	330,9	294,0	295,2	325,5	322,1	314,0	290,9	299,7
A1DW-3	314,4	289,9	271,6	261,4	247,1	271,8			237,7		301,0	279,9	246,5	
A1DW-4	314,0	287,4	274,1		285,4	238,4		282,1					289,8	
A1DW-5		312,2	294,4	344,6	302,6	330,0	335,7	297,0	311,6	289,1	318,1	282,1	296,3	315,4
A2DW-1	201,9	310,6	214,1	228,0	213,5	202,0	215,5	212,6	220,8	215,8	211,3	212,8	207,5	214,7
A2DW-2	197,9	195,2	208,9	204,5	201,8	212,3	227,7	206,0	215,0	203,0	227,6	206,0	197,2	210,1
A2DW-3	242,5													
pH														
	Jul-15	Aug-15	Sep-15	Oct-15	Nov-15	Dec-15	Jan-16	Feb-16	Mar-16	Apr-16	May-16	Jun-16	Jul-16	Aug-16
JDW-1	7,75	7,98	7,91	7,72		7,99	7,84	7,86	7,72	7,82	7,91	7,67	7,93	8,05
JDW-2	7,77	7,93	7,75	7,89		7,95	7,84	7,97	7,83	7,90	7,71	7,90	7,98	7,83
JDW-3	7,74	7,83	7,82	7,84	7,81	8,00	7,89	7,98	7,79	7,92	7,79	7,88	7,87	7,78
JDW-4	7,83	7,88	7,93	7,86	7,78		7,96	7,96	7,79	7,93	7,73	7,93	7,87	7,98
JDW-5	7,70	7,84	7,89	7,82	7,76	7,87	7,84	7,86	7,79	7,87	7,77	7,86	7,60	7,91
A1DW-1	7,81	7,89	7,84	7,80	7,78	7,84	7,80	7,94	7,72	7,73	7,83	7,98	7,88	8,02
A1DW-2	7,82	7,98	7,83	7,76	7,78	7,98	7,86	8,03	7,74	7,81	7,93	7,86	8,00	8,02

A1DW-3	7,76	7,85	7,87	7,86	7,81	7,89			7,87		7,57	7,98	8,02	
A1DW-4	7,77	7,86	7,93		7,84	8,02		7,89					7,83	
A1DW-5		7,91	7,37	7,78	7,80	7,79	7,83	7,99	7,76	7,94	7,80	7,93	8,01	7,94
A2DW-1	7,83	7,88	7,91	7,86	7,86	7,99	7,98	7,89	7,77	7,82	7,95	7,85	8,03	7,99
A2DW-2	7,82	7,88	7,61	7,83	7,84	7,82	8,00	8,03	7,73	7,94	7,77	7,92	7,93	7,86
A2DW-3	7,82													

Appendix G

Local Climatic Data

Temperature

Legend

*** indicates that data is missing or not yet available in the current month
Temperatures in °C

Day	JAN	FEB	MAR	APR	MAY	JUN	JUL	AUG	SEP	OCT	NOV	DEC
1	25,6	25,2	24,6	24	15,9	20,3	15,9	18	20,1	28	***	27,6
2	25,1	25,6	24,4	25,8	14,9	20,5	16,2	7,3	21,5	26,1	***	27,5
3	22,1	27,6	26,7	23,7	17,1	17,9	17	9,6	23,6	24,9	***	29,2
4	23,5	25,8	17,5	23,4	20,1	16,9	18,4	12,3	20,6	24,3	26,8	29,2
5	25	28,2	19	25,1	20,5	20,3	19,9	12,7	20,2	24,3	26,7	26,8
6	27,2	21,3	20,7	24,9	22,2	21,9	22	18,2	22,7	26,4	20,8	28
7	26,8	22,7	24,4	25,7	17,5	21,6	17,7	21,3	21	26,7	22,7	30,1
8	26,2	20,2	26,4	24,8	16,5	19,8	17,6	24	20,7	22,5	26,1	26,3
9	20,9	23	26,6	20,8	16,9	19,6	18,5	23,8	22,6	23,1	27,6	30,3
10	19,4	26	26,9	15,8	18,5	19,9	21,1	18,7	24,9	24,1	27,8	29,1
11	24,8	22,6	26,1	20,5	19,5	17,8	19,9	20	25,7	23,3	31,1	20,5
12	23,2	24,1	25,3	20,8	21,4	21	19,8	24	26,1	24,4	26,7	25,4
13	25,7	24,9	20,6	***	***	22,7	19	22,5	23,2	25,5	17,9	29,1
14	26,6	26	17,7	***	20,9	15,7	17,4	21,5	24	26	26,8	30,9
15	26	25,7	22,5	***	20,6	16,5	19,3	20,4	25,6	26,8	28,8	32,7
16	26,8	27	15,1	***	20,8	16,7	19,1	13,5	25,2	28	25,6	31,2

17	27,1	27,9	***	***	20	17	18,9	18,9	18,8	28,7	23,4	28,3
18	26,8	28,1	***	15	20,7	18,1	21,3	19,5	16,3	27,3	23,8	30,3
19	27,4	27,9	***	18,5	15	17,3	21,1	21,5	21,1	23,9	17,3	***
20	24,8	28,6	***	22,4	11,9	17,9	20,3	21,5	22,3	27,8	21,4	***
21	24,6	26,4	***	22,2	11,6	19,4	20,6	18,3	22	27	25,9	24,1
22	24,3	25,8	***	20,6	14,2	17,6	19,1	19,4	21,3	29,9	27,7	25,4
23	24,8	23,8	***	19,5	14,8	15,9	18,8	16	25,6	30	26,2	25,4
24	19,2	25,4	19,5	17,8	13,8	18,4	19,9	15,4	27,2	32,7	26,6	27,1
25	26,5	26,5	18,1	18,1	14,7	17,9	22,3	15,5	26,5	33,1	29,8	***
26	24,3	20,8	24,2	18,7	17,2	14,8	22,6	16,4	21,5	24,5	21,9	***
27	25,2	19,3	24,5	19,4	20,6	10,2	21,9	17,6	24,1	***	26,8	***
28	25,1	24,6	18,9	20,5	21,2	11,5	21,8	19,8	24,9	***	29,7	***
29	27,3	***	19,3	20,6	19,5	13,3	21,4	23,2	27,2	***	28,5	***
30	26	***	19,8	20	20,7	14,4	20,2	15	27,9	***	30,2	***
31	26	***	20,8	***	20,7	***	17,6	17,7	***	***	***	***
Avg	25	25	22.1	21.1	18.0	17,8	19,6	18,2	23,1	26.5	25.7	27.9
Day	JAN	FEB	MAR	APR	MAY	JUN	JUL	AUG	SEP	OCT	NOV	DEC
1	***	25,7	30,5	12,3	22	20,6	17,7	22,7	28,7	21,1	24,1	25,2
2	***	27,7	30,3	24,9	22,6	14,8	14,4	23,8	31	20	27,6	27,2
3	26,2	28,3	30,2	23,9	24,1	17,9	13,5	24,5	29,3	23,7	27,4	21,2
4	***	30,8	30,3	24,2	23,4	17,7	13,2	23,2	29,7	25,6	28,5	24,4
5	***	30,5	30,3	24,5	23,4	19,3	13,2	16,9	30,5	23,5	28,2	26,7
6	***	31,2	30,4	26,8	23,5	14,3	15,3	16,5	30,6	17,9	25,1	24,8
7	***	25,6	27,5	24,5	25	13,5	16,9	12	25,5	24	22,3	21,8
8	27,9	29,5	22,9	24	24,5	15,1	16,5	17,9	26,2	27,5	21,9	20,5
9	27,4	30,3	24,7	23,8	24,2	16,6	16,6	19,8	29,1	16,8	28,3	24,2
10	26,7	28,1	24,8	25,2	24,7	18,7	18,1	21,4	29,7	21,9	27,4	26,8

11	28,7	22,8	28,3	27,6	23,1	21,5	18,5	23	29,4	14,3	26,5	28,3
12	30,3	25	28,9	16,4	24,7	21,9	19,7	24,4	31,4	23	28,6	27
13	30,4	24,8	29,4	***	25,1	21,9	20,7	23,1	31,3	24,4	30,4	25,3
14	29,4	28,3	29,7	***	25	19,7	19,6	25,2	28,8	25,8	31,5	26,6
15	25,2	29	30,4	***	***	18,5	22,3	18,6	27,3	27,6	31,8	28,1
16	27,5	31,6	30,8	27,2	***	19,6	20,9	17,8	30,2	25,6	27,8	23
17	27,7	28,3	29,7	26,7	23,8	19,2	21,6	19,5	26,2	28,1	26,8	25,1
18	26,7	29	27,1	16	24,3	20,2	19,1	19,6	26,8	25,2	16,8	22,3
19	***	30,6	23,8	23,3	24,3	20,2	20,3	22	28,4	21,3	28,4	19,7
20	24,3	30,9	27,3	24,6	23,1	18,8	19,8	24,6	29,1	21,7	28,6	22,8
21	***	31,5	30,1	26	10,1	18,9	21,8	27,9	30,1	24	24,5	27,2
22	26,5	32,3	29,5	25,2	9,7	18,7	21,4	28,2	30,9	24	26,7	29
23	29,6	29,7	27,1	24,5	12,3	17,3	23,2	25,8	28,6	25,6	26,2	28,7
24	28,5	30,1	25,2	24,1	15,3	17,7	22,9	23	28,9	25,8	24,2	28,8
25	27,1	30	25,7	25,4	16,4	17,8	22,9	19,5	23,1	15,8	26	24,6
26	28,7	26,9	25,8	26,7	17	18,6	19,9	18,6	18,6	12,2	20,2	27,5
27	28,4	28,8	21,9	26	19,2	7,4	22,4	22,8	14,5	14,1	27,7	28,7
28	25,7	30,2	22,7	15	20	15,9	13,3	20	18,5	23,9	19,2	26,3
29	28,8	***	23,1	16,5	21,6	18,9	16,7	22,9	22,3	24,4	17,2	26,7
30	29,6	***	22,6	22,2	21,4	20,1	18,7	26,1	21,1	25,6	19,6	27,1
31	25,1	***	23	***	22,6	***	23,2	27,8	***	22,2	***	29,3
Avg	27.7	28,8	27,2	23.2	21.3	18	18,8	21,9	27,2	22,5	25,7	25,6
Day	JAN	FEB	MAR	APR	MAY	JUN	JUL	AUG	SEP	OCT	NOV	DEC
1	30,6	28,9	25,4	24	22,9	22,3	19,5	23,4	19,8	31,1	30,8	24,9
2	29,7	28	28,6	23,4	16,8	20,5	19,5	22,9	23,3	28,9	31,2	29,7
3	31,7	28,5	28,2	22,2	12,8	19	20,3	22,3	25,8	30,1	31,4	30
4	22,6	27,3	28,6	25,7	15,5	15	20,2	16,1	24,2	26	27,7	27,8

5	26,5	25,6	26,2	23,8	19,5	17,4	16,9	20,7	28,6	26,4	***	27,7
6	26,8	26,3	25,6	24,6	23,5	19,8	14,4	22,5	26,7	23,7	***	27,1
7	26	27,8	25,8	24,4	24,5	21,6	18,7	22,4	27,7	24,2	***	24,7
8	28,1	26	24,7	24,1	24,2	20,9	21,5	22,7	31,2	27,2	***	29,8
9	17,5	24,5	25,5	22,4	24,2	16,3	21,7	21,9	31,8	26,1	16	29,7
10	15	23,9	27,6	23,6	23,4	14,3	12,5	21,5	30,5	26,9	22,5	28,8
11	17	24,8	27,6	22,5	25,3	16,6	12,7	19,8	25,9	26,8	19,1	29,3
12	22,9	25,8	27,7	22,3	22,3	19	10,9	19,7	19,7	29	24,1	29,1
13	27	24,2	26	22,2	24	20,4	15,4	21,9	20,5	31,3	24,4	28,1
14	28	25,1	20,2	20,7	24,5	20	17,7	23,4	22,5	32,2	25,6	27,4
15	27,6	27,7	20,8	21,6	24,3	22,1	18,9	23,6	25,1	28,8	26,9	25,5
16	29,2	27,8	15,3	23,8	24,4	17,7	21,3	23,2	28,7	28,8	29,6	24,3
17	27,2	28,3	11,4	26	25,2	15,3	20	16,8	28	30	27,9	27,4
18	21,5	29,5	14,5	25,8	20,4	17,9	16,7	16,1	23,8	28	25,7	27,3
19	20,5	29,6	22,8	25,1	19,8	***	18,2	16,9	27,4	26,7	22,8	29
20	19,3	28,2	23,9	22,1	18,4	***	18,9	23,9	22,9	28,6	23,9	30,1
21	21	28,3	22,5	14	19,2	***	19,6	24,2	17,6	28,4	23,3	32
22	20,8	28,4	21	18,9	20,5	20	20	26,1	23,9	30,2	25,7	30,6
23	22,3	28	24,4	21	19,8	20,2	18,3	26,5	27,3	23	28,8	31
24	21,6	27,6	24,3	21	17,6	17,8	16,8	25,2	24,8	22,6	31	25,5
25	22,9	27,7	25,8	22,6	12,9	20,1	17,9	26,3	26,1	24,8	31,6	26,4
26	25	17,9	25,9	23,6	18,1	19,9	18,8	25	29,1	22,8	28,5	25,3
27	25,5	***	25,8	24,7	16	20	20,2	25,8	24,6	25,8	28,4	27,4
28	27	28,7	26,4	23,8	20,3	19,6	20,1	24,9	20,4	28,6	29,1	25
29	26,5	27,2	24,5	22,2	20,8	19,7	17,8	25,7	25,7	29,7	30,7	28,7
30	27,6	***	22,5	22	20,6	18,9	22,1	26,8	29,3	27,8	29,2	31,2
31	28,9	***	24,2	***	21,6	***	22,7	23,2	***	30,3	***	30,1
Avg	24,6	26.8	24	22,8	20,8	19.0	18,4	22,6	25,4	27,6	26.8	28,1
Day	JAN	FEB	MAR	APR	MAY	JUN	JUL	AUG	SEP	OCT	NOV	DEC

1	27,5	25,6	24,8	24,1	21,6	19,3	15,8	11,8	27,8	24,1	24,6	26,4
2	28,2	27,2	25,6	26,2	19,7	22,1	15,4	13,3	27,9	23,9	25,4	25,5
3	28,4	24,8	26,9	24,8	17,8	22,1	16,4	16,6	28,3	23,1	23,6	28
4	30,2	22,5	25,7	23,8	23,7	23,3	13,1	19,7	27,5	20,6	19,7	28,6
5	28,8	20,5	24,1	24,6	24,7	23,3	14,5	22,6	27,7	20,3	25,2	28,1
6	28,8	26,2	25,7	26,5	21,3	23,2	16	23,5	26,8	28	27,8	27,4
7	30,7	25,8	26,8	23,3	23,5	23	17	21,2	27,4	30,4	23,8	29
8	29,4	26,6	28	24,7	21,3	14,7	17,5	20,7	28	32	28,2	26
9	29,2	27,5	25,8	25,2	17,6	14,6	20,1	21,4	27,8	30,4	24,4	25,3
10	24,5	26,1	22,3	25,6	18,6	10,8	21,2	23,3	21,2	29,9	26,8	27,5
11	26,7	25,4	22,1	25,1	19,7	12,1	20	24,5	23,4	22,4	27,8	26
12	25	20,2	25,7	27,1	20,4	17,3	18,7	23,6	24,2	25,1	29,4	25,5
13	22,7	23,8	23,6	26,8	20,1	18,7	19,9	17,8	25,2	27,6	29,6	29,7
14	28,1	26,2	25,3	21,5	19,5	21,1	14,7	18,4	29,2	27,8	28,6	18,9
15	27,3	26,8	22,4	25	20,6	22,4	16,7	20,1	29,1	27,9	28,8	21,4
16	29,4	28,1	24,8	26,1	18,2	20,2	15,1	19,7	30,7	29,5	26,5	30,7
17	29,6	28,3	27,5	25,3	17,7	19,3	17,1	17,1	30,1	26,3	14,3	31,6
18	28,5	27,2	23,8	26	20,2	19,6	17,4	17,5	23	26,6	12,7	32,8
19	28,9	28,8	23	26,8	22,8	17,1	18,2	18,2	24	27	18,4	31,4
20	26,1	27,9	21,1	26,6	20,2	16,7	17,5	14,9	22,4	24,8	11,9	28,2
21	26,8	28,8	23,1	16,9	16,3	19,3	17,4	20,7	26,3	29,7	18,9	22,1
22	22,7	27,7	23,6	19,1	20,5	20	17,4	20,3	27,5	28,1	24,2	29,7
23	23,4	25,5	26,2	21,3	21,7	16,6	15,3	22,3	24,2	27,6	26,3	30
24	26,4	21,3	25,7	22,2	21	14,6	11,6	21,3	26,4	27,8	27,3	30,7
25	27,3	25,7	26,7	23,7	22,4	17,9	13,2	20,8	20,7	25,8	28	29,6
26	26,8	27,8	28,1	21,9	22,4	12,6	16	23,7	27,6	25,5	30,6	27,5
27	27,3	24,8	27	21,7	21,9	16,5	17,1	21,5	29,2	24,4	29	28,5
28	21,2	24,9	28,4	24,7	22,4	17,5	16,6	21,4	29,4	26,3	28,4	25,1

29	20,3	***	27,1	26,1	22,2	15,9	18,4	24,2	18,4	25,8	27,9	29,4
30	23,1	***	25,9	25,5	20,6	14,7	19,1	26,8	20,2	23	27,2	27,4
31	27,6	***	27,7	***	18,6	***	19,8	27	***	20,5	***	29,4
Avg	26,8	25,8	25,3	24,3	20,6	18,2	16,9	20,5	26,1	26,2	24,8	27,7
Day	JAN	FEB	MAR	APR	MAY	JUN	JUL	AUG	SEP	OCT	NOV	DEC
1	29,6	27,2	27,8	20,1	20	17,4	17,7	20,6	27,2	29,2	26,7	27,9
2	27,2	29	29,3	17,5	21	18,1	15,6	21,4	28,7	30,5	27,5	29,8
3	23,9	28	25,6	24,6	14,7	19,1	17,8	22	26,6	31,7	29,4	24,8
4	25,4	27,4	24,7	23,9	20	19,6	15	21,2	27,1	31,5	30,2	30,2
5	18,4	26,8	24,4	19,7	22,5	21,2	15,7	21,4	28,8	27,7	28,4	31,6
6	25,4	27,5	26,2	22,6	23,6	23,6	17,4	21,8	29,2	28,3	29	30,3
7	29,8	28	24,8	23,9	22,3	23,1	19,4	20,5	29	28,6	28,2	24,4
8	25,5	29,7	24,8	25,7	23,4	22,9	17,6	22,1	25,7	29,3	27,2	27,5
9	24,2	28,3	26,8	21,6	22,9	19,5	17,1	19,2	26,5	31,8	20,8	27,7
10	24,8	28,1	28,7	26,9	23,1	18,1	19,6	15,5	26,5	30,8	23,3	29,7
11	26	29,6	30,7	22,4	21,7	16,9	20	14,7	21,8	31,5	26,3	29,4
12	27	31,2	31,4	26,3	21,7	19,3	10,8	16	25,9	31,6	30,4	20,2
13	26,1	32,8	30,9	27,5	19,8	21	13,3	19,1	28,6	23,9	33	21,8
14	25,1	27,3	28,5	26,2	23	20,3	15,8	23,9	28	21,8	30,7	23,1
15	26,4	27,6	27	25,7	23,9	11,5	16,8	25,4	28,2	23,6	21	***
16	27,7	27,8	25,3	25,4	21	10,7	11,8	25,3	30,4	22,1	24,6	24,1
17	27,7	26,2	27,6	24,6	21	12,4	19,4	22,5	23,1	21	23,9	28,6
18	22,2	26,4	28	25,6	22,8	15	18,5	24,2	25,1	25,7	16,3	29,3
19	27,7	27,6	25,4	23,5	23,1	14,4	18,9	25,5	27,4	27,4	24,1	28
20	23,9	26,4	25,1	20,6	21,6	17,7	19,1	19,6	27,8	29,5	29,3	24,9
21	20,4	27,9	25,6	20	21,1	18,8	18,1	21,4	27	30	29,1	24
22	25,3	27,8	24,1	21,7	21,2	19,6	19,5	25,7	24	29,3	26,1	28,1

23	26,9	26,4	26,1	22,5	21,8	17,6	19,9	21,6	28,1	28	29	29,8
24	26,3	26,2	19,1	13,2	23,1	20,1	19,4	21,7	28,8	28,3	24,8	28,7
25	27,7	19,9	26,9	16	23,3	22,7	21	20,5	28,8	26,9	24,6	31,2
26	25,1	24,4	27,4	13,5	22,3	25,2	20,8	21,8	28,4	28,1	25,3	25,9
27	24,8	23	26	14,2	21,4	22	22,1	25,8	24,1	27,6	28,2	25,1
28	27,2	26,5	28	21,1	23,1	14,8	21,8	26,3	17,6	26,5	29,4	***
29	27,5	***	20	22,5	21,1	16,7	21,8	27,5	23,2	27,7	31,7	***
30	24,7	***	25,3	22,8	13,9	18,7	18,3	25,9	27,3	30	24,8	27
31	26,3	***	26,6	***	15,3	***	18	25,3	***	30,3	***	27
Avg	25,7	27,3	26,4	22,1	21,3	18,6	18	22,1	26,6	28,1	26,8	27.1
Day	JAN	FEB	MAR	APR	MAY	JUN	JUL	AUG	SEP	OCT	NOV	DEC
1	22,5	25,2	27,4	27,5	18	15,6	16,7	18,3	25,4	22,7	23,6	25,4
2	26,5	23,9	27,5	25,5	20,4	19,7	19,9	17,1	27,5	19	25,2	27,5
3	27,4	25	29,4	27,1	19,9	22,1	19,6	17,3	25,1	22,8	25	31,8
4	27,6	24,9	28	25,6	23,5	21,3	13,5	19	25,6	22,1	28,1	26,1
5	25,3	25,4	27,6	18,5	22,4	22,3	9	21,5	27,2	22,1	25,7	26,6
6	23,7	26,4	28,2	16,7	22,2	21,3	14,7	20,1	27,4	20,6	28	30,1
7	23,1	28,1	28	23,3	17,9	19	15,5	16,7	27,8	22,7	26,5	33,3
8	22,6	28,3	28,2	23	22	13,3	15,5	21,1	26,2	25,2	30	29,8
9	23,1	28,3	28,5	22,8	20,5	9,4	15,1	21,3	27,1	26,3	33,4	18,2
10	27,1	28,2	28,4	24,9	20,9	14,9	13,9	21,5	29,2	27,7	33,2	20,7
11	26,3	28,4	29,8	23,6	22,2	20,5	16,5	23,1	25,1	27,4	31,4	26,4
12	26,9	29,6	30,9	***	22,1	19,4	16,7	25	25,5	28,6	32,2	29,8
13	27,7	25,1	28,7	***	21,8	19,2	15,4	24,9	26	27,6	33,8	30,4
14	22,5	27,4	20,7	***	18,6	19,1	15	21,6	25,3	27,5	29,7	25,8
15	24,4	27,3	26,8	***	21,7	18,6	16,1	11,2	25,2	28,9	27,8	29,6
16	23,3	26,8	24	***	21,2	20,9	16,8	12,4	23,8	29,1	30,3	30,8

17	24	24	26,2	***	22,5	14,7	18	15,5	22,4	25,9	32,9	29,1
18	22,6	21,6	27,6	14,5	22,7	16,8	18,5	17,1	26,6	24,5	31,2	30,5
19	27,5	25,4	20,9	20,5	21,6	19,8	20,4	19,4	25,7	25,8	30,5	32,9
20	27,6	28,2	23,3	20,5	20,9	20,1	21,6	22,5	23	21,6	24,1	30,9
21	27,2	26,3	25,7	20,6	21,9	20,2	22,7	23,6	25,6	24	25,8	32,2
22	26,8	25,7	26,8	21,8	22,5	19,7	22	23,8	25,8	28,1	25,3	29
23	27,4	26,3	29	18,2	22,3	19,6	21,1	24	26,4	33,7	33,3	29,9
24	26,5	25,9	29,4	18,4	23,4	10,6	20,3	18,7	17,2	35,3	23,8	22,2
25	24,3	25,7	27,4	23,2	17,1	9,8	18	23,4	22	33,3	24,4	27,7
26	23	25,4	23,5	21,1	13,3	15,8	11,4	27,9	25,7	33,2	25,8	25,8
27	25,5	25,8	20,2	20,3	16,6	17,5	16,7	27,5	29,2	30,2	27,1	24,2
28	27,9	28,2	26,3	18,8	16,8	19,4	16,3	18,2	28,3	30,5	27,6	29,1
29	27	***	26,3	20,4	20,5	20,1	10,3	22,2	29,1	26,7	27,4	27,6
30	28,3	***	28,8	21,3	20,5	20,6	16,8	25,4	27,7	27,6	24	27
31	26,8	***	28,2	***	14,4	***	17,2	26,4	***	28,2	***	25,2
Avg	25,6	26,3	26,8	21.6	20,4	18	16,8	20,9	25,8	26,7	28,2	27,9
Day	JAN	FEB	MAR	APR	MAY	JUN	JUL	AUG	SEP	OCT	NOV	DEC
1	29,6	30,1	27,3	21,8	28,7	21,2	23,5	16,8	24,8	27	19	20
2	31,9	30,3	27,3	21,4	27,7	20,9	22,8	20,6	23	29,5	21,3	20
3	33,5	30,1	27,9	23,5	27,1	22,2	22,5	21,6	25,9	30,3	24,3	20
4	32,1	31,5	31,2	25,2	28,5	20,2	21,9	23,2	26,4	32,6	28,5	25,6
5	33,3	28,9	30,9	24,7	29,3	19,4	23,4	22,7	16,2	32,1	32,1	27,7
6	32,1	27,2	25,7	23,6	26,7	20,6	20,3	18	11,7	31,6	32,5	24,7
7	30,1	27	27,2	22,8	27	21	20,2	5,1	14	31,8	30,8	27,1
8	29,8	31	27,3	24,6	23,6	21	16,8	12,5	18,5	26,9	22,6	30,1
9	25,3	25,4	29,6	24,9	25,4	10,5	19,8	16,8	23,2	22	21,2	29,3
10	29,9	23,5	29,8	22,2	25,1	12,9	20,7	20,4	24,7	26,5	26,9	25,4

11	31,3	28,5	28	23,5	25,4	16,3	21,1	22,1	24,7	24,6	26,2	22,2
12	30,9	29	27,1	23,2	23	20,5	19,8	13,4	23,7	17,7	26,7	22
13	29,3	30	29,4	22,3	22,2	22	18	18,4	25,1	21,5	29,5	24,9
14	26,7	30,9	29,6	22,5	23,3	17	14,4	21,1	26,1	22,8	27	27,7
15	27,7	31	19	23,6	21,5	16,1	12,3	24,8	14,7	23,5	28,2	26,2
16	27,7	31,6	19	24,7	20,7	16,4	14,9	23,3	18,6	28,4	31,8	28,1
17	26,7	31,1	26,9	24,7	23,4	15,2	19,3	22,7	20,4	24,9	31,7	28
18	25,2	28,7	27,5	24	22,8	20,8	19,2	17,3	26	27,6	29,4	27,1
19	28,5	29,7	26,1	23,4	24,5	19,7	20,3	21,6	27,9	30,4	31,6	26,7
20	29,5	28,2	28,1	25,6	22,1	20,5	21,5	26,5	28,5	24,2	33,2	28,5
21	30,4	30,2	26,8	25,3	18,6	16,5	22,5	27,3	25,9	23,8	32	25,9
22	29	30,7	28,5	23,4	18,8	15,3	23,3	26,9	23,8	26,7	27,1	27,5
23	29,7	29,7	27,4	20,6	21,7	18,1	21,8	28,8	24	24,9	27,8	29,3
24	29,3	26,6	27,8	18,3	24	13,8	18,8	29	23,5	17,6	19,9	30,7
25	27,9	27,4	26,6	15,2	22,7	13,5	20,8	28,8	25,2	20	23,5	29,8
26	28,4	28,5	27,5	21,9	23,1	17,6	21,2	28,3	25,6	24,9	26,9	24,7
27	30,3	28	28,1	24,3	20,7	21,6	21,2	23,6	28,4	26,9	28,4	26,2
28	29,9	27,6	24,8	26,9	18,6	21,2	21,1	24,1	27,3	24,5	27,1	29,1
29	28,4	27,4	24	27,2	19,9	23,4	19,8	25,7	19,4	24,1	29,5	30,6
30	30	***	21,7	28,3	22	24,8	20,4	27	25,6	26,4	29,2	31
31	32,7	***	21,4	***	20,7	***	19,9	27,8	***	22,5	***	27,4
Avg	29,6	29	26,8	23,5	23,5	18,7	20,1	22,1	23,1	25,7	27,5	26,6
Day	JAN	FEB	MAR	APR	MAY	JUN	JUL	AUG	SEP	OCT	NOV	DEC
1	29	27,3	24,7	26	23,8	23,9	23,6	19,1	17	22,6	26,5	25,4
2	26,5	29,4	23,9	26,9	24,1	23,5	22,7	***	21,6	27,8	25,7	25,5
3	27,1	31,4	27,6	22,5	24,4	22,9	23,2	***	25,1	30,3	23,7	24,2
4	30,8	30	28,7	18,4	20,5	24,7	21,4	***	26,5	29,5	28,5	28

5	24,6	26,3	28,4	22,1	20,1	23,7	14,6	15,9	25	30,7	30,1	26,6
6	27,9	25,2	30,5	25,5	20,8	22,9	16	18,5	25,8	32	30,4	23,6
7	30,4	30,1	25,2	27,5	19,6	23,9	21,6	20,9	25,7	28,1	28,4	24,2
8	31,2	29,4	27,2	28,7	21,2	23,4	23	22,8	28,4	25,8	30,8	24,7
9	32	28,6	31,1	29	23,7	15,2	22,7	19,7	30,4	29,9	31,1	24,6
10	33	26,8	25,1	27,5	23	16,1	18,3	19,1	28,9	30,3	29,8	16,9
11	27,4	27,9	23,4	18,6	18,2	18,5	16,9	19,5	29,6	31,8	28,7	25,5
12	26,8	27,6	24,3	18	20,6	20	17,9	16,3	25,9	33,3	29,1	26,5
13	28,4	28,5	25	20,1	22,1	21,4	18,7	23,4	27	27	31,7	29
14	30,6	31	23,4	25,5	22,5	22,3	20,1	21,9	29,5	24,5	31,3	29,3
15	30,1	31,4	25,9	27,1	21,3	19,2	18,9	22,7	30,3	26,3	30,6	31,2
16	26,3	27,8	27,3	28,5	23	18,2	21,5	20,8	31,4	30,4	29,8	31,1
17	26	28,6	30,3	28,5	22,2	19,2	22,5	26	30,3	29,5	30,8	27,8
18	21,7	28,1	28,8	20	19,6	16,6	17,1	18,9	30,6	29,2	32	27
19	24,1	31,7	30,5	15,9	18,5	18,7	18,5	19,7	28,5	27,5	29,5	23,9
20	20,6	32,1	28,2	12,6	20,4	21,3	18,8	20,6	29,1	14,2	29	25,6
21	27	29,6	29,4	19,5	21,7	21	19	23	20,7	19,1	22,4	28,8
22	28,1	30,3	32	21,8	22,1	21,8	17,8	20,8	15	21,8	23,6	29,7
23	31,6	32,8	31,4	23,3	22,5	19,3	18,9	18,9	22,5	21,8	27,4	28,1
24	32,7	30,8	28,1	21,6	23	19,9	22,6	23,2	30,9	21,7	25,7	22,4
25	34,4	24,6	28,4	24,3	23,6	21,8	22,5	25,4	31,4	25	26,5	21,3
26	30,3	30,3	24,5	24,5	24,3	23,7	22,8	23,1	31,3	26,1	29,4	24,6
27	29,4	32,3	23,2	25,6	24,4	23,6	23,9	24,4	29,6	26,9	29,6	24,8
28	30,7	30,7	25,8	25,8	23,7	20,2	23	26,2	28,3	20,7	23,6	27,3
29	28,1	***	27,4	25,7	23,3	22,3	19,8	25	25	24,6	22,5	20,1
30	27	***	26	22,7	25,2	23,9	17,7	26,1	17,4	28,3	30	25,7
31	29,9	***	24,3	***	25	***	18,4	12,9	***	28,2	***	28,7
Avg	28,5	29,3	27,1	23,5	22,2	21,1	20,1	21.2	26,6	26,6	28,3	25,9
Day	JAN	FEB	MAR	APR	MAY	JUN	JUL	AUG	SEP	OCT	NOV	DEC

1	28,8	28,1	22,9	23,3	26,8	26,7	21,3	22,8	21,1	24,9	27	27,6
2	31,3	29,4	18,5	25	28,1	25,8	18,8	22,1	22,3	24,2	20,9	28,3
3	31	21,5	20,5	25,9	28,2	24,5	19,8	20,8	22,9	24,9	23,1	28,6
4	30,5	26,1	21,1	24,1	26,1	23,4	18,8	20,3	23,9	22,3	24	30,7
5	29,5	27,2	21,2	25,9	25,5	22,6	20,7	23,2	24	25	25,2	31,9
6	24,8	28,1	26,2	24,5	20,2	11,8	20,4	24,8	26,3	26,5	26,7	29,1
7	27,4	27,7	25,6	24,5	21,1	17	17,1	24	28,8	27,5	29	29,1
8	26,8	29,1	26,5	23,5	22,4	18,5	11,6	20,6	31	31	28,1	25,7
9	29	26,2	24,2	21,6	25,1	20,3	13,3	17,7	28,7	32	29,4	20,2
10	30,6	28,7	21	23,6	25,2	19,3	15,5	21	30,8	29,5	22,3	26,1
11	29,9	30,7	20,4	23,2	22,7	19	15,9	20,8	30,3	22	17,4	28,4
12	30,1	31,1	25,1	24,1	21,1	18,9	17,9	21	31,3	29	18,2	25,7
13	32,7	29,2	22,1	23,1	24,2	19,8	20	22	29,8	32,5	26,8	27,1
14	29	27,7	18,2	18,2	23,9	21	20,6	25,2	31,3	29,7	30,9	25,9
15	27,9	27	25,4	24,2	24,9	23,8	18,6	25,1	30,8	25,7	24,1	27,6
16	31,8	29,1	27,3	22	25,2	21,8	21,3	17,4	29,9	27,2	24,6	20,4
17	32,5	28	26,2	18,4	23,6	21,9	22,3	18,3	30,4	21	19,8	23
18	32,4	30,1	26,7	24	18,3	23,4	24,3	21,8	30,2	23,6	19,9	26,5
19	26,4	28,7	27,1	26	19,7	15	18,3	25,9	23,7	28,8	23,3	27,7
20	28,7	28,1	28,4	26,2	18,4	20,2	20	25,9	24,1	30,5	25,1	30,1
21	27,9	25,9	24,4	26,1	21,3	20,5	19,8	25,1	22,9	30,4	27,3	30,8
22	27,8	26,7	23,7	24,7	18,8	19,5	19,9	17,7	24,3	29,3	28,7	30,2
23	28,3	27,9	27,2	19,8	22,9	19,8	22,9	19,2	25,8	29,1	21,9	28,3
24	30,6	26,5	26,3	22,2	21,7	20,8	24,5	19,4	25,9	30,3	26,9	28,9
25	31,7	28	25,5	22,5	21,2	20,8	23,3	21,6	28,9	29	29,7	31,3
26	27,7	27	27,4	24,5	24,4	22,7	18,6	24,8	30,6	19,4	29,9	30,3
27	24,8	26,7	27,3	24	25,9	22,9	18,9	25,2	31	23,3	19	22,7
28	26,3	27,9	24,5	21,4	23,8	18,2	21,5	25,6	26,3	26,3	26,7	24,9

29	29,6	***	24,6	25	24,9	21,5	18,6	12,9	23,9	29,7	28,1	27,8
30	29	***	26,4	27,9	25,8	21,4	18,8	18,8	26,1	32,7	26,5	30,6
31	26,1	***	25,8	***	26,2	***	20,6	20,3	***	31,6	***	26,5
Avg	29,1	27,8	24,4	23,6	23,5	20,8	19,5	21,7	27,2	27,4	25	27,5
Day	JAN	FEB	MAR	APR	MAY	JUN	JUL	AUG	SEP	OCT	NOV	DEC
1	25,7	29,2	25,9	27,3	25,7	23,3	19,6	19,8	26,1	28,5	35,6	33,6
2	28,5	28,9	23,7	28,9	25,6	20,6	21,4	19,5	22,7	27,3	24,4	31,2
3	28,8	30,4	25	26	26,7	16,1	21	21,2	22,4	29,9	23,2	26,1
4	31,7	31,4	28,1	24,5	27,2	13,8	21,3	23,9	12,4	32,1	23,5	31,1
5	31,3	31,4	28,9	26,1	28,1	16,9	22,4	22,3	13,8	33,2	26	33,7
6	32,2	31,8	28,7	27	28,4	16,2	23,3	22,7	15,6	32,8	27,7	36,2
7	29,3	30,4	25,1	20,7	24,4	16,9	18,9	24,1	22,1	33,3	31,6	35,7
8	28,8	31	28,6	21,9	23,1	19,6	19,7	24,5	24,7	33,8	32,2	29,6
9	30,7	32,2	27,9	21,9	25,1	20,9	22,4	24,5	26,6	33,5	35,5	31
10	29,4	33,1	29,5	20,8	23,6	18,6	20,8	24,9	30,6	31,6	36	33,5
11	28,4	33,5	29,9	24	23	15,7	18,6	19,6	30,2	33	36,5	34,1
12	30	31	26,9	25	23,1	18,3	21,7	20,4	22,6	30,8	34,4	28,9
13	28,2	30,3	29,2	25,3	25,5	20,5	23,2	23,7	24,8	32,5	31,3	32,2
14	24,4	28,9	29,3	27	27	21,3	20,9	26	24,7	28,3	30,2	29,4
15	27,8	29,1	30,2	25,8	27,9	22,6	20,6	25,6	25,5	27,2	32,3	28,4
16	27,7	27,2	29,8	26,2	28,1	22,3	22,4	27,6	28,4	29,4	27	28,7
17	30,4	26,1	30,3	22,8	26,6	12,6	14,6	26,5	29,9	24,8	26,1	30
18	25,9	29,7	28,4	21	24,7	18	20,4	27,4	29,2	28,8	26,3	31,2
19	27,8	31	27,5	21,5	25,3	20,6	23,4	26,6	24,4	31	27	33,8
20	27	31,8	29,6	23,7	25,8	18,2	23,8	24,7	***	28,5	28,5	33,2
21	28	21,9	27,3	25,7	26	19,1	22,3	26,6	***	29	28,7	33,6
22	29	30,2	20,8	23	23,9	20,6	19,5	28,8	17,3	28,1	26,1	33,7

23	31,1	27,4	25,2	25,1	20,9	20,6	17	26,7	29,8	29	28,8	33,1
24	30,2	28,9	25,5	21	23,5	21,5	15,5	26,5	31,5	31,1	31,3	35
25	31	26,7	23,2	26,1	24,6	21,4	13,1	27,4	30,9	31,6	31,8	26,8
26	29,4	28	25,8	27,1	25,3	19,9	15,3	27,8	31,9	31	32,5	29,8
27	30,3	26,9	28,2	28,4	25,7	12,2	18,4	27,6	28,5	26,9	32,9	29,9
28	21,4	26,4	24,3	27,1	25,5	18,2	18,6	28,1	30,5	29,2	22,3	32,1
29	27,2	***	26,3	27,2	26	21,4	21,4	29,5	32,5	28,1	28,5	33
30	27,3	***	25,1	25,1	26,2	20,9	21,4	29	31,7	31,2	31	31,7
31	26,2	***	25,5	***	25,1	***	13,9	29	***	34,2	***	31,1
Avg	28,6	29,5	27,1	24,8	25,4	19	19,9	25,2	25.8	30,3	29,6	31,7
Day	JAN	FEB	MAR	APR	MAY	JUN	JUL	AUG	SEP	OCT	NOV	DEC
1	33,3	29,4	30,2	29,4	19,7	20,5	22,7	15,3	25	28,6	31,7	31,9
2	29,6	31,6	31,4	30,1	23,2	20,2	17,4	20,3	26,2	24,9	29,6	29,7
3	31,8	30,7	30,3	30,1	24,9	***	16,6	19,7	27,2	20,5	27,7	30,1
4	33,6	32,1	30,8	27	23,5	***	16,2	17,1	27	19,1	30,9	33,4
5	35,5	26	31	25,1	24,3	***	16,8	21,3	26,9	26,4	26	27,8
6	38,3	29,3	31,6	19,5	24,2	19,9	21,6	24,7	28	31,9	29,1	27,3
7	38,8	31,5	30,9	19,3	23	19,4	19,7	25,4	28,7	32,9	25,6	29,1
8	33,9	29,7	26	21,2	17,7	20,5	18,9	24,7	30,9	28,2	28,8	30,1
9	28,4	28,6	20,9	23,4	20	21	21,3	21,5	30	25,7	28,4	31,2
10	29,2	28,7	24,6	24,7	19,3	23	19,9	24	28,9	27,7	29,5	30,9
11	28,9	32,2	27,1	25,9	24,2	19,1	19,4	23,8	24,8	32	22	27,8
12	27	34,2	26,4	27,4	25,4	13,8	19,9	23,1	25,3	32,5	27	25,7
13	29,2	34,5	28,2	28,1	23,9	8	19,2	22,7	27,8	29	28,7	26,3
14	26,1	33,2	26,9	28,8	14,6	10,5	18,7	24,6	20,1	26,7	28,7	25,4
15	29,6	32	26,6	27,1	16,6	20,2	18,5	25,6	26,5	30	24,3	27,4
16	23,6	33,7	26,7	28	20,7	21,3	18,9	20,4	28,2	29,8	25	29,8

17	27,4	30,4	20,1	30,3	22,9	20,5	18,3	20,8	22,9	29,9	29,8	30,1
18	25,4	31	26,6	28,9	20,7	19,4	19,3	20,8	10,7	23,5	29,3	29,8
19	27,1	31,1	29,2	28,1	21,6	22,1	19,9	22,1	21,1	20,6	22,9	31,7
20	26,1	32,2	28,3	28,6	21	22,7	22,1	25,5	23,4	25,1	27,6	31,7
21	25,6	32,8	28,9	18,1	20,2	22,6	23,1	26,2	27,4	25,1	23,3	30,8
22	28,2	32,1	25,9	26,4	21,2	18,1	24,4	19,5	30	29,9	29,8	32,1
23	27	29,5	24,1	27,9	21	18,2	21,9	19,9	30,7	29,6	27,6	32,7
24	24	29,7	28,6	27,2	21,2	19,5	19,1	23	28,7	29,7	19,8	26,8
25	29,8	28,6	27,7	28,4	20,3	20	14,5	25,7	28,9	30,5	25,9	20,5
26	28,3	28,3	25,5	28,4	18,8	20,3	17,1	27,7	26,2	29,2	26	19,7
27	29,3	28,2	27,5	25,2	19,1	19,8	14,8	25,5	26,9	32,3	26	25,9
28	29,7	25	28,2	27	20,8	20,6	17,1	26,5	26,1	32,6	30,8	23,8
29	29,6	28,4	29,6	28,7	21,6	20,8	17,9	28,8	26	33,9	32,6	27,3
30	30,8	***	30	25,2	21,5	20,1	19	28,7	27,8	34,3	32,8	27,1
31	30,4	***	29,7	***	21,5	***	20,3	26,7	***	35,3	***	29
Avg	29,5	30,5	27,7	26,5	21,2	19.3	19,2	23,3	26,3	28,6	27,6	28,5
Day	JAN	FEB	MAR	APR	MAY	JUN	JUL	AUG	SEP	OCT	NOV	DEC
1	25,1	26,9	28,2	28,4	18,7	15,9	18,2	19,1	26,6	24,3	24,2	26,1
2	27,6	25,6	29,4	25,8	20,4	19,1	20,2	18,3	29,3	20,1	25,3	27,9
3	28,7	25,8	31,3	28,8	21,9	20,7	20,3	17,9	26,6	24,5	25,1	30,4
4	28,5	25,9	29,9	27,1	24,7	21,3	16,4	18,8	26,9	23,8	29,3	26,1
5	26,4	26,2	28,7	20,7	22,2	22,1	11,3	21,9	27,5	23,5	27	24,3
6	25	27,8	29,5	18,3	22,6	21,9	16,4	20,7	28,9	21,1	28,4	28,1
7	24	29,5	29,5	25,6	18,9	21,1	17,1	17,5	29	24,5	27,2	32
8	23,8	27,9	29,5	24,1	23,3	14,3	16,6	20,3	27,2	26,5	30,8	29,3
9	23,6	28,6	29,1	22,7	21,7	10,8	16,1	23,1	28,3	27,9	***	18
10	27,7	29,2	30	25,7	21,4	17,5	15,9	23,3	29,5	28,9	33,5	21

11	27,3	29,1	31,6	25	22,9	20,1	17,8	24,4	26,7	28,9	32,4	25,9
12	27,7	31	31,7	24,8	23,2	20,7	17,1	24,7	26,4	29,6	32,2	28,9
13	29,4	27,8	31,6	22	22,7	20,8	16,6	25,5	27	28,7	33,8	29,5
14	22,2	29	22,3	22,6	19,5	18,5	16	22,7	26,8	28,2	28,7	24,1
15	24,6	28,2	26,7	23,3	22,9	18,8	17,4	13,8	26,7	29,4	29,6	***
16	24,4	28,6	24,6	15,4	22,5	21,1	18	14,3	25,8	30,2	31,6	***
17	27,1	23,7	27,1	21	23,1	17	19,3	16,7	23,2	27,3	32,9	28,5
18	23,7	21,6	27,2	15,4	24	17	19,5	17,9	26,8	26,5	31,7	30,5
19	28,9	26,3	23	21,3	23,5	18,7	20,4	19	27,3	26,6	32	32,6
20	28	29,8	24,9	21,7	21,7	21,5	22,3	22,7	24	23,7	26,5	***
21	27,7	27,6	26,7	18,7	23,6	19,8	23,4	24,2	26,3	25,1	25,7	31,3
22	27,1	27,1	28,3	22,9	22,7	19,2	22,6	25,2	27	29	25,8	30,5
23	27,8	27,5	30,3	18,9	22,3	19,6	21,3	26	26,7	35,1	22,9	27,9
24	27,1	27,4	30,3	19,6	23,5	11,8	20,7	20,2	18,6	36,2	24,7	20,8
25	25	26,7	28,7	23,1	18,4	11,1	20,1	23,5	23,2	33,6	25,1	26,8
26	25,1	27	25,5	21,4	14,8	16,9	13,7	26	26,3	33,9	26,7	27
27	27,2	26,5	21	21,5	16,7	17,1	18,5	28,8	30	31,6	27,5	24,6
28	28,2	28,6	27	20,7	16,8	19,6	17,3	20,3	29,2	31,9	27,2	26,8
29	29,7	***	26,2	20,6	19,9	20,5	11,4	22,6	29,1	27	27,6	27,5
30	30,5	***	30,8	22	21,2	22,3	17,9	25,4	29,5	***	24,2	24,9
31	27,7	***	29,3	***	16,3	***	18,9	26,9	***	27	***	25,9
Avg	26,7	27,4	28,1	22,3	21,2	18,6	18	21,7	26,9	27.8	28.3	27.0
Day	JAN	FEB	MAR	APR	MAY	JUN	JUL	AUG	SEP	OCT	NOV	DEC
1	28,5	28,9	28,2	22,8	29,1	21,6	23,6	18,8	25,9	27,2	19,9	21,2
2	30,9	30	29,7	22,8	27,7	22,1	22,5	19,8	23,3	29,6	22,3	20,1
3	32,7	29,8	30	24,2	27,1	22,7	22,7	22,6	26,8	30,7	24,4	21,6
4	31,8	31	33,6	25,8	28,9	19,7	21,7	23,2	26,5	32,6	28,3	27,6

5	32	28,4	32,7	25	29,1	19,5	23,3	23	17,6	32,7	31,8	28,2
6	30,9	28,3	27,3	23,2	26,4	20,6	19,9	19,1	13,9	32,4	33,5	24,6
7	29	28,2	28,2	23,3	27,2	20	21,3	7,1	14,4	32,2	31,7	27,3
8	30,5	30,6	29	25,7	23,9	21,5	18,1	12,3	19,4	27,7	23,5	31,5
9	24	25,3	30,8	25,5	26,5	12,6	19,9	17,8	22,4	24	22,4	30,1
10	28,5	23,7	30,8	23,1	26,1	14,5	21,8	19,9	25,9	26,7	27,6	26,6
11	29,6	28,4	28,4	24	25,9	16,2	22,1	23,2	24,2	28,9	27	22
12	30,8	28,5	28,8	24,2	23,1	18,8	20,2	14	23,9	16,1	28,1	23,3
13	31,5	29,2	30,6	23,2	23,4	21,5	19,4	21,3	25,5	22	30	25,4
14	29,8	30,2	30,1	22,4	23,6	17,9	15,4	25	26,9	22,7	28,1	27,8
15	28,2	31,7	20,2	23,1	23,3	16,6	14,3	23	16,2	23,8	28,6	27,8
16	28,1	31,5	19,6	25,4	21,6	16,8	15,9	23,8	19	27,6	31,7	29,7
17	28	30,7	27,9	24,5	23,2	16,9	20	18,7	20,2	26	32,3	28,4
18	25,9	29,9	27,9	25,3	24,3	21	19,3	21,7	26,9	27,4	30,7	27,7
19	27,6	29,6	25,5	23,9	24,3	20,8	20,2	26,3	29	26	31,2	28,1
20	29,5	29	28,5	25,7	23,1	21,4	20,5	26,1	28,8	24,4	33,1	30,1
21	29,8	30,2	28,5	25,3	19,8	17,9	22,3	27,3	26,5	27,1	32	25,7
22	29,5	30,9	29,2	23,8	19	18	22,9	26,9	25,5	17	28,1	28,1
23	27,7	31,1	28,2	23,7	21,6	19,6	21,9	28,9	25,5	24,9	27,7	30,4
24	28,3	27,9	28,3	20,3	25	15,8	18,9	29,1	25	17,9	21,3	30,9
25	28,5	29,7	27,4	17,5	23,8	15,7	21,5	28,9	24,7	20,1	24,6	31,4
26	27,1	29,6	28,6	22,3	23,3	17,4	21,1	28,2	25,8	25,1	26,2	26,3
27	28	29,5	29,8	24,8	21	23,5	22,1	23,1	29	27,7	27,8	27,4
28	28,6	29,9	26,7	27,5	19,8	20,2	22,3	24,9	28,9	24,5	27,3	30,6
29	26,8	29,7	24,2	28,1	20	21,7	19,3	25,8	20,1	28	29,5	31,8
30	28,6	***	22,1	28,7	23,4	25,2	20	26,7	25	25,7	29,5	32,9
31	32	***	22,3	***	21,3	***	20,5	27,6	***	22,7	***	27,4
Avg	29,1	29,4	27,8	24,2	24,1	19,3	20,5	22,7	23,8	25,9	28	27,5
Day	JAN	FEB	MAR	APR	MAY	JUN	JUL	AUG	SEP	OCT	NOV	DEC

1	29,9	28,7	24,1	***	***	25	23,5	19,6	18,3	23,2	27,2	***
2	27,4	30,1	26,2	27,2	25,2	24,7	22,5	19,6	22,2	28,8	26,9	***
3	26,9	32,6	28,4	20,3	24,3	23,7	22,9	19,3	24,7	31,1	24,2	***
4	31,7	30,9	28,9	21	21,7	24,4	21,8	19,2	26,4	28,9	28,5	28,2
5	24,7	27,3	28,9	24	20,7	24,7	16,9	21,5	25,5	30,7	31	27,6
6	28,6	25,1	31,7	27,2	20,6	22,4	16,7	18,5	26,7	33,2	31,3	22,4
7	31,5	30,6	26	29	19	22,6	21,3	21,3	25,7	29,5	28,3	24,4
8	31,8	29,5	27,3	28,8	21,2	23,4	21,6	23,4	27,7	26,6	31,8	26
9	33,6	29,6	31,4	29,2	23,7	16	22,2	20,1	30,5	28,5	31,6	25,3
10	34,2	27	25,3	27,8	23,6	17	19,3	19,4	29,5	30,2	31,2	17,9
11	27,4	29,4	23,2	19,5	19,7	17,8	17,3	19,7	29,2	32,3	29,5	26,3
12	28,7	28,5	24,9	17,5	21,2	20	18,1	18,2	27,3	34,5	29,3	27,8
13	30,3	29,3	26,4	20	22,3	22,5	19,3	22,7	27,4	28,2	31	28,1
14	32,8	32,4	23,5	26,4	22	23,6	20,4	22,7	29,8	24,7	31,9	30,3
15	30,9	32,4	26,6	28,5	21,1	22	19,2	22,3	31,6	26,3	31,8	32,1
16	27,3	29	28,2	28,6	22,8	19,7	21,7	22	31,7	31,1	30,8	31,9
17	27,4	29,8	30,8	28,9	23,1	19,6	23,1	25,3	30,2	31	32,1	28,6
18	21,3	30,1	29,1	22,6	20,6	16,1	18	20,3	30,8	30,6	32,2	27,1
19	24,7	32,4	31,3	18,6	19,1	19,4	18,6	20,1	28,3	29,7	30,1	23,2
20	21,6	32,4	28,8	14,2	21,8	20,8	20,2	19,9	29,9	15,5	30,4	25,8
21	29	30,9	29,8	20,5	22,6	20,4	19,6	23,2	21,9	22	23,7	29,2
22	29,1	32	32,6	22,8	22,1	22,2	17,3	22	15,8	22,9	24,4	31,4
23	32,6	33,6	30,6	23,9	23,9	19,5	18,6	20,2	23	22,7	28,7	30
24	32,6	31,7	28,5	22	23,5	18,8	21,6	22,7	30	23,4	26,2	25,3
25	35,1	25,4	28,9	24,3	24,2	20,8	22,7	25,7	32,7	25	26,9	22,2
26	30,1	30,6	25,1	24,9	23,8	23,1	23,4	22,6	31,6	27,2	30,7	24,9
27	30,4	33,7	24,6	24,8	24	23,1	24,5	24,2	30,7	23,1	29,5	25,4
28	30,8	32,3	26,8	25,9	24,4	20,2	24,5	26,2	29,5	23,1	25,1	28,4

29	28,4	***	27	26,3	23,2	21,4	20,3	25,5	25,7	25,7	22	21,2
30	27,7	***	27,1	22,4	24,9	23,4	17,9	27,1	18,6	29,3	30,4	26,4
31	29,9	***	25,1	***	25	***	19,6	13,9	***	29,1	***	29,9
Avg	29,3	30,3	27,6	24.0	22.5	21,3	20,5	21,6	27,1	27,4	29	26.7
Day	JAN	FEB	MAR	APR	MAY	JUN	JUL	AUG	SEP	OCT	NOV	DEC
1	29,8	28,1	23,3	23,9	26	25,7	21,4	***	***	26,7	28,5	29
2	32,4	29,4	20	26	28,4	25,6	19,7	22,6	22,5	25,4	22,2	28,2
3	32,7	24,2	20	26,4	28,2	24,5	19,5	21,1	22,7	25,6	25,4	29,8
4	31,2	27,3	22,5	23,1	25,8	23,8	19,5	21,1	24	23,8	25,4	31,1
5	29,9	28,4	22,4	25,7	26,6	23,3	21	23,5	23,5	25,1	27,3	33,2
6	24,3	28,4	26,9	24,5	21,6	13,1	20,9	25,2	26,6	27,5	27,2	29,7
7	28,6	28,7	26,6	25	20,5	16,7	18,6	25,2	29,6	28,8	30	30,5
8	27,3	30,2	26,6	23	22,9	17,9	12,2	21,8	30,9	31,5	29,4	27
9	29,8	26,3	21,5	22,5	24,7	19	13,7	19,3	28,6	33,1	30,9	21,9
10	32,3	28,6	20,7	23	25,4	20,1	15,7	22,4	29,6	30,4	21,8	27,2
11	30,4	30,9	27,3	23,7	23,8	19	16,1	20,9	30,2	23,8	19,5	28,3
12	29,9	31,7	23,8	24,4	22,5	19,9	17,5	21,2	31,5	30,1	19,4	25,6
13	31,8	29,9	18,9	22,3	24,3	20,9	20,8	22,1	29,7	34,1	27,3	28,2
14	28,9	29,2	25,2	18,1	24,6	21,8	20,1	24,5	31,3	30,3	31,8	25,6
15	29,4	27,7	28,1	23,8	24,2	24,2	18,6	25,1	30,3	26,9	24,4	28,3
16	33,4	29,6	26,7	23,5	24,6	21,8	20,6	19	30,4	28,2	26,5	21,2
17	33,7	28,5	26,6	16,8	24,9	21,9	21,5	20	30,5	22,9	21,4	23,5
18	33,5	31,4	27,7	23,3	19,8	22,5	23,7	21,9	31,7	25,1	20,9	26,2
19	26,9	29,2	27,5	26,1	19,5	16,2	18,5	25,7	24,9	30,4	24,7	28,6
20	30,1	28,9	28,9	26,4	18	19,8	19,9	26,4	24,5	31,3	26,9	29,3
21	29,1	28,5	24,5	25,8	21,8	19,8	19,8	25,6	24,1	31,4	28,3	31,9
22	29,4	27,5	24,6	24,7	20,2	20	19,2	18,8	25,9	30,3	28,9	27,2

23	29,3	28,5	26,9	21	22,1	19,3	22,6	19,8	26,8	29,4	22,1	29,6
24	32,2	27	26,7	23,1	22,1	20,1	24,7	20,9	27,4	31,9	27,4	31,6
25	32,4	25,9	25,5	22,2	22,7	21,7	23,1	24,4	29,7	30,3	31	31,9
26	28,4	27,6	26,8	23,4	25,1	22	20,4	25,5	31,3	20,6	31,1	30,9
27	26,8	25,9	26,3	25,4	25,4	23,5	19,1	26,9	31,8	24,4	19,4	23,4
28	***	27,7	25	21,6	23,1	19,2	21,2	14	27,9	27,3	27,9	27,3
29	***	***	24,6	25,9	24,9	20,8	19,2	19,4	25,9	30,7	28,6	27,9
30	***	***	26,8	28	26,8	22,3	18,8	20,4	28	33,4	26,4	30,4
31	26,7	***	25,7	***	26,2	***	22	20,3	***	33,1	***	27,6
Avg	30.0	28,4	25	23,8	23,8	20,9	19,7	22.2	28.0	28,5	26,1	28,1
Day	JAN	FEB	MAR	APR	MAY	JUN	JUL	AUG	SEP	OCT	NOV	DEC
1	***	29,3	27,6	27,7	25,3	23,3	***	***	26,9	***	***	34,1
2	29,1	30,3	24,7	28,4	25,1	21,4	20,3	19,1	23,7	27,9	25,3	32,1
3	29,8	32	26,1	26,1	27,2	18,3	20,2	20,8	22,7	30,2	24,3	26,7
4	32,5	31,9	28,7	24,3	26,9	15,6	20,3	23,6	14,2	32,4	23,7	31,1
5	31,2	31,9	30,3	26	27,4	17,2	21,9	22,7	14,2	33,6	26,2	34,5
6	32,2	33,2	30,1	27,8	29,3	16,3	23,5	22,5	16,9	33,3	27,6	36,6
7	29,7	32,4	27,9	21,8	24,4	16,7	19,4	23,5	21,8	33,6	31,7	36,7
8	30	31,4	29,4	22,4	23,1	19,6	19,1	25,1	25,3	34,4	33,4	30
9	31	32,4	28,7	22,7	25,1	20,9	22,3	25,3	26,9	34,1	36,4	31,5
10	30,6	34,1	30,4	21,2	25,3	18,5	20,4	24,6	31,1	32,3	36,5	33,4
11	30,3	34,3	30,6	24	24,3	16,6	18,8	19,9	30,8	33,6	37	34,9
12	30,6	31,1	27,6	24,8	23,8	18,8	21,4	20,9	22,4	31,5	35,8	30,6
13	30,9	30,4	30,4	24,9	25,6	20,7	***	25	24,6	32,4	31,9	33
14	24,6	30	30,3	26,8	27,7	22,4	21,5	26,7	24	29,4	30,5	30,6
15	28,7	30,5	31,4	26,8	28,3	23,1	***	26,1	26,2	27,6	32,8	28,5
16	27,7	28	30,2	26,4	27,8	21,9	***	27,1	28,5	30,3	27,7	28,8

17	32,3	26,6	31,4	23	26,8	13,9	15,7	26,3	31,1	24,3	26,6	31,4
18	27,6	29,8	29	20,4	24,4	17,5	***	26,4	29,5	29,6	27,3	31,3
19	29,4	32,7	29	21,4	25,4	19,6	***	26,4	25,8	31,2	27,9	33,5
20	27,6	32,8	29,1	23,8	26,2	17,7	***	25,6	21,9	30,3	28,6	33,9
21	29,7	24,6	28,4	26,2	25,3	19,8	***	26,4	21,7	30,4	29	33,5
22	32	31,3	23	23	24,8	19	***	29,5	27,1	28,6	27,2	34,1
23	31,7	29,2	26,3	25,2	21,4	20,7	***	26,3	30,3	29	29,2	33,4
24	31,7	30,7	26,5	22,5	22,5	20,8	***	26,3	31	31,5	31,4	35,4
25	32,3	27,6	24,5	25,6	25,5	21,6	***	27,7	31	31,9	32,7	26,6
26	30,7	29,7	25,8	27,5	25,7	20,4	***	28,1	31,3	31,2	33,3	29,3
27	32,3	27,8	28,7	27,9	25,9	14,2	***	28	28,8	28,1	33,2	31,2
28	22,3	27,6	25,2	27,5	25,7	18,2	***	27,8	31	30,3	22,6	33,2
29	26,9	***	25,7	27,3	26,8	21,4	***	29,8	33	28,6	28,5	33,2
30	28,9	***	26	26,3	26,4	20,8	***	29,1	32,4	31,2	32	32,3
31	28,8	***	24,7	***	24,7	***	***	29,3	***	34,9	***	32,7
Avg	29.8	30,5	28	25	25,6	19,2	20.4	25.5	26,2	30.9	30.0	32,2
Day	JAN	FEB	MAR	APR	MAY	JUN	JUL	AUG	SEP	OCT	NOV	DEC
1	35,1	30,1	30,5	28,6	18,9	***	21,9	***	***	***	32,1	***
2	***	33	32,2	29,9	22,8	20,2	18	19,6	25,6	25,6	30,3	30,7
3	30,5	31,2	31,5	29,2	24,7	20	15,9	19,8	27,4	21	27,5	30,5
4	23,6	31,9	32	26,1	23	20,8	16,2	17,9	27	20,8	31,4	34,1
5	34	26,1	31,5	24,7	23,5	20	15,9	21,4	26,9	26,8	27,8	28,3
6	37,1	29,8	32,3	22	23,7	19,6	20,2	24,4	28	32	29,6	26,8
7	38,3	32	31,8	20,7	23,4	19	19,6	23,8	28,7	33,9	26,3	30,3
8	35	30,5	26,8	20,7	18,5	19,7	19,2	25	31	29,5	28,8	30,5
9	29,7	28,1	22,6	23	19,8	20,4	21,1	21,1	30,5	26,5	29,9	31,8
10	28,4	28,5	24,3	25,1	19,9	22,4	19,2	23,8	28,8	28,1	30,1	30,4

11	29,6	31,2	27,9	26	23,6	19,9	18,5	23,1	25,6	32,1	22,8	27,6
12	26	33,6	25,4	28,1	24,6	14,6	20,3	22,5	25,7	33,3	27,8	26,2
13	28,8	33,5	27,9	28,3	24,2	9,8	19	22,3	28,4	28,8	30	26,9
14	24,9	33,1	24,9	28,9	15,6	11,4	17,8	24,2	21,6	27,2	29,7	25
15	29,3	33	26,5	27,5	17,4	18,4	18,4	25,4	27,9	30,3	23,9	26,4
16	24,8	35,2	27,2	27,5	20,2	21,4	18,8	20,8	29,3	31	25,1	31,6
17	26,8	32	20,6	29,3	22,3	20,6	18,2	20,8	23,9	31,2	30,9	30,1
18	25,6	31,3	26,9	28,5	20,6	18,8	18,2	21,2	12,2	23,4	31,1	30,8
19	28,1	31,4	29,8	27,7	20,3	22,1	20,5	22	21,3	20,7	22,9	32,2
20	27,8	34,2	28,6	30,3	21,6	22,5	22,4	25,2	23,2	25,2	27,5	31,7
21	26,1	33,9	28,9	18,4	18,8	22,6	23,6	26,5	27,1	24,5	24,4	30,7
22	27,5	33,6	26,2	25,5	20,4	17,9	24,2	20,8	30,4	29,7	30	32
23	29,8	29,3	23,9	28,8	19,7	18,3	22,5	20,1	31,8	29,6	27,7	32,6
24	24,3	30,9	27,8	27,3	20,3	19,4	19,9	23,4	28,9	30,3	21,2	25,7
25	28,9	30,1	28	27	20,8	19,5	17	25,3	29,2	31	26,8	21,2
26	29,3	29	25,4	29,5	18,8	19,7	17,7	27,9	27	29,9	26,4	19,9
27	29,7	28,3	28,1	24,8	19,6	20,2	13,9	24,4	27,9	31,7	26	25,4
28	30,8	25,1	28,7	27	20,1	21,1	17,4	26,2	26,8	33,4	31,3	23,5
29	30	28,2	29,1	28	21	19,8	18,8	28	27,2	34,7	33,7	28,1
30	31,4	***	29,1	25,9	20,6	19,1	19,9	28,1	28,6	35,5	33,8	27,3
31	31,1	***	29	***	21,2	***	20,2	26,3	***	35,9	***	29
Avg	29.4	31	27,9	26,5	21	19.3	19,2	23.4	26.8	29.1	28,2	28.6

Precipitation

Krugersdorp			Johannesburg Bot Gardens			Lanseria		
Month	Year	Tot Rain (mm)	Month	Year	Tot Rain (mm)	Month	Year	Tot Rain (mm)
Jan	2006	114,5	Jan	2006	151,4	Jan	2011	178
Feb	2006	160,5	Feb	2006	119	Feb	2011	47
Mar	2006	62	Mar	2006		Mar	2011	93
Apr	2006	2	Apr	2006		Apr	2011	101
May	2006	0	May	2006		May	2011	6,8
Jun	2006	0	Jun	2006	0	Jun	2011	45,6
Jul	2006	0	Jul	2006	0,6	Jul	2011	0
Aug	2006	35,5	Aug	2006	29,8	Aug	2011	1,6
Sep	2006	3	Sep	2006	2,8	Sep	2011	1,4
Oct	2006	54,5	Oct	2006	54,4	Oct	2011	33,8
Nov	2006	117	Nov	2006		Nov	2011	
Dec	2006	152	Dec	2006		Dec	2011	
Jan	2007	87	Jan	2007		Jan	2012	103,6
Feb	2007	18	Feb	2007	10,8	Feb	2012	9,6
Mar	2007	26	Mar	2007		Mar	2012	87
Apr	2007	45	Apr	2007		Apr	2012	2,4
May	2007	0	May	2007		May	2012	0
Jun	2007	5	Jun	2007		Jun	2012	3,4
Jul	2007	0	Jul	2007	0,2	Jul	2012	0
Aug	2007	0	Aug	2007	0	Aug	2012	0
Sep	2007	0	Sep	2007	33,4	Sep	2012	92,6
Oct	2007	120	Oct	2007	113,2	Oct	2012	73,8
Nov	2007	33	Nov	2007		Nov	2012	75,2

Dec	2007	86	Dec	2007	90,4	Dec	2012	95
Jan	2008	223	Jan	2008	146,6	Jan	2013	57,6
Feb	2008	11	Feb	2008		Feb	2013	54,4
Mar	2008	165	Mar	2008	142	Mar	2013	68,6
Apr	2008	2	Apr	2008	10,4	Apr	2013	103,2
May	2008	31	May	2008	47,6	May	2013	1,8
Jun	2008	17	Jun	2008		Jun	2013	0
Jul	2008	0	Jul	2008		Jul	2013	0
Aug	2008	0	Aug	2008	0	Aug	2013	0
Sep	2008	0	Sep	2008	0	Sep	2013	2,2
Oct	2008	27	Oct	2008	75,4	Oct	2013	73,4
Nov	2008	115	Nov	2008		Nov	2013	61,4
Dec	2008	124	Dec	2008	150,4	Dec	2013	
Jan	2009	147	Jan	2009	212	Jan	2014	
Feb	2009	113	Feb	2009		Feb	2014	7,6
Mar	2009	54	Mar	2009		Mar	2014	
Apr	2009	0	Apr	2009	4	Apr	2014	2,4
May	2009	21	May	2009	13,8	May	2014	1
Jun	2009	21	Jun	2009	15	Jun	2014	
Jul	2009	0	Jul	2009	3	Jul	2014	0
Aug	2009	30	Aug	2009	7,8	Aug	2014	10
Sep	2009	0	Sep	2009	10,2	Sep	2014	1,4
Oct	2009	82	Oct	2009	24,8	Oct	2014	26,2
Nov	2009	101	Nov	2009	66,4	Nov	2014	91
Dec	2009	138	Dec	2009	186,8	Dec	2014	42
Jan	2010	103	Jan	2010	349	Jan	2015	58,4
Feb	2010	91,5	Feb	2010	76,6	Feb	2015	56,4
Mar	2010	98	Mar	2010	39	Mar	2015	71,6
Apr	2010	91,4	Apr	2010	130	Apr	2015	36,2

May	2010	12	May	2010	37,8	May	2015	0,4
Jun	2010	0	Jun	2010	0,8	Jun	2015	1,8
Jul	2010	0	Jul	2010	0	Jul	2015	
Aug	2010	0	Aug	2010	0	Aug	2015	0
Sep	2010	0	Sep	2010	0	Sep	2015	54,8
Oct	2010	0	Oct	2010	35,6	Oct	2015	2,4
Nov	2010	73	Nov	2010	51,6	Nov	2015	32,2
Dec	2010	289,5	Dec	2010		Dec	2015	60,8
Jan	2011	299	Jan	2011	111,2	Jan	2016	100,6
Feb	2011	109	Feb	2011	82	Feb	2016	70,6
Mar	2011	44	Mar	2011	157,6	Mar	2016	148
Apr	2011	69	Apr	2011		Apr	2016	3,8
May	2011	14	May	2011	22,8	May	2016	49,2
Jun	2011	53	Jun	2011	46,4	Jun	2016	12,6
Jul	2011	0	Jul	2011		Jul	2016	24,8
Aug	2011	0	Aug	2011	3,2	Aug	2016	0,2
Sep	2011	0	Sep	2011	2,2	Sep	2016	6,4
Oct	2011	0	Oct	2011	40	Oct	2016	36,4
Nov	2011	30	Nov	2011		Nov	2016	92
Dec	2011	90	Dec	2011	83,8	Dec	2016	
Jan	2012	95	Jan	2012	77			
Feb	2012	195	Feb	2012				
Mar	2012	108	Mar	2012	26,4			
Apr	2012	31	Apr	2012	4,4			
May	2012	0	May	2012				
Jun	2012	0	Jun	2012	1,6			
Jul	2012	0	Jul	2012	0			
Aug	2012	0	Aug	2012	0			
Sep	2012	37	Sep	2012	15			

Oct	2012	48	Oct	2012	29			
Nov	2012	0	Nov	2012				
Dec	2012	0	Dec	2012	146,8			
Jan	2013	22	Jan	2013	59,4			
Feb	2013	47	Feb	2013	43,4			
Mar	2013	40	Mar	2013	26,8			
Apr	2013	0	Apr	2013	62			
May	2013	0	May	2013	5,6			
Jun	2013	0	Jun	2013	0			
Jul	2013	0	Jul	2013	0			
Aug	2013	0	Aug	2013				
Sep	2013	0	Sep	2013	4,4			
Oct	2013	68	Oct	2013	78			
Nov	2013	38,5	Nov	2013	104			
Dec	2013	152,5	Dec	2013	83,6			
Jan	2014	27,5	Jan	2014	61			
Feb	2014	175	Feb	2014	62,4			
Mar	2014	242	Mar	2014	62			
Apr	2014	27	Apr	2014	0			
May	2014	0	May	2014	0			
Jun	2014	0	Jun	2014				
Jul	2014	0	Jul	2014				
Aug	2014	0	Aug	2014	0			
Sep	2014	0	Sep	2014	37			
Oct	2014	0	Oct	2014	68,6			
Nov	2014	0	Nov	2014				
Dec	2014	0	Dec	2014	151,2			
Jan	2015		Jan	2015	189,2			
Feb	2015		Feb	2015	91			

Mar	2015	50	Mar	2015	81,6			
Apr	2015	40	Apr	2015				
May	2015	0	May	2015	1,2			
Jun	2015	2	Jun	2015	1,6			
Jul	2015	0	Jul	2015	20,6			
Aug	2015		Aug	2015				
Sep	2015		Sep	2015				
Oct	2015		Oct	2015				
Nov	2015	0	Nov	2015	45,2			
Dec	2015	0	Dec	2015				
Jan	2016		Jan	2016	98			
Feb	2016		Feb	2016				
Mar	2016	224	Mar	2016	198,2			
Apr	2016	10,4	Apr	2016	11,6			
May	2016	77,6	May	2016	59,8			
Jun	2016	16,4	Jun	2016				
Jul	2016	36	Jul	2016	21			
Aug	2016	0	Aug	2016	0			
Sep	2016	5	Sep	2016	2,6			
Oct	2016	57,6	Oct	2016	57			
Nov	2016	118,6	Nov	2016	153			
Dec	2016	132,4	Dec	2016	83,8			